The University Of Sheffield.

Through-plane Gas Permeability of Carbon-Based Porous Media In Polymer Electrolyte Fuel Cells

By:

Narvin David Neehall

A thesis submitted in partial fulfilment of the requirements for the degree of Doctor of Philosophy

The University of Sheffield
Faculty of Engineering
Department of Mechanical Engineering

October 2019

The candidate confirms that the work submitted is his own, except where work which has formed part of jointly authored publications has been included. The contribution of the candidate and the other authors to this work has been explicitly indicated below. The candidate confirms that appropriate credit has been given within the thesis where reference has been made to the work of others.

Abstract

The ever-growing need for energy security, depletion of fossil fuel reserves and rising environmental concerns has encouraged a shift from the conventional, fossil fuel dependent generation technologies to more environmentally friendly ones. It has been suggested that the hydrogen economy is a potential alternative, with the fuel cell identified as the energy generating technology. Polymer electrolyte fuel cells (PEFCs), specifically, has a great potential to replace fossil fuel dependent sources in portable, automotive and stationary applications due to their high efficiency, size flexibility, high power density and fast start-up times. There are still, however, certain aspects of its operation hindering widespread deployment of this technology. Two aspects need to be resolved further, specifically, water and thermal management are crucial in influencing the efficiency and performance of the cell.

The gas diffusion media (GDM) consisting of a gas diffusion layer (GDL) and microporous layer (MPL) is one of the major components which needs to be optimized and tailored in order to have high mass transport properties to successfully manage the water and heat produced from the operating cell. Even though, the basic structure of the fuel cell is simple, the individual components can be quite complex. Many researchers often try to improve the design of the PEFC through modelling and as such, PEFC models require accurate transport parameters as inputs. Diffusion is the main mode of transport in the PEFC; however, experimental investigations to measure the diffusion coefficient are inconvenient and may have a high deal of inaccuracy. As such, many researchers tend to measure the gas permeability which gives an indication of how porous the medium is to fluid flow.

This thesis focuses on the experimental investigation of the through-plane permeability of the GDM. Certain aspects are investigated, particularly, the structure of the GDL, the carbon

powder used in the MPL, the carbon loading or thickness of the MPL, surface morphology and optimization through certain ancillary techniques such as composite mixtures of different carbon powder types, sintering of the MPL and ink homogenization of the MPL ink slurry. The main findings are that the structure of the GDL used in conjunction with the type of carbon powder is crucial in determining the final gas permeability of the GDM. The ancillary techniques investigated have shown tremendous potential in predicting the final structure of the GDM.

Acknowledgements

I would like to express my sincere gratitude to my supervisors: Professor Mohammed Pourkashanian, Professor Lin Ma, Professor Derek Ingham, Dr. Kevin Hughes and Dr. Mohammed Ismail for their tremendous support and advice. A special thanks to Dr. Mohammed Ismail for his continuous support, day to day guidance and many useful discussions over the years. I would also like to acknowledge the technical assistance of Mr Paul Crosby and Mr. Dmitry Govorukhin in Energy 2050 at the University of Sheffield for their help with my experimental work.

I highly appreciate the support and love of my family and friends back in Trinidad and Tobago who have constantly aided me through all the hurdles I faced during my PhD. I am extremely grateful to my father (David Neehall), mother (Radicca Neehall), sisters (Kala and Ana Neehall) and brother (George Neehall). A special thanks to my father and mother who have always supported and encouraged me and helped me out financially as well.

Finally, I wish to acknowledge my sponsor, the Scholarships and Advanced Training Division (SATD) - Ministry of Education in Trinidad and Tobago for their financial support.

Table of Contents

List of Figures

List of Tables

Journal Publications

Journal Papers

1. **N.D. Neehall**, M.S. Ismail and K.J. Hughes, "Effect of gas diffusion layer substrate structure and PTFE content on the through-plane gas permeability of PEFC porous media**," In preparation for submission to the Journal of Hydrogen Energy. Chapter 4**.

2. **N.D. Neehall**, M.S. Ismail and K.J. Hughes, "Effect of Sintering time and Composite Carbon Mixtures on the through-plane gas permeability of PEFC porous media**," In preparation for submission to the Journal of the Energy Institute. Chapter 5**.

3. **N.D. Neehall**, M.S. Ismail and K.J. Hughes, "Influence of MPL ink slurry homogenization on the through-plane gas permeability of PEFC porous media**," In preparation for submission to the Journal of the Energy Institute. Chapter 6**.

Nomenclature

Roman Letters

D	Diameter of porous medium, µm
D_k^{eff}	Effective diffusion coefficient, m^2s^{-1}
g	Acceleration due to gravity, ms^{-2}
h	Height of porous medium in terms of its thickness, µm
k_g	Gas Phase Permeability, m^2
k_{GDL}	Permeability of gas diffusion layer, m^2
k_{GDM}	Permeability of coated gas diffusion layer, m^2
k_{MPL}	Permeability of microporous layer, m^2
L	Thickness of porous medium, µm
L_{GDL}	Thickness of gas diffusion layer, µm
L_{GDM}	Thickness of gas diffusion media, µm
L_{MPL}	Thickness of microporous layer, µm
P	Pressure, Pa
P_{rm}	Room pressure, Pa
Q	Volume flow rate, m^3s^{-1}
R	Universal gas constant, $Jmol^{-1}K^{-1}$
r	Radius of porous medium, m
$S_{95\%}$	95% confidence interval
t	Time, s
T	Temperature, K

T_{rm}	Room temperature, K
u_g	Gas Phase Velocity, ms^{-1}
V	Volume, m^3
wt.	Weight of sample, kg
wt.%	Percentage by weight

Greek Characters

β	Inertial coefficient, m^{-1}
ε	Porosity of porous medium
μ	Fluid viscosity of air flow, Pa.s
π	Pi
ρ	Density, kgm^{-3}
∇	Math symbol for gradient
$\Delta wt.$	Weight difference of samples, kg

Subscripts/ Superscripts

eff	Effective value
g	Gas phase
GDM	Gas diffusion medium
GDL	Gas diffusion layer
k	Species, k
MPL	Microporous layer
rm	Room value

Abbreviations

AB	Acetylene black
AEM	Anion exchange membrane
AFC	Alkaline fuel cell
BET	Brunauer-Emmett-Teller
BP	Bipolar plate
BP-2K	Black Pearls 2000
CCL	Cathode catalyst layer
CL	Catalyst layer
CNT	Carbon nanotube
DM	Diffusion medium
DMFC	Direct methanol fuel cell
FEP	Fluorinated ethylene propylene
FIB	Focused ion beam
GE	General Electric
GDL	Gas diffusion layer
GDM	Gas diffusion media
GFC	Gas flow channel
IEM	Ion exchange membrane
MEA	Membrane electrode assembly
MPL	Microporous layer
MWCNT	Multiwalled carbon nanotube

MCFC	Molten carbonate fuel cell
OECD	Organisation for Economic Co-operation and Development
PBI	Polybenzimidazole
PEMFC	Polymer electrolyte membrane fuel cell
PEFC	Polymer electrolyte fuel cells
PAFC	Phosphoric acid fuel cell
PAN	Polyacrylonitrile
PDMS	Polydimethylsiloxane
PPM	Parts per million
PTFE	Polytetrafluoroethylene
PVDF	Polyvinylidene fluoride
SAB	Shawinigan acetylene black
SEM	Scanning electron microscope
SLPM	Standard Litre per Minute
SOFC	Solid oxide fuel cell
SPFC	Solid polymer fuel cell
UK	United Kingdom
UNFCC	United Nations Framework Convention on Climate Change
USA	United States of America

Chemical Symbols

Al	Aluminium
e^-	Electron

CO	Carbon monoxide
CO_2	Carbon dioxide
CO_3^{2-}	Carbonate ion
H_2	Hydrogen molecule
H^+	Proton ion
H_2O	Water molecule
H_3PO_4	Phosphoric acid
K	Potassium
KOH	Potassium hydroxide
Li	Lithium
$LiAlO_2$	Lithium aluminate
N_2	Nitrogen
Na	Sodium
O_2	Oxygen molecule
OH^-	Hydroxide ion
SO_2	Sulphur dioxide

Chapter 1

Introduction

1.1 Energy Overview

The industrialization of developing nations and the growing world population have resulted in a rapid growth in worldwide energy consumption. Such a growth can be naturally attributed to the never-ending quest for improvement in the quality of life through economic development. The majority of energy demand today is supplied from the combustion of fossil fuels which has resulted in substantial degradation of the global environment. Pollutants gases, such as CO_2, CO, SO_2, NO_x, soot and ash which are admitted into the atmosphere through combustion of fossil fuels have been the cause of greenhouse gas effects which has led to global warming, air pollution and acid rains [1]. As a result, the world is now at a crucial stage to combat the climate change brought about by these emissions. Since 1995, greenhouse gas emissions have risen by more than 25% and atmospheric concentrations have reached as high as 435 parts per million carbon dioxide equivalent (ppm $CO_{2\text{-eq}}$) [2]. The groups which make up the United Nations Framework Convention on Climate Change (UNFCC) met in December 2015 and put in place a global agreement of limiting greenhouse gas emissions in order to achieve on average no more than a 2 °C rise in global warming this century. In order to achieve this, a reform of the energy sector is required, which accounts for two-thirds of all greenhouse gases at present [2]. It should be pointed out that in 2014, the rate of growth of CO_2 emissions from the energy sector grew at its slowest rate since 1998 [3].

The energy sector is one of the major contributors to economic development, such that, it is the source of electricity generation, heating and transportation. In order to achieve successful globalization and environmental protection, the security of the world's energy supply is of

great importance. Concerns for a reliable and sufficient amount of energy at a reasonable price most likely peaked in the 1970s. The world economy suffered and struggled to overcome the effects of the oil crises of 1973-1974 and 1979-1980 which was the result of inflation in prices [4]. Fossil fuels, namely, coal, oil and natural gas, have a finite supply. It is estimated that within the next 70-150 years that oil supply will be depleted and unless an alternative solution is present by 2015, where it is estimated that the consumption for oil will be greater than production, the world will face another energy crisis [5]. However, this was not the case by 2014, in which the global consumption of oil and gas was less than the production. In 2014, oil and coal prices fell, whereas gas prices fell in Europe, remained consistent in Asia but rose in North America [3].

The need for energy security, depletion of fossil fuel reserves and the rising global environmental concerns have precipitated the need for energy technologies which are more efficient than conventional technologies, such as the internal combustion engine. Energy sources with minimal or no emissions are undoubtedly required. It has been suggested that a hydrogen economy is a potential solution with the fuel cell being identified as the source of energy supply which will be able to solve the energy security and pollutant problems, whilst stabilising the fossil fuel supplies, facilitating economic growth and providing sustainable development [1].

Sustainable development strategies involve three major changes: (i) Energy savings, (ii) efficient energy production, and (iii) replacement of fossil fuels with various renewable energy sources. The drawbacks of utilising renewable energy sources stem mainly from their variable outputs and as such there will need to be diversification in the technologies. Therefore, any sustainable development strategy or policy should account for this through high supplies and it has been suggested in [6] that transportation be included in such policies

as well. Even though oil still accounts for 32.6% of the global consumption of energy in 2014, prospects for renewable energy technologies do look enticing, with renewable energy being the fastest growing form of energy each year in which the energy consumption has slowed down drastically. Renewable energy accounted for 3% of the world energy [3] and 22% of the electricity generation (a 7% growth) in 2014 [7] with the Organisation for Economic Co-operation and Development (OECD) non-member countries dominating [7].

1.2 Fuel Cells

Hydrogen is an excellent choice for an energy carrier since it is the lightest, most efficient and cleanest fuel [8]. A fuel cell is an energy conversion device which electrochemically converts the chemical energy contained in two reactants supplied to the device (a fuel and an oxidant) into electrical energy. The fuel of choice is typically hydrogen and the oxidant is usually oxygen which may be pure or from the ambient air [9]. The utilization of hydrogen in an electrochemical process allows for a higher efficiency of energy conversion when compared to that of internal combustion engine or thermal power plants. This can be attributed to the fact that electrochemical engines are not limited by the Carnot Cycle. Furthermore, unlike batteries, which are similar to fuels cells, once supplied continuously with reactant fuels, fuel cells can continuously produce power. It is due to this fact that fuel cells, namely the polymer electrolyte fuel cell (PEFC), are the ideal choice for the automotive industry [8]. Research in this thesis will focus specifically on PEFCs.

The simple cell device consists of an anode (electrically negative electrode), a cathode (electrically positive electrode), an electrolyte placed between the two electrodes (allows for the conduction of ions) and an external circuit which connects the two electrodes [9]. There are six major categories of fuel cells which have received extensive research focus:

(i) PEMFC or polymer electrolyte fuel cell (PEFC).

(ii) Solid oxide fuel cell (SOFC).

(iii) Alkaline fuel cell (AFC).

(iv) Phosphoric acid fuel cell (PAFC)

(v) Molten carbonate fuel cell (MCFC)

(vi) Direct methanol fuel cell (DMFC) [9], [10].

There are numerous other types of fuel cells apart from the ones listed above. Sharaf et al. [11] has provided a comprehensive list of various types of fuel cells and rates the research activity being conducted on these devices. Even though the unit cell device structure may be simple, for example in PEMFC, the phenomena occurring within this device during operation are quite complex and usually involve heat transfers, species and charge transport, multi-phase flows and electrochemical reactions which can take place in the various components, namely, in the membrane electrode assembly (MEA) which comprises the porous catalyst layer (CL) and membrane, the gas diffusion layer (GDL) and microporous layer (MPL) which are sometimes collectively termed the diffusion media (DM), the gas flow channels (GFCs) and the bipolar plates (BP) [10]. Table 1.1 provides a comparison of the major fuel cells listed above. It should be noted that this thesis specifically deals with the gas diffusion media (GDM) used in PEFC.

Table 1. 1 Comparison of the major fuel cells [11].

Fuel cell type	**Electrolyte**	**Operating temperature (℃)**	**Fuel type**	**Charge carrier**	**Efficiency (%)**
PEFC	• Solid Nafion (low temperature). • Solid composite Nafion or polybenzimidazole (PBI) doped in phosphoric acid (high temperature).	• 60-80 (low temperature) • 110-180 (high temperature)	Hydrogen	H^+	• 40-60 (low temperature) • 50-60 (high temperature)
SOFC	• Solid yttria stabilized zirconia (YSZ).	• 800-1000	Methane	O^{2-}	• 55-65
AFC	• Potassium hydroxide (KOH) water solution. • Anion exchange membrane (AEM).	• Below 0-230	Hydrogen	OH^-	• 60-70

PAFC	• Concentrated liquid phosphoric acid (H_3PO_4) in silicon carbide (SiC).	• 160-220	Hydrogen	H^+	• 36-45
MCFC	• Liquid alkali carbonate (Li_2CO_3, Na_2CO_3, K_2CO_3) in lithium aluminate ($LiAlO_2$).	• 600-700	Methane	CO_3^{2-}	• 55-65
DFMC	• Solid Nafion.	• Ambient – 110	Liquid methanol-water solution	H^+	• 35-60

1.3 Research motivation and objectives

It can be said, that even though the basic device structure of a fuel cell is simple, the various components can be quite complex. For example, the GDL and MPL structures are extremely complicated and the mass transport properties such as effective gas diffusivity are difficult to measure experimentally, which is why numerical and stochastic reconstruction such as in [12]–[18] are typically performed. The GDL structure is anisotropic which means that experimental measurements such as in [19]–[30] of the effective diffusivity are required in both the in-plane and through-plane directions. The majority of experimental techniques

used in the literature for measuring the effective diffusivity have been limited to mainly through-plane direction [17], [19], [20], [23], [24], [26]–[29] with very few measuring the in-plane diffusivity [21], [22], [30]. Furthermore, experiments measuring the effective diffusivity of the MPL are also very scarce [22], [24], [31].

Diffusion is the main method of transport through the porous media of the PEFC. The above experiments have shown that it is inconvenient to estimate the effective diffusivity experimentally and have shown to have a high degree of uncertainty [19], [30]. As a result, an easier method of determining how "diffusive" the porous media in PEFC is, would be to measure the gas permeability, since both transport properties scale with porosity [32]. The motivation for this thesis is derived from the losses which occur due to the components of the MEA, that is, GDL, MPL and CL. One of the major challenges which occur in an operating fuel cell is water management. Water management is directly related to the ability of the gas diffusion media (GDM) which aids in the regulation of water created in an operating PEFC. GDLs and MPLs are typically imbued with a hydrophobic agent (PTFE) to aid in water management. Furthermore, optimization of reactant gas transport is crucial in determining the efficiency of the PEFC, such that, the gas diffusion media (GDM) must demonstrate high transport properties for the CL to have sufficient amount of reactant gases. It should be noted that term GDM in this thesis refers to MPL coated GDLs.

Gas permeability is one of these transport properties which needs to be accurately determined since it describes how efficient the convective transport is in the PEFC. The GDLs which aid in regulation of the gas transport in PEFCs can be classified into two main types: (1) Non-woven carbon fibre paper and (2) Woven carbon cloths. Furthermore, non-woven carbon fibre paper can be sub-divided into two main categories: (1) straight fibres and (2) felt/spaghetti fibres [33]. This thesis focuses on the through-plane gas permeability

of the GDL and MPL structures which is measured experimentally by investigation of the pressure gradient of the flowing gas as a function of fluid velocity. Gas permeability, similar to effective diffusivity, can be measured in two principal directions, namely: (1) Through-plane, (2) In-plane (0° and 90°; that is, two orthogonal directions). This thesis focuses only on the through-plane permeability of GDL and MPL structures.

The aim of this thesis is as follows:

I. To experimentally investigate the through-plane gas permeability of GDLs and GDMs for different carbon paper structures.
II. To investigate the effect of PTFE in the GDL and how this affects the through-plane permeability of GDMs.
III. To experimentally measure the through-plane permeability of GDMs for various MPL compositions with a focus on carbon loading and carbon powder types.
IV. To experimentally determine the through-plane permeability of composite mixtures (a mixture of two different carbon black types) of carbon powders in the MPL.
V. To investigate the effect of sintering time for various GDMs utilizing different GDL substrates and different PTFE loaded commercial GDMs.
VI. To investigate the effects of homogenization techniques in creating the MPL ink slurry on through-plane permeability.

1.4 Scope and Outline of thesis

This thesis is divided into seven (7) chapters. Chapter 1 serves as in introductory chapter which provides general information related to the thesis. It provides a general overview of energy and different types of fuel cells. The research motivation and objectives of the thesis are clearly identified with a focus on the work involving the porous media in PEFCs.

Chapter 2 presents a thorough and critical literature review on works involving gas permeability in PEFC porous media. Additionally, the history of the major milestones in fuel cells and the history of the MPL are discussed with a general overview of PEFCs operations.

Chapter 3 discusses the detailed description of the procedures, materials and methods to be used in the investigation of gas permeability of PEFC porous media. The analysis used in determining the gas permeability from the experimental results is also discussed.

Chapter 4 investigates the effect of carbon loading and carbon black types as materials used in the MPL for various structures GDLs on through-plane permeability. The effects of PTFE in the GDL regarding different MPL carbon loadings and carbon black types is also investigated. Lastly, the effect of MPL thickness on through-plane permeability with and without penetration is analytically investigated.

Chapter 5 investigates the effect of composite mixtures in the MPL. Also, the effect of sintering time on MPL permeability is determined for a single carbon loading and for different PTFE loadings in the MPL

Chapter 6 involves the investigation of homogenization techniques used to prepare MPL ink slurries and how this affects the through-plane permeability of GDMs with a focus on types of GDL substrates, MPL surface morphology and different carbon powder types. The effect of dispersion time of the MPL ink is explored for bath sonication and how this impacts the through-plane permeability and surface morphology of the GDMs.

Chapter 7 concludes the thesis and provides a summary of the knowledge gained from the experimental investigations listed in Chapter 4 to 6. This section also provides possible future investigations which can be performed.

Chapter 2

Literature Review

Fuel cells are rapidly becoming an alternative to fossil fuel based conventional generation technologies, particularly for automotive, portable and stationary applications due to their capability of producing high power densities and high efficiencies with quick start up times and size flexibility [34], [35]. Fuel cells are typically classified by the type of membrane used, for example, PEFCs employ a polymer electrolyte membrane (Nafion) as shown in Table 1.1 and have the capability of producing low or even zero emissions. PEFCs are quite promising since they produce zero emissions (see Section 2.2) with the by-products of the electrochemical reactions being only water and heat. Water and heat management are therefore crucial in influencing the efficiency and performance of the fuel cell [8].

The membrane electrode assembly (MEA) forms the “heart” of the PEFC. The MEA comprises of the gas diffusion layer (GDL), microporous layer (MPL) and the catalyst layer (CL) and the impermeable polymer electrolyte membrane. The concept of water management in PEFC is somewhat conflicting in that a deficiency of water in the membrane reduces the ionic conductivity while leading to increased contact resistance between the membrane and CL and increased ohmic heating. Alternatively, excessive water produced, particularly at the cathode CL (CCL) in the MEA hinders reactant transport to the catalytic sites and adversely affects mass transport through the porous media. Water flooding is responsible for the unreliability, unpredictability and unrepeatability under identical operating conditions, in an operating fuel cell [35]–[37]. Ideally, water management is crucial in determining the overall performance of a PEFC.

Thermal management is another key issue which needs to be resolved before PEFC can be commercialized since the overall heat from the electrochemical reactions limits the efficiency of the fuel cell to 50% [38], [39]. Temperature has a great effect on catalyst activity, polymer membrane water content and mass transfer effects [40], [41]. The sources of heat in the PEFC can be: (1) Entropic, (2) Irreversible due to voltage losses and (3) due to phase changes through condensation and evaporation [42], [43]. Aslam et al. [42] suggested that it would be more meaningful to consider thermal and water management simultanesously, due to the fact that heat is transferred through the fuel cell mainly through conduction and eventually removed by the reactant gas in the flow fields.

The gas diffusion media (GDM) consisting of the gas diffusion layer (GDL) and microporous layer (MPL) is a crucial component in regulating water and heat throughout the components of the fuel cell and will be discussed in more detail in a later section of this chapter. As such, some of the characteristics of these layers need to be tailored in order to improve cell performance while facilitating efficient water and thermal management. Gas permeability is one of the mass transfer characteristics which needs to be improved and studied in greater detail. This chapter provides a thorough and critical review of the components or materials which comprise the gas diffusion media used in PEFCs and identifies areas which can be improved on.

2.1 History of PEFC with a focus on diffusion media development

In 1834, Sir William Grove invented the first fuel cell by reacting oxygen and hydrogen on separate platinum electrodes in sulphuric acid inside a five-cell gas voltaic battery. However, it was not until 1933-1959 that the first practical fuel cell was introduced by Francis Thomas Bacon using AFC technology. A summary of the milestones in general fuel cell development

is given in Table 2.1. This section will focus on the major developments of the diffusion layers in PEFC history.

Thomas Grubb and Leonard Niedrach at General Electric (GE) were the pioneers of the present PEFC which they referred to as an ion-exchange membrane (IEM) fuel cell. They utilized a sulfonated, cross-linked polystyrene in the form a sheet which was held together by an inert binder. The metal electrodes used were nickel screens activated by platinum black but some experiments were performed with platinized platinum and palladium foil electrodes. The electrodes were in direct contact with the ion-exchange membrane. Also, an indication of keeping the membrane hydrated is also given and it was accomplished by passing the input gases (hydrogen and oxygen) through water and by water being formed in the reactions in the cell [44].

These electrodes still did not resemble the dual layer carbon electrodes used today (microporous substrate affixed to the macro porous GDL). Further work by Niedrach [45] showed the use of hydrocarbons as fuel for the ion exchange membrane fuel cell. No difference in the electrode structure was observed, that is, platinum or palladium black catalysts coated onto the membrane with the use of a metal screen as a current collector. A different membrane was used - a reinforced sulfonated phenol formaldehyde casting resin but this cell showed inferior performance to the hydrogen-oxygen cell [45].

The technology developed by Grubb and Niedrach [44] at GE was used in NASAs Gemini Space program in the 1960s. The advantages of such a system were the high current densities, simple stack assembly and the absence of corrosive liquid electrolytes; however, this technology had a limited lifetime. Due to high production cost and high catalyst loadings used at the time in comparison to other technologies at the time, the solid polymer fuel cell (SPFC) would see little improvements until the mid-1980s [46]. Also, the power densities

which were achieved at the time of the Gemini Space Program were still not high enough (< 50 mW cm^{-2}) and the polystyrene sulfonate membrane was not stable and this made the AFC the chosen cell for the Apollo Space Program. In the late -1960s, the operation lifetime of the SPFC- what it was called at the time, was increased with the introduction of the Nafion membrane. GE further developed the solid polymer electrolyte for use in water electrolysis; however, no indication in the change in electrode structure was made - high surface area unsupported platinum electrodes were used in GE fuel cells in the 1980s. The GE technology was purchased by Hamilton-Standards United Technology Corporation (GE/HS-UTC). However, the electrode structures still utilized high platinum loadings (4 mg cm^{-2}) on the anode and cathode which were mixed with Teflon and hot pressed to the membrane. A wet-proofed carbon fiber paper was attached to the catalyst layer to prevent flooding and membrane intrusion into the current collector. No indication was given about the use of a MPL at the time [46].

In early 1984, Ballard Technologies Corporation in Canada along with the Canadian Department of National Defense (DND) was determined to investigate the potential of SPFCs for military and commercial needs. Their initial work focused on stack level hardware in order to develop the SPFC to operate effectively on air and pure hydrogen by improving the distribution of air to the porous cathode, effective removal of the water product and the manifolding of cells in the stack, reformed hydrocarbon fuels and reduction in fuel costs to improve the fuel cell performance. In 1987, Ballard Technologies began experimenting with a new ion-conducting polymer membrane created by the Dow Chemical Company. This new membrane, at ½ to ¾ of the weight of the commonly used Nafion membrane, showed greater conductivity and water retention and produced about four times the current and power as compared to the Nafion membrane when operating at the same voltage [47], [48]. Also, Eisman [46] stated that the tests performed with this new membrane significantly reduced

the internal resistance in the cell which directly relates to the increase in performance and cell efficiency. Further advances in PEFC technologies at the time included carbon supported platinum catalysts with low platinum loadings of ~0.35 mg cm^{-2}, as shown in [49], and water management through the use of internal water transport to humidify the gases and the membrane (this was done by Ergenics Power Systems Inc) and differential pressurization was utilized in the GE/HS-UTC cell to overcome water management issues [48]. Water management with an MPL was not used in the 1980s and early 1990s.

It was not until the mid to late 1990s that an MPL was added to the general structure of the PEFC. However, it should be noted that this structure of adhering a layer of carbon black mixed with PTFE onto a macroporous carbon substrate (GDL) dates back possibly to the mid-1980s, as shown in [50], and was used in the PAFC technology. The introduction of carbon to the various components of PAFCs made this technology economically feasible. It was first introduced in the form of graphite endplates (1968-1969) and eventually it was used as current collectors in the form of felts (around 1970), electrode substrates and as catalysts supports (1972-1973) [51]. Cameron [52] highlighted that the knowledge gained from the PAFC technology enabled the use of inexpensive carbon materials in PEFC. Kato [53] investigated the following ratios of PTFE to carbon black (between 10:90 and 60:40 with a preferential ratio of 20:80 or 50:50). It was also indicated that the amount of PTFE was crucial in water management and the amount of carbon black used was necessary for conductivity and porosity. Also, both [53] and [54] indicated that the thickness of this layer is important in gas diffusion and conductivity, such that, a thinner layer showed increased performance.

There has been a tremendous amount of research conducted to determine the MPL properties and improve them. Properties such as pore-structure, wettability, carbon loadings have been

improved through the use of new carbon-based materials and different fabrication processes. Some of these investigations have involved the use of different carbon-based materials in the fabrication process and are involved mainly at improving the water management during fuel cell operation. For example, Passalacqua et al. [55] prepared MPLs using Asbury graphite 850, Mogul L, Vulcan XC-72 and Shawinigan acetylene black (SAB) in which SAB resulted in better fuel cell performance due to a higher pore volume and smaller pore size. More recently, Chun et al. [56] have shown that the structure of the MPL has been extended to incorporate a hydrophilic and hydrophobic MPL. It was shown that the sample with the hydrophobic MPL at the surface resulted in better cell performance due to the water generated in the catalyst layer being absorbed by the hydrophilic MPL after passing through the hydrophobic MPL surface.

Attempts have been made by Kong et al. [57] to modify the pore structure through the use of a pore former, Li_2CO_3, and a heat treatment process at 350 °C. Their results indicated an increase in cell performance due to an increase in macropores (5-10 μm) in the MPL; this increase in macropores enhanced the mass transport processes which occur during the fuel cell operation. Wang et al. introduced an interlayer between the CL and macroporous substrate comprised of silica particles and polydimethylsiloxane (PDMS). The resulting structure when coated on to the diffusion media created a super hydrophobic surface with the internal pores of the gas diffusion media being hydrophilic. A thorough review of the investigations conducted on the improvements to the MPLs structure and composition is given in [35] and discussed in greater detail later in this chapter.

Table 2. 1 Summary of the milestones in fuel cell development [11], [52], [58]-[62].

Year (s)	Accomplishments
1800	William Nicholson and Sir Anthony Carlisle discover the inverse process to that occurring in a hydrogen fuel cell (that is, water electrolysis).
1838	Christian F. Schoenbein discovers the basic principle of fuel cells.
1839	William R. Grove and Christian F. Schoenbein independently test and develop the "gaseous voltaic battery" using hydrogen and oxygen what would be later called the fuel cell.
1882	Lord Rayleigh develops a new gas battery in an attempt to improve the efficiency of the platinum electrode. Hydrogen and coal gas as fuel were tested; however, the gas battery produced an inferior current.
1889	Ludwig Mond and Carl Langer developed porous electrodes to deal with the problem of electrode flooding, identify carbon monoxide poisoning and were able to generate hydrogen from coal.
1889	Alder Wright and Thompson reintroduce a previous device which they develop in 1887 by introducing "aeration plates" as electrodes and foresaw the use of liquid fuels as energy.
1893	F.W. Ostwald describes the function of different components and the electrochemistry of fuel cells.
1896	William Jacques builds a fuel cell that operates on coal.
1921	E.Baur and H.Preis begin experimenting with solid oxide electrolytes.
1933-1959	Francis Thomas Bacon introduces AFC technology.

1937-1939	E.Baur and H.Preis develop the SOFC out of a need to have a more manageable electrolyte as opposed to molten electrolytes.
1950	Polytetrafluoroethylene (PTFE) or Teflon was introduced and was used with platinum electrodes/acid electrolytes and carbon electrode/alkaline electrolytes.
1955-1958	Thomas Grubb at GE in 1955 developed an ion exchange polystyrene membrane and Leonard Niedrach at GE in 1958 developed a way to deposit platinum on to the membrane to act as a catalyst. PEMFC technology was developed at GE.
1958-1961	G.H.J. Broers and J.A.A. Ketelaar abandoned electrolyte oxides to use molten salts thereby introducing MCFC technology.
1960	Apollo space program at NASA utilizes AFC technology based on F.T. Bacon's work.
1961	G.V. Elmore and H.A. Tanner introduce the PAFC technology.
1962-1966	Gemini Space program at NASA uses the PEMFC technology introduced by GE.
1968	Nafion is introduced by DuPont.
1992	Jet Propulsion Lab at NASA in conjunction with the University of Southern California developed the DMFC.
1990s	Extensive focus on PEMFCs.
2000s	Early commercialization of fuel cell technology.

2.2 Overview of operation principles and performance of PEFCs

PEFCs are electrochemical devices which allow the conversion of chemical energy to electrical energy through a direct electrochemical reaction. The membrane electrode assembly (MEA) constitutes the primary components which defines the PEFC. The MEA, as stated in Section 1.2, consists of a polymer membrane which acts as an electrolyte sandwiched between an anode and cathode. The membrane functions as a proton conductor, alternatively termed proton-exchange membrane, and as an impermeable gas separator between the anode and cathode side gases. Adjacent to the membrane are two electrically conducting porous electrodes (they are porous to facilitate the diffusion of gases), typically, carbon fibre paper or carbon cloth. The interface between these two layers are catalyst particles, typically platinum supported on carbon, where the electrochemical reactions take place (See Figure 2.1) [8], [58].

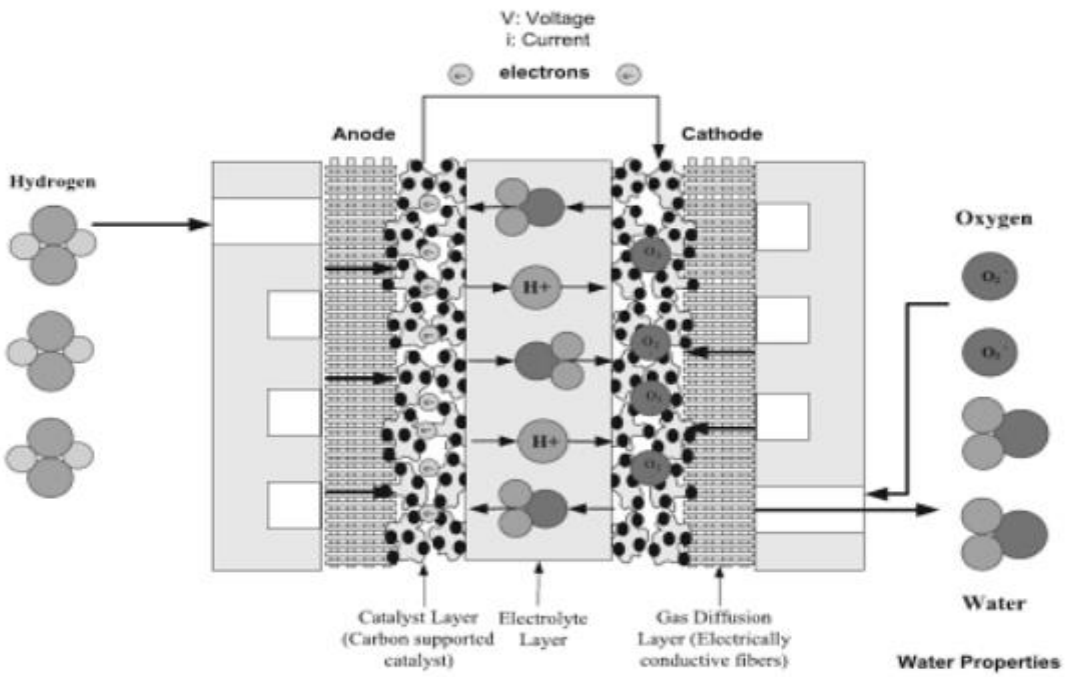

Figure 2. 1 The basic principle and structure of PEFCs [58].

The fuel cell can operate continuously provided that the fuel and oxidant are constantly supplied. Hydrogen is transported to the anode from the anode flow field channel whereas

oxygen or air is delivered to the cathode through a similar process. Decomposition of the hydrogen atom at the membrane allows for one proton to be transported through the membrane and one electron to travel through the electrodes, current collectors and then to the external circuit. At the cathode catalyst layer, the protons re-combine with the electrons and oxygen molecules to form water which is removed from the cell through the excess flow of oxygen. The electrochemical reactions at the anode (equation 2.1) and cathode (equation 2.2) are as follows [8], [58]:

$$H_2 \rightarrow 2H^+ + 2e^- \tag{2.1}$$

$$\frac{1}{2}O_2 + 2H^+ + 2e^- \rightarrow H_2O + heat \tag{2.2}$$

Accordingly, the overall reaction can be written as follows:

$$\frac{1}{2}O_2 + H_2 \rightarrow H_2O + heat \tag{2.3}$$

The electrochemical reactions taking place at the membrane directly influence the fuel cell performance. Polarization curves are commonly used to characterize the fuel cell performance by evaluating the cell voltage with respect to the current density under operating conditions. Consequently, evaluation of different cell components on the fuel cell performance can be achieved with the comparison of polarization curves. Voltage losses in fuel cells are characterized into three categories: (i) activation losses, (ii) ohmic losses and (iii) concentration losses (See Figure 2.2).

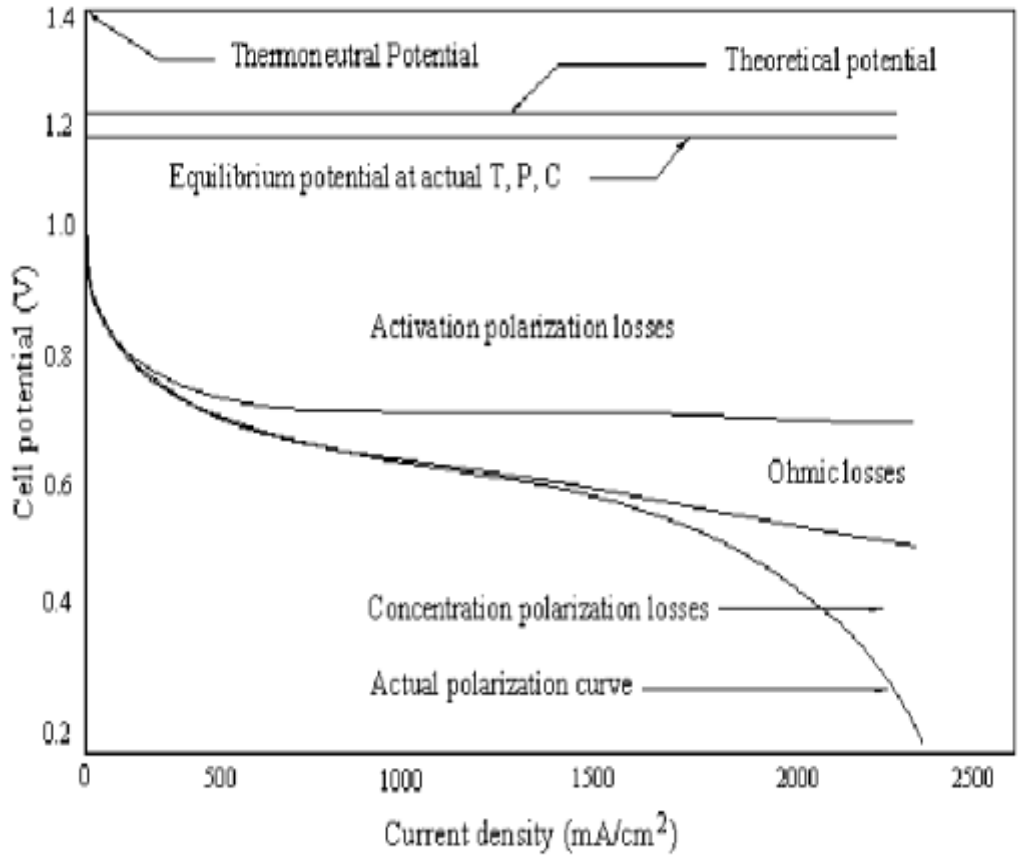

Figure 2. 2 Schematic diagram of an ideal polarization curve depicting the cell losses with their corresponding regions [8], [59].

The activation losses (low current density region) are mainly attributed to the sluggish electrode kinetics, namely the oxygen reduction reaction at the cathode catalyst layer which requires higher overpotentials and is slower than the hydrogen oxidation at the anode. The ohmic losses, which are almost linear, are the result of the resistance to electron flow through the electrically conducting components. Concentration losses arise when a gradient is established due to rapid consumption of reactants. This is directly related to the current density, which is high in this region, resulting in a low surface concentration and a drastically high consumption rate as compared to the supply rate [8], [59].

2.3 Overview of the Functions of Porous Media in PEFCs

As stated previously, the three main porous regions of the MEA are the: (i) GDL, (ii) MPL and (iii) catalyst layer. Since the focus of this thesis is the mass transport properties in the GDL and MPL, only these will be discussed here further. Figure 2.3 shows a schematic of the porous regions of the MEA.

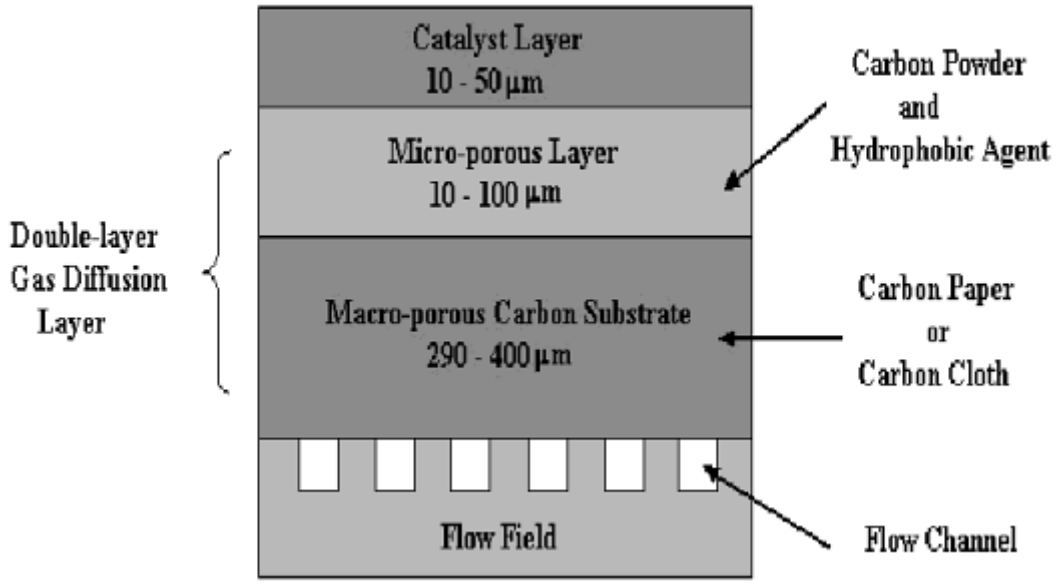

Figure 2. 3 Schematic showing the porous regions of the MEA [59].

The GDL exists between the catalyst layer and bi-polar flow field plates and facilitates the diffusion of gases to the catalyst layer and acts as an electrical conductor between the catalyst layer and flow field plate. They are typically constructed from porous carbon fibre-based materials and are usually in the form of a non-woven carbon paper or woven carbon cloth. There has been greater interest in carbon paper GDLs due to lower costs and the availability to easily apply the MPL to it [60], [61]. The main functions of the GDL are as follows:

(i) There is a need for a sufficiently porous GDL to allow the flow of reactant gases and product water.

(ii) The pores must be of a sufficient size to allow proper distribution of gases to the reactant catalyst sites.

(iii) It must be electrically and thermally conductive to allow the flow of electrons and allow the removal of heat, respectively.

(iv) It must be mechanically rigid to support the MEA but flexible enough to be in good electrical contact with nearby components [59]–[61].

The GDL is normally made hydrophobic with the use of PTFE. PTFE is applied in the form of an aqueous suspension which is eventually heat-treated to sinter particles allowing them to adhere to the GDL surface. Additionally, an MPL is applied to the GDL, forming a dual layer structure. The dual layer structure consists of either carbon-fibre woven cloth or non-woven carbon paper as the GDL and a thin layer of carbon black powder (Vulcan XC-72R or Acetylene black being the most commonly used) bonded with a hydrophobic agent such as PTFE which serves as the MPL [35], [62]. The pore-diameter of the MPL is usually in the range $0.02 - 0.5$ μm as compared to the GDL pores which range from $10 - 100$ μm [36], [62], [63]. The main functions of the MPL are as follows:

(i) The MPL reduces contact resistance between the catalyst layer (CL) and GDL (macroporous layer).

(ii) Improves cell performance by enhancing water management in the cell in the form of:

- The smaller pore size of the MPL and the enhanced hydrophobicity leads to a higher saturated pressure in the MPL as compared with the GDL which makes the MPL less vulnerable to flooding issues.
- The GDL with an MPL attached forces the macrosubstrate to have a two-fold function, forcing water to the membrane which keeps it hydrated and allows for the buildup of pressure to force water through less hydrophobic GDL into the cathode flow channels.

- GDLs lose hydrophobicity over long hours of operation and as such, the presence of an MPL reduces the loss of hydrophobicity in the macroporous GDL substrate [36], [62]–[64].

(iii) It was reported in [63] and [65] that the MPL also increases the catalyst utilization and overall cell performance depending on its structure.

The MPL is typically prepared by the doctor blade technique in which an MPL paste, consisting of carbon powder and PTFE in a solvent, is spread over the GDL with the use of a metal strip. The solvent is then allowed to slowly evaporate to prevent cracks at the surface of the layer. Finally, the substrate is heat treated to sinter the binder [35], [60].

2.4 GDL materials and fabrication

As stated previously, there are two main categories of GDLs, namely: (1) Woven carbon cloths and (2) non-woven carbon fibre paper [60], [61]. Non-woven carbon fibre paper GDLs will be the primary materials used in this thesis and as such, only the manufacture of these materials will be discussed. It should be noted, however, that there are metal based GDLs which are usually fabricated in the form of a metal foam, mesh or micro-machined substrate [66], [67] for use primarily in DMFCs due to their ability to positively aid in the transfer of liquid water and fuels. Some of the metals used in the literature include copper [68]–[70], titanium [67], [71]–[73] and stainless steel [74], [75]; however, corrosion of the metal based GDLs becomes a major flaw due to the fact that it promotes membrane degradation [76]–[78].

Non-woven carbon fibre papers undergo four (4) major manufacturing steps: (i) papermaking, (ii) resin impregnation, (iii) moulding and (iv) heat treatment (carbonization and graphitization). The most attractive precursor of choice in the production of non-woven

carbon fibre papers is typically copolymer made up of >90% polyacrylonitrile (PAN) due to the low cost, high carbon fibre yield (50%) and appealing material properties. The PAN copolymer is then transformed into PAN fibres through a process of solvent spinning followed by stabilization in air at 230 °C which creates a thermoset material from the thermoplastic polymer. This allows the fibres to remain as isolated filaments even after subsequent heating processes. These stabilised carbon fibres are then heated to approximately 1200-1350 °C in nitrogen reducing its weight by 50% and yields fibres with >95% carbon. The resulting tows or untwisted bundles of continuous carbon fibre filaments are then cut into 3-12 mm lengths before the papermaking process. Rolls of carbon fibre paper are created from a wet-laid conventional papermaking technique (it should be noted that there are other techniques to create the carbon fibre paper as shown in Figure 2.4). The tows are dispersed in water with a typical binder such as polyvinyl alcohol. Rotating porous drums or wire screens with a vacuum dryer are used to remove and dry the rolls. The rolls of carbon fibre paper can then be impregnated, typically, with a phenolic resin. The impregnated rolls are then compression moulded in a batch process and dried at 175 °C under a pressure of 400-500 kPa. This process allows for a desired thickness of carbon fibre paper to be obtained. Lastly, the fibres undergo graphitization at >2000°C in an inert environment which changes the amorphous carbon into crystalline graphite fibre of >99% carbon content with more appealing mechanical, electrical and chemical properties in comparison with the amorphous carbon. Woven carbon cloth is created from spun PAN yarns followed by graphitization. A full description of alternative processes can be found in [79].

It is to the author's best knowledge that there are only a few works in the literature which focus on the manufacturing of the GDL substrates apart from the generic process of fabrication described above. Typically, researchers tend to describe GDL fabrication in either a one or two stage "fabrication" process which takes place after the manufacturing of

the GDL substrate. In the one-stage process, the GDL substrate is typically coated with a hydrophobic material such as PTFE or fluorinated ethylene propylene (FEP) which not only improves the hydrophobicity but also the surface smoothness reducing the contact resistance of the catalyst layer adjacent to it [80], [81]. The most common way of applying the PTFE to the carbon substrate is by dipping the medium in an aqueous suspension of the hydrophobic material followed by heat treatment at 350°C to remove the remaining solvent and fixing the PTFE to the surface. Typically a range of 5% to 30% by weight PTFE is applied to the carbon substrate [79]. Furthermore, the two-stage process involves not only applying the hydrophobic material to the carbon substrate but also the application of a microporous layer consisting of carbon or graphite particles and a polymeric binder such as PTFE. Typically a PTFE loading of 15-20% by weight leads to optimum performance [80], [82]. The majority of this thesis focuses on MPLs with 20% PTFE by weight. The MPL can be applied by either brushing, printing, spraying or doctor blade, on either one or both sides of the carbon substrate [79], [80]. It should be noted that the material properties such as, porosity, thickness, bulk density permeability, hydrophobicity and electrical and thermal conductivity of the microporous layer can be directly affected by the application method and even by the materials used. For example, even the nature of an alternative binder, such as, polyvinylidene fluoride (PVDF) can affect the structure of the MPL created [79], [80]. Figure 2.4 and Figure 2.5 illustrates the total fabrication process of the non-woven carbon fibre substrates. It should be noted that sintering of the substrates would be discussed in a later section of this chapter.

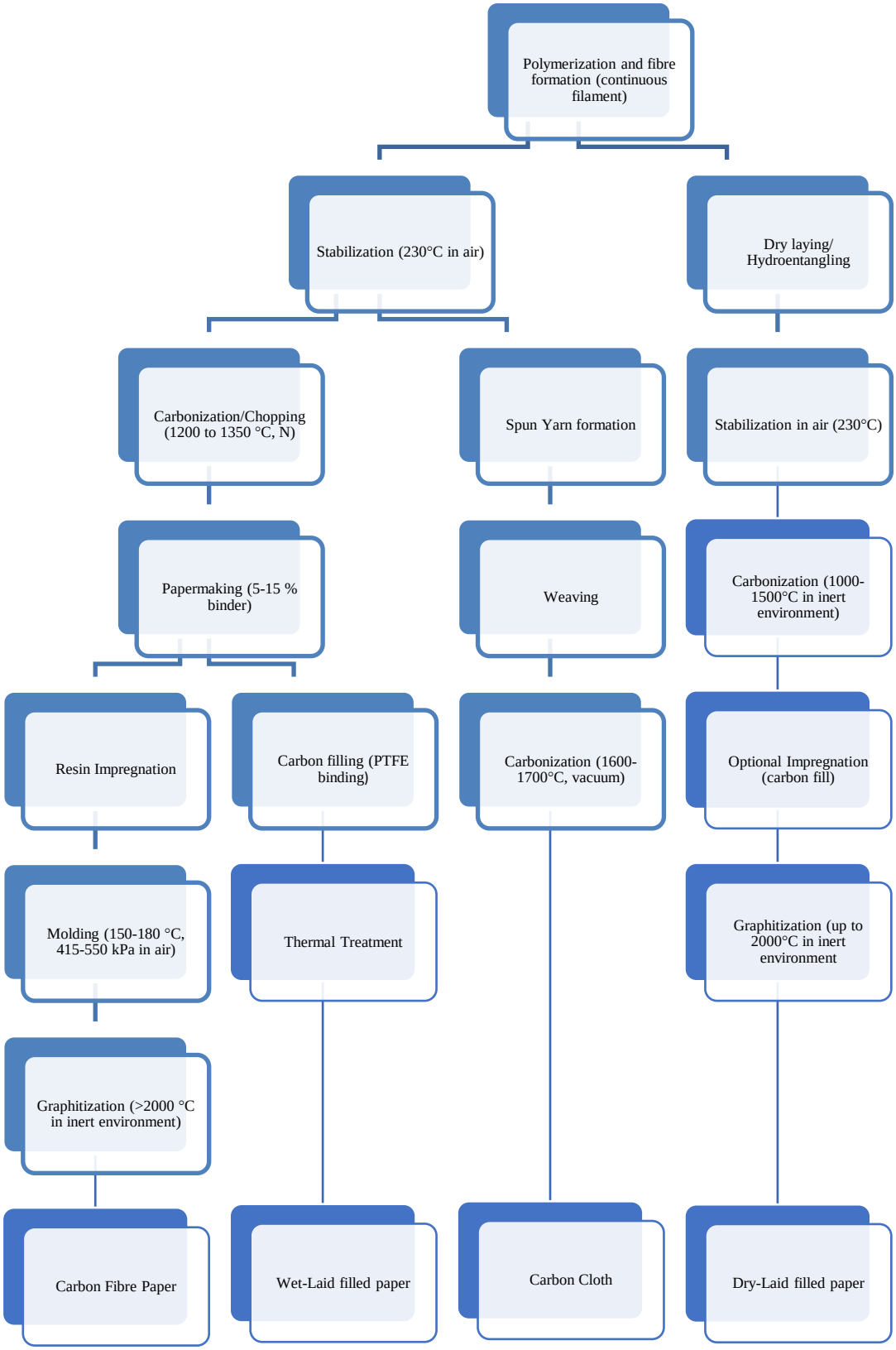

Figure 2. 4 Carbon substrate fabrication process [79].

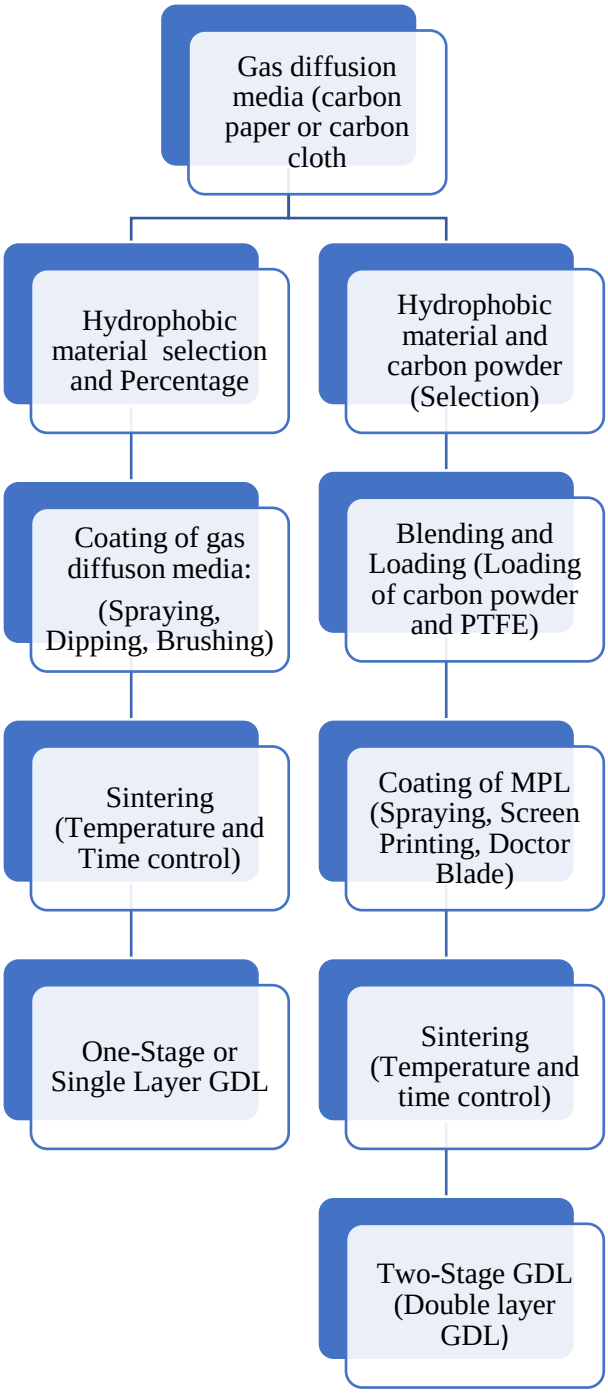

Figure 2. 5 Carbon substrate treatment and coating process [80].

2.5 Gas Transport in PEFC porous media

Diffusion is considered the primary mode of mass transport within porous media in a polymer electrolyte fuel cell (PEFC) [19]. Operating the fuel cell at high current densities results in the electrochemical reactions occurring within the cell being limited by the diffusive flux through the gas diffusion layer (GDL); as such, a thorough understanding of the GDL structure and how operating conditions affect mass transport is desirable in order to obtain improved designs of PEFC porous media [19], [23].

The GDL consists of graphitized carbon fibres which are manufactured into either randomly oriented carbon paper and held together with a binder or woven into carbon cloth. The anisotropic structure of the GDL is highly porous with a porosity of about 70% and consists of a wide range of pore sizes [19]. Numerical models are often employed to obtain a greater understanding of the GDL's structure and use the conservation equations of mass, momentum, species, charge and energy to simulate various transport phenomena. In order to account for the random structure of the GDL, transport coefficients need to be adjusted and are usually referred to as effective transport coefficients [23].

Diffusion in porous media can be characterized as mainly: Ordinary or Knudsen diffusion [83]. Equation (2.4) is typically used to express the effective gas diffusion coefficient D_k^{eff} and has been modified to account for structural features of the porous media [19]:

$$D_k^{eff} = f(\varepsilon) D_k \tag{2.4}$$

where D_k^{eff} is the effective diffusion coefficient or effective diffusivity, ε is the porosity of the medium and D_k is the normal diffusion coefficient of species k. The porosity describes the pore-volume or void fraction within the porous media. There are many different models which can be used to describe the diffusivity in porous media with the most common being

the Bruggeman expression $f(\varepsilon) = \varepsilon^{1.5}$ [19], [23], [83]. The type of diffusion is dependent on the pore size such that ordinary diffusion occurs if the mean free path (average distance traversed by a particle between successive collisions) is short compared to the pore size, that is, molecule to molecule collisions occur more frequently in ordinary diffusion. If the mean free path is long compared to the pore size, Knudsen diffusion is dominant and the molecule to wall collisions are more frequent [83], [84]. Knudsen diffusion is dominant for pore sizes ranging from 2-50 nm and as such, it is expected that both ordinary and Knudsen diffusion coexist in the MPL and GDL which have pore sizes ranging from tens of nanometres to tens of micrometres respectively [84]. Other mathematical models for the effective diffusivity can be found in [12]–[17]. Furthermore, since these models do not accurately define the GDL properly, there have been numerous experimental works in the literature to estimate the effective diffusion coefficient [19]–[22], [24], [26], [27], [30], [31]. Alternatively, there have been attempts to reconstruct the GDL using X-ray tomography such as in [85]–[89] and focused ion beam (FIB) SEM [90], [91]; however, these techniques are limited by the technology currently used and size of the samples used.

Convective gas flow resistance is typically characterized using Darcy's law to determine the permeability of the porous media which is proportional to the convective flow. Permeability, similar to the effective diffusion coefficient, gives an indication as to how porous the medium is to fluid flow. Typically, permeability is obtained by measuring the pressure drops across the porous medium in relation to the fluid flow velocity through the medium. As indicated in [92], the contribution of through-plane convection is small, typically, in the MPL which reduces the gas flow due to size of the pores; however, convection is significant in the in-plane direction (parallel to the flow channels) due to the high pressure difference between adjacent flow channels in the flow field plates and the high in-plane permeability as compared to the low through-plane permeability [79], [92]. This property is further

discussed in greater detail in Chapter 3 as it is one of the transport properties which relates the flow of gases to the catalyst layers and forms the core of the investigations conducted in this thesis.

2.6 Experimental investigations of Gas Permeability of the GDM

As stated previously in Section 2.3, the gas diffusion media in the PEFC needs to have high transport properties in order to facilitate reactant gas flow to the catalyst layer whilst maintaining proper water and heat management. Even though gas diffusion is the main mode of transport in the PEFC, experimental investigations into gas diffusivity are inconvenient to measure experimentally and some have a high deal of inaccuracy [19], [30], [32]. Subsequently, many researchers tend to measure the gas permeability of the porous media which scales with porosity (similar to gas diffusivity), giving an indication of how "diffusive" the GDM is. Furthermore, since the GDL's morphology is anisotropic, researchers then to measure the gas permeability in as many as three directions: (i) through-plane (z-direction), that is, in the plane from the flow field to the catalyst layer and (ii) two in-plane directions (x and y direction) orthogonal to each other [30], [93], [94]. Many researchers tend to investigate the gas permeability of the porous media in PEFCs using in-house built experimental setups with the use of Darcy's law [80]. Darcy's law will be discussed in more detail in Chapter 3.

Gurau et al. [94] investigated the absolute through-plane and in-plane permeability for different PTFE loadings and carbon types in the MPL. They concluded that a higher PTFE loading in the MPL resulted in higher permeability in both the through and in-plane directions. This was attributed to the increase in volume of the intra-agglomerate pores and the fact that under compression, the gas diffusion media was able to maintain a higher porosity due to increased rigidity of the media. Gurau et al. [94], however, did not indicate

the type of carbon black used in the MPLs. A similar conclusion was reported by Dohle et al. [95] for in-plane permeability measurements of a single type of diffusion layer with varied PTFE loadings. Ismail et al. [93] also showed similar findings for increased PTFE loading in the MPL on in-plane permeability; however, an increase in PTFE loadings in the GDLs resulted in a decrease in permeability. Pharoh et al. [96] indicated, however, that the in-plane permeability plays a more significant role when compared to the through-plane permeability especially in the case where MPLs are used due to the fact that the addition of a MPL significantly reduces the through-plane permeability by several orders of magnitude beyond a computational threshold value of 1×10^{-13} m^2 after which convective flow is no longer significant; however, it was shown that the in-plane permeability remains unchanged. Tehlar et al. [97] confirmed this relationship experimentally by testing the in-plane permeability of Toray TGP-H-60 with and without an MPL and showed that the in-plane permeability remained almost unchanged. Feser et al. [98] investigated the in-plane permeability of carbon cloth (Avcarb 1071-HBC), non-woven carbon fibre paper (SGL 31BA) and carbon fibre paper (Toray TGP-H-60) and showed that woven and non-woven carbon fibre paper showed higher in-plane permeability than carbon fibre paper.

Ismail et al. [99] measured the through-plane permeability of various carbon substrates (GDLs) with different PTFE loadings. The results concluded by Ismail et al. [99], however, was surprising such that the carbon substrate with 0% PTFE loading showed a lower permeability than the substrate with 5% PTFE and the substrate with 20% PTFE loading showed the lowest permeability when compared to the various substrates investigated. This should not be the case as reported by Bevers et al. [100] and Park et al. [101] in which the higher PTFE loading in the carbon substrates results in a decrease in through-plane permeability due to the fact that the PTFE block a portion of the pores. Ismail et al. [32] extended investigations into through-plane permeability by considering commercial GDLs

with a MPL. The results showed similar findings to that of Gurau et al. [94] such that the increase in PTFE loading of the MPL resulted in an increase in through-plane permeability. Ismail et al. [32], [99] also investigated the effect of compressibility of the gas when solving Darcy's law and showed that if it is not accounted for, resulting values of through-plane permeability of MPL coated GDLs are underestimated by up to 11% and up to 9% for bare GDL substrates. Gurau et al. [94] did not consider gas compressibility for through-plane permeability but for in-plane permeability assuming that pressure drop in the short through-plane path was negligible compared to the longer in-plane path.

Gostick et al. [102] investigated the in-plane and through-plane permeability of several GDLs without MPLs. Furthermore, in-plane permeability was reported for two in-plane directions perpendicular to each other. The results showed that the in-plane permeability was higher than the through-plane permeability and the permeability of the two perpendicular in-plane directions showed significant anisotropy such that the in-plane permeability differed by a factor as much as 2. Ismail et al. [93] investigated the effect of PTFE the in-plane permeability of SGL 10BA in two orthogonal in-plane directions and showed similar findings to that of Gostick et al. [102] that in-plane permeability in the direction parallel to the fibre orientation was greater than that normal to the fibre orientation. Feser et al. [98] investigated the in-plane permeability of carbon cloth (Avcarb 1071-HBC), non-woven carbon fibre paper (SGL 31BA) and carbon fibre paper (Toray TGP-H-60) and showed similar findings to Gostick et al. [102] and Ismail et al. [93], such that, an inverse relationship exists between in-plane permeability and compression ratio. It should be pointed out that experimental investigations into the in-plane permeability of the GDMs used in PEFC allows the effect of compression to be investigated with the used of feeler gauges such as in [93], [102] or brass shims [98] which allow the compression effects to be directly incorporated without removing the sample from the setup.

To the author's best knowledge there are only a few communications which investigated the effect of compression on through-plane permeability [85], [97], [103]. Compression was achieved in the through-plane ex-situ with the use of a universal test machine [103] or clamping the samples between two highly permeable sintered frits and controlling the compression with spacers [85], [97]. The results presented in [85], [97], [103] showed an inverse relationship between through-plane permeability and both compression ratio and PTFE content; however, increased PTFE content was far less influencing that the effects of compression.

Williams et al. [104] investigated the through-plane permeability of several commercial based GDLs (carbon fibre paper and carbon cloths) with microporous layers. The microporous layer consisted of carbon black (Vulcan XC-72R) with 14 wt.% PTFE loading. The in-house constructed paper utilised Toray TGP-H-120 carbon fibre paper as the GDL and showed a reduction in through-plane permeability with the addition of a microporous layer by approximately 80%; however, no indication of the carbon loading was given. SGL 10BB, a non-woven carbon fibre paper with an MPL, showed a reduction in through-plane permeability in the order of two magnitudes lower when compared to the base GDL, SGL 10BA. Carbon cloths with a microporous layer were found to have lower permeability when compared to the GDM utilising carbon fibre paper as the GDL. Similar findings were shown by Ihonen et al. [105]; however, the permeability of the bare carbon cloths are typically higher than carbon fibre papers [102], [106].

Mangal et al. [107] investigated the effect of PTFE loadings using Toray TGP-H-90 carbon fibre paper. The experimental investigations in the literature discussed thus far have utilised one sample in the experimental setup. Mangal et al. [107] investigated the effect of stacking samples and found that three showed the best repeatability; however, it should be noted that

the exposed area of the sample to the flowing gas was small (9.5mm in diameter) as compared to 20 mm used in [32], [99]. The results indicated agree with the investigations discussed above, such that, increasing PTFE content in the GDL reduces through-plane permeability; however, 10% PTFE loading showed the highest but this was attributed to sample preparation and variability.

2.7 Composition and Preparation of the Microporous Layer

The MPL composition typically describes the addition of a mixture of carbon powder and a hydrophobic agent as stated earlier in Section 2.3 [35]. The morphology of the MPL is therefore controlled by the type, loading and particle size of the carbon powder used in conjunction with the type hydrophobic agent; the former determines the surface smoothness, for example, carbon powders with finer sizes result in smoother surfaces and smaller pores whereas the later directly affects the pore properties [78], [80]. Furthermore, the deposition and ink preparation methods can have significant impacts on the structure and GDM properties [81], [108]–[114].

Passalacqua et al. [55] investigated the effects of various carbon blacks, namely, Asbury graphite, Shawinigan Acetylene Black (SAB), Mogul L and Vulcan XC-72R, with different surface areas on fuel cell performance. SAB showed the best fuel cell performance due to higher pore volume and smaller pore sizes which was characterized using a mercury intrusion porosimeter (MIP). Carbon loadings were varied between 2.5 to 5 $mgcm^{-2}$ and the MPL was spray-coated onto a Toray TGP-H-90 carbon paper sheet.

Antolini et al. [115] investigated the effect of a single carbon loading of 3.0 $mgcm^{-2}$ of SAB and Vulcan XC-72R coated on two sides of carbon cloth GDL to form a triple-layer GDM (MPL/GDL/MPL). The substrates coated with SAB showed higher cell performance; however, optimized cell performance at high pressures indicated the use of Vulcan XC-72R

carbon powder on the catalyst side and SAB on the gas side (SAB carbon powder MPL/GDL/ Vulcan carbon powder MPL. Chen et al. [116] compared the relative humidity for different flow rates for MPLs containing Vulcan XC-72R and Ketjenblack EC-600JD. MPLs containing the later showed to contain more water vapour due to its large surface area and micro-pores compared to the former.

Han et al. [117] explored the effects of carbon and PTFE loading on cell performance. MPLs containing 40% PTFE with varying carbon loadings of 2-8 $mgcm^{-2}$ and fixed carbon loading of 6 $mgcm^{-2}$ with varying PTFE (10-60%) were created using Vulcan XC-72R as the carbon black and sintered at 340 °C for one hour. Experimental investigations revealed that the carbon powder loading affects the fuel cell performance in all three polarization areas (activation, mass transport and ohmic) such that low carbon loadings reduce the support of the catalyst layer resulting in less active catalyst sites causing an increase in activation over-potential. An increase in the carbon loading resulted in higher performance due to more efficient water management and catalyst utilization; however, excessive carbon loadings result in a decrease in porosity and an increase in the diffusion path causing a concentration over-potential. As such, the results presented by Han et al. [117] indicates that there exists and optimal carbon loading. Furthermore, the increase in PTFE loading affects the cell performance in the ohmic and mass transport polarization regions such that PTFE loading directly affects the contact resistance between the diffusion media and catalyst layer and the porosity of the diffusion media. Excessive PTFE loading (60%), however, was shown to affect catalyst utilization.

Stampino et al. [109] investigated a MPL consisting of a composite mixture of Vulcan XC-72R and carbon nanotubes (CNTs) in a ratio of 90 wt.% of the former and 10 wt.% of the later and 14 wt.% PTFE. The mixture was sonicated for fifteen minutes and then stirred for

one hour and coated onto a commercial carbon cloth using the doctor blade technique. Of particular note, the thickness of the final MPL containing CNTs was found to be twice that of the MPL containing Vulcan XC-72R. Cell performance was found to be better with the CNTs MPL which also showed a far lower ohmic resistance even though the thickness of the MPL was doubled.

Gharibi et al. [118] also investigated a MPL of multi-walled carbon nanotubes (MWCNTs) in a composite mixture with Vulcan XC-72R for various combinations of MWCNT to Vulcan XC-72R with a PTFE loading of 30% which was determined to be the optimized PTFE loading with MWCNTs. Gharibi et al. [118] suggested that the MWCNTs in the MPL structure allow for higher surface concentrations of reactants at the catalyst layer was achieved due to MWCNTs being able to adsorb oxygen onto their surfaces.

Wang et al. [113] also constructed a composite MPL using two different carbon blacks - Acetylene black (AB) and Black Pearls 2000 (BP-2K) and investigated the effect of the composite mixture in terms of fuel cell performance. The carbon loading was held constant at 1.0 $mgcm^{-2}$ with a ratio of 80 wt.% AB and 20 wt.% BP with 30 wt.% PTFE loading. The mixture was sonicated and applied to a Toray TGP-H-30 carbon fibre paper using a doctor blade technique. The physical properties of the composite mixture were investigated: the specific area of the composite mixture was found to be 335.3 m^2g^{-1} which was in-between that of the two carbon powders- 62 m^2g^{-1} (AB) and 1501.8 m^2g^{-1} (BP-2K). Furthermore, other physical properties such as pore volume and contact angle showed similar trends such that the composite mixture tended to lie nearer to those of AB since the mixture consisted mostly of AB. Through-plane permeability of the composite mixture showed a similar trend as well; however, the permeability was only reported for the 80 wt.% AB and 20 wt.% BP-2K combination. Lastly, the effect of different ratios of AB to BP-2K were investigated and

it was shown that there existed an optimum ratio of 10 wt.% BP in terms of fuel cell performance.

Kannan et al. and associates [119]–[121] also investigated the effects creating a MPL by adding a nano-fibrous carbon (VCGF-H Showa Denko America Inc., New York) to PUREBLACK® 205-110 Carbon (Superior Graphite Co., Chicago, IL, USA) in a ratio of 50-50 wt.% (carbon loading of 3.0 $mgcm^{-2}$) and 30 wt.% PTFE followed by sonication and magnetic stirring. The new structure created exhibited no cracks in the MPL and showed structural robustness when compared with the Pureblack. This group further investigated the effect of adding a dispersion agent, Novec-7300 to the isopropanol used in previous studies. The resulting ink slurry of 75 wt.% Pureblack, 25 wt.% VCGF and 25 wt.% PTFE was coated using a wire rod system (EC26, Coatema) which was used to control the carbon loading of 2.6-3.0 $mgcm^{-2}$ through the slurry composition and wire thickness of the rod. The surface morphology obtained from the addition of the dispersion agent showed a more homogenous structure when compared with simply using isopropanol as the dispersion agent for the ink slurry.

Ozden et al. [122] recently compared a MPL created using graphene powder to that of Ketjenblack EC-600JD. The MPLs were created for a carbon loading of 2.0 $mgcm^{-2}$ with a 20 wt.% PTFE loading dispersed in isopropanol followed by sonication for two hours. The ink slurry was spray coated onto an Avcarb GDS3250 GDL. The through-plane permeability of the GDMs and several physical characteristics such as porosity, wettability, thickness, surface area, pore volume, pore size and bulk density were determined for the two carbon powders. The surface areas of the two carbon powders varied significantly: 305.5 m^2g^{-1} and 1255.1 m^2g^{-1} for graphene and Ketjenblack EC-600JD respectively. Surface morphology showed a smooth and dense structure for the MPLs derived from the graphene powder as

compared with Ketjenblack EC-600JD which showed large cracks on the surface. Furthermore, the MPL thickness varied significantly for the 2.0 $mgcm^{-2}$ carbon loading with MPL thicknesses of 13-17 µm for the graphene and 97-103 µm for the Ketjenblack EC-600JD. The through-plane permeability of the graphene based MPL was significantly lower by an order of magnitude compared with the Ketjenblack EC-600JD MPL due to the dense packing and stack ability of graphene flakes. Lastly, the MPL with graphene powder showed superior performance capabilities (approximately 55%) under low and intermediate humidity operation with comparable performance to that of the Ketjenblack EC-600JD at high humidity conditions.

Hydrophobicity of the PEFC GDL is typically controlled with the addition of PTFE; however, there have been other materials which have been explored such as polyvinylidene fluoride (PVDF) [123], [124] and fluorinated ethylene propylene (FEP) [61], [125]. Park et al. [123] investigated the effects of various loadings of PVDF on electrical resistance and gas permeability. The results indicated an increase in both conductivity and permeability for decreased PVDF loadings. Furthermore, surface morphology indicated an MPL with few cracks and pores and that the produced MPL had great potential to enhance mass transport due to small pore sizes. Ong et al. [124] investigated the physical properties such as electrical resistance, gas permeability and microstructure of an MPL which utilised PVDF in the MPL and two types of carbon (Vulcan XC-72R carbon powder and Timrex HSAG 300 graphite) as the electrically conductive filler. The ratio of PVDF to Vulcan XC-72R was explored for 5% and 10% PVDF. The results indicated a significant reduction of 97.6% in gas permeability with the increase of PVDF loading from 5 to 10%.

Lim and Wang [61] investigated the effect of varying levels of FEP- 10wt. % to 30 wt. %- in the GDL on fuel cell performance for an air breathing fuel cell. The results indicated

higher power densities at 10 wt.% FEP compared with the 30 wt.% and this was attributed to the substantial blocking of pores with increasing FEP loading. Park et al. [125] investigated the effects of a FEP based MPL to a PTFE based MPL on a carbon cloth GDL. The electrical resistance and permeability of the MPL based on FEP were slightly lower and higher respectively and this was based on the difference in surface morphology such that the FEP based MPL showed much fewer crack formations.

Park et al. [63] investigated the effect of varying levels of PTFE and carbon loading in the MPL on fuel cell performance. The carbon loading was varied between 0.2 and 2.0 $mgcm^{-2}$ and the PTFE between 6% and 40% for acetylene black spray coated on to a commercial SGL 10CA substrate. They determined the best fuel cell performance at 0.5 $mgcm^{-2}$ carbon loading and for 20% PTFE loading at this carbon loading which agreed with the results presented in a simulation study by Weber and Newman [126] for a thin MPL layer which directly correlates to the carbon loading. Jordan et al. [82] obtained better cell performance for carbon loadings between 1.25 to 1.9 $mgcm^{-2}$ for acetylene black with a PTFE loading of 10wt. %.

Orogbemi et al. [127] investigated the effects of through-plane gas permeability for varying PTFE loadings in the MPL between 0 and 50 wt.% for five carbon loadings of 0.5, 1.0, 1.5, 2.0 and 2.5 $mgcm^{-2}$ utilising Ketjenblack EC-300J as the carbon powder which was spray coated onto an SGL 10BA substrate. The through-plane permeability was found to be the lowest at 20% for the investigated carbon loadings but was found to increase between 20 and 50% PTFE loading in the MPL. This finding was found to agree with that of [32], [99]. The permeability for increased carbon loading was also found to decrease as the PTFE loading was increased from 10-20%. Orogebemi et al. [128] extended the work conducted on the effect of carbon loading on through-plane permeability of GDMs. Two carbon blacks,

namely, Vulcan XC-72R and Ketjenblack EC-300J were used for the five carbon loadings investigated in [128]. The results indicated a decrease in through-plane permeability with increased carbon loading for the two carbon powders with the permeability of the GDMs coated with Vulcan XC-72R being higher for carbon loadings less than 1.5 $mgcm^{-2}$. It should be noted that these investigations [127], [128] involved the use of a single GDL substrate with no consideration of how the trends in through-plane permeability would differ for different GDMs. Furthermore, the GDL substrate used contained a fix PTFE loading of 5%. El-Kharouf et al. [33] identified that there are significant property differences for various commercial substrates and the author believes that GDL properties would, undoubtedly, influence the final GDM properties.

Most of the investigations thus far have only considered MPL compositions in terms of carbon types, various carbon loadings, hydrophobic agent types and hydrophobic loadings. GDM structures, as stated previously, can be affected by preparations methods such as the ink preparation techniques and coating techniques. Zhiani et al. [129] investigated the in-plane permeability and through-plane resistance of MPL coated Toray TGP-H-60 carbon fibre paper focusing on the ink slurry homogenization methods. Four techniques: (i) Pulse probe sonication, (ii) continuous probe sonication, (iii) bath sonication and (iv) magnetic stirring were used. The results showed signification variations in the properties investigated due to the various morphologies derived from each technique. It was shown that bath sonication produced achieved the highest fuel cell performance. There was no indication on how the through-plane permeability was affected with the various homogenization techniques, only one carbon type (Vulcan XC-72R) and GDL substrate were used in the investigations and the ratio of carbon to PTFE was held constant at 90% and 10% by weight respectively.

Yu et al. [108] employed a dry deposition technique to deposit a mixture of carbon powder and PTFE onto a Toray TGP-H-60 carbon substrate. Three different types of powders, Vulcan XC-72R, Ketjenblack EC-600JD and Denka were investigated in terms of cell performance with the Denka carbon powder performing the best due to the fact that its small surface area resulted in large amounts of micropores which allowed it to facilitate gas transport to the catalyst layer longer until its micro and meso-pores become filled with liquid water. It was shown by Yu et al. [108] that cell performance increased with a decreasing surface area of the carbon powder used. Furthermore, the dry deposition technique allows mass production of the MPL with greater repeatability as opposed to a wet method and allows the thickness of the MPL to be controlled.

Stampino et al. [110] investigated the rheology of the MPL inks and its effect on the MPL thickness and morphology. The doctor blade technique was used for coating onto two different carbon substrates (SEAL SCCG5N carbon cloth and SGL 10CA carbon fibre substrate) and the composition of the ink slurry was changed for different PTFE loadings. Their results indicated that the rheology of the ink slurries was almost the same for different PTFE loadings; however, the GDL morphology had a significant different on final MPL thickness. Sitanggang et al. [111] developed an x-y robotic spray technique to coat an MPL ink slurry onto carbon cloth. It was shown that the technique was able to control the thicknesses of the MPLs produced along with the porosity. Pozio et al. [114] investigated different coating techniques used in MPL application in terms of feasibility, surface morphology, permeability, cell performance. It was shown that spray coating allowed a homogenous MPL to be created in terms of its thickness; however, approximately 20-30% material is lost in the process of spray coating. Hand coating was not able to control the thickness of the MPL. A cold rolling process was deemed the best in terms of obtaining a desired thickness and surface morphology. Spray coating allowed for the highest gas

permeability and stable performance at high current densities. Cold rolling allowed for the production of compact MPL structures in which permeability as a function of PTFE loading.

2.8 Sintering of the microporous layer

Sintering involves the heat treatment of the gas diffusion media in an effort to provide a more homogenous distribution of PTFE such that the gas diffusion media is rendered more hydrophobic [82], [130]. As indicated in [100], [131] the effect of sintering typically is investigated on its effect on fuel cell performance by considering the amount of PTFE in relation to electrical conductivity, mass transport (gas diffusion and permeability) and hydrophobicity.

Bevers et al. [100] investigated the influence of PTFE in the GDL on sintering time and temperature. Initially, the samples were heat treated at temperatures below 200 °C followed by sintering at a desired temperature and time. Samples with different PTFE content were investigated at a constant sinter temperature of 390 °C for twenty minutes and at different temperatures with a constant PTFE of 180 wt.% for fifteen minutes. Even though direct gas permeability was not directly reported, the pressure drop of gas flow over the samples was determined. The experiments revealed that the pressure drop decreases with increasing sinter temperatures due to the fact that increasing temperatures allow the PTFE to be dispersed more thoroughly from the voids between fibres to the fibres themselves thus allowing the gas to flow more freely. Alternatively, the increase in PTFE content lead to increasing pressure drops and this was attributed to the fact that the void between fibres become filled with PTFE resulting in greater restriction of gas flow. It should be noted that the experimental work conducted by Bevers et al. [100] focused solely on the effect of PTFE in the GDL and not for MPL coated GDLs. Furthermore, the effect of sintering time on gas permeability was not clearly represented.

Jordan et al. [82] experimentally investigated the effect of sintering on fuel cell performance taking into consideration different carbon black types. The experiments conducted involved sintering a Toray TGP-H-120 sample coated with a MPL of various carbon loadings (0.7 – 2.5 $mgcm^{-2}$) and 10% PTFE for two different carbon black types at 350 °C for thirty minutes. The investigations revealed that sintering significantly affects performance of the fuel cell at high current densities for carbon loadings between 1.25-1.9 $mgcm^{-2}$. Two carbon types, namely, Vulcan XC-72R and Acetylene black, were used to construct the MPL. The experiments conducted indicate that cell performance was noticeably better using Acetylene black due to the smaller pore volume (in the range of 10-100 μm) which allowed less water to permeate through the gas diffusion media. Furthermore, a sintered gas diffusion media, allowed for more efficient water management by rendering the gas diffusion media more hydrophobic, allowing the catalyst layer to be partially hydrated while maintain proper gas transport through the layer. The effect of MPL composition on cell performance was explored; however, no investigations were performed with regard to MPL composition on mass transport properties. Furthermore, sintering time for the coated GDLs was held constant at thirty minutes.

Aslam [132] experimentally investigated the effect of heat treatment of three commercial gas diffusion media (SGL 10CA, Toray TGP-H-60 and SGL 10BC) on through-plane permeability. The temperatures investigated were 200, 500, 800 °C for SGL 10CA and Toray TGP-H60 and 200, 500, 800 and 1000 °C for the MPL coated sample SGL 10BC. The through-plane permeability was found to increase with increasing temperatures up to 800 °C which was due to the reduction in PTFE on the surface of the fibres as the temperature incremented. For temperatures up to 500 °C, the through-plane permeability increased for SGL 10BC; however, there was a significant reduction in the permeability for the temperatures 800 °C and 1000 °C. SEM images indicated that at 1000 °C, the surface

morphology changed when compared to lower temperatures showing that the entire surface seemed to be less porous and the size of the cracks of the MPL surface were shown to be smaller which could explain the reduction in permeability.

Orogbemi et al. [128] investigated the effect of sintering by experimentally comparing the through-plane gas permeability of MPL coated GDLs before and after sintering. An MPL consisting of two different carbon black types (Vulcan XC-72R and Ketjenblack EC-300J) for five carbon loadings (0.5, 1.0, 1.5, 2.0 and 2.5 $mgcm^{-2}$) with a constant PTFE loading of 20% were spray coated onto a SGL 10BA carbon substrate. The samples were first heat treated for at 120 °C for one hour, 280 °C for thirty minutes and then sintered at 350 °C for thirty minutes. The results indicated that sintering decreased the through-plane permeability of the gas diffusion media and the general trend was to be invariant of the carbon black type. It was indicated that sintering caused a "spreading effect" which in turn narrows the cracks in the MPL thereby reducing mass transport resistance. It was also shown that depending on the carbon black type, at low carbon loadings, samples coated with Ketjenblack EC-300J were found to show a greater reduction in permeability due to the larger fraction of micro pores when compared to Vulcan XC-72R.

Lo et al. [133] and associates [134] experimentally investigated the effect of sintering time on gas permeability. Toray TGP-H-90/ Toray TGP-H-120 carbon paper was chosen as the GDL onto which an MPL consisting of Triton carbon powder, PTFE and isopropyl alcohol as a pore former. The MPL was scraped onto the wet-proofed (20% PTFE) carbon paper, dried at 80 °C for one hour and finally sintered at 350 °C for one, five, nine and thirteen hours. The results showed that the gas permeability, measured with a capillary flow porometer, showed that increasing the sintering time resulted in an increase in through-plane permeability and cell performance; however, there was only a slight increase in permeability

from the nine hour to thirteen hour measurements which both showed increases in cell performance when compared to a sintering time of one or five hours. It was not specifically stated which GDM assembly was used to investigate the effect of sintering time on gas permeability; however, the author believes that a GDL/MPL assembly consisting of Toray TGP-H-120 was used as the base GDL with 20% PTFE loading and the MPL consisted of 40% PTFE loading with a thickness of 84 µm.

It should be noted that the results presented in [133] contradict the results determined by Orogbemi et al. [128] such that the later indicated a decrease in permeability with sintering; however, it is difficult to compare both of these results since different carbon powder types and MPL application techniques were used. Furthermore, Orogbemi's [128] conclusion that that sintering results in a reduction in permeability was based on a thirty minute sintering time. The effect of sintering time on through-plane gas permeability for MPL coated GDLs is still unclear as reported above. Further experiments are therefore required to verify the findings reported in the literature. As such, the effect of carbon powder type and PTFE loadings in the MPL are investigated with regard sintering times in this thesis.

2.9 Summary

Water and gas management remains a challenge in PEFC operation. In order to overcome the concentration losses in the PEFC, these issues need to be resolved and can be by optimization of the porous components of the MEA. This chapter provides a thorough review of history, operations principles and functions of the porous media in the PEFC literature. The focus of this review was primarily on two major components of the MEA which comprises the GDL and MPL. Emphasis was placed on fabrication and composition of these two layers, particularly, on how gas permeability was affected by the materials and techniques used to produce these layers. Also, a thorough review of the experimental

measurements of gas permeability was provided. Finally, the review helped to identify the gaps in the literature and determined the technical objectives of the subsequent chapters of this thesis as shown in Figure 2.6 below.

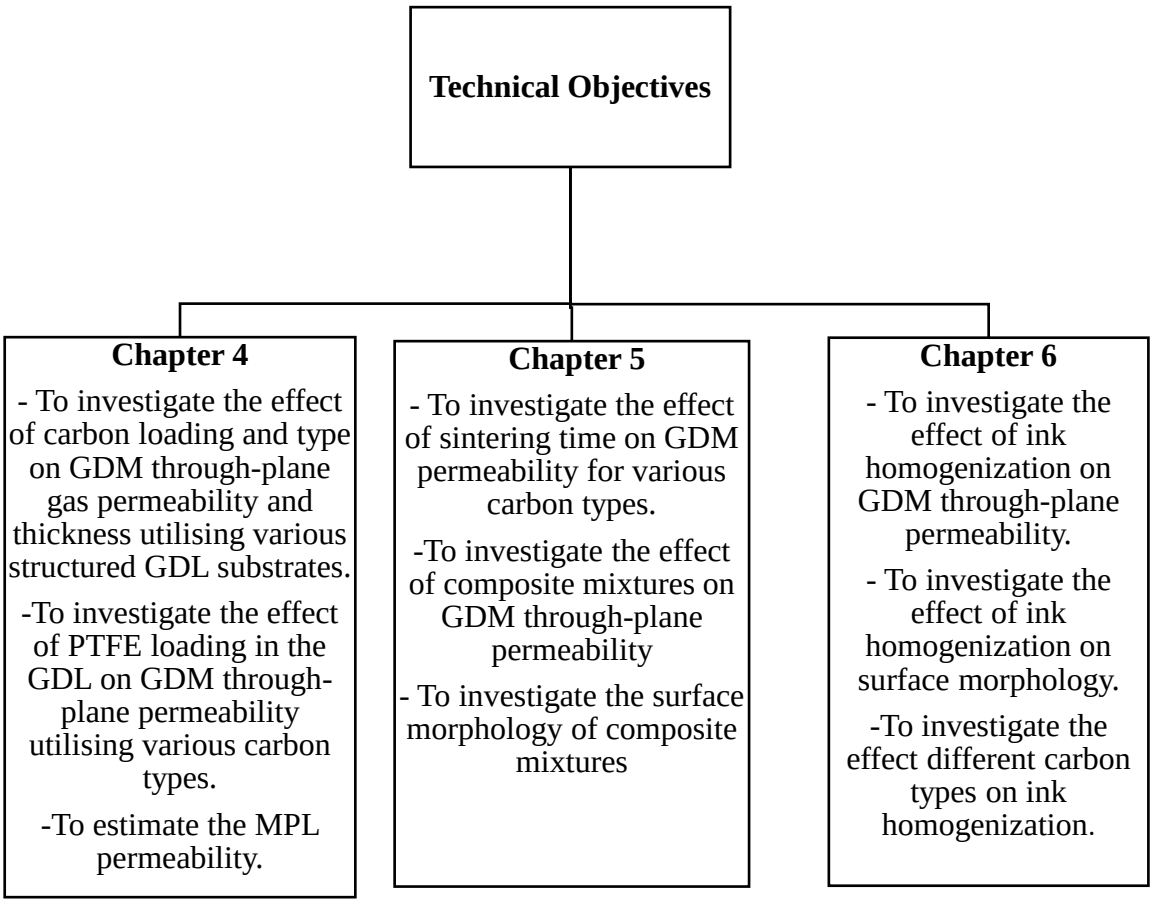

Figure 2. 6 Technical Objectives of thesis.

Chapter 3

Materials and Methods

3.1 Introduction

This chapter details the techniques used, research methodology, materials and data analysis used in order to determine the through-plane gas permeability of PEFC porous media, mainly, the GDL and the MPL. The research methodology is simple and can divided into three main steps, as follows:

1. Preparation of the sample.
2. Measurement of the through-plane gas permeability before and after coating the MPL onto the GDL.
3. Analysis of the results obtained.

Similar to many authors [32], [99], [102], [127], [128] , an in-house experimental setup was used to measure the pressure drop across the sample, after which the through-plane gas permeability could be obtained. The schematic diagram shown in Figure 3.1 identifies the porous layers under investigation in this thesis.

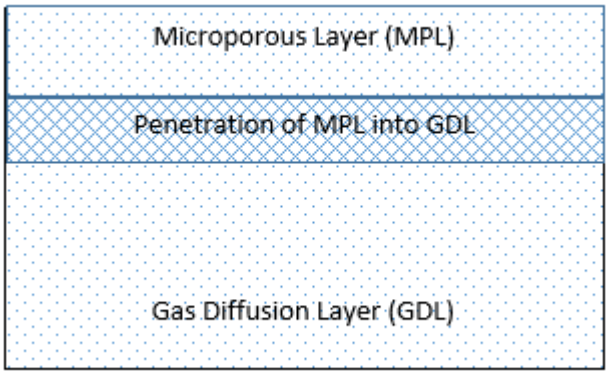

Figure 3. 1 Schematic diagram showing the porous media under investigation.

The full experimental approach adopted was similar to that performed in [127], [128] and can be described fully in Figure 3.2. The general processes indicated in Figure 3.2 were used to investigate the following characteristics:

1. Carbon Loading with two different carbon blacks, namely, Vulcan XC-72R and Ketjenblack EC-300J.
2. GDL and MPL thickness.
3. MPL composition.
4. Penetration of the GDL into the MPL.
5. Sintering times.
6. Dispersion technique, that is, bath sonication versus magnetic stirring.

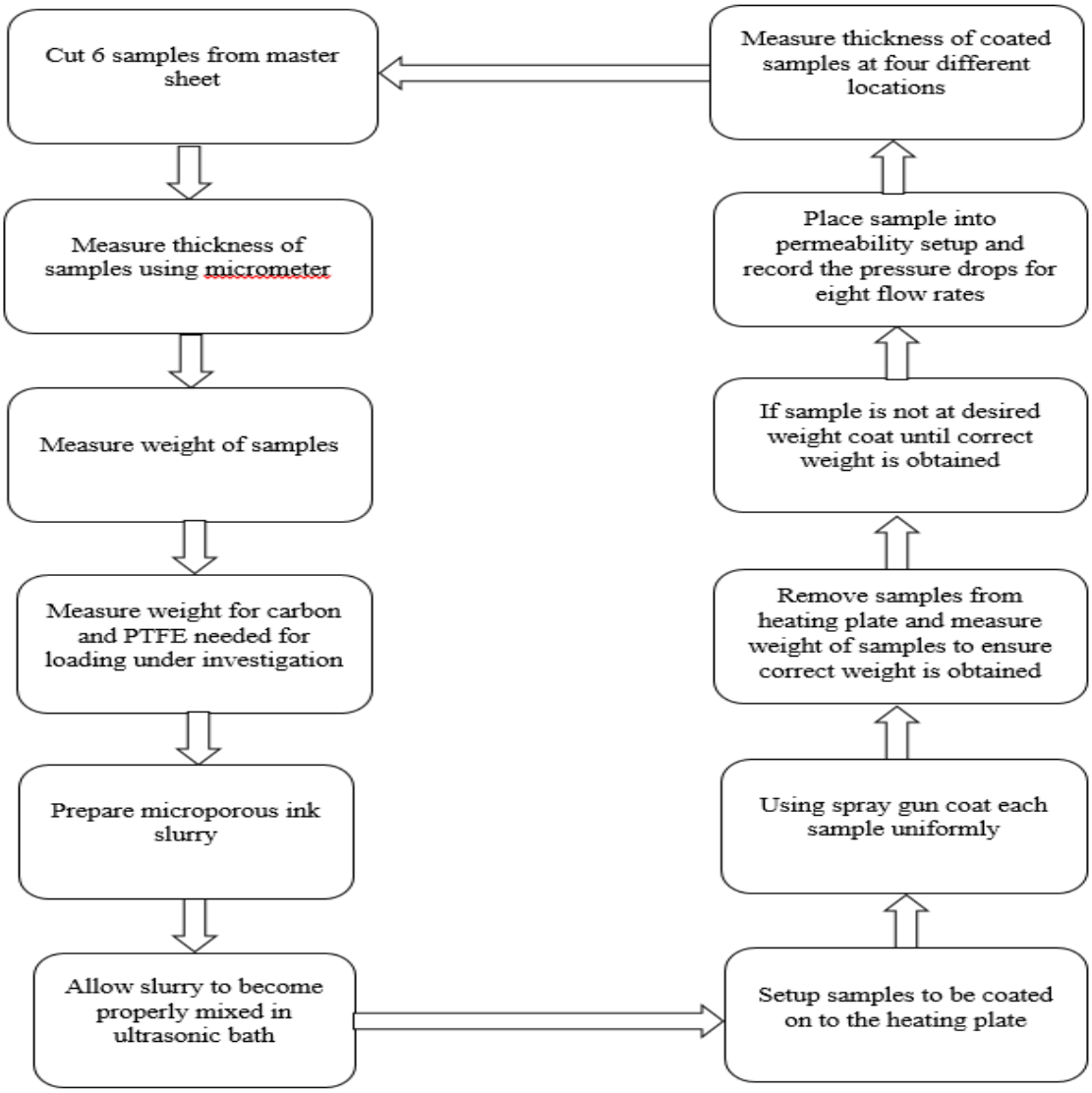

Figure 3. 2 Flow diagram illustrating the steps involved in the preparation process of the MPL.

3.2 Materials

This section describes the materials used in the investigations of the through-plane gas permeability of the porous media in PEFC. Several commercial gas diffusion layers were used in the investigations. The following GDLs (1-7) and GDMs (8-9) were used in this thesis:

1. Toray TGP-H-120.
2. Toray TGP-H-90.

3. Toray TGP-H-60.
4. SGL 10CA.
5. SGL 10DA.
6. SGL 10EA.
7. SGL 35BA.
8. SGL 10BC.
9. SGL 10BE.

In each investigation, for example, preparation of an MPL with a carbon loading of 1.0 $mgcm^{-2}$, the carbon fibre sheets were from the same batch. Table 3.1 indicates the manufacturer's data for each substrate obtained from SGL Carbon GmbH, Meitingen, Germany and Toray International, UK.

Table 3. 1 Manufacturer's data for the gas diffusion layers under investigation.

Gas Diffusion Layer/ Gas Diffusion Media	**Physical Parameters**			
	Thickness (µm)	**Areal Weight (gm^{-2})**	**Porosity (%)**	**PTFE loading in GDL (%)**
Toray TGP-H-120	370	-	78	5
Toray TGP-H-90	280	-	78	5
Toray TGP-H-60	190	-	78	5
SGL 10CA	400	90	-	10
SGL 10DA	400	100	-	20
SGL 10EA	374	112.9	-	30

SGL 35BA	300	54	-	5
SGL 10BC	415	135	-	5, 20-25[a]
SGL 10BE	367	139	-	5, ~50[a]

[a] Indicates the PTFE loading in the MPL.

The microporous layer was constructed using two different carbon black powders, namely, Vulcan XC-72R (Cabot Corporation, USA) and Ketjenblack EC-300J (AkzoNobel, Netherlands). The physical properties such as pore volume, bulk density, surface area, particle diameter, pH and volatile content allowed the author to investigate the difference in through-plane gas permeability using two distinct carbon black powders as well as a combination of both, that is, a composite mixture. Table 3.2 compares the difference in physical properties of the two carbon black powders.

Table 3. 2 Physical properties of carbon black powders provided by the manufacturer.

Properties	**Ketjenblack EC-300J**	**Vulcan XC-72R**
Pore Volume (ml/100g)	310-345	178
Apparent bulk density (kgm^{-3})	125-145	20-380
Surface Areas (m^2g^{-1})	950	254
Particle Diameter (nm)	30	30
pH	9.0-10.5	2-11
Volatile (by weight % max)	1.0	2-8

Two other materials were necessary in the preparation of the microporous layer. A binding agent was necessary to hold the particles together. Polytetrafluorethylene (PTFE) was used as the hydrophobic binding agent; Sigma Aldrich, UK PTFE with 60 wt.% aqueous dispersion emulsion was used. Isopropanol was used as a dispersant for the mixture and was also supplied by Sigma Aldrich W292907-8KG-K, UK with a 99.7% concentration. These three materials, that is, carbon black powder, PTFE and isopropanol were used in the preparation of the MPL ink slurry to be coated onto the GDLs and the process will be described in a later section of this chapter.

3.3 Methods

The process of applying a microporous layer to the GDL through the use of a microporous ink slurry was adopted from [127], [128], [135] . A similar procedure was used here to create an MPL with three different carbon loadings: 0.5 $mgcm^{-2}$, 1.0 $mgcm^{-2}$ and 2.0 $mgcm^{-2}$. The concentration of carbon black to PTFE was kept constant such that each mixture contained 80 wt.% carbon powder and 20 wt.% PTFE.

3.3.1 Microporous layer ink slurry preparation

The process of creating the MPL ink slurry is described in this section. In order to determine the amount of carbon and PTFE needed to create the ink, the ratio of carbon powder to PTFE needs to be chosen. In this case, the experiments conducted in this thesis all used 80 wt.% carbon powder and 20 wt.% PTFE. It was necessary to determine a mass for carbon black powder and PTFE for each carbon loading, that is, 0.5 $mgcm^{-2}$, 1.0 $mgcm^{-2}$ and 2.0 $mgcm^{-2}$. A sample calculation for a carbon loading of 0.5 $mgcm^{-2}$ using an 80 wt.% carbon and 20 wt.% PTFE is shown below. Also, it should be noted that the calculations were based on applying an ink mixture to six (6) samples.

$$Area\ of\ sample, A = \frac{\pi}{4}(2.54)^2 = 5.069\ \text{cm}^2$$

$$Area\ of\ \ 6\ samples, A = (5.069\ \times 6\ ) = 30.41\ \text{cm}^2$$

$$For\ a\ loading\ of\ 0.5\ \text{mgcm}^{-2}$$

$$Amount\ of\ carbon\ black\ powder\ required, C = 0.5\ \text{mgcm}^{-2}\ \times 30.41\ \text{cm}^2 = 15.21\ \text{mg}$$

$$Assuming\ a\ loss\ factor\ of\ 3$$

$$C = 3\ \times 15.21 = 45.62\ \text{mg}\ C$$

$$To\ determine\ the\ amount\ of\ PTFE\ needed\ for\ a\ 80\ wt.\%: 20\ wt.\%\ Carbon\ to\ PTFE:$$

$$PTFE\ required = \frac{20\ \text{mg}\ PTFE}{80\ \text{mg}\ C}\ \times 45.62\ \text{mg}\ C\ \times \frac{100\ \text{mg}\ PTFE}{62.6\ \text{mg}\ PTFE} = 18.22\ \text{mg}\ PTFE$$

Therefore, 45.62 mg carbon black powder and 18.22 mg PTFE were mixed to coat six samples. Table 3.3 summarises the amount of carbon black powder and PTFE needed for the following loadings 0.5 $mgcm^{-2}$, 1.0 $mgcm^{-2}$ and 2.0 $mgcm^{-2}$.

Table 3. 3 Amount of carbon black powder and PTFE needed by weight for MPL ink slurry.

Quantities	**Carbon loadings ($mgcm^{-2}$)**		
	0.5 $mgcm^{-2}$	**1.0 $mgcm^{-2}$**	**2.0 $mgcm^{-2}$**
Carbon needed (mg)	45.62	91.24	182.48
PTFE (mg)	18.22	36.44	72.88

After determining the theoretical weight of carbon powder and PTFE needed for a specific carbon loading, a calibrated scale (Denver Instrument with a calibration certificate traceable to International prototype kilogram through NIST- CE09-01-011, M, 24608827, Denver Instrument Germany) was used to measure the mass of each substance. Once the desired masses were achieved, isopropanol was added to the paste-like mixture consisting of the carbon powder and PTFE. The solution was then manually mixed, followed by bath sonication for three hours to form a homogenous solution with the use of an ultrasonic bath (Ultrawave U-300H, Ultrawave, UK). Bath sonication for all experiments throughout this thesis, were conducted using the above-mentioned ultrasonic bath for an operating frequency of 44 kHz and an isothermal bath temperature of 40 ℃. The procedure described above is illustrated in Figure 3.3 (a-d).

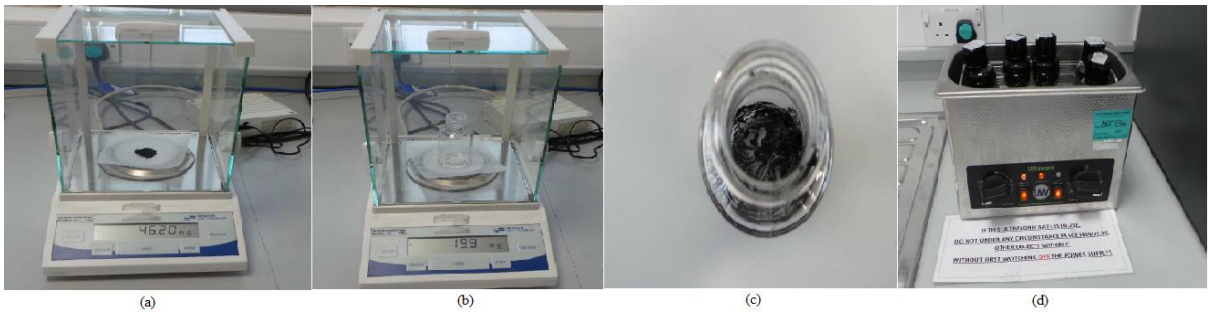

Figure 3. 3 (a) Carbon powder needed by wt.%, (b) PTFE needed by wt.%, (c) Paste-like ink slurry and (d) Ultrasonic bath used to prepare a homogenous solution.

It should be noted that for any given carbon loading, for example, it was not always possible to achieve the exact estimate of carbon powder or PTFE needed as shown in the data recorded in the Appendices. Figure 3.3 illustrates the ink preparation in order (a) to (d). Six (6) samples were used for each carbon loading for the following samples: (i) Toray TGP-H-120, (ii) Toray TGP-H-90, (iii) SGL 10CA, (iv) SGL 10EA and (v) SGL 35BA in Chapter 4. Toray TGP-H-60 and SGL 35BA samples were used in the investigation involving sintering times and dispersion technique; a total of eight (8) samples each (four for each carbon powder under investigation, that is, Vulcan XC-72R and Ketjenblack EC-300J) were used for a carbon loading of 1.0 mgcm^{-2} only in Chapter 5. SGL 10BC and SGL 10BE were used in investigations of sintering time for different PTFE loadings in the MPL; four (4) of each substrate were sintered. A total of sixteen (16) samples of SGL 10DA and Toray TGP-H-60 were used, in Chapter 6, in the investigation of dispersion technique (bath sonication versus magnetic stirring) for a carbon loading of 1.0 mgcm^{-2} (eight samples were used for each carbon black under investigation; that is, four samples were coated for each dispersion technique). The investigations into the impact of sintering times and dispersion technique on the through-plane permeability will be discussed later in this chapter. The actual carbon loadings for the various samples with the mean and 95% confidence interval around the mean value are recorded in the Appendices for the results from Chapter 4, 5 and 6.

In order to determine the theoretical mass of carbon powder and PTFE combination necessary to obtain the carbon loadings shown in Table 3.4, the following sample calculation is performed:

$$Area\ of\ sample, A = \frac{\pi}{4}(2.54)^2 = 5.069\ \text{cm}^2$$

$$For\ carbon\ powder\ loading, C:$$

$$0.5\ \text{mg}cm^{-2}: 0.5\ \text{mg}cm^{-2}\ \times 5.069\ \text{cm}^2 = 2.535\ \text{mg}\ C$$

$$For\ 20\%\ wt.PTFE\ required:$$

$$\frac{20\ \text{mg}\ PTFE}{80\ \text{mg}\ C}\ \times 2.535\ \text{mg}\ C = 0.634\ \text{mg}\ PTFE$$

$$Therefore, the\ theoretical\ mass\ of\ of\ carbon\ powder\ and\ PTFE\ needed\ for\ 0.5\ \text{mgcm}^{-2}\ loading$$

$$for\ a\ ratio$$

$$80\ wt.\%\ Carbon, 20\ wt.\%\ PTFE\ composition:$$

$$2.535\ \text{mg}\ C + 0.634\ \text{mg}\ PTFE = 3.169\ \text{mg}\ (C + PTFE)$$

The value 3.169 mg is the theoretical mass of the ink slurry coated onto the GDL substrate which must be added to the mass of GDL substrate in order to achieve a carbon loading of 0.5 mgcm^{-2}. Table 3.4 summaries the theoretical mass of carbon power and PTFE solution necessary to achieve the carbon loadings of 0.5 mgcm^{-2}, 1.0 mgcm^{-2} and 2.0 mgcm^{-2}.

The sample calculation given below illustrates how the actual carbon loading of a sample was determined:

$$Mass\ of\ GDL\ substrate\ before\ coating = 84.90\ \text{mg}$$

$$To\ achieve\ a\ carbon\ loading\ of\ 0.5\ \text{mgcm}^{-2}\ for\ a\ ratio\ 80\%\ Carbon\ to\ 20\%\ PTFE$$

$$Expected\ mass\ of\ coated\ sample\ for\ a\ loading:\ 0.5\ \text{mgcm}^{-2} = 84.90 + 3.169$$

$$= 88.069\ \text{mg}$$

$$Actual\ mass\ of\ coated\ sample = 88.2\ \text{mg}$$

$$Difference\ between\ actual\ and\ uncoated\ mass = 88.2 - 84.9 = 3.3\ \text{mg}$$

$$Therefore\ actual\ carbon\ loading = \frac{3.3\ \text{mg}}{5.069\ \text{cm}^2} \times 0.8 = 0.52\ \text{mgcm}^{-2}$$

Table 3. 4 Actual mass of carbon powder and PTFE needed to obtain the expected carbon loading.

Carbon loading ($mgcm^{-2}$)	**Expected mass of carbon powder and PTFE needed to achieve the appropriate carbon loading (mg)**
0.5	3.169
1.0	6.336
2.0	12.72

3.3.2 GDL pre-processing

Pre-processing of the GDLs involved measuring the thickness, permeability (equipment used to measure the permeability is discussed in a later section of Chapter 3) and mass of the bare substrates before application of the MPL ink slurry. Six (6) samples were cut from the master sheets; samples were circular with a diameter of 25.4 mm. The thickness of each sample was measured at four (4) locations equally spaced across the sample with the use of a micrometre (See Figure 3.4) after which, the average thickness of the samples was

determined. SEM (Scanning Electron Microscopy) images were also taken for the bare substrates in order to study the surface morphology before the samples were coated with the MPL ink slurry. The model of the scanning electron microscope used was JEOL JSM-601LA as shown in Figure 3.5.

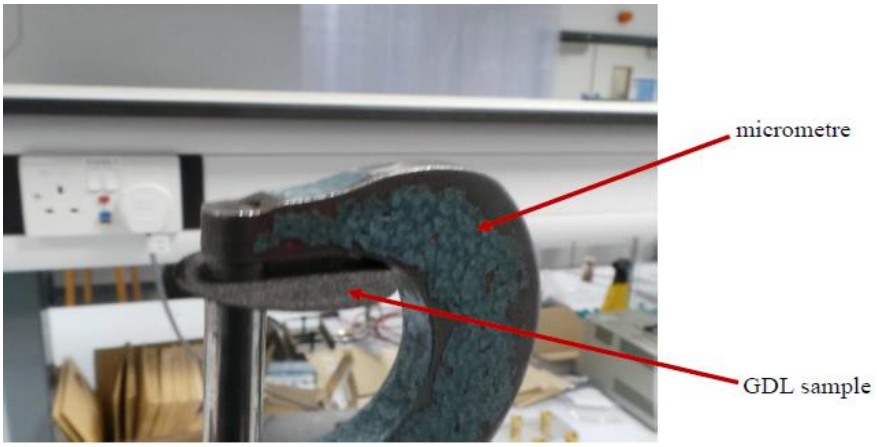

Figure 3. 4 Micrometre used for measuring the thickness of the GDL samples before and after coating [136].

Figure 3. 5 Scanning Electron Microscope used for image processing.

3.3.3 Application of the microporous ink slurry to bare GDL substrates

After pre-processing of the bare substrates, the samples were mounted onto a heating plate, as shown in Figure 3.6. The temperature of the heating plate was set the 80 °C; this allowed the volatile components of the ink slurry to be evaporated quickly. The ink slurry was applied to the bare substrates with the use of a spray gun (Badger 100^{TM} LG, USA). A nitrogen gas supply was attached to the spray gun in order to apply the MPL ink slurry to the uncoated samples.

Figure 3. 6 Heating plate showing the coated six samples.

Once the achieved mass of the coated samples was determined, that is, the addition of the initial mass of the uncoated samples to the values provided in Table 3.4 for each carbon loading, the permeability of the coated samples were then measured with the in-house permeability setup.

3.3.4 Gas Permeability Setup

The through-plane gas permeability of the samples was measured using an in-house built experimental setup. As discussed by Blanco et al. [137], the majority of experimental techniques used to measure the through-plane permeability of the gas diffusion media in PEFC mainly report the viscous permeability coefficients based on Darcy's law; this will be discussed in more detail in Section 3.3.5. The through-plane permeability setup, described in this section, was employed in [32], [99], [127], [128], [132] . The approach used was similar to that adopted from Gurau et al. [94] and discussed in detail in Blanco and Wilkson [137]. Figure 3.7 shows the actual experimental setup used in measuring the through-plane permeability of the GDM investigated in this thesis; Figure 3.8 shows a schematic view of the experiment.

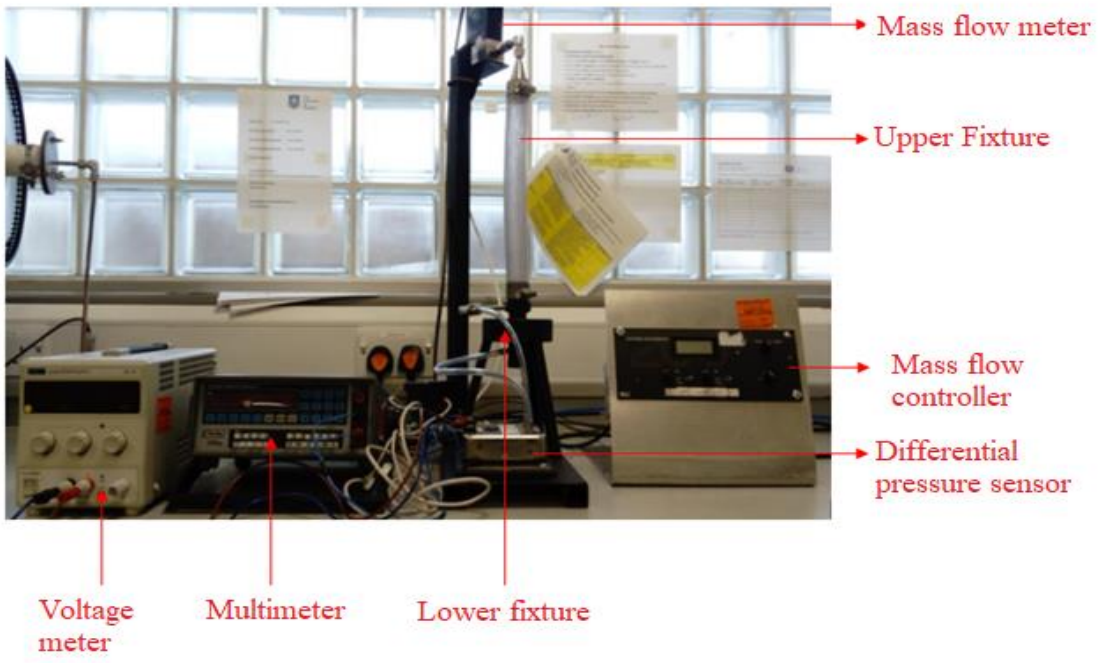

Figure 3. 7 In-house gas permeability setup used to measure the through-plane permeability of the GDM.

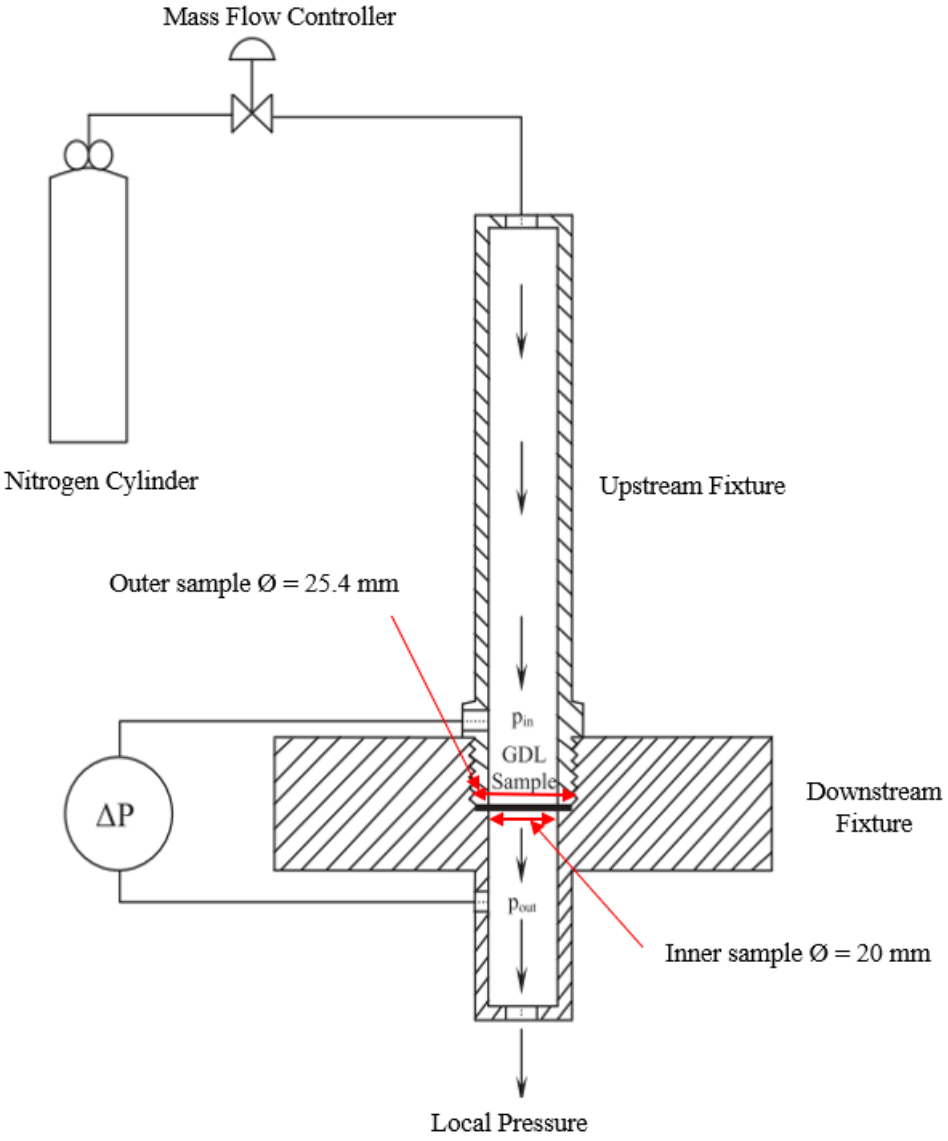

Figure 3. 8 Schematic diagram of the experimental setup [32], [99], [127], [128], [132].

The in-house experimental setup consists of an upper and lower fixture used to facilitate the nitrogen gas flow through the sample, which is positioned between the fixtures as shown in Figure 3.9.

Figure 3. 9 Image of the lower fixture without the sample (L) and with the samples (R) [60].

As stated in section 3.3.2, the samples are circular with a diameter of 25.4 mm; however, the actual diameter of the sample exposed to the gas flow is 20 mm. The sensitivity of the samples to compression on the outer circumferential as a result of clamping of the upper fixture to the lower fixture was investigated by Ismail [60] and was found to have a negligible effect on the through-plane permeability. The gas leakage through the narrow gap between the upper and low fixtures was also investigated by Ismail [60] and was found to be negligible.

Eight (8) equally spaced flow rates controlled by the flow controller (HFC-202 Teledyne Hastings, UK) with a range of 0.0 to 0.5 SLPM were used in conjunction with a differential pressure sensor (PX 653 Omega, UK) with a range of ± 12.5 Pa, to determine voltage signals for the different steady-state flow rates. These voltage signals measured by the multimeter were used to determine the pressure gradient across the samples. Also, temperature and pressure were measured and recorded for each experiment. It was noticed that the pressure drop across the carbon substrates were considerably lower than the coated substrates. Furthermore, for the carbon loadings 1.0 $mgcm^{-2}$ and 2.0 $mgcm^{-2}$ utilising the carbon powder Vulcan XC-72R on the Toray TGP-H-90 and Toray TGP-H-120 samples exceeded the range of the pressure sensor used; as a result, eight (8) lower, equally spaced flow rates were used. The analysis of the data is discussed in more detail in the next section.

3.3.5 Data Analysis

Manufacturers of carbon fibre papers or carbon cloths normally give the through-plane permeability of these materials in the manufacturer's specification sheets, even though, it is not always specified as through-plane permeability. Commercial instruments such as permeameters and Gurley method instruments are used by manufacturers to specify the permeability of the samples. Manufacturers tend to report the permeability with the units in $cm^3cm^{-2}s^{-1}$; however, the more fundamental unit for reporting the permeability is given in m^2 which can be obtained by using Darcy's Law [99], [137].

The viscous resistance to fluid flow is the major cause of the pressure gradient across the porous media for single phase flow at low fluid velocities (Reynolds number < 3 in this case). A linear relationship is created between the volume averaged fluid velocity and pressure gradient [32], [99], [137]–[139]. Darcy's law is expressed mathematically in Equation 3.1.

$$\overline{u_g} = -\frac{k_g}{\mu_g}\left(\nabla P_g - \rho_g \bar{g}\right) \tag{3.1}$$

where $\overline{u_g}$ is the superficial gas velocity, k_g is the gas-phase permeability, μ_g is the gas-phase viscosity, P_g is the gas-phase pressure gradient, ρ_g is the gas-phase density and $\bar{g}$ is the gravitational constant. Neglecting gravity, Equation 3.1 can be expressed as follows:

$$-\nabla P_g = \frac{\mu_g}{k_g}\overline{u_g} \tag{3.2}$$

In the case of high fluid velocities, the inertial resistance to fluid flow caused by the acceleration or deceleration of the fluid through the tortuous path of the diffusion media

become more signification and as such, an additional term is introduced to Equation 3.1. This additional term is called the non-Darcy or Forchheimer term.

$$-\nabla P_g = \frac{\mu_g}{k_g}\overline{u_g} + \beta_g \rho_g |\overline{u_g}|\overline{u_g} \tag{3.3}$$

The first term in Equation 3.3 is the Darcy term and β_g is the gas phase inertial coefficient [32], [99], [137]. For the purposes of this thesis, Equation 3.1 can be simplified to:

$$\frac{\Delta P_g}{L} = \frac{\mu_g}{k_g} u_g \tag{3.4}$$

where L is the thickness of the sample. Further to this, u_g can be determined as follow:

$$u_g = \frac{Q}{\pi \frac{D^2}{4}} \tag{3.5}$$

where Q is the volumetric flow rate and D is the diameter of the sample exposed to gas flow [127], [128], [132]. The gas permeability of the bare carbon substrates was determined by fitting the experimental data of the pressure gradient across the substrate to the fluid velocity. The MPL permeability was estimated by utilising an equation derived from the fact that the pressure gradient across the GDM (GDL and MPL combined) is equal to the sum of the pressure gradient across MPL and GDL, such that:

$$\Delta P_{GDM} = \Delta P_{MPL} + \Delta P_{GDL} \tag{3.6}$$

where ΔP_{GDM}, ΔP_{MPL} and ΔP_{GDL} are the pressure gradient across the entire coated substrate, the microporous layer and the gas diffusion layer respectively. Substituting Equation 3.6 into Equation 3.4 yields the following equation:

$$\frac{\mu_g L_{GDM}}{k_{GDM}} u_g = \frac{\mu_g L_{MPL}}{k_{MPL}} u_g + \frac{\mu_g L_{GDL}}{k_{GDL}} u_g \tag{3.7}$$

where L_{GDM}, L_{MPL} and L_{GDL} are the thicknesses of the coated substrate, MPL and GDL substrate respectively and k_{GDM}, k_{MPL} and k_{GDL} are the gas permeability values of the coated substrate, MPL and GDL substrate respectively. Equation 3.7 can be rearranged to solve for the permeability of the MPL, k_{MPL}, such that [32], [99], [127], [128]:

$$k_{MPL} = \frac{L_{MPL}}{\frac{L_{GDM}}{k_{GDM}} - \frac{L_{GDL}}{k_{GDL}}} \tag{3.8}$$

The thickness of the MPL, L_{MPL}, was determined by subtracting the thickness of the carbon substrate, L_{GDL} , from the total thickness of the GDM, L_{GDM} as used by Gurau et al. [94]. In order to minimise uncertainties in the permeability measurements carried out, the average permeability was determined with error bars which represented a 95% confidence interval across the mean.

3.3.6 Uncertainty and Error Analysis

Experimental measurements conducted in this thesis focused on the thickness and through-plane permeability of the substrates before and after application of the MPL, the percentage reduction of the through-plane permeability of original substrate after application of the MPL and the actual carbon loadings in the MPL. Measurement errors were reduced using several samples and the mean and standard deviation obtained with errors bars representing

the 95% confidence interval about the mean. The following steps were performed in order to determine the 95% confidence interval about the mean [140]:

1. The mean, $\bar{x}$ of a set of n observations was determined (for example, $n = 6$ for six samples of which a gas permeability measurement was obtained).

$$Mean\ (\bar{x}) = \frac{\sum_{i=1}^{n}(x_i)}{n} \tag{3.9}$$

2. The standard deviation, $s\ (x)$, for the 95% confidence interval is determined from the following equations:

$$s\ (x) = \sqrt{\frac{\sum_{i=1}^{n}(x_i - \bar{x})^2}{n-1}} \tag{3.10}$$

$$s_{95\%} = \frac{(n-1) \times s\ (x)}{\sqrt{n}} \tag{3.11}$$

where $(n-1)$ represents the degrees of freedom, df. df was obtained from a Student's *t*-distribution table [141] for n observations minus the number of calculated quantities.

3. The maximum and minimum values of the error bars were represented as follows:

$$Mean\ (\bar{x}) \pm s_{95\%}$$

3.3.7 Sintering or heat treatment experimental setup

The heat treatment of samples was carried out in Chapter 5, with the use of a cylindrical tube furnace (VCTF, Vecstar Ltd, UK) and a nitrogen supply controlled by a flow controller

shown in Figure 3.10 below. The furnace was set to three different stages: 120 ℃ for one (1) hour, 280 °C for thirty (30) minutes and the final stage was set to 350 °C for the following times: thirty (30) minutes, two (2) hours, four (4) hours, six (6) hours and eight (8) hours, in order to investigate the sintering time on through-plane permeability. The nitrogen supply was set to 2 Litres per minute with the help of the flow controller. After each timed stage in the final sintering step, the gas permeability of the coated samples, for two different carbon blacks (Vulcan XC-72R and Ketjenblack EC-300J) with the carbon loading held at 1.0 $mgcm^{-2}$, were measured. A total of eight (8) samples for the following substrates (four samples per carbon powder type): (1) Toray TGP-H-60 and (2) SGL 35BA. The effect of different levels of PTFE in the MPL for various sintering times was investigated using two (2) commercial samples: (1) SGL 10BC and (2) SGL 10BE. The commercial samples were also heated for thirty (30) minutes, two (2) hours, four (4) hours, six (6) hours and 8 (hours) and the permeability was measured during each step. For the investigations involving the use of the furnace, four (4) samples were used and the mean permeability and 95% confidence interval across this mean were reported. Samples were positioned in a glass crucible with the MPL side of the GDM facing upwards before placing them into the furnace.

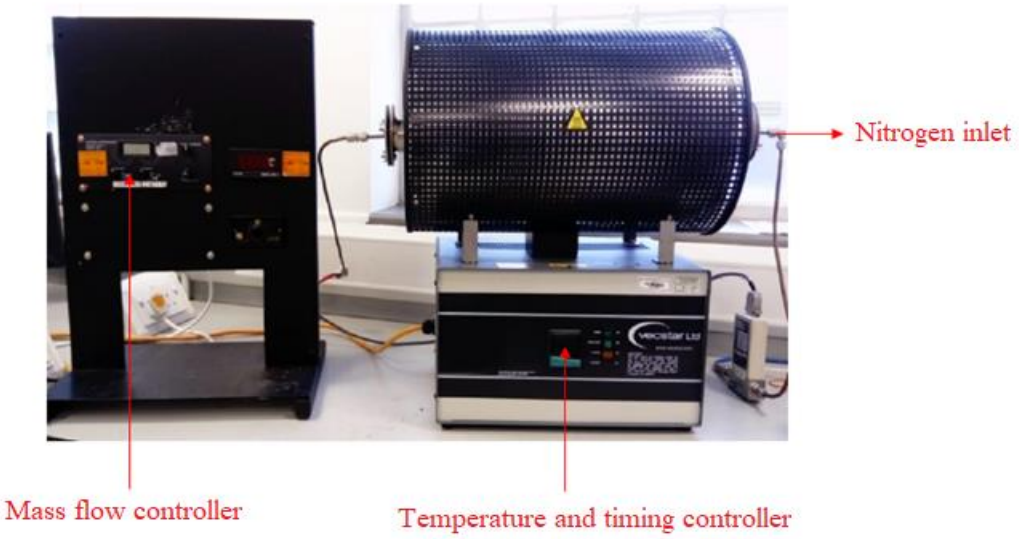

Figure 3. 10 Cylindrical tube furnace for sintering.

3.3.8 Calibration of mass flow controller

The mass flow controller (HFC-202 Teledyne Hastings, UK) was calibrated in [136] for several set points on the controller. This was achieved by measuring the time (t) taken (in seconds), using a stopwatch, for a soap film to travel between a set distance (two marked positions) indicated on a cylindrical tube. The time taken to move between the two marked positions was repeated five times and the average time recorded. The soap film was produced by squeezing a rubber bulb (which held a solution of soap water) in order to create bubbles; several bubbles were formed until a well-formed bubble film was achieved. A nitrogen gas supply, attached to the tube inlet above the bulb, was necessary to move the soap film between the two marked positions after which the gas was vented through the open-ended outlet. Figure 3.11 illustrates the calibration equipment used. The volumetric flow rate, Q, was then determined for each set point and calculated using the following equation:

$$Q = \frac{V}{t} = \frac{\pi r^2 h}{t} \tag{3.12}$$

where V is the volume of the cylinder (m^3), t is the time taken (s) for the soap film to move a distance, h (m) and r (m) is the radius of the cylindrical tube. The actual volumetric flow rate, Q_{act}, was corrected for variations in temperature and pressure and converted to litres per minute (multiplied by (6×10^4)) as follows [138]:

$$Actual\ volumetric\ flow\ rate, Q_{act} = Q \times \frac{T}{T_{rm}} \times \frac{P_{rm}}{P} \times (6 \times 10^4) \quad (3.13)$$

where T is the standard temperature (273.15 K), P is the standard pressure (1013.25 mb), T_{rm} is the temperature of the room (295.65 K) determined from a thermometer and P_{rm} is the room pressure (1015 mb) recorded on the day of the experiment, determined the BBC weather. Variations in the recorded temperature and pressures were found to be negligible.

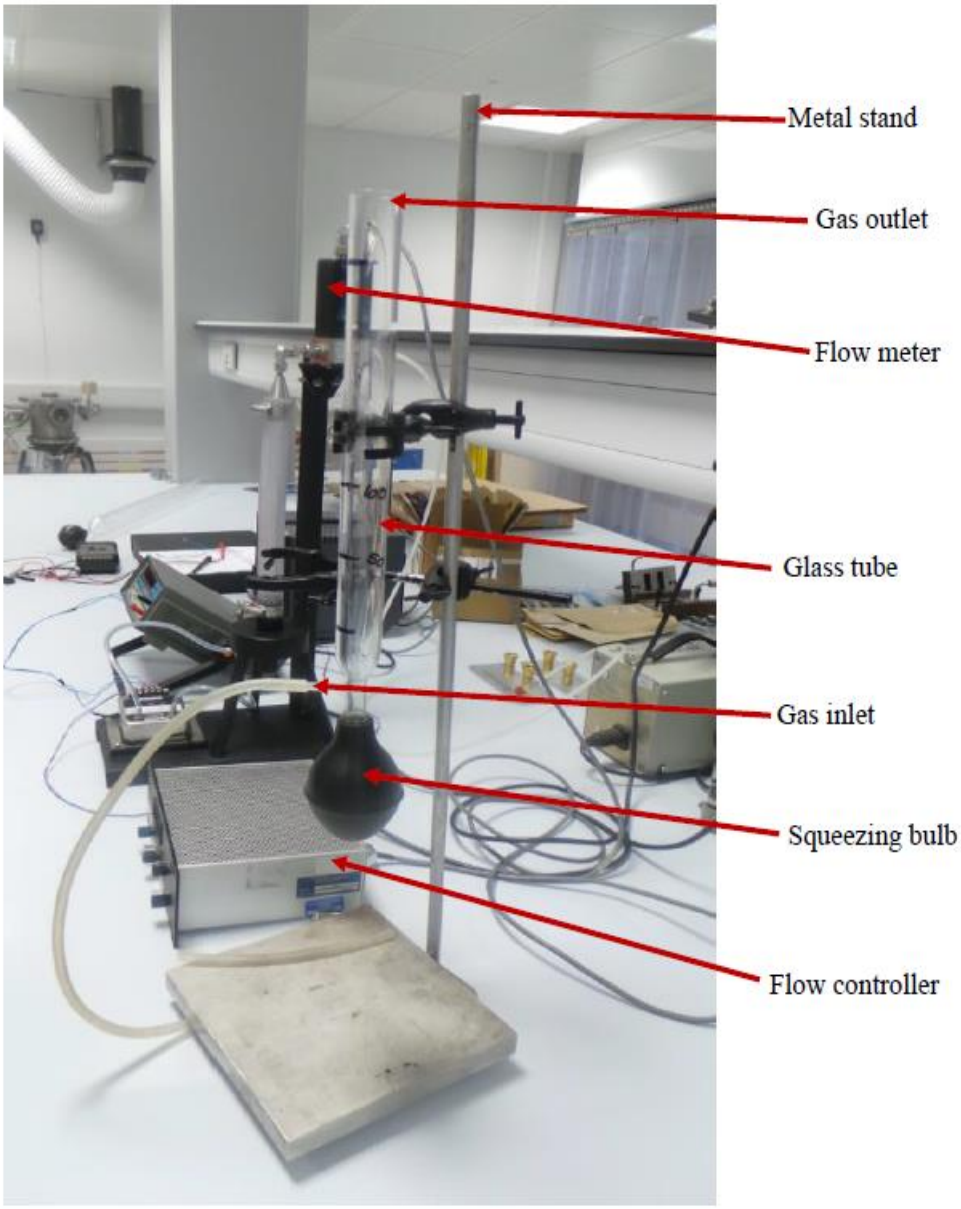

Figure 3. 11 Experimental setup used to calibrate the mass flow controller [136].

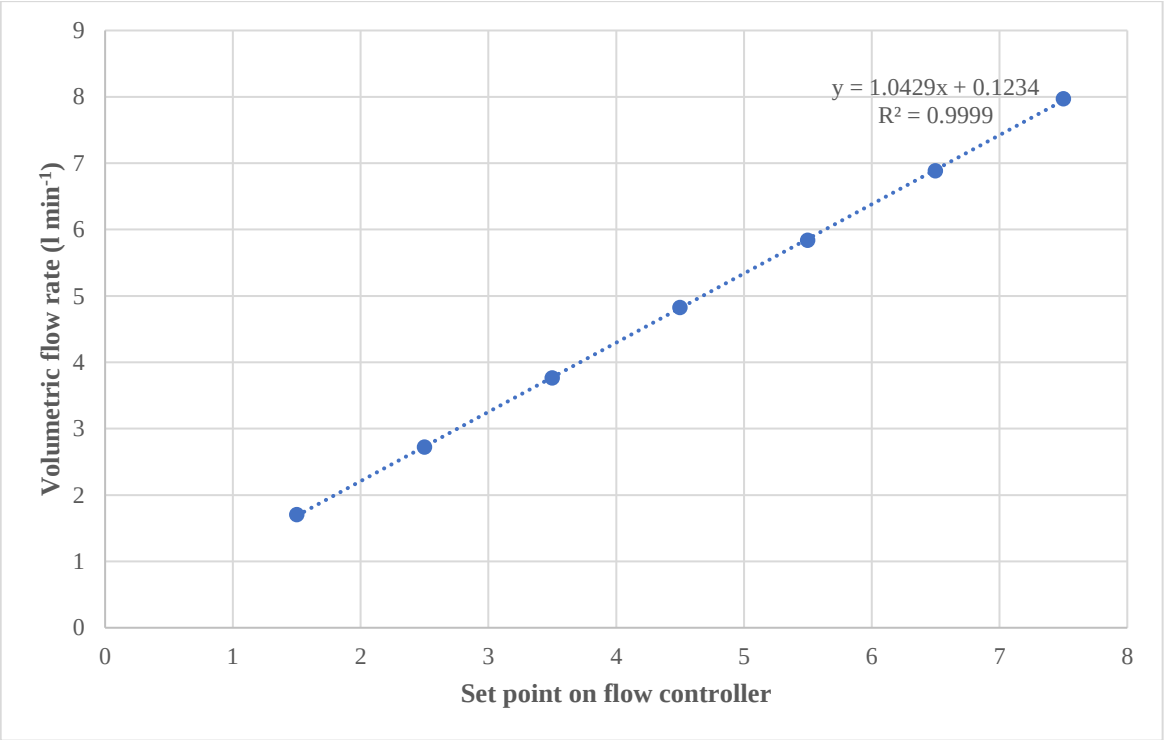

Figure 3. 12 Mass flow controller calibration curve used to determine the pressure drop across the samples [136].

3.4 Summary

This chapter presents the materials, methodology and research techniques used to measure the through-plane permeability and investigate the surface morphology of the porous media in PEFC. The experimental techniques used to measure the thickness and preparation of the MPL to the GDL were also presented along with the heat treatment processes to investigate the sintering time on through-plane permeability.

Chapter 4

Effects of gas diffusion layer substrate structure and PTFE content on the through-plane permeability of PEFC porous media

4.1 Introduction

GDM fabrication typically describes the altering of the GDL substrate by the addition of a hydrophobic material such as PTFE or the addition of a thin layer referred to as a MPL which consists of carbon powder and a binding agent such as PTFE or both [80], [81]. The physical properties of this thin layer are determined from the type, loading and particle size of the carbon powder used in conjunction with the type of hydrophobic agent, such that, the former controls the surface morphology and the later the pore properties [78], [80]. There are numerous studies in the literature which focus on MPL composition on the performance of the fuel cell [55], [61], [63], [82], [108], [109], [113], [115], [117], [119]–[121], [126]. Furthermore, there are many investigations on the MPL which can be characterized by the type and loading of the hydrophobic agent used [61], [63], [117], [118], [123]–[125], [127], [128] and the type and loading of the carbon powder used [55], [63], [82], [109], [113], [115], [116], [127], [128].

Passalacqua et al. [55] investigated different carbon blacks with different surface areas for varied carbon loadings of 2.5 to 5 $mgcm^{-2}$ on a Toray TGP-H-90 carbon paper. Their results showed that Shawinigan Acetylene Black (SAB) performed the highest due to a higher pore volume and lower pore size. Antolini et al. [115] compared, for a single carbon loading of 3.0 $mgcm^{-2}$ the effects of a triple layer GDM consisting of SAB and Vulcan XC-72R on cell

performance. Cell performance was optimized at high pressures with the use of Vulcan XC-72R in the MPL positioned on the catalyst side and SAB on the gas side. Han et al. [117] reported that an optimum carbon loadings exists by exploring various PTFE loadings for a carbon loading of 6 $mgcm^{-2}$ with Vulcan XC-72R used as the carbon powder and the effect of various carbon loadings of 2-8 $mgcm^{-2}$ for a fixed PTFE loading of 40 wt.%. The results in [117] revealed that low carbon loadings results in less active catalyst sides, an increased carbon loading resulted in high catalyst utilization and management and excessive carbon loading reduces porosity and leads to concentration over-potentials. The impact of increased PTFE loadings affected the performance in the ohmic and mass transport polarization regions by affecting the contact resistance between the GDM and catalyst layer and reduces porosity of the diffusion media.

Park et al. [63] also determined an optimum carbon and PTFE loading by varying the carbon loading of acetylene black between 0.2 and 2.0 $mgcm^{-2}$ and PTFE loading between 6 and 40 wt.%. The results showed a low carbon loading of 0.5 $mgcm^{-2}$ and a PTFE loading of 20 wt.% had the best performance and the results were in agreement with those of Weber and Newman [126]. Jordan et al. [82] investigated fuel cell performance by considering different carbon types (Acetylene black and Vulcan XC-72R for carbon loadings between 0.7 and 2.5 $mgcm^{-2}$. The investigations indicated an increased cell performance at high current densities for loadings between 1.25 and 1.9 $mgcm^{-2}$ for acetylene black which had a smaller pore volume which allowed it hinder water permeation through the diffusion media whilst maintaining sufficient hydration of the catalyst layer.

One of the key properties of the PEFC porous media is its gas permeability as it describes how effective the convective gas transport is within the porous regions of the fuel cell. As such, these porous media, namely the GDL and MPL need to effectively demonstrate high

transport properties to allow gas to be transported to the catalyst layer while minimising concentration losses [103]. There have been numerous investigations [32], [93], [102]–[104], [106], [107], [127], [128], [142], [94]–[101] into the gas permeability of the PEFC porous layers; however, very few [127], [128] have looked at the effect of microporous layer composition on through-plane gas permeability.

Orogbemi et al. [127], [128] investigated the effect of through-plane permeability for various carbon loadings and various PTFE loadings for two carbon black types. The through-plane permeability was found to be the lowest at 20 wt.% PTFE for the investigated carbon loadings but was found to increase between 20 and 50 wt.% PTFE loading in the MPL. This finding was in agreement with that of [32], [94]. The permeability for increased carbon loading was also found to decrease as the PTFE loading was increased from 10-20 wt.%. Orogebemi et al. [128] extended the work conducted in [127] on the effect of carbon loading on through-plane permeability of GDMs. Two carbon blacks, namely, Vulcan XC-72R and Ketjenblack EC-300J were used for the five carbon loadings investigated in [128]. The results indicated a decrease in through-plane permeability with increased carbon loading for the two carbon powders with the permeability of the GDMs coated with Vulcan XC-72R being higher for carbon loadings less than 1.5 $mgcm^{-2}$. The investigations conducted by Orogbemi et al. [127], [128] were based on a single GDL substrate, SGL 10BA. El-Kharouf et al. [33] reported the through-plane permeability of many commercial substrates with and without a MPL and indicated how non-woven carbon fibre papers vary in structural configurations, namely, straight non-woven or felt/spaghetti non-woven. Based on the investigations conducted in [33] it is evident how the properties of various substrates differ tremendously.

The focus of this chapter extends the work conducted in [127], [128] to include the impact of different structured GDLs on the through-plane gas permeability of the GDM and to investigated the effects of PTFE loading in the GDL on the overall GDM permeability. Two carbon blacks, namely, Vulcan XC-72R and Ketjenblack EC-300J are used for various carbon loadings and the impact on the gas permeability before and after application of an MPL are investigated. Through-plane permeability of the MPL is compared for the cases with and without consideration of penetration into the GDL. SEM images were used to investigate surface morphology and MPL thickness.

4.2 Materials and Methods

An in-house gas permeability setup was used to determine the through-plane permeability. Preparation of the samples and data analysis used in the investigations was described previously in Section 3.3. The through-plane gas permeability was investigated for six (6) samples coated (for each carbon substrate) with two different carbon powders (Vulcan XC-72R and Ketjenblack EC-300J) for three carbon loadings of 0.5, 1.0 and 2.0 $mgcm^{-2}$. The composition of the MPL for each carbon loadings was kept constant at 80 wt.% carbon powder and 20 wt.% PTFE. Several commercial GDLs were chosen as the base substrates for this investigation. The non-woven straight carbon fibre papers utilised were, Toray TGP-H-90, Toray TGP-H-120 and SGL 35BA; the felt/spaghetti type carbon fibre papers used were, SGL 10CA and SGL 10EA. SGL 10CA and SGL 10EA were used to investigate the effects of different PTFE loadings in the GDL on through-plane permeability of GDMs. Lastly, SEM micrographs were used to determine the surface morphology and MPL thickness to determine the impact of neglecting the penetration of the MPL into GDL.

4.3 Results and Discussion

4.3.1 Through-plane gas permeability of gas diffusion layer substrates

The through-plane gas permeability of the GDL substrates listed in Table 4.1 were determined initially, before application of a microporous layer onto the substrate. Gas permeability was estimated experimentally by fitting the data, determined from the dependence of fluid velocity on pressure drop, to Eq. 3.4. The through-plane permeability and thickness of all uncoated GDL substrates under investigation are presented in Table 4.1. The listed values represent the mean and 95% confidence interval limits for the gas permeability and thickness of thirty-six samples. Figure 4.1 illustrates the relationship between the pressure gradient across the substrates to the fluid velocity used in the estimation of the gas permeability of the samples. Figure 4.2 shows the pressure gradient as a function of fluid velocity for each individual GDL with the error bars representing the 95% confidence interval for the samples used. The linearity of the pressure gradient to fluid velocity relationship for the samples investigated, justifies the use of Darcy's law given in Equation 3.4 ($\frac{\Delta P_g}{L} = \frac{\mu_g}{k_g} u_g$; where, k_g is the gas-phase permeability, $\mu_g$is the nitrogen viscosity, P_g is the gas-phase pressure gradient, u_g is the gas velocity and L is the thickness of the sample.

Table 4. 1 Through-plane permeability of tested GDL substrates.

GDL substrates	**Permeability** $k \times 10^{-12}(\mathrm{m}^2)$	**Thickness** $(\mu\mathrm{m})$
Toray TGP-H-090	6.906 ± 0.125	291.181 ± 0.839
Toray TGP-H-120	5.701 ± 0.130	358.333 ± 1.831
SGL 35BA	39.867 ± 0.797	294.549 ± 1.686
SGL 10CA	21.856 ± 0.456	353.750 ± 5.205
SGL 10EA	18.772 ± 0.972	376.354 ± 6.431

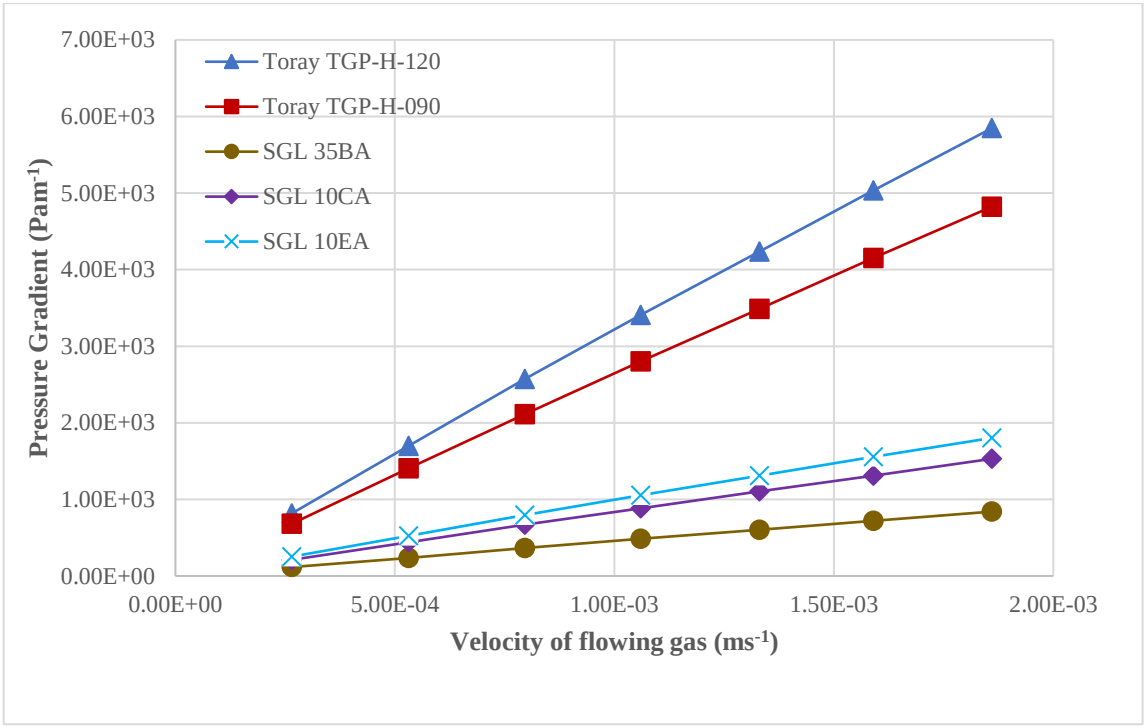

Figure 4. 1 Experimental data for the pressure gradient as a function of fluid velocity for the GDL substrates used.

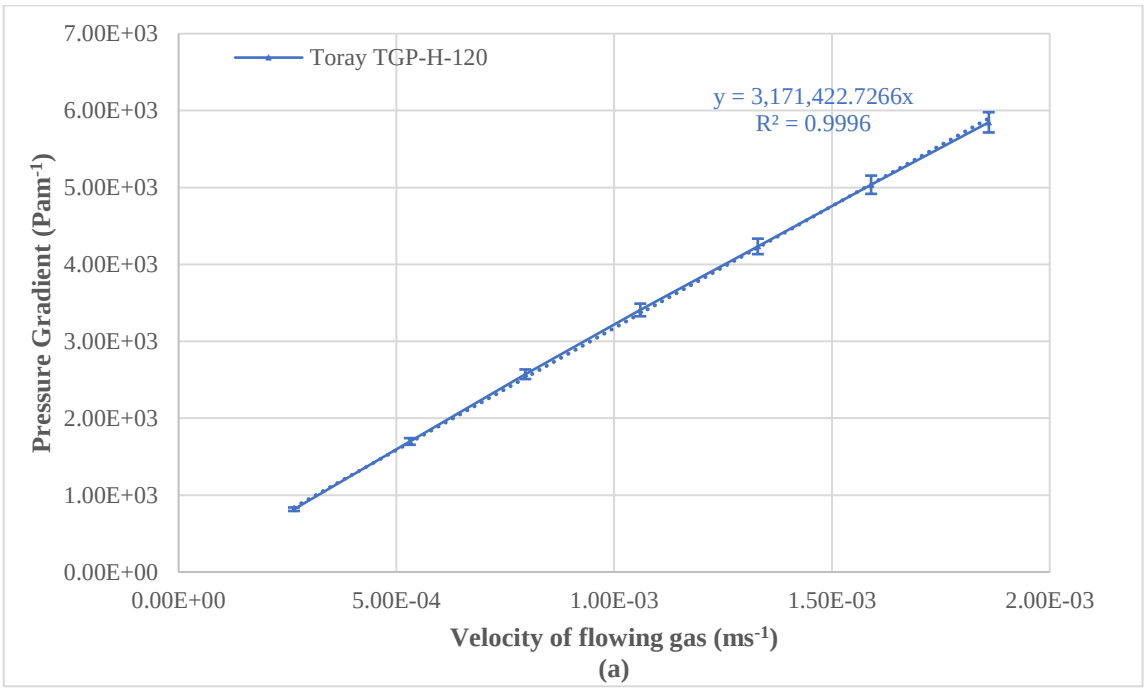

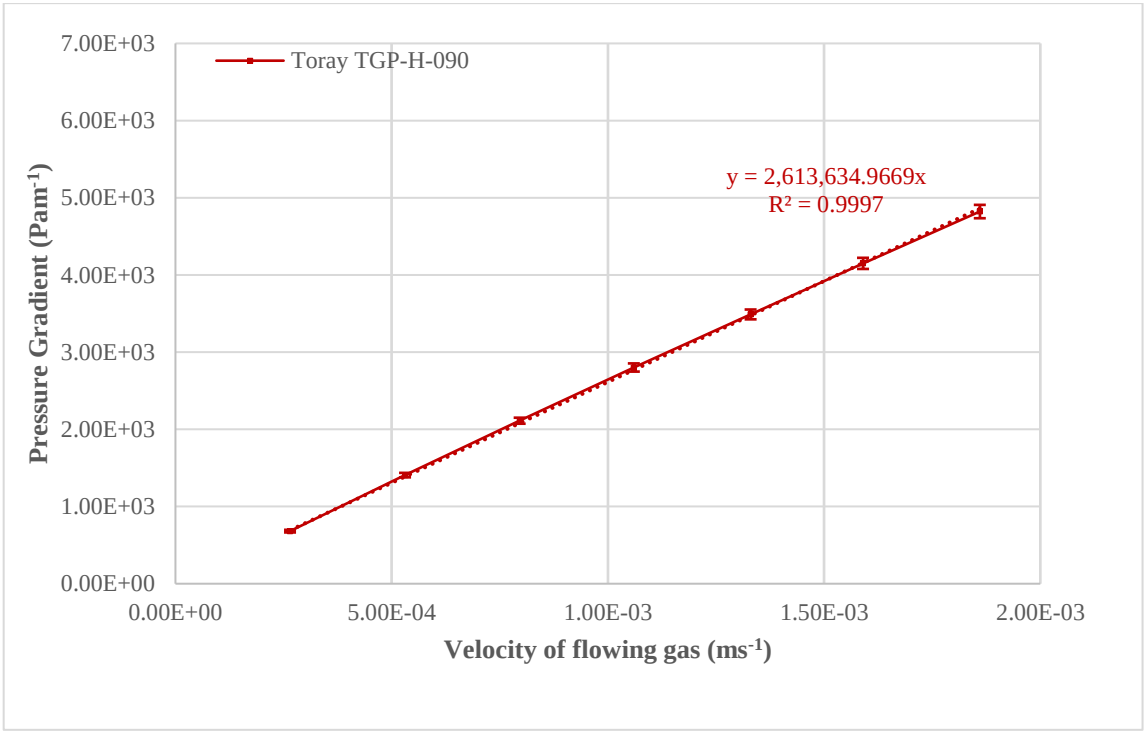
Toray TGP-H-090
y = 2,613,634.9669x
R² = 0.9997
Pressure Gradient (Pam-1)
Velocity of flowing gas (ms-1)
7.00E+03
6.00E+03
5.00E+03
4.00E+03
3.00E+03
2.00E+03
1.00E+03
0.00E+00
0.00E+00
5.00E-04
1.00E-03
1.50E-03
2.00E-03

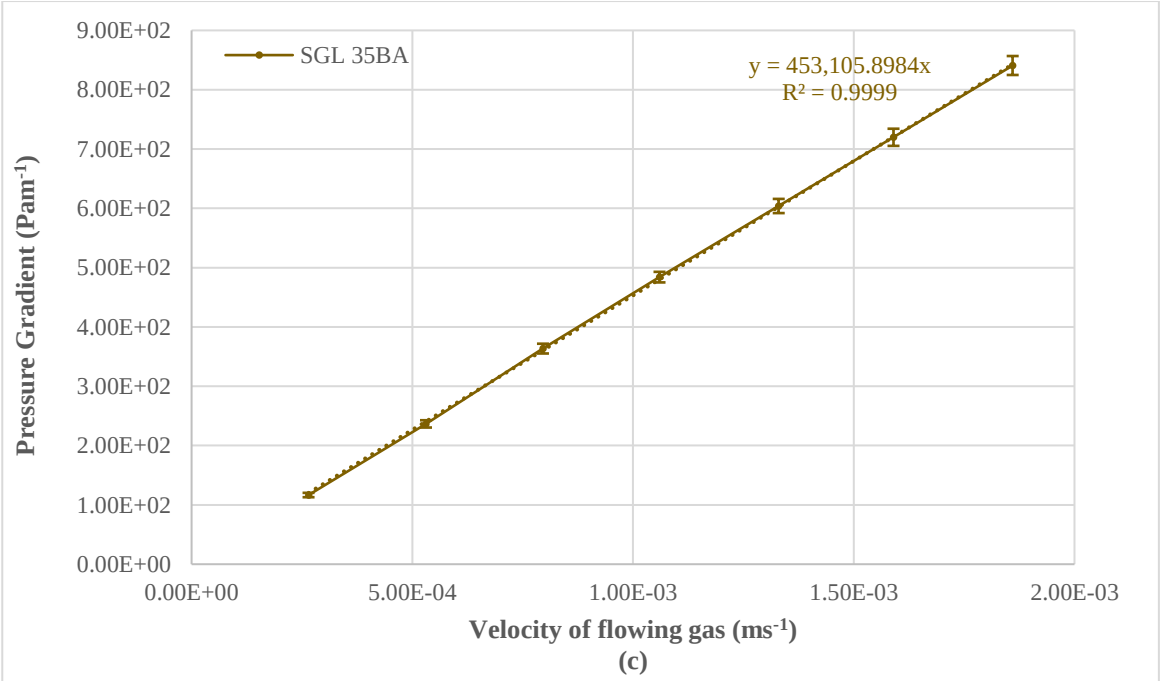
SGL 35BA
y = 453,105.8984x
R² = 0.9999
Pressure Gradient (Pam-1)
Velocity of flowing gas (ms-1)
9.00E+02
8.00E+02
7.00E+02
6.00E+02
5.00E+02
4.00E+02
3.00E+02
2.00E+02
1.00E+02
0.00E+00
0.00E+00
5.00E-04
1.00E-03
1.50E-03
2.00E-03

(c)

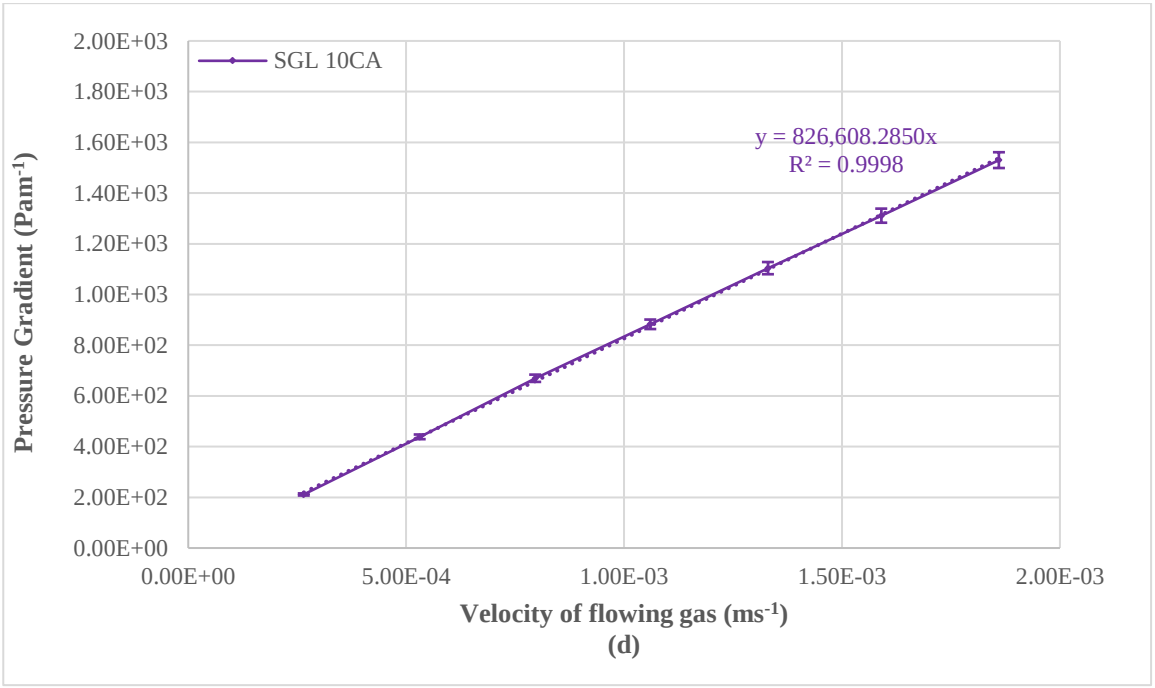

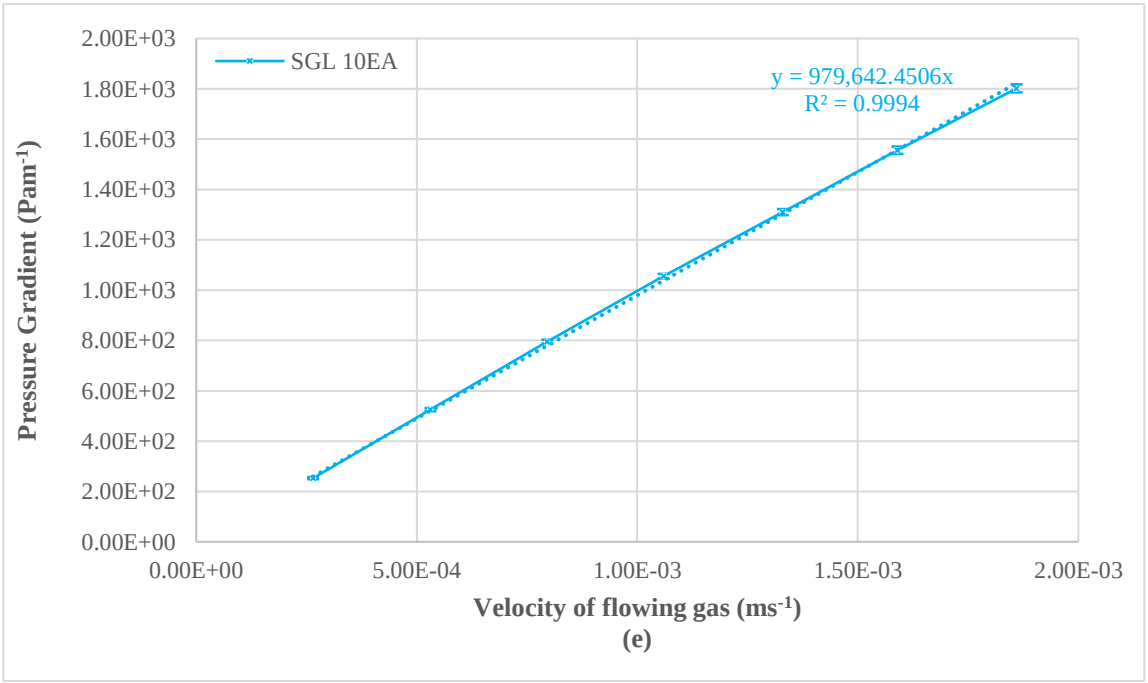

Figure 4. 2 Experimental data for pressure gradient as a function of fluid velocity for (a) Toray TGP-H-120, (b) Toray TGP-H-090, (c) SGL 35BA, (d) SGL 10CA and (e) SGL 10EA showing the 95% confidence interval for each sample.

Comparison of the through-plane permeability of the GDL substrates to the available literature shows good agreement. Ismail et al. [99]measured the through-plane permeability of SGL 10CA (10% PTFE) and SGL 10EA (30% PTFE) to be 22.2×10^{-12} m^2 and

23.9×10^{-12} m^2 respectively. Previous studies [94], [100], [101] have shown a decrease in through-plane permeability with increase in the amount of PTFE due to the partial occupation of the pores by the PTFE particles which subsequently leads to a reduction in the porosity of the medium. This trend is reiterated in the present study. It should be noted that eight of the SGL 10EA samples, in this study, cut from a different sheet showed through-plane permeability within the range $21.4 - 25.1 \times 10^{-12}$ m^2. This emphasizes the variability of samples between different sheets, which may be a result of fabrication uncertainties as suggested in [31]. Gostick et al. [102] reported a value of 8.99×10^{-12} m^2 for Toray TGP-H-90 and Mangal et al. [107] reported a value of 8×10^{-12} m^2 for Toray TGP-H-90 in the through-plane direction for samples with 0% PTFE compared to the 5% PTFE loading in the samples used in this investigation which would explain the reduction in permeability as shown in Table 4.2. Toray TGP-H-90 and Toray TGP-H-120 are structurally similar and the reduction in permeability of Toray TGP-H-120 was due to the increased thickness [102]. Williams et al. [104] tested the through-plane permeability of Toray TGP-H-120 and obtained a value of 8.69×10^{-12} m^2. El-Kharouf et al. [33] reported values of 4.53×10^{-12} m^2 , 3.90×10^{-12} m^2 and 53.1×10^{-12} m^2 for Toray TGP-H-090, Toray TGP-H-120 and SGL 35BA respectively. SGL 35BA shares is similar structure to that of Toray TGP-H-090 and Toray TGP-H-120; they are all categorized in [33] as non-woven carbon papers with straight fibres. The significant difference in through-plane permeability was due to increased porosity due to lower bulk density and increased pore diameters of the SGL 35BA samples as reported in [33]. Figure 4.3 shows the SEM images of the base carbon substrates used in this study.

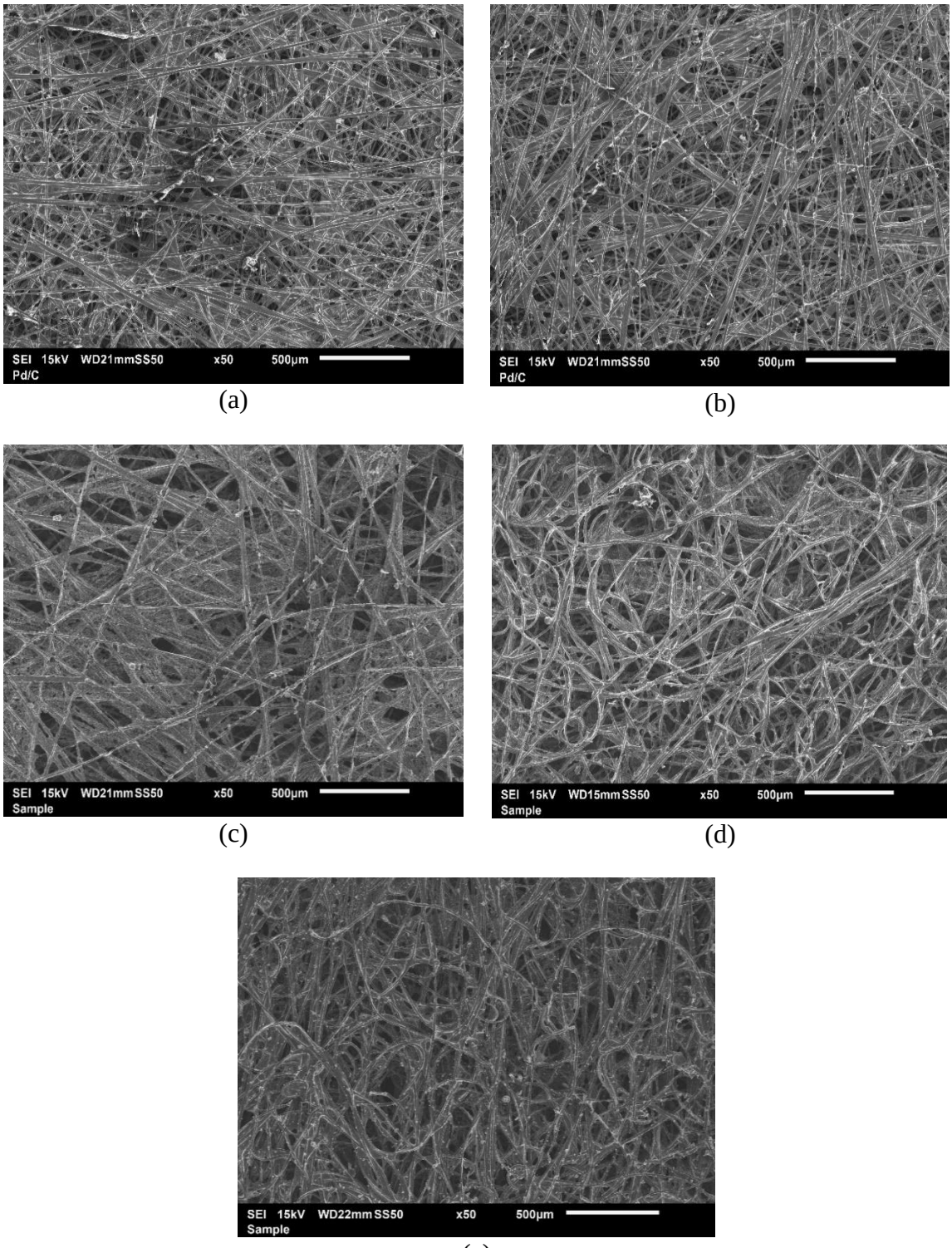

Figure 4. 3 SEM micrographs for (a) Toray TGP-H-120, (b) Toray TGP-H-090, (c) SGL 35BA, (d) SGL 10CA and (e) SGL 10EA.

4.3.2 Through-plane gas permeability of Gas Diffusion Media

The through-plane gas permeability of GDMs was investigated in this section for two carbon black types, namely, Vulcan XC-72R and Ketjenblack EC-300J. The MPL composed of 20% PTFE and 80% carbon black which was held constant for three carbon loadings, 0.5 $mgcm^{-2}$, 1.0 $mgcm^{-2}$ and 2.0 $mgcm^{-2}$. This MPL composition value has been widely used in previous studies in the literature namely [143], [144]. Gas permeability of the GDMs was calculated similar to that of the bare substrates with the use of equation 3.4. Figure 4.4 and Figure 4.5 shows the pressure gradient as a function of fluid velocity for the various carbon loadings and the different substrates for samples coated with Vulcan XC-72R and Ketjenblack EC-300J respectively.

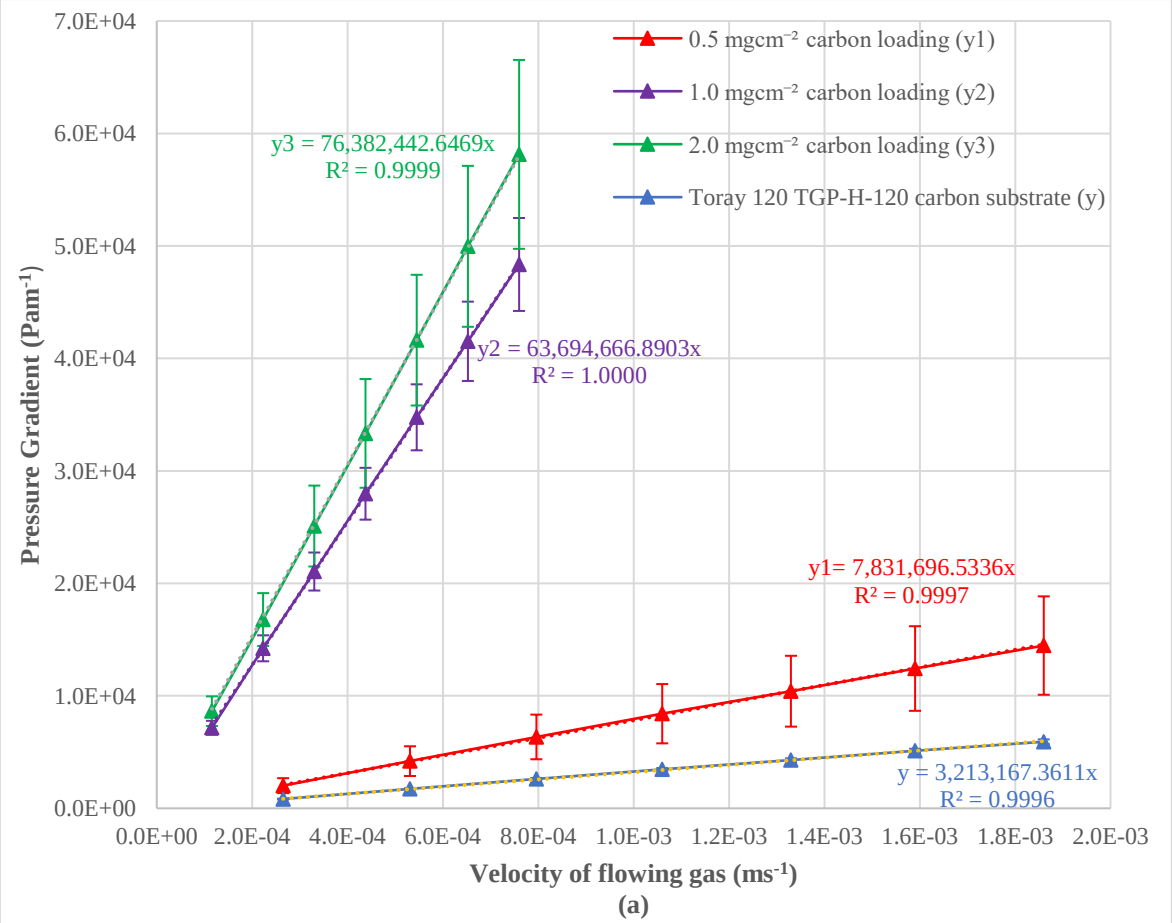

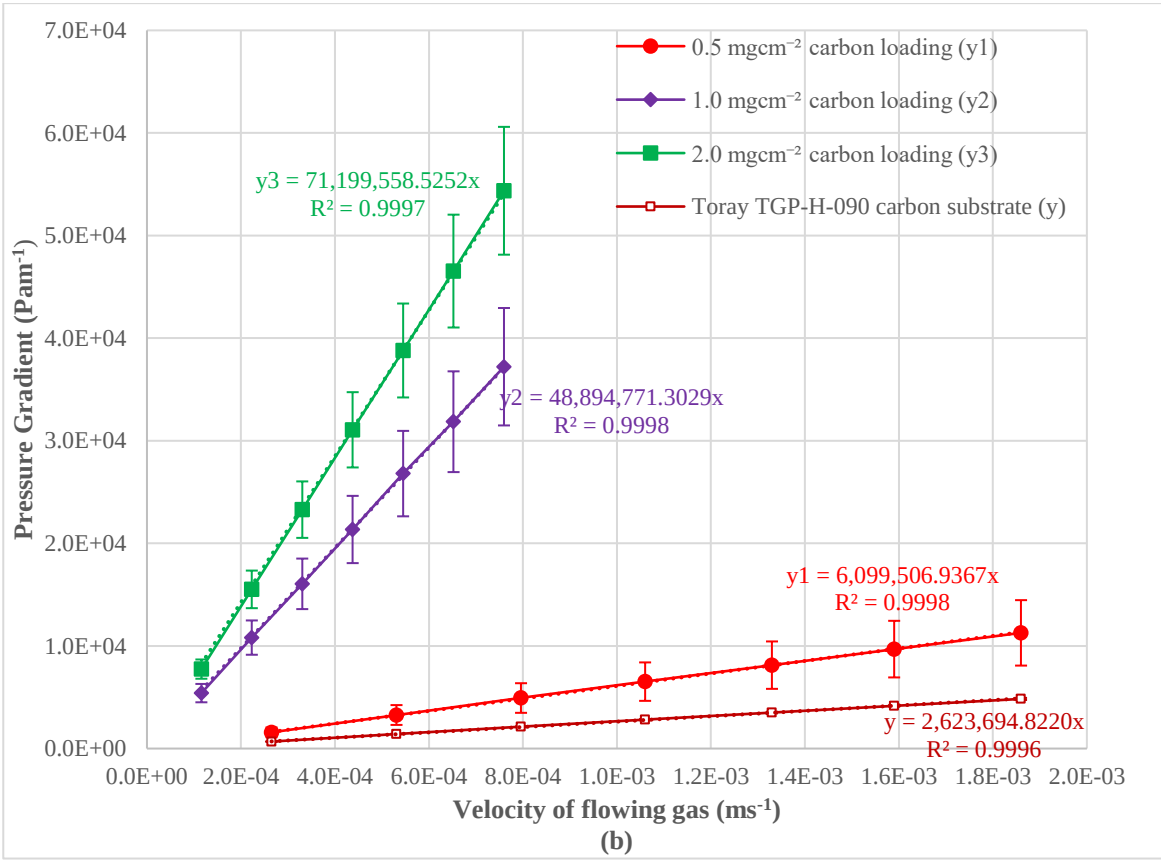
7.0E+04
6.0E+04
5.0E+04
4.0E+04
3.0E+04
2.0E+04
1.0E+04
0.0E+00
Pressure Gradient (Pam-1)
0.0E+00 2.0E-04 4.0E-04 6.0E-04 8.0E-04 1.0E-03 1.2E-03 1.4E-03 1.6E-03 1.8E-03 2.0E-03
Velocity of flowing gas (ms-1)
0.5 mgcm-2 carbon loading (y1)
1.0 mgcm-2 carbon loading (y2)
2.0 mgcm-2 carbon loading (y3)
Toray TGP-H-090 carbon substrate (y)
y3 = 71,199,558.5252x
R² = 0.9997
y2 = 48,894,771.3029x
R² = 0.9998
y1 = 6,099,506.9367x
R² = 0.9998
y = 2,623,694.8220x
R² = 0.9996

(b)

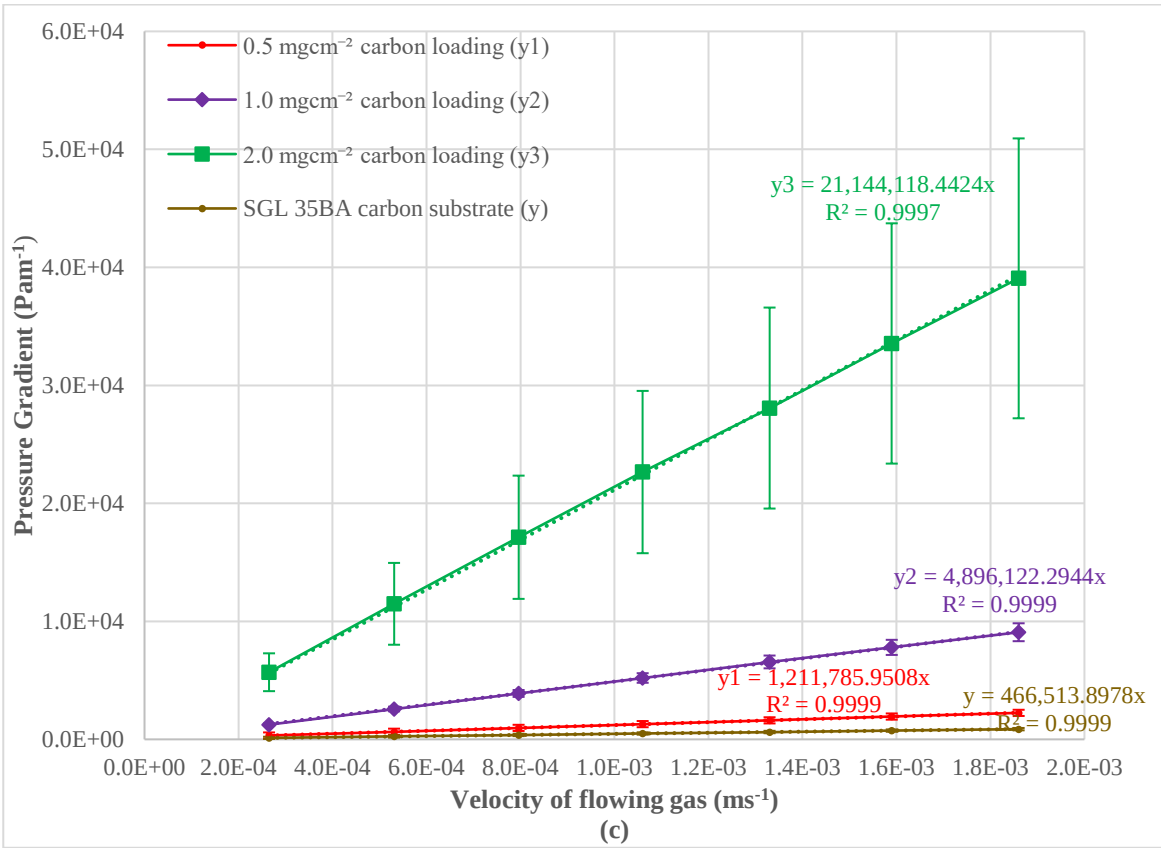
6.0E+04
5.0E+04
4.0E+04
3.0E+04
2.0E+04
1.0E+04
0.0E+00
Pressure Gradient (Pam-1)
0.0E+00 2.0E-04 4.0E-04 6.0E-04 8.0E-04 1.0E-03 1.2E-03 1.4E-03 1.6E-03 1.8E-03 2.0E-03
Velocity of flowing gas (ms-1)
0.5 mgcm-2 carbon loading (y1)
1.0 mgcm-2 carbon loading (y2)
2.0 mgcm-2 carbon loading (y3)
SGL 35BA carbon substrate (y)
y3 = 21,144,118.4424x
R² = 0.9997
y2 = 4,896,122.2944x
R² = 0.9999
y1 = 1,211,785.9508x
R² = 0.9999
y = 466,513.8978x
R² = 0.9999

(c)

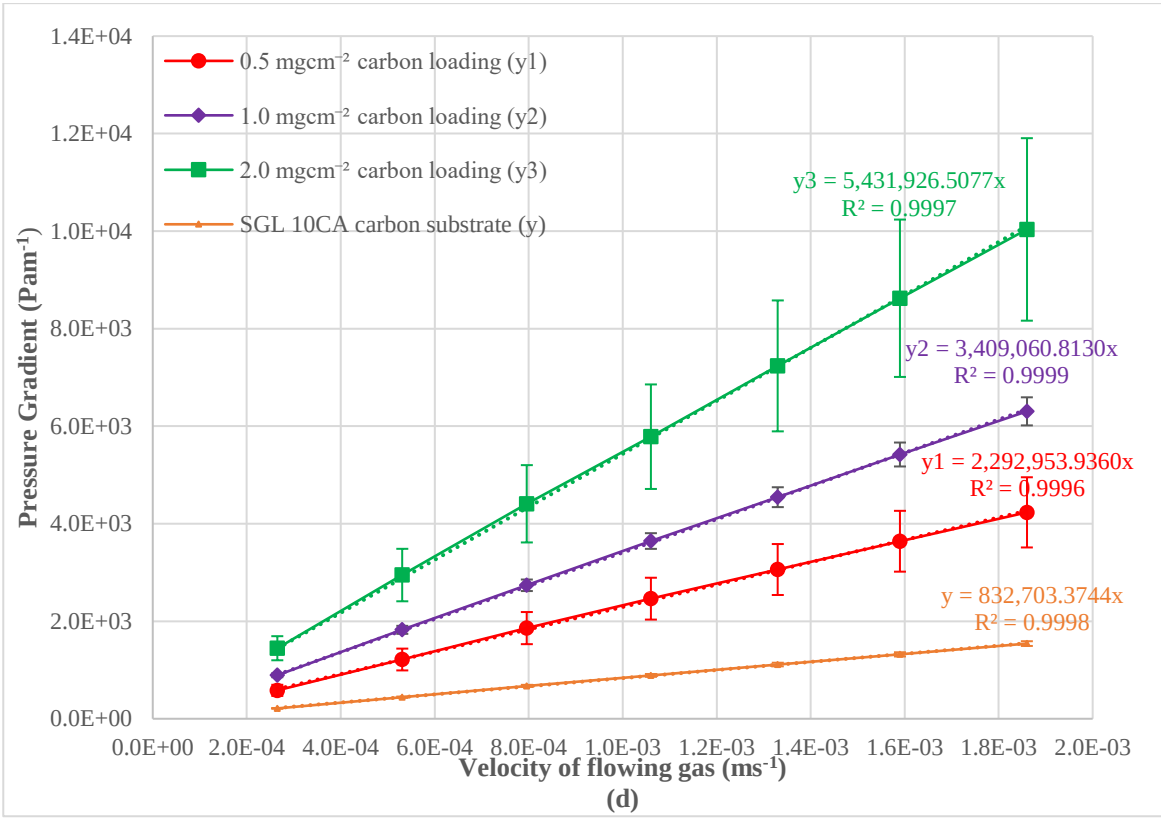

(d)

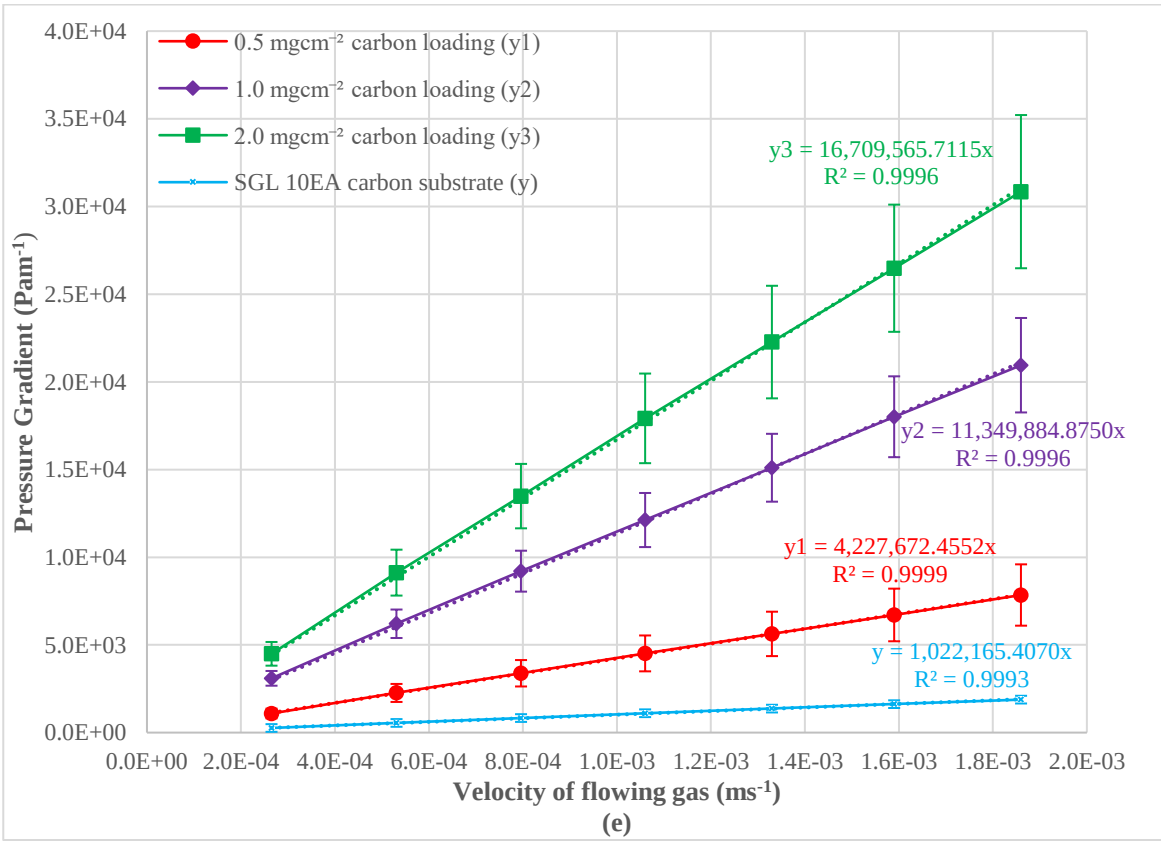

(e)

Figure 4. 4 Experimental data for the pressure gradient as a function for fluid velocity for substrates coated using Vulcan XC-72R, (a) Toray TGP-H-120, (b) Toray TGP-H-90, (c) SGL 35BA, (d) SGL 10CA and (e) SGL 10EA.

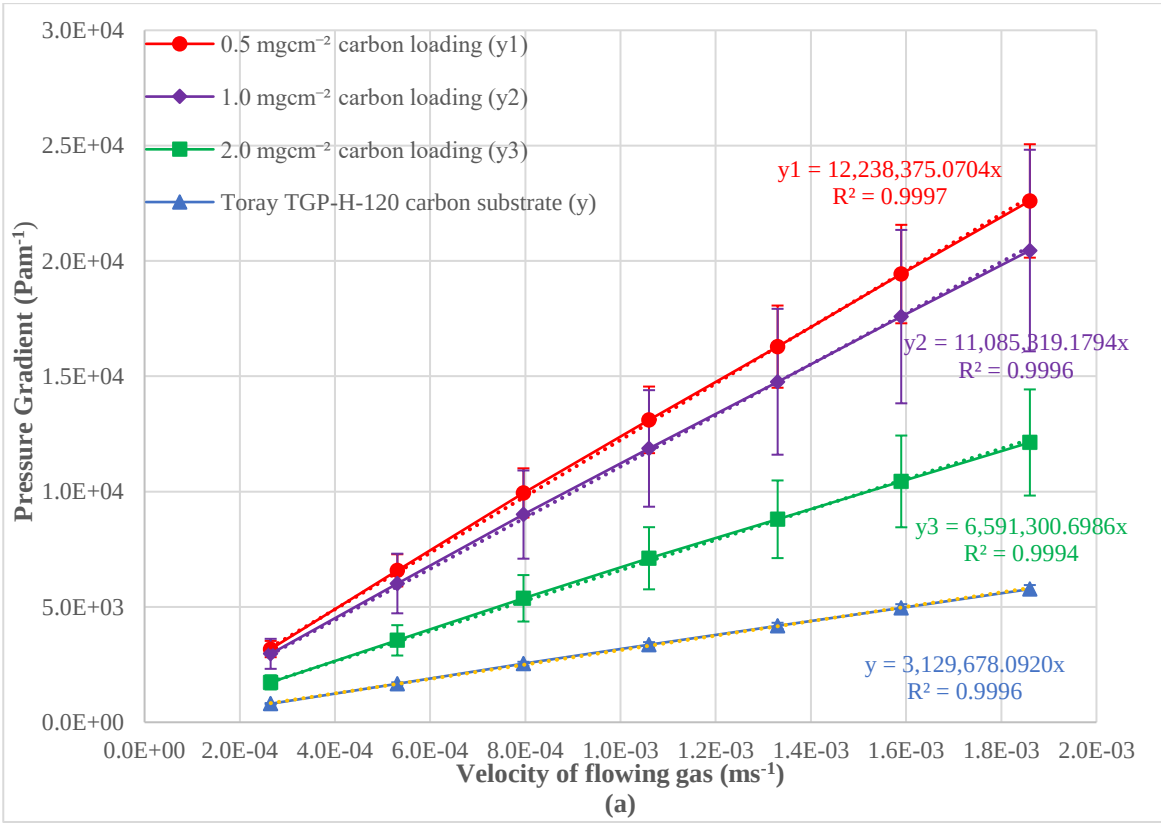
0.5 mgcm⁻² carbon loading (y1)
1.0 mgcm⁻² carbon loading (y2)
2.0 mgcm⁻² carbon loading (y3)
Toray TGP-H-120 carbon substrate (y)
y1 = 12,238,375.0704x
R² = 0.9997
y2 = 11,085,319.1794x
R² = 0.9996
y3 = 6,591,300.6986x
R² = 0.9994
y = 3,129,678.0920x
R² = 0.9996
Pressure Gradient (Pam⁻¹)
Velocity of flowing gas (ms⁻¹)
3.0E+04
2.5E+04
2.0E+04
1.5E+04
1.0E+04
5.0E+03
0.0E+00
0.0E+00 2.0E-04 4.0E-04 6.0E-04 8.0E-04 1.0E-03 1.2E-03 1.4E-03 1.6E-03 1.8E-03 2.0E-03

(a)

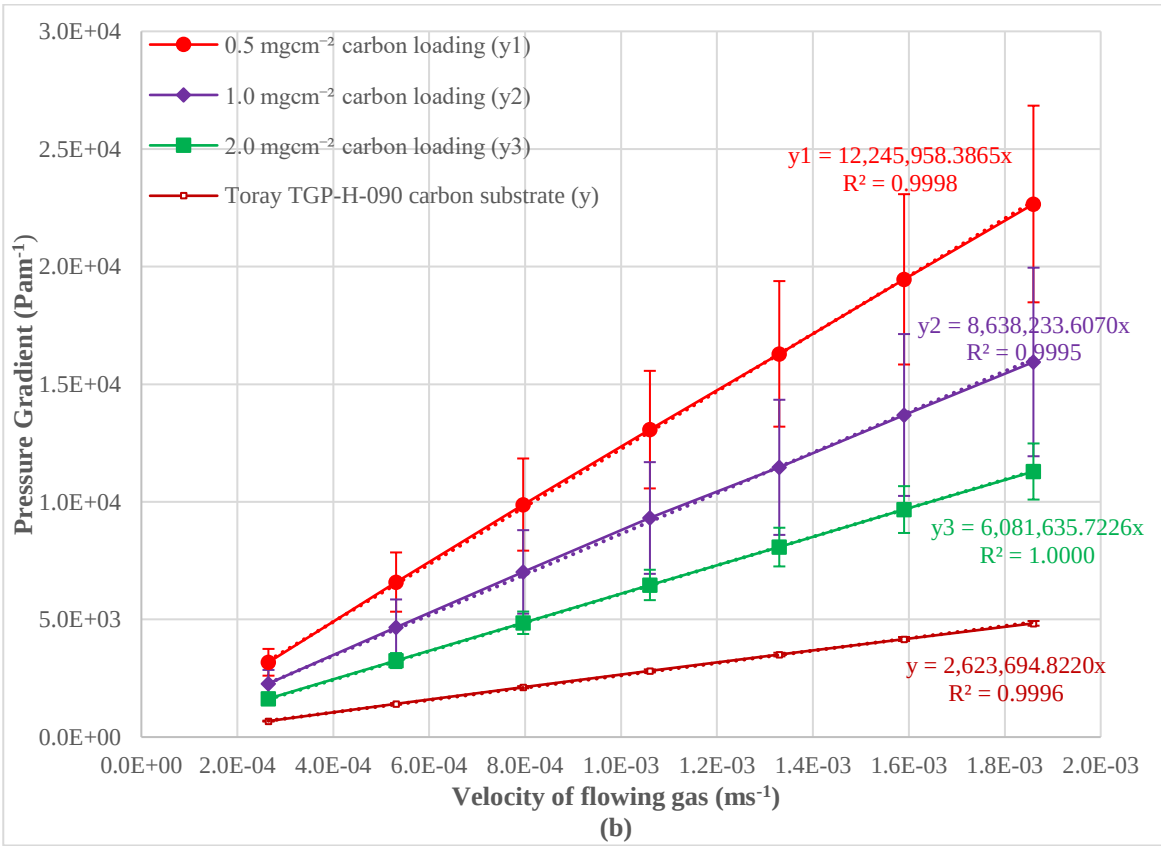
0.5 mgcm⁻² carbon loading (y1)
1.0 mgcm⁻² carbon loading (y2)
2.0 mgcm⁻² carbon loading (y3)
Toray TGP-H-090 carbon substrate (y)
y1 = 12,245,958.3865x
R² = 0.9998
y2 = 8,638,233.6070x
R² = 0.9995
y3 = 6,081,635.7226x
R² = 1.0000
y = 2,623,694.8220x
R² = 0.9996
Pressure Gradient (Pam⁻¹)
Velocity of flowing gas (ms⁻¹)
3.0E+04
2.5E+04
2.0E+04
1.5E+04
1.0E+04
5.0E+03
0.0E+00
0.0E+00 2.0E-04 4.0E-04 6.0E-04 8.0E-04 1.0E-03 1.2E-03 1.4E-03 1.6E-03 1.8E-03 2.0E-03

(b)

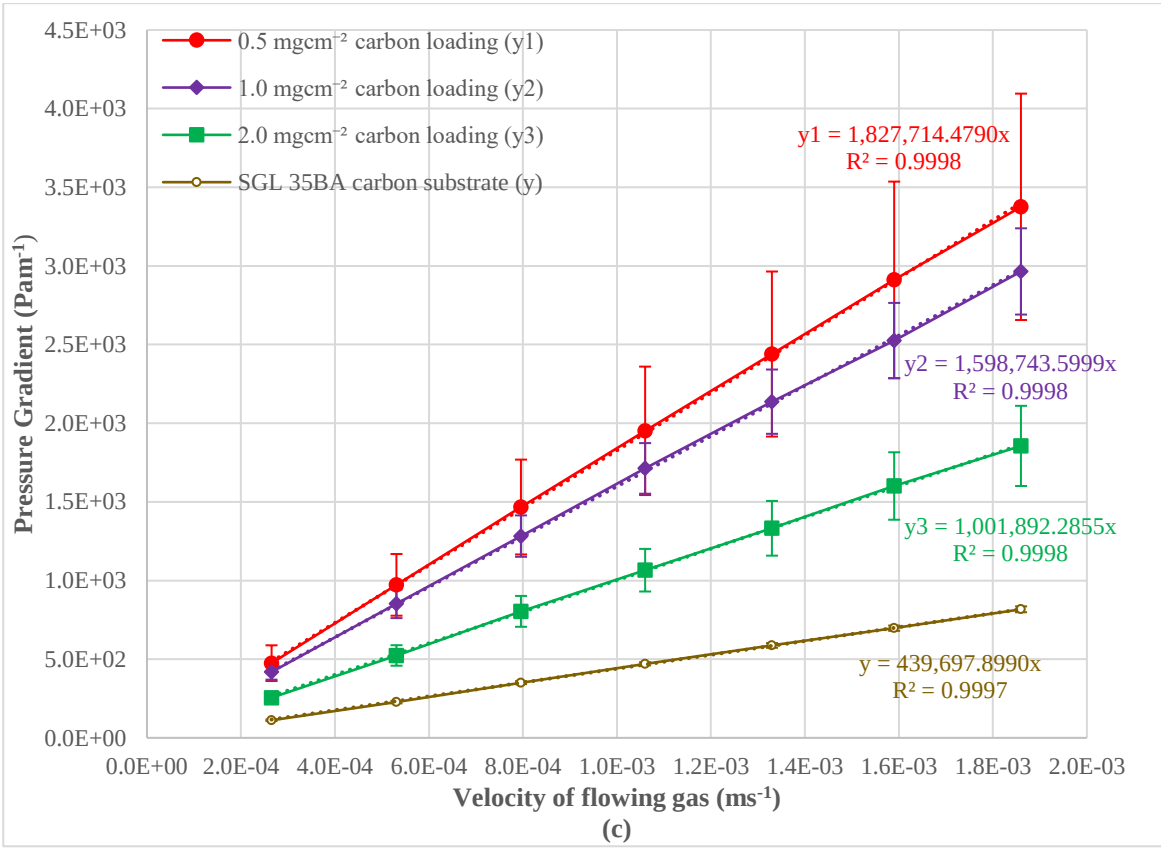
0.5 mgcm⁻² carbon loading (y1)
1.0 mgcm⁻² carbon loading (y2)
2.0 mgcm⁻² carbon loading (y3)
SGL 35BA carbon substrate (y)
y1 = 1,827,714.4790x
R² = 0.9998
y2 = 1,598,743.5999x
R² = 0.9998
y3 = 1,001,892.2855x
R² = 0.9998
y = 439,697.8990x
R² = 0.9997
Pressure Gradient (Pam⁻¹)
Velocity of flowing gas (ms⁻¹)
4.5E+03
4.0E+03
3.5E+03
3.0E+03
2.5E+03
2.0E+03
1.5E+03
1.0E+03
5.0E+02
0.0E+00
0.0E+00 2.0E-04 4.0E-04 6.0E-04 8.0E-04 1.0E-03 1.2E-03 1.4E-03 1.6E-03 1.8E-03 2.0E-03

(c)

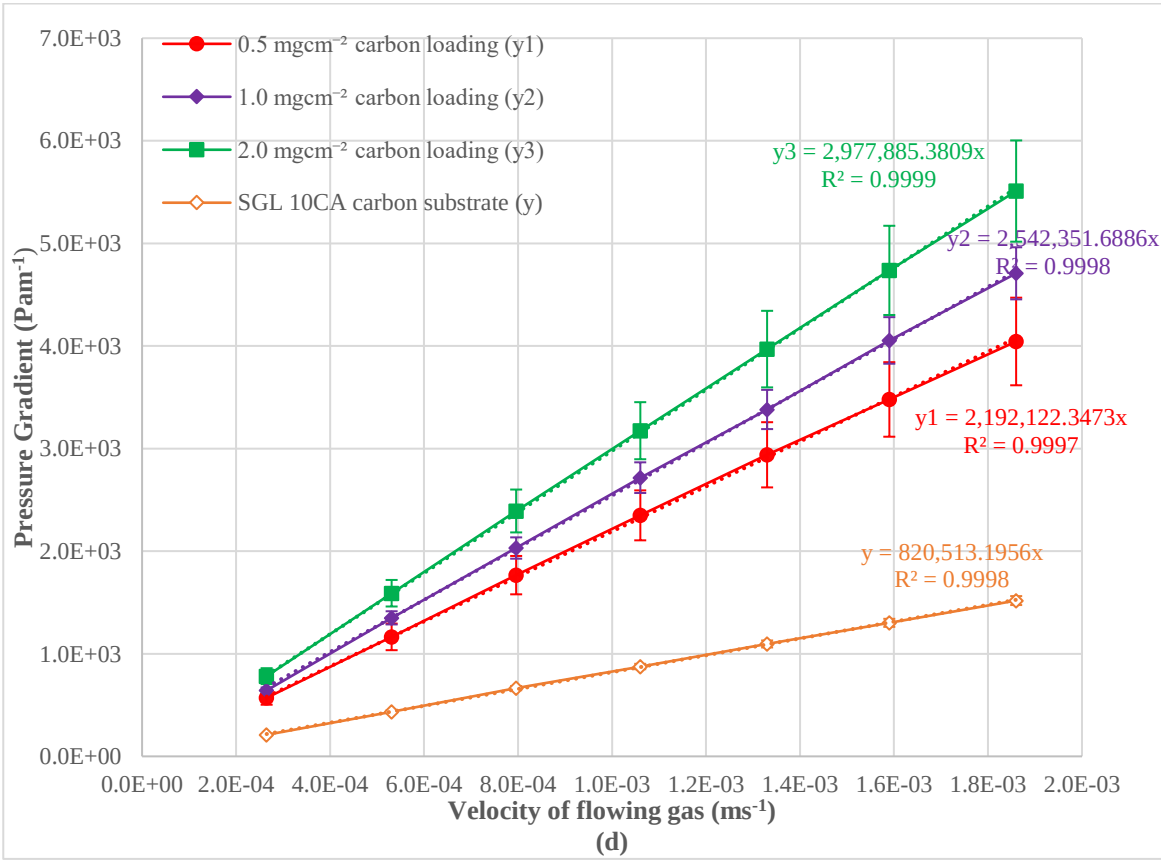
0.5 mgcm⁻² carbon loading (y1)
1.0 mgcm⁻² carbon loading (y2)
2.0 mgcm⁻² carbon loading (y3)
SGL 10CA carbon substrate (y)
y3 = 2,977,885.3809x
R² = 0.9999
y2 = 2,542,351.6886x
R² = 0.9998
y1 = 2,192,122.3473x
R² = 0.9997
y = 820,513.1956x
R² = 0.9998
Pressure Gradient (Pam⁻¹)
Velocity of flowing gas (ms⁻¹)
7.0E+03
6.0E+03
5.0E+03
4.0E+03
3.0E+03
2.0E+03
1.0E+03
0.0E+00
0.0E+00 2.0E-04 4.0E-04 6.0E-04 8.0E-04 1.0E-03 1.2E-03 1.4E-03 1.6E-03 1.8E-03 2.0E-03

(d)

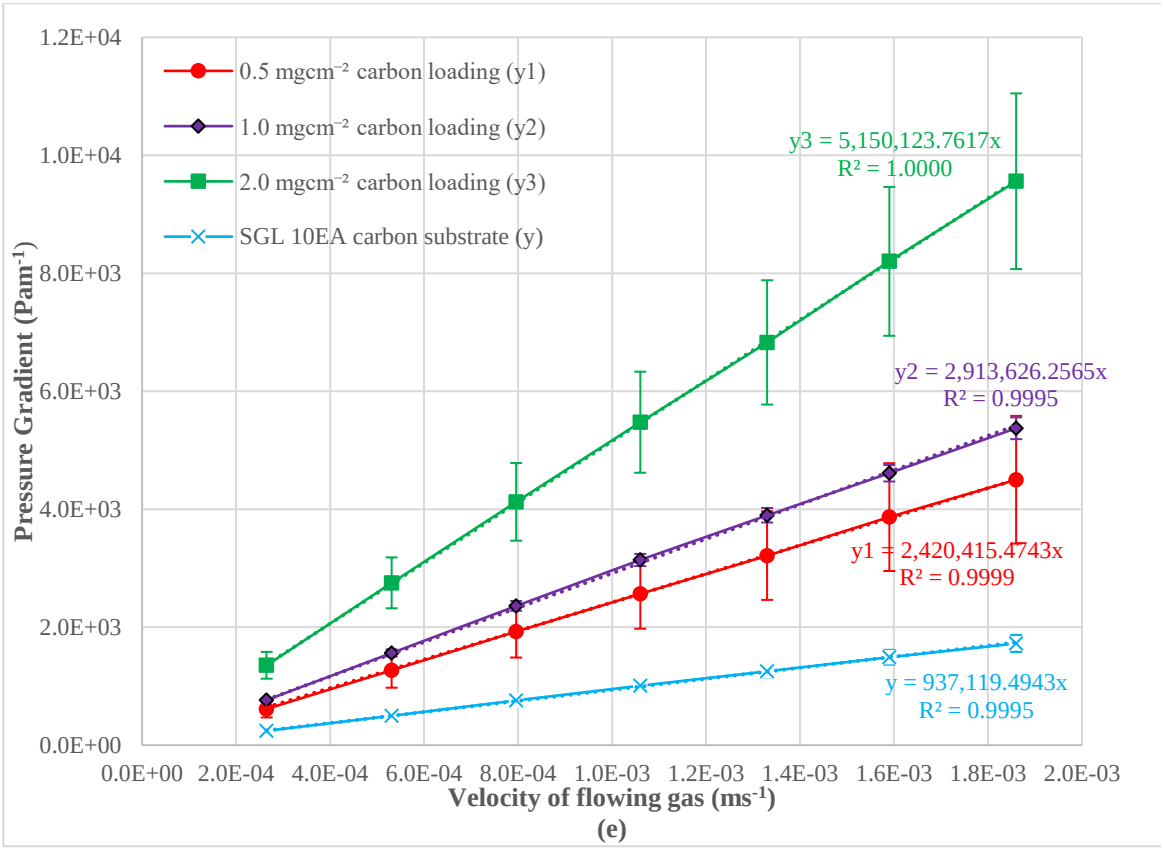

Figure 4. 5 Experimental data for the pressure gradient as a function for fluid velocity for substrates coated using Ketjenblack EC-300J, (a) Toray TGP-H-120, (b) Toray TGP-H-90, (c) SGL 35BA, (d) SGL 10CA and (e) SGL 10EA.

It should be noted from Figure 4.4, that the pressure gradient increases with the increase in carbon loading for a given velocity. This trend is seen for both non-woven straight fibre carbon papers (Toray TGP-H-120, Toray TGP-H-90 and SGL 35BA) as well as for felt/spaghetti-like carbon fibre papers (SGL 10CA and SGL 10EA). These results are consistent with those reported by Orogbemi et al. in [127], [128] for substrates coated with Vulcan XC-72R due to the increase in thickness of the substrates with increased carbon loading. This trend is also seen for the felt/spaghetti-like carbon papers when Ketjenblack EC-300J is used; however, from Figure 4.5, the opposite effect occurs for the non-woven straight fibre carbon papers when coated using Ketjenblack EC-300J. For a given velocity, the pressure gradient decreases with the increase in carbon loading. Comparisons between carbon type, carbon loading and substrate structure will be discussed in the subsequent sections.

4.3.2.1 Effect of carbon loading and carbon black type in the MPL

The previous section has demonstrated the significant effect of the increase in carbon loadings in the MPL with the different types of carbon blacks. This varies from what has been reported by Orogbemi et al. [127], [128] and the author believes that the type of substrate used in combination with the type of carbon black in the MPL has been severely overlooked in previous studies. Figure 4.6 demonstrates the through-plane gas permeability of the substrates used as a function carbon loading for the two carbon black types used.

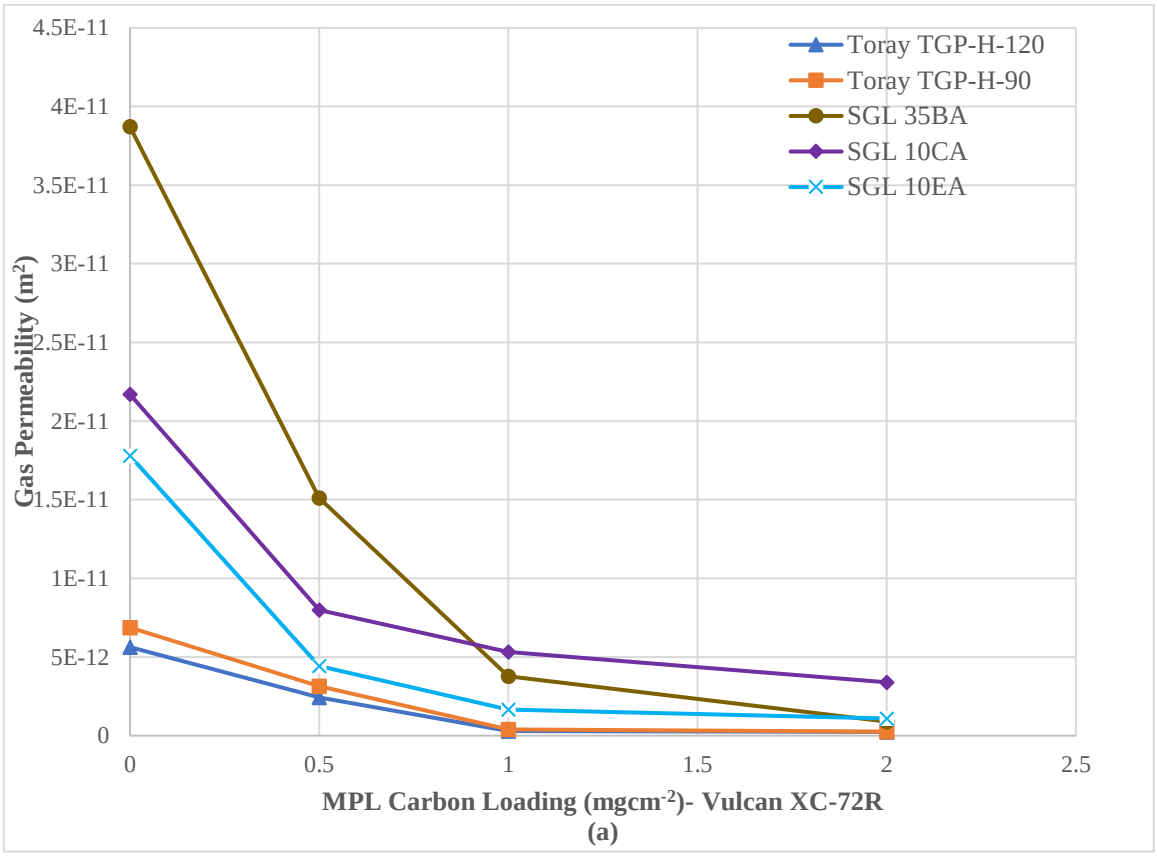

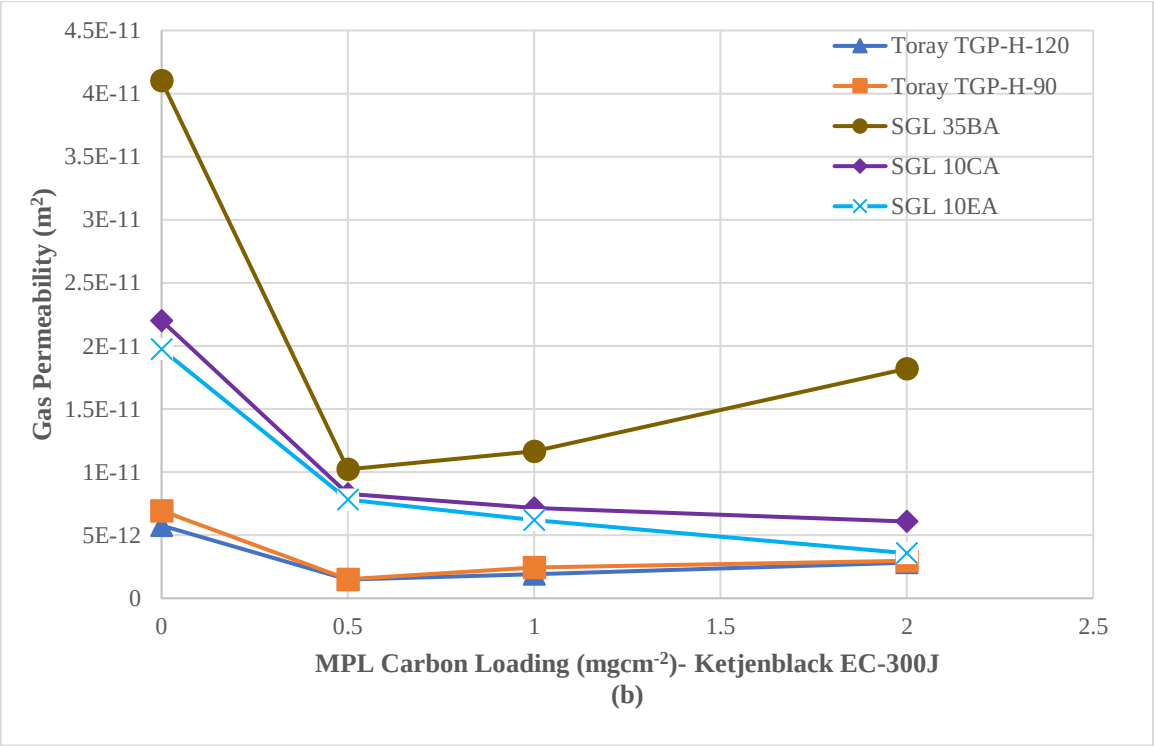

Figure 4. 6 Through-plane gas permeability of GDM for various substrates coated with (a) Vulcan XC-72R and (b) Ketjenblack EC-300J.

In the majority of cases, the increase in carbon loading results in a decrease is through-plane permeability due to the increase path the fluid travels through the porous medium from the resulting increase in thickness of the coated sample; however, the permeability of samples on which the Ketjenblack EC-300J were coated onto, particularly, the non-woven straight fibre carbon papers shows an opposite trend, that is, 0.5 mgcm^{-2} carbon loading has the lowest through-plane gas permeability. Figure 4.7 and Figure 4.8 show the SEM images for each carbon loading for the samples coated with Vulcan XC-72R and Ketjenblack EC-300J respectively. As shown, in Figure 4.7, as the carbon loading increases there is a clear distinction that the pathways are being closed when the carbon loadings were increased from 0.5 mgcm^{-2} to 2.0 mgcm^{-2} as a result of the increased thickness. The reductions in the through-plane permeability were at least one order of magnitude lower and in some cases two orders for carbon loadings between 1.0 mgcm^{-2} and 2.0 mgcm^{-2}. This is in agreement with [127], [128], [145]. As shown in Figure 4.8 (a-i), the increase in carbon loading from

0.5 $mgcm^{-2}$ to 2.0 $mgcm^{-2}$ demonstrated that there was a general increase in the surface crack formations on the MPL. The 0.5 $mgcm^{-2}$ case for the three different non-woven straight fibre carbon papers, clearly showed that the samples had been coated almost thoroughly which would indicate that the carbon loading showed the lowest through-plane permeability as compared to the 0.5 $mgcm^{-2}$ cases with the Vulcan XC-27R in Figure 4.7.

As such, the combination of the various base substrate and type of carbon black played an important role in the resulting through-plane gas permeability of the GDM. The properties such as porosity and pore size distribution of the GDM were significantly affected by the carbon loadings which determined the micro, meso and macro pores of the MPL as suggested by [63], [146]. Furthermore, the final structure was significantly affected by the properties of the carbon black type used in combination with the base structure of the GDL. The resulting increase in through-plane permeability for the GDMs which used a combination of non-woven straight fibre carbon papers and Ketjenblack EC-300J was primarily due to the large surface area of the Ketjenblack EC-300J as compared to the Vulcan XC-72R. High surface area carbon powders form large cracks and thicker layers compared to low surface area carbon powders which form smoother surfaces with a dense, thin layer with less cracks [122]. This is corroborated in Figures 4.7 and 4.8.

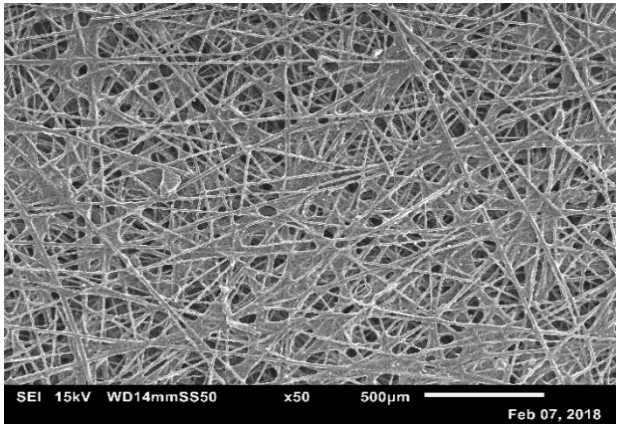

(a) 0.5 mgcm^{-2}

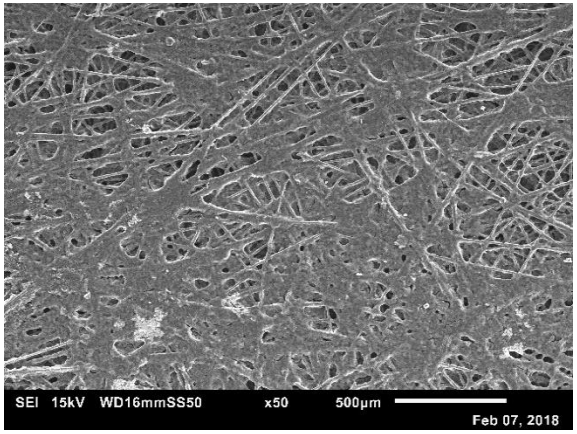

(b) 1.0 mgcm^{-2}

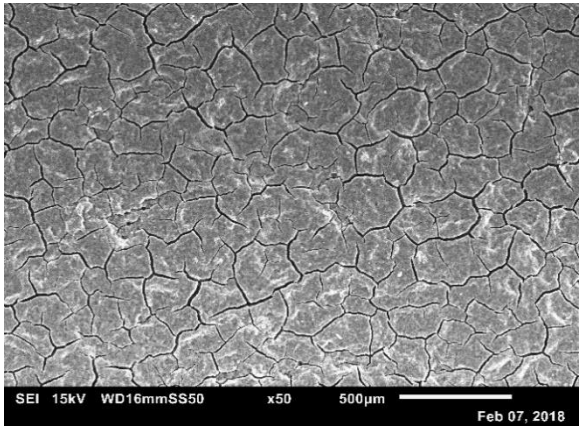

(c) 2.0 mgcm^{-2}

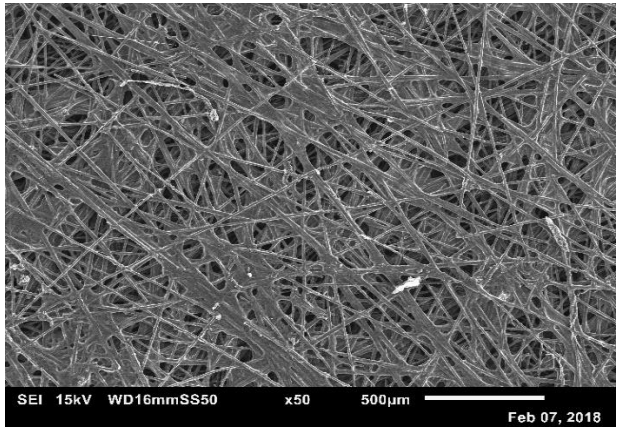

(d) 0.5 mgcm^{-2}

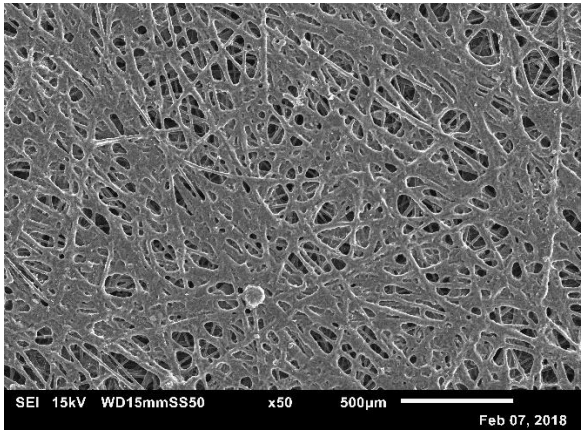

(e) 1.0 mgcm^{-2}

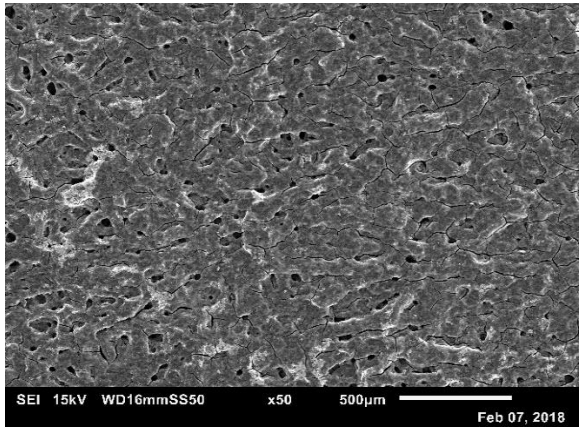

(f) 2.0 mgcm^{-2}

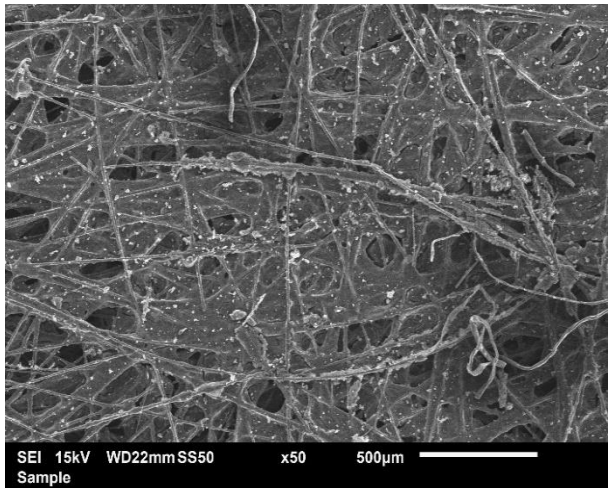

(g) 0.5 mgcm^{-2}

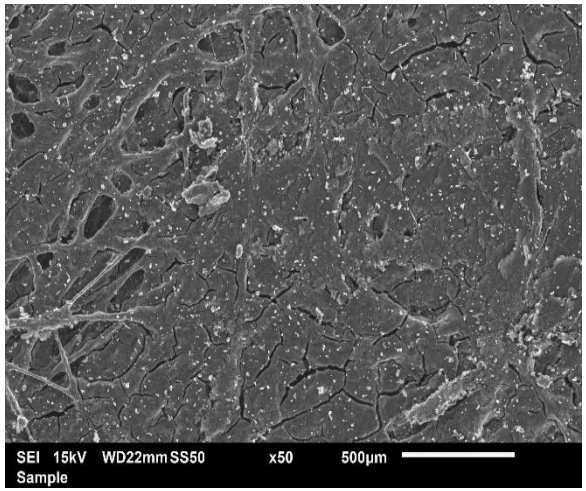

(h) 1.0 mgcm^{-2}

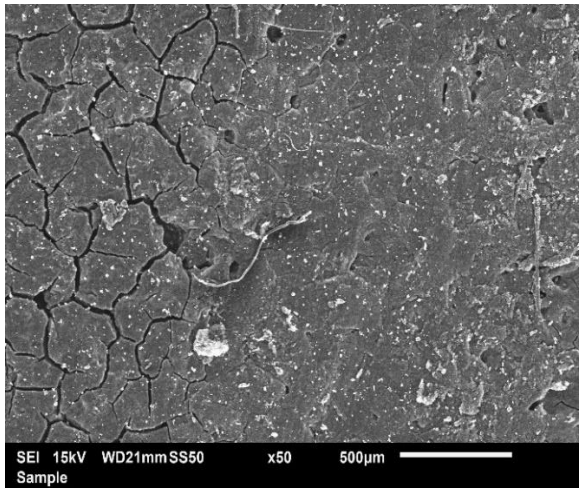

(i) 2.0 mgcm^{-2}

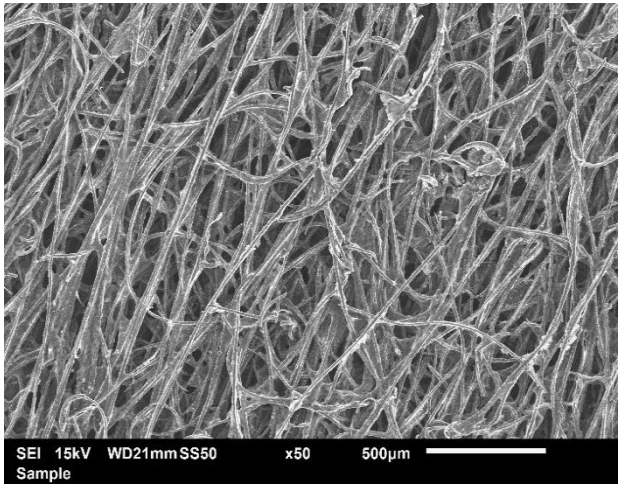

(j) 0.5 mgcm^{-2}

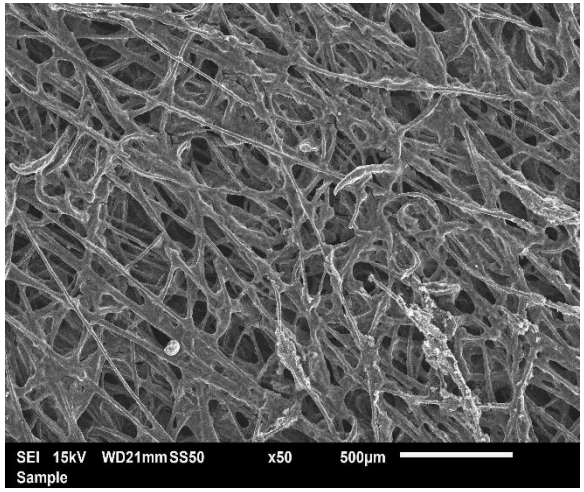

(k) 1.0 mgcm^{-2}

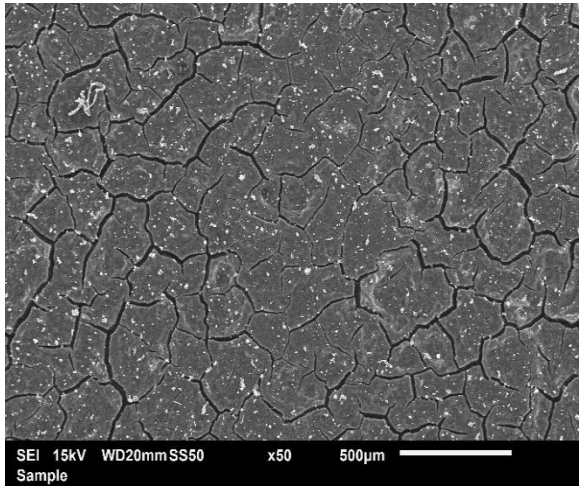

(l) 2.0 mgcm^{-2}

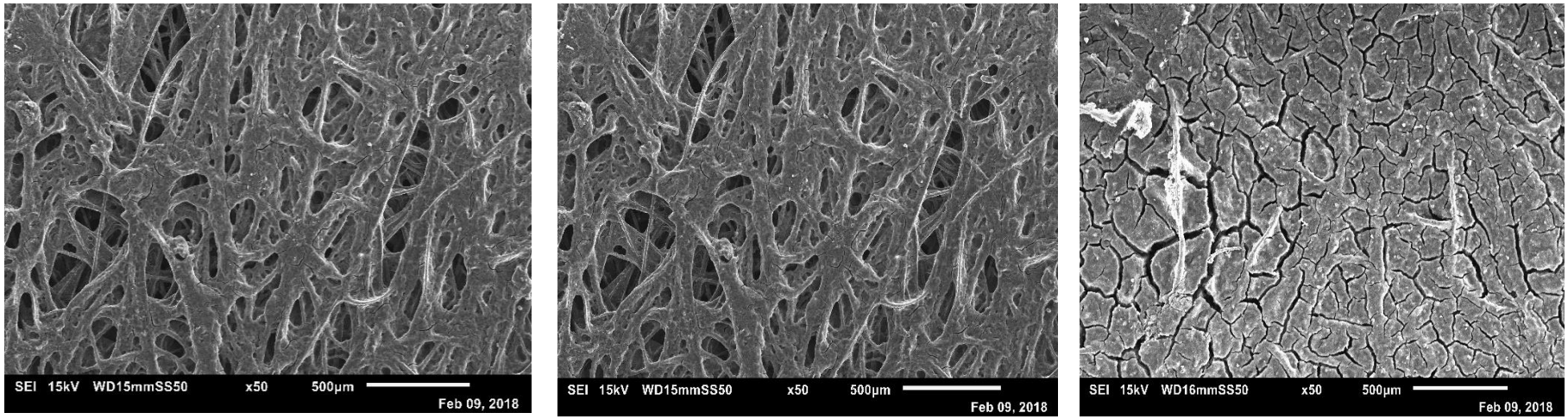

(m) 0.5 mgcm^{-2} (n) 1.0 mgcm^{-2} (o) 2.0 mgcm^{-2}

Figure 4. 7 SEM images of substrates coated with Vulcan XC-72R (a-c) Toray TGP-H-120, (d-f) Toray TGP-H-90, (g-i) SGL 35BA, (j-l) SGL 10CA and (m-o) SGL 10EA.

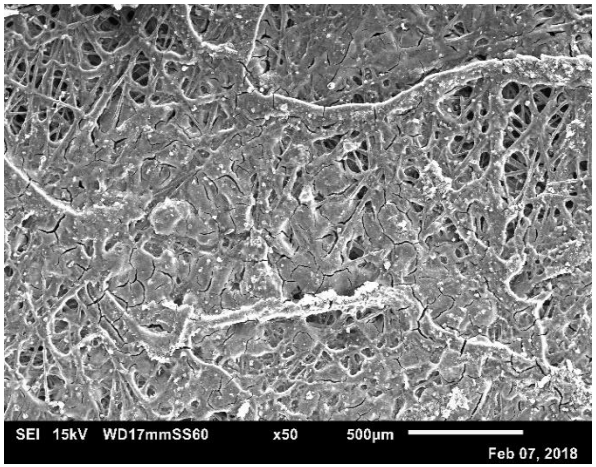

(a) 0.5 mgcm^{-2}

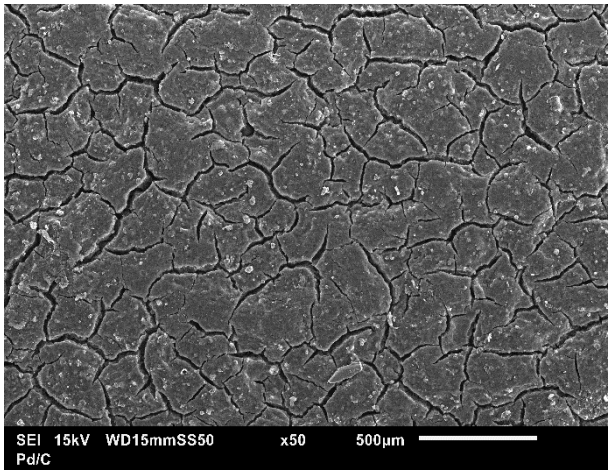

(b) 1.0 mgcm^{-2}

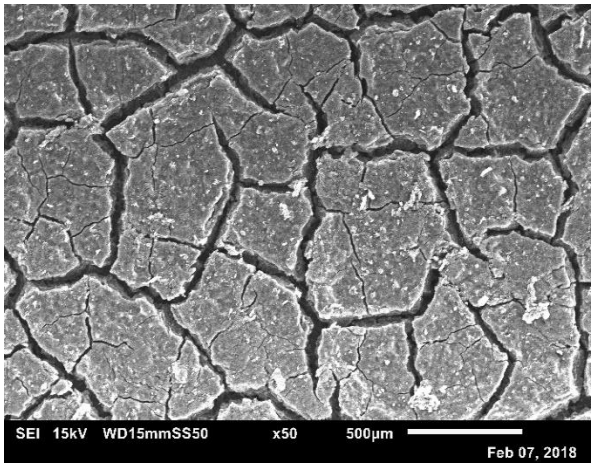

(c) 2.0 mgcm^{-2}

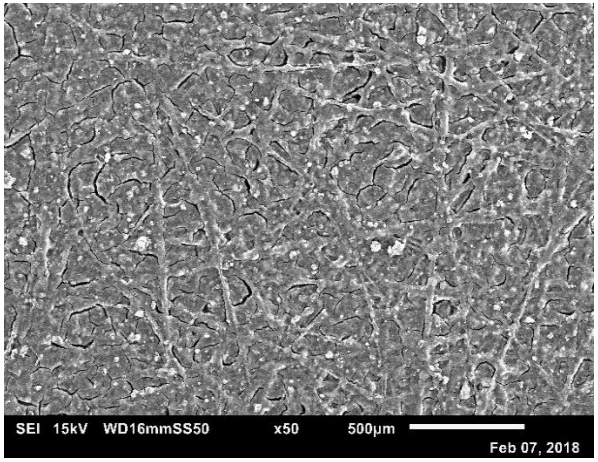

(d) 0.5 mgcm^{-2}

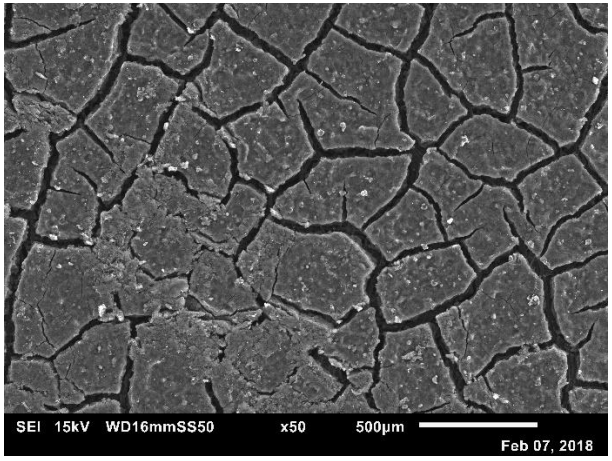

(e) 1.0 mgcm^{-2}

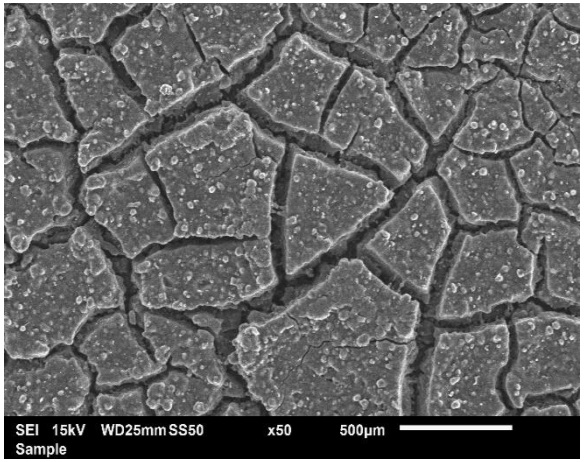

(f) 2.0 mgcm^{-2}

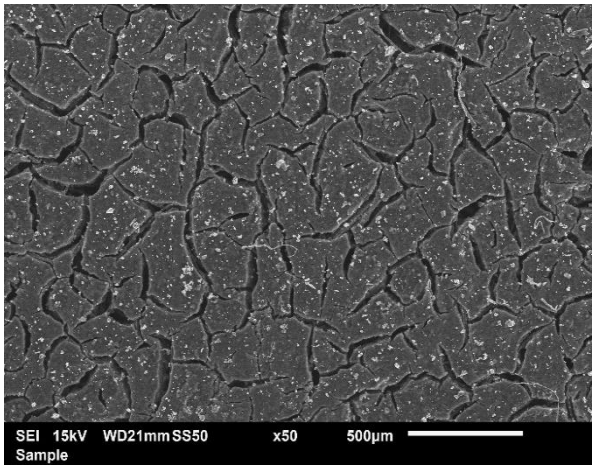

(g) 0.5 mgcm^{-2}

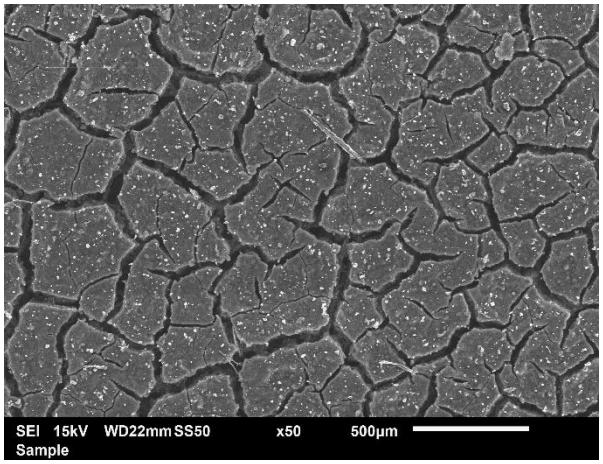

(h) 1.0 mgcm^{-2}

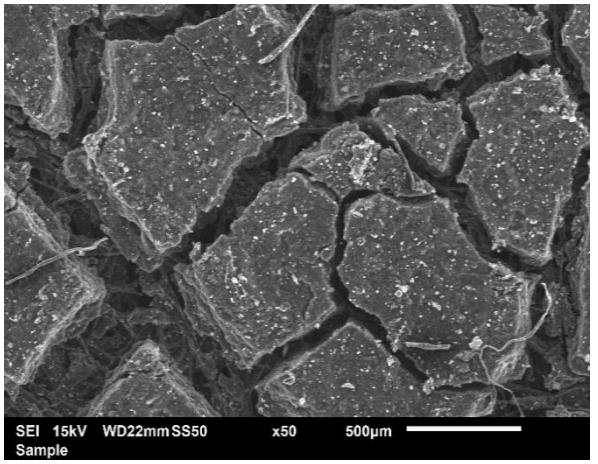

(i) 2.0 mgcm^{-2}

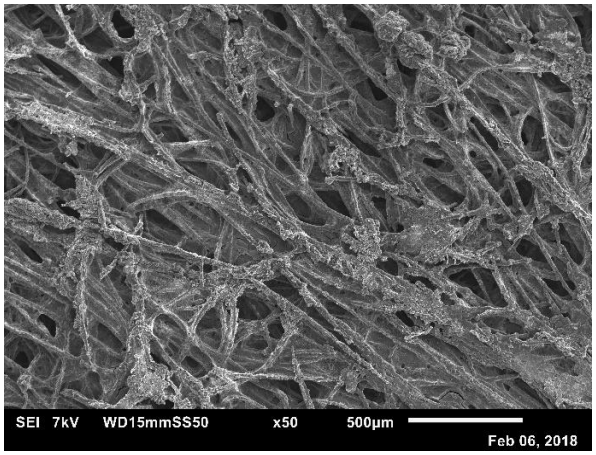

(j) 0.5 mgcm^{-2}

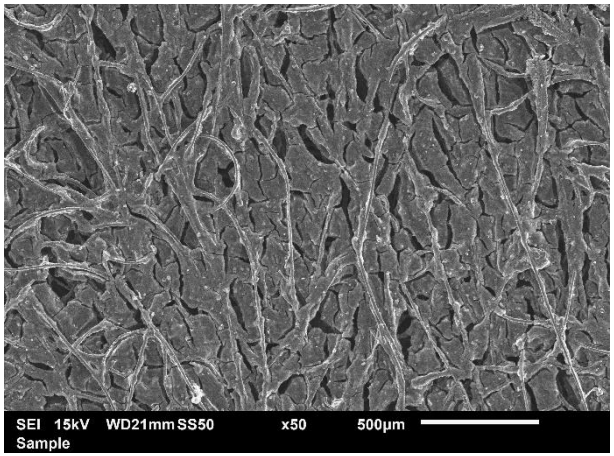

(k) 1.0 mgcm^{-2}

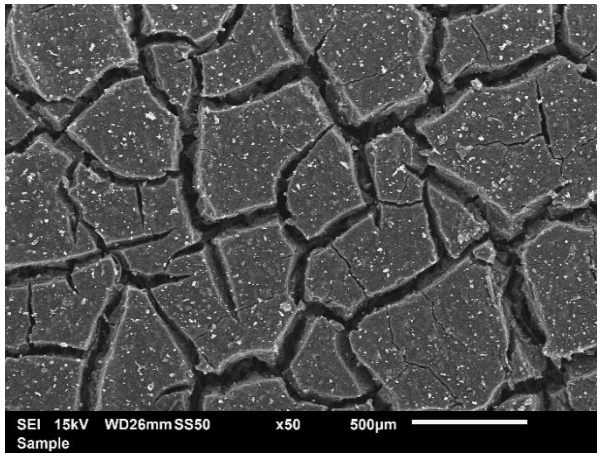

(l) 2.0 mgcm^{-2}

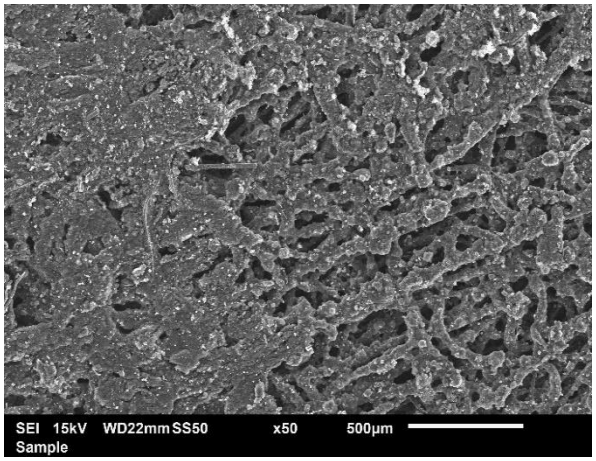

(m) 0.5 mgcm^{-2}

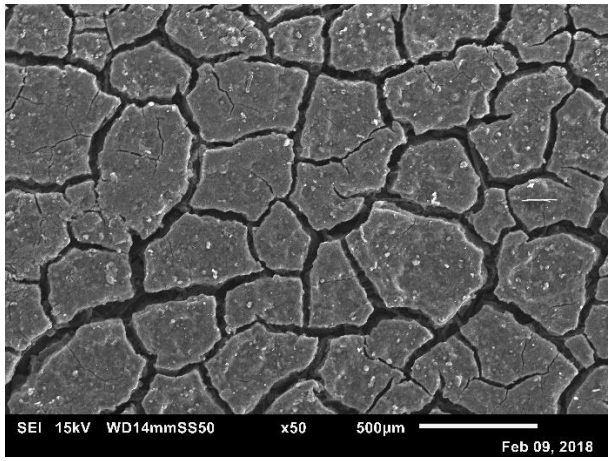

(n) 1.0 mgcm^{-2}

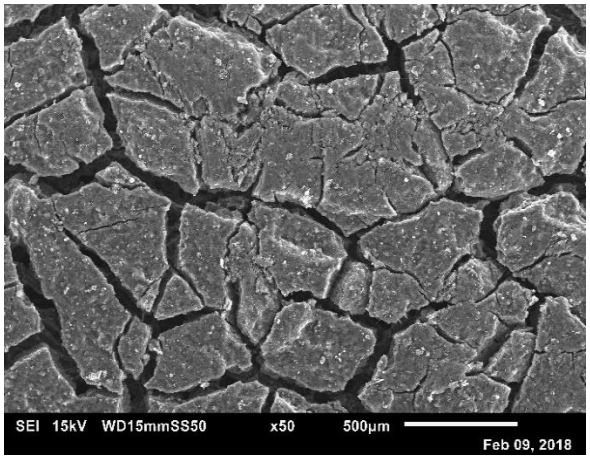

(o) 2.0 mgcm^{-2}

Figure 4. 8 SEM images of substrates coated with Ketjenblack EC-300J (a-c) Toray TGP-H-120, (d-f) Toray TGP-H-90, (g-i) SGL 35BA, (j-l) SGL 10CA and (m-0) SGL 10EA.

As stated previously, the increase in carbon loadings in the MPL increases the thickness of the general GDM (that is, visible MPL thickness). Figure 4.9 illustrates the increase in thickness with the increase in carbon loading for the various substrates and carbon black types with the error bars representing the 95% confidence interval for six samples of each substrate coated and carbon loading used.

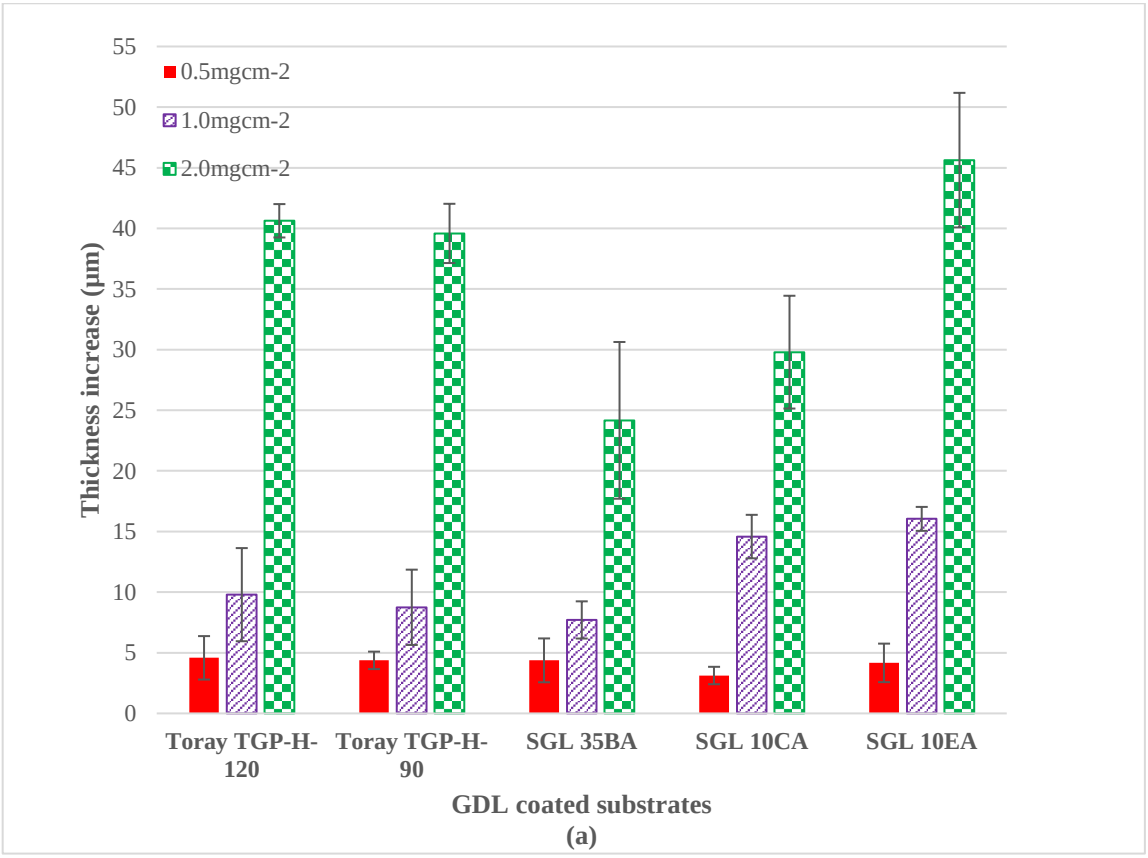

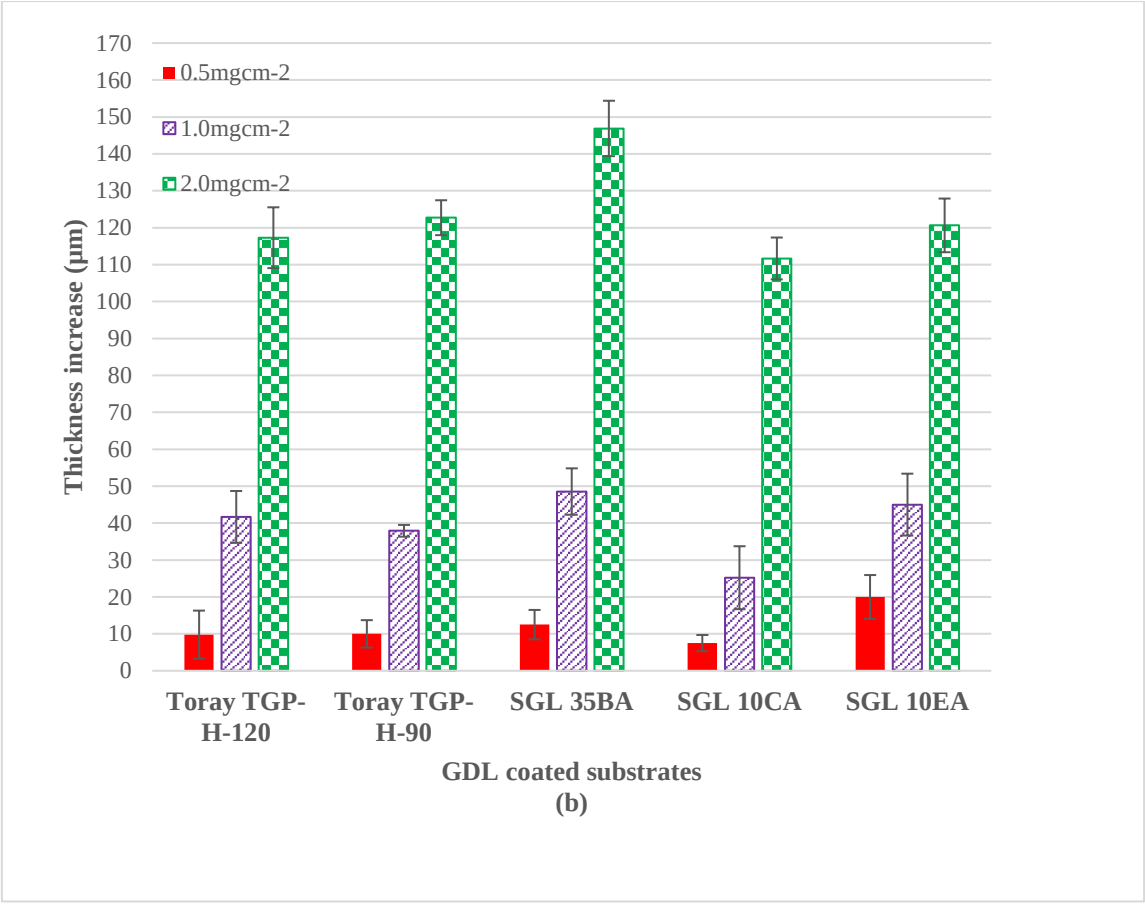

Figure 4. 9 GDL thickness increase for each carbon loading for the various substrates used and coated with the two types of carbon blacks (a) Vulcan XC-72R and (b) Ketjenblack EC-300J

Figure 4.9 (b) clearly identifies the significant increase in thickness for the GDLs coated with Ketjenblack as opposed to Vulcan XC-72R shown in Figure 4.9 (a). As indicated in [82], [127], [128], [144] these variations in thickness were the result of MPL dispersion and penetration into the GDL substrates. Furthermore, such variations in the thickness indicate that the properties of the carbon black affect the properties of the MPL in terms of porosity, pore size distribution and surface morphology [33], [63]. Clearly, in all cases there is an increase in thickness with an increase in carbon loading and this result is independent of the type of carbon black used. This result is in agreement with literature [132], [133], [150]. El-Kharouf et al. [33] indicated Toray TGP-H-120 and Toray TGP-H-90 share similar properties such as porosity and tortuosity. Tortuosity represents the actual path length the fluid passes through the pores to the shortest linear path between two points and porosity

indicates the void or pore-space fraction of the GDM [20]. SGL 35BA was reported to have a slightly higher increase in porosity; however, the tortuosity when compared to that of the Toray carbon papers was found to be far less which would indicate the far less increase when coated with Vulcan XC-72R as shown in Figure 4.9 (a). For the felt like/spaghetti type carbon papers, there is a noticeable increase in thickness with the increase in PTFE in the GDL, as shown in Figure 4.9.

Figure 4.6 shows the through-plane gas permeability as a function of carbon loading. In order to compare the samples, a comparison of percentage reduction in gas permeability as a function of carbon black type and carbon loading would be beneficial to compare similar like structures. Figure 4.10 shows the percentage reduction of through-plane gas permeability from the original sample after coating with each type of carbon black used in this work.

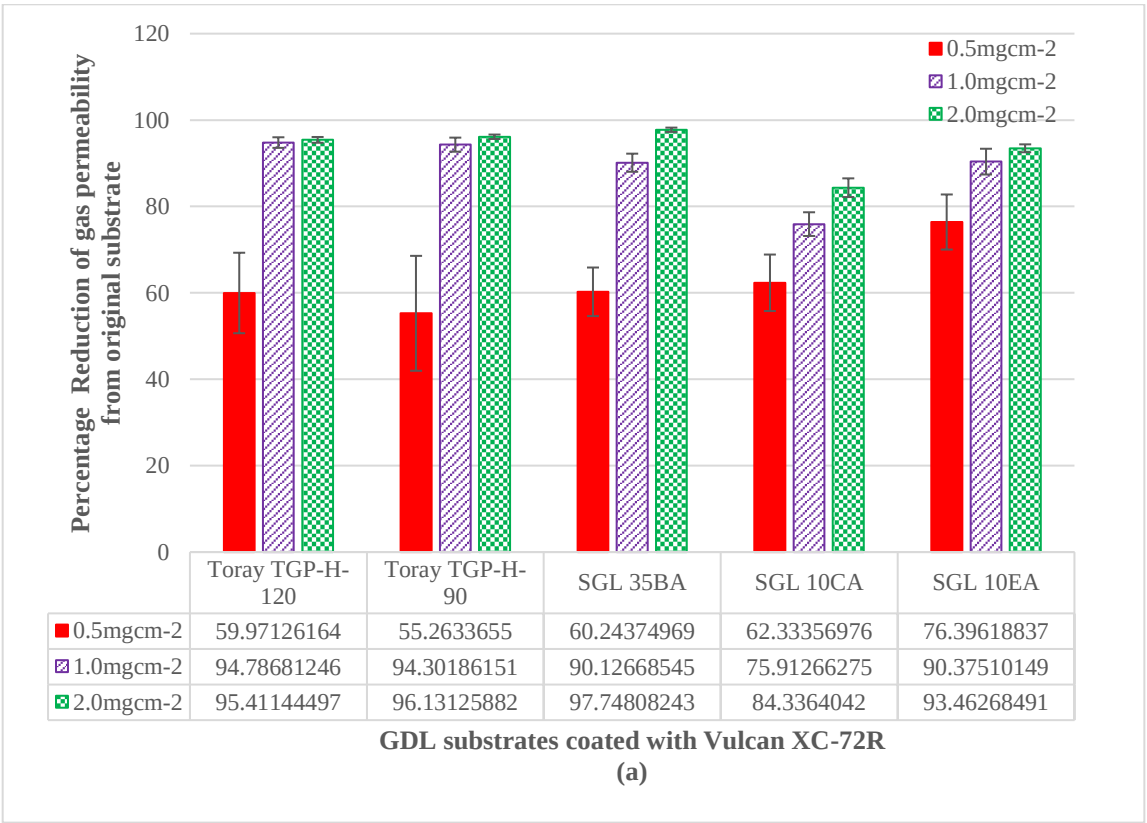

	Toray TGP-H-120	Toray TGP-H-90	SGL 35BA	SGL 10CA	SGL 10EA
0.5mgcm-2	59.97126164	55.2633655	60.24374969	62.33356976	76.39618837
1.0mgcm-2	94.78681246	94.30186151	90.12668545	75.91266275	90.37510149
2.0mgcm-2	95.41144497	96.13125882	97.74808243	84.3364042	93.46268491

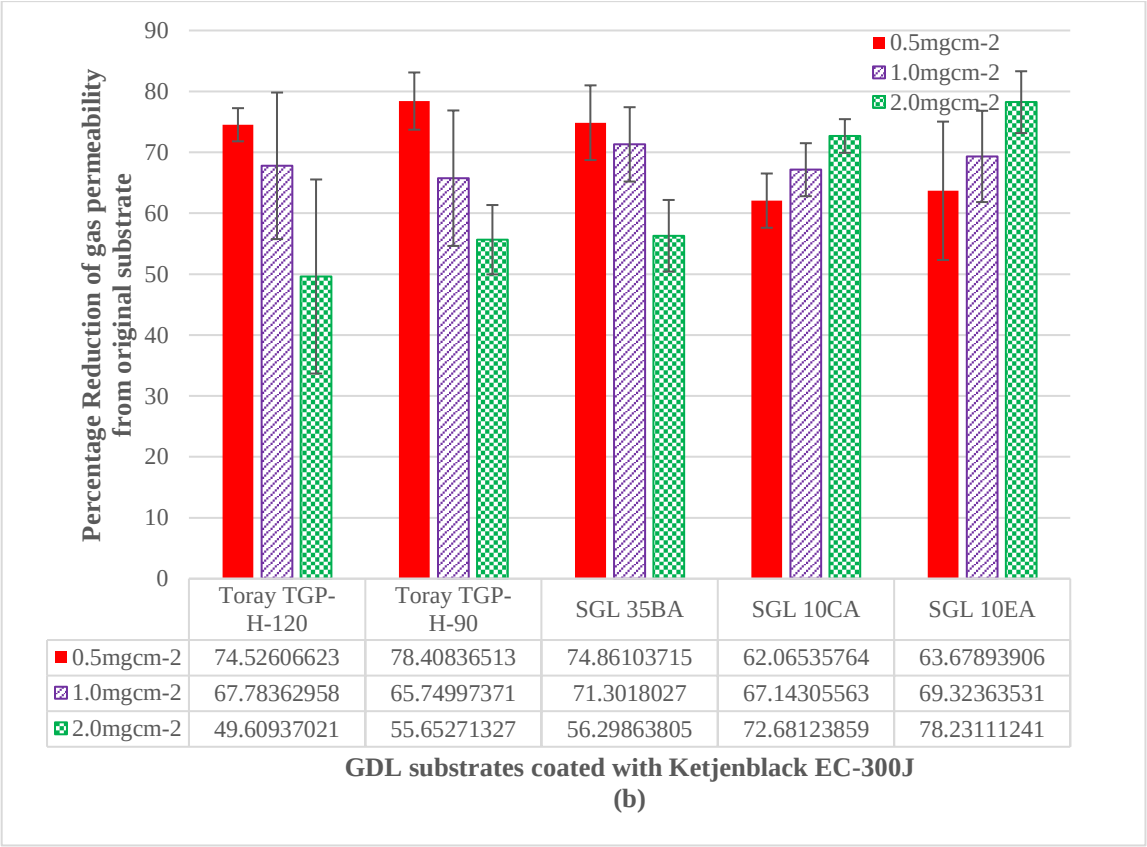

Figure 4. 10 Percentage Reduction in gas permeability from the original substrate for different carbon loadings coated with (a) Vulcan XC-72R and (b) Ketjenblack EC-300J.

A comparison between the percentage reductions in gas permeability for the non-woven straight fibre carbon papers shows similar reductions for each carbon loading and for each carbon type used. In the felt/spaghetti type structures there is a clear distinction in the reduction of gas permeability. This can be attributed to the level PTFE which has resulted in increased thickness as the amount of PTFE was increased as shown in Figure 4.9; Figure 4.7 and 4.8 illustrate the blocking of the pores as the carbon loading increases. It should also be noted that for the samples SGL 10CA and SGL 10EA coated with Vulcan XC-72R there is a noticeable difference in the percentage reduction caused by the level of PTFE increase in the GDL substrates when compared with the relatively small reductions when coated with Ketjenblack EC-300J as the carbon loading was increased. This would imply that the reduction in through-plane gas permeability of the GDM varies depending on the type of carbon black and substrate used; however, depending on the type of carbon black, the level

of PTFE may either have a huge impact or only slight reduction with an increase in carbon loading.

4.3.2.2 Through-plane gas permeability of the microporous layer

The through-plane gas permeability of the MPLs coated onto the various substrates were calculated using equation 3.8 for the two types of carbon blacks used. Two approaches were used to compare the MPL gas permeability, that is, (i) considering no penetration into the GDL (adopted from [94]): this approach considers only the visible thickness of the MPL and the thickness used, that is, L_{MPL}, was determined by simply subtracting the thickness of the GDM, L_{GDM}, from the thickness of the bare carbon substrate, L_{SUB} and by (ii) considering penetration into the GDL with the use of SEM micrographs to determine the actual MPL thickness into the GDL [32], [127]. The through-plane permeability of the MPL when calculated using the actual MPL thickness derived from the SEM images resulted in no distinct trend, which was found not to be in agreement with the results reported in [127] which showed a reduction in MPL permeability with increased carbon loading. This should not be the case as argued by Orogbemi et al. [127] and Ismail et al. [32] Ideally, since the composition of the MPL is the same for all cases, that is, 20 wt.% PTFE and 80 wt.% carbon, regardless of carbon loading the permeability of the MPL should be the same since the gas permeability is an intrinsic property [32], [127]. Figure 4.11 illustrates the MPL permeability, ignoring the penetration into the carbon substrate, that is, using the visible MPL thickness. Figure 4.12 illustrates the MPL gas permeability with increased carbon loading for the case where SEM images are used to determine the actual MPL thickness.

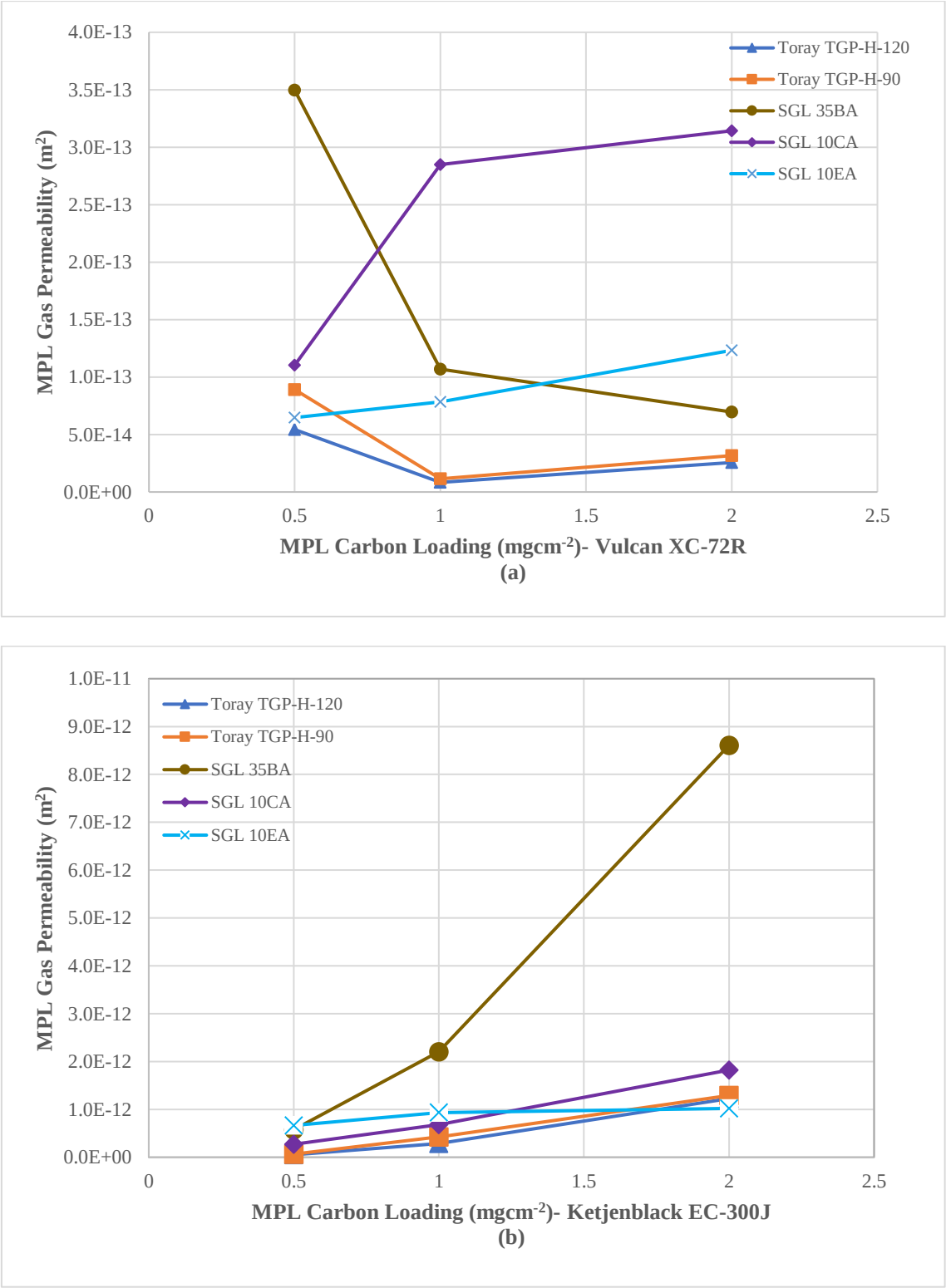

Figure 4. 11 Through-plane gas permeability of the MPL only as a function of increased carbon loading for the carbon black types using the visible thickness determined from the micrometre for GDLs coated with (a) Vulcan XC-72R and (b) Ketjenblack EC-300J.

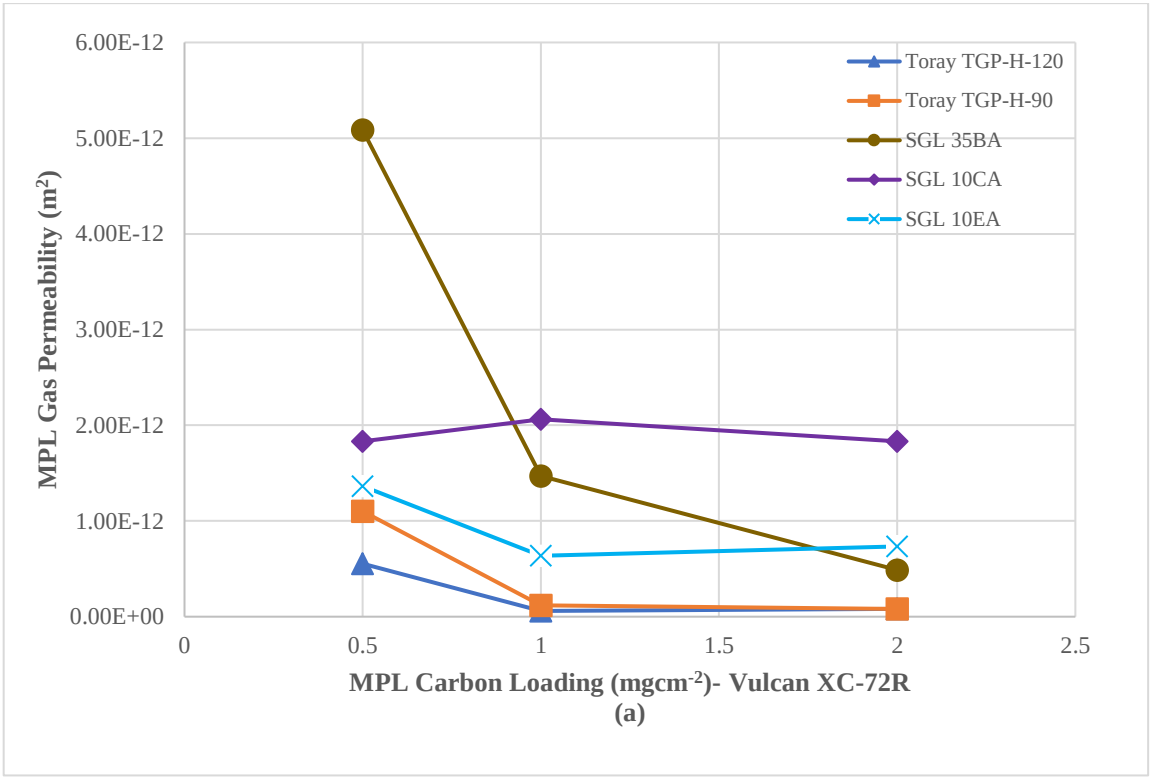

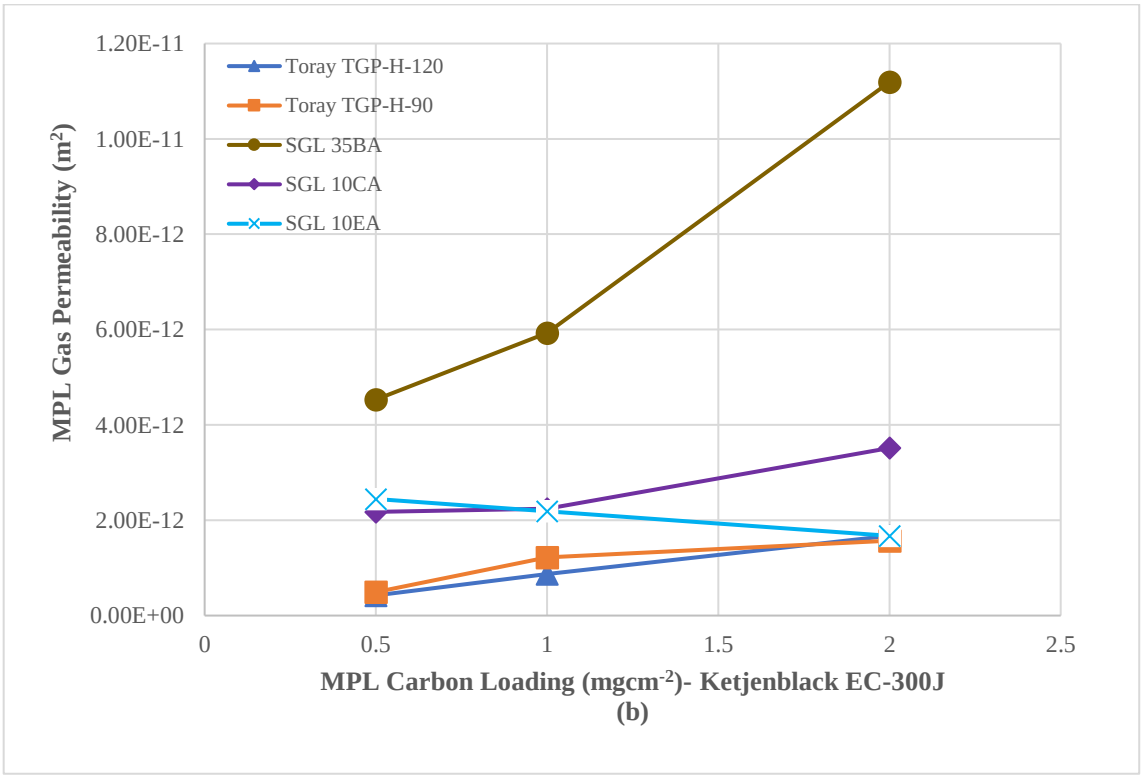

Figure 4. 12 Through-plane gas permeability of the MPL only as a function of increased carbon loading for the carbon black types using the actual MPL thickness derived from SEM cross-section images for GDLs coated with (a) Vulcan XC-72R and (b) Ketjenblack EC-300J.

As such, neither using the results from micrometre measured thickness nor SEM images can truly determine true through-plane permeability of the MPL and this can be attributed to the variations in penetration of the MPL into the GDL. However, what is clear, is that without considering the penetration into the GDL structure, there is a significantly lower value of the MPL permeability. Figure 4.13 and Figure 4.14 illustrates the cross-section SEM images for the three MPL carbon loadings with each GDL substrate for Vulcan XC-72R and Ketjenblack EC-300J respectively. The actual MPL thicknesses are given in Table 4.2 and Table 4.3 for GDLs coated with Vulcan XC-72R and Ketjenblack EC-300J respectively with the listed values representing the mean and 95% confidence interval limits. As shown in Figures 4.13 and 4.14, it is evident that the MPL thickness varies considerably due to variations in the penetration into the GDL substrate and is non-uniform. A comparison between actual MPL thicknesses determined from the SEM images in Figure 4.13 and Figure 4.14 to the MPL thickness determined from the micrometre (shown in Table 4.2 and Table 4.3) shows that the actual MPL thickness is severely underestimated due to the penetration of the MPL into the GDL substrate.

Table 4. 2 Comparison between actual MPL thickness derived from cross-section SEM images for GDLs and thickness increase determined from the micrometre for GDLs coated with Vulcan XC-72R.

Samples	**Thickness of MPL determined from SEM images for carbon loadings (µm)**			**Thickness of MPL determined from micrometre for carbon loadings (µm)**		
	0.5 mgcm^{-2}	**1.0 mgcm^{-2}**	**2.0 mgcm^{-2}**	**0.5 mgcm^{-2}**	**1.0 mgcm^{-2}**	**2.0 mgcm^{-2}**
Toray TGP-H-120	53.334 ± 4.177	72.500 ± 4.816	130.002 ± 13.016	4.583 ± 1.793	9.792 ± 3.840	40.625 ± 1.376
Toray TGP-H-90	63.333 ± 14.685	86.428 ± 15.013	101.820 ± 13.273	4.375 ± 0.719	8.750 ± 3.105	39.583 ± 2.443
SGL 10CA	67.058 ± 14.208	108.571 ± 3.661	172.668 ± 13.805	4.375 ± 1.808	7.708 ± 1.534	24.167 ± 6.463
SGL 10EA	55.342 ± 14.662	115.456 ± 12.446	237.272 ± 16.420	3.125 ± 0.719	14.583 ± 1.793	29.792 ± 4.651
SGL 35BA	96.552 ± 21.405	113.750 ± 32.490	278.572 ± 52.212	4.167 ± 1.589	16.042 ± 0.988	45.625 ± 5.551

Table 4. 3 Comparison between actual MPL thickness derived from cross-section SEM images for GDLs and thickness increase determined from the micrometre for GDLs coated with Ketjenblack EC-300J.

Samples	**Thickness of MPL determined from SEM images for carbon loadings (µm)**			**Thickness of MPL determined from micrometre for carbon loadings (µm)**		
	0.5 mgcm^{-2}	**1.0 mgcm^{-2}**	**2.0 mgcm^{-2}**	**0.5 mgcm^{-2}**	**1.0 mgcm^{-2}**	**2.0 mgcm^{-2}**
Toray TGP-H-120	83.848 ± 5.785	138.750 ± 14.790	185.264 ± 31.430	9.792 ± 6.503	41.667 ± 7.025	117.292 ± 8.232
Toray TGP-H-90	81.905 ± 19.725	125.909 ± 8.863	157.273 ± 11.565	10.000 ± 3.171	37.917 ± 1.589	122.708 ± 4.724
SGL 10CA	114.000 ± 2.829	144.667 ± 13.216	203.634 ± 19.926	7.500 ± 2.195	48.542 ± 6.288	146.875 ± 7.503
SGL 10EA	65.220 ± 6.236	89.000 ± 9.749	239.790 ± 21.139	7.500 ± 2.195	25.208 ± 8.520	111.667 ± 5.669
SGL 35BA	84.668 ± 19.205	113.600 ± 31.223	241.600 ± 9.334	20.000 ± 5.926	45.000 ± 8.380	120.625 ± 7.270

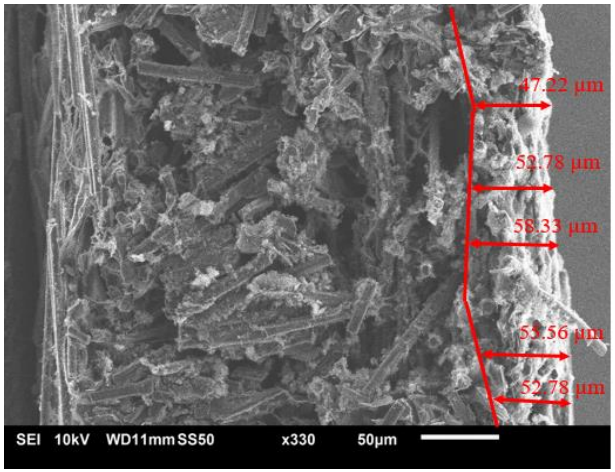

(a) 0.5 mgcm^{-2}

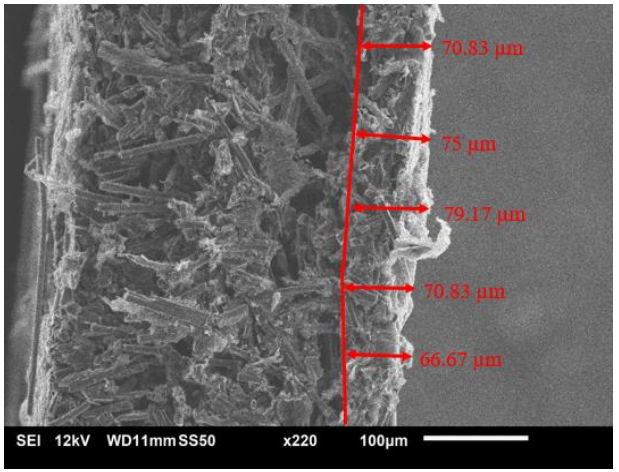

(b) 1.0 mgcm^{-2}

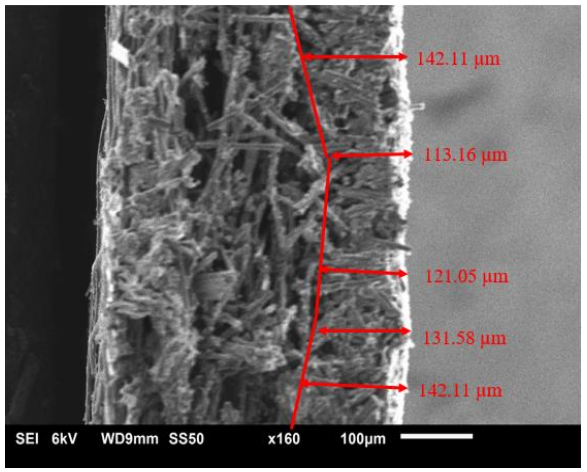

(c) 2.0 mgcm^{-2}

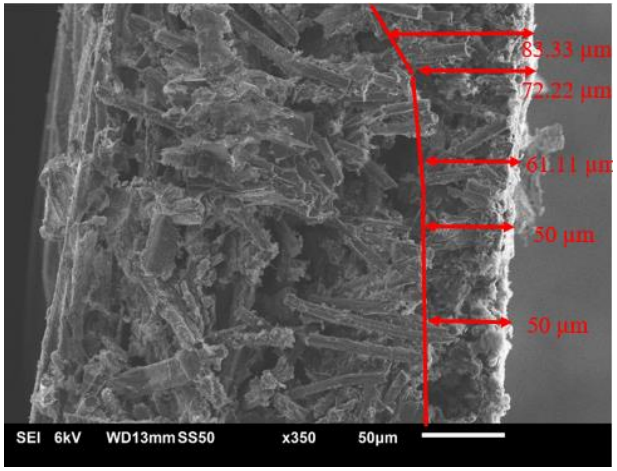

(d) 0.5 mgcm^{-2}

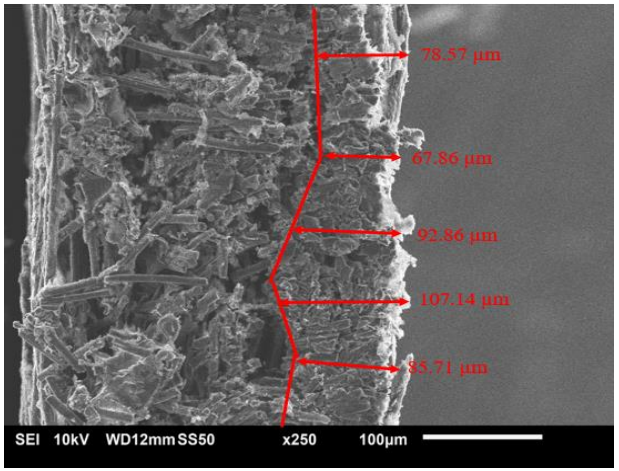

(e) 1.0 mgcm^{-2}

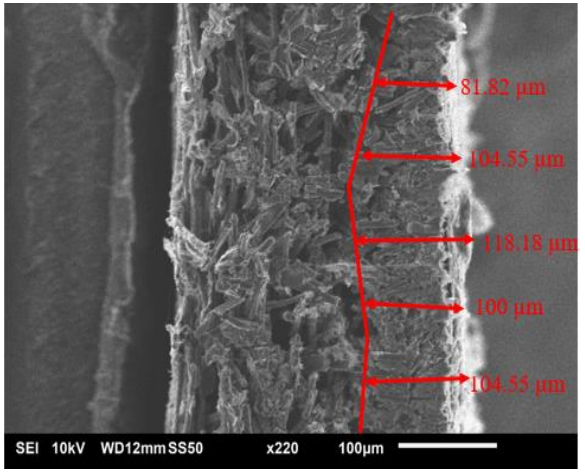

(f) 2.0 mgcm^{-2}

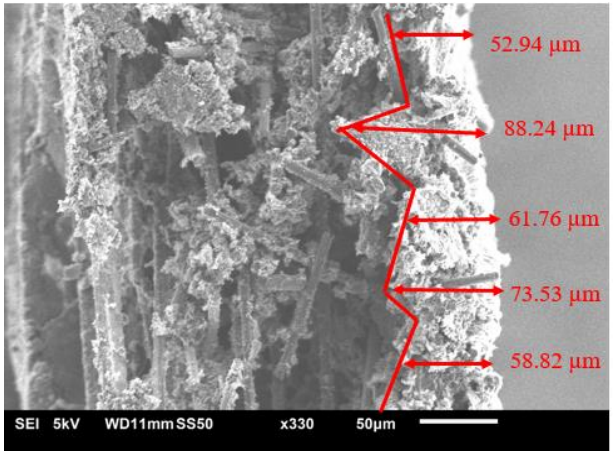

(g) 0.5 mgcm^{-2}

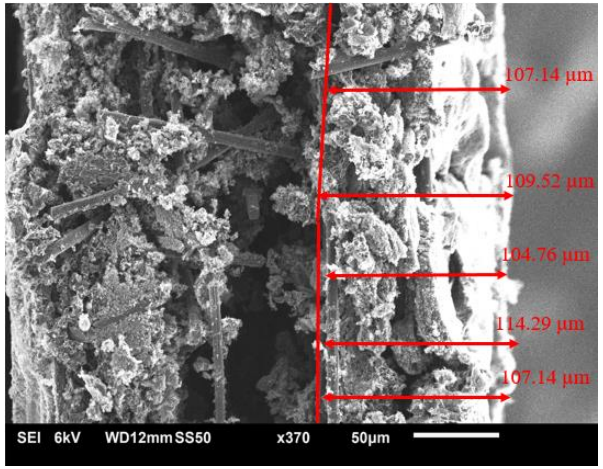

(h) 1.0 mgcm^{-2}

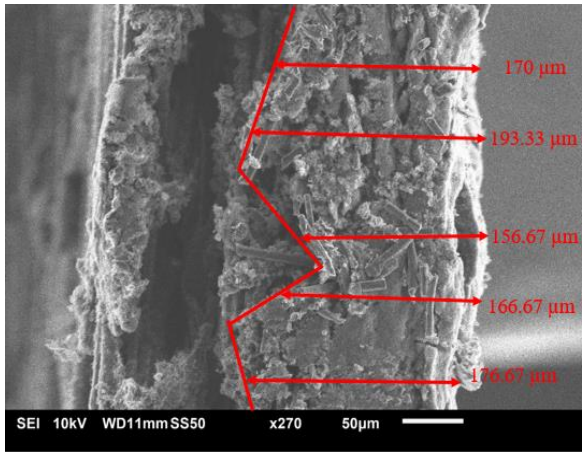

(i) 2.0 mgcm^{-2}

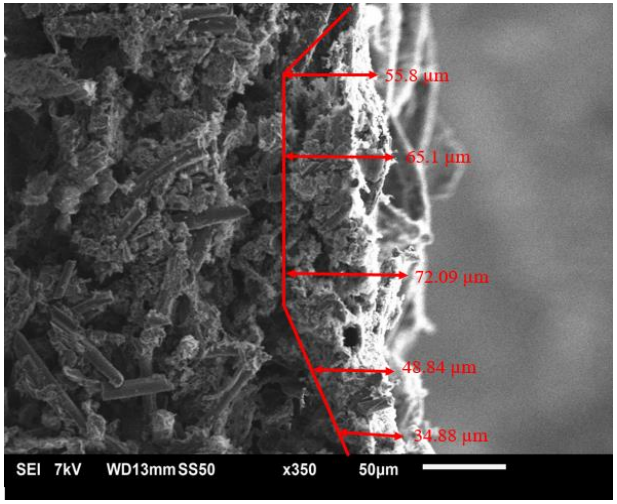

(j) 0.5 mgcm^{-2}

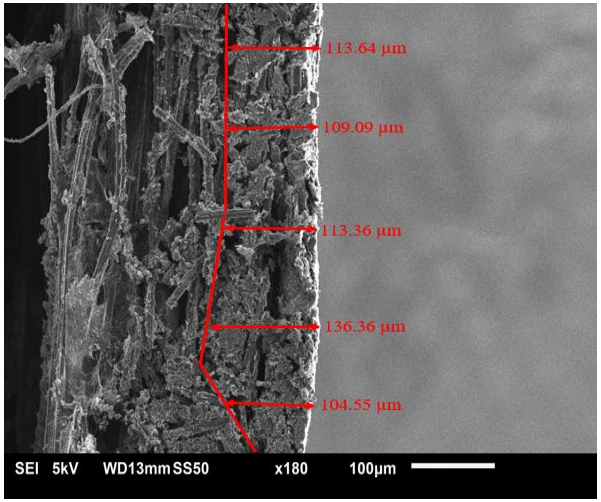

(k) 1.0 mgcm^{-2}

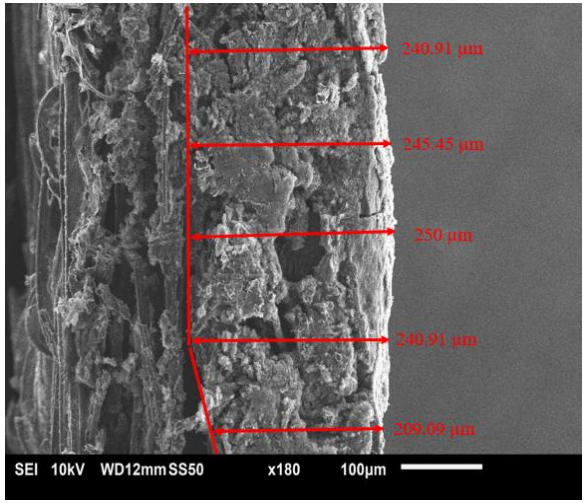

(l) 2.0 mgcm^{-2}

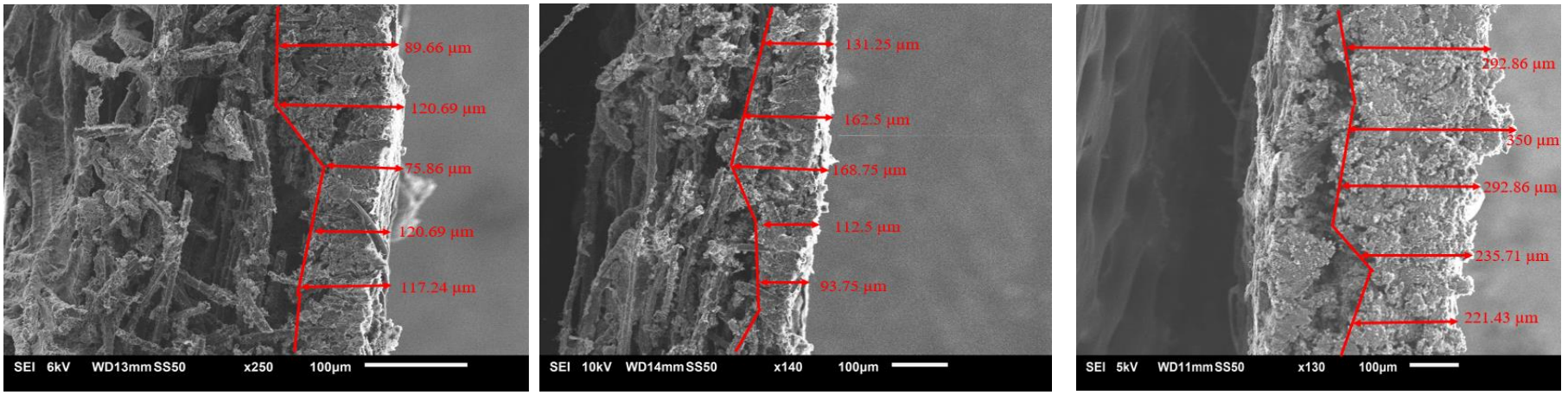

(m) 0.5 mgcm^{-2} (n) 1.0 mgcm^{-2} (o) 2.0 mgcm^{-2}

Figure 4. 13 Cross-section SEM images of substrates coated with Vulcan XC-72R (a-c) Toray TGP-H-120, (d-f) Toray TGP-H-90, (g-i) SGL 35BA, (j-l) SGL 10CA and (m-0) SGL 10EA.

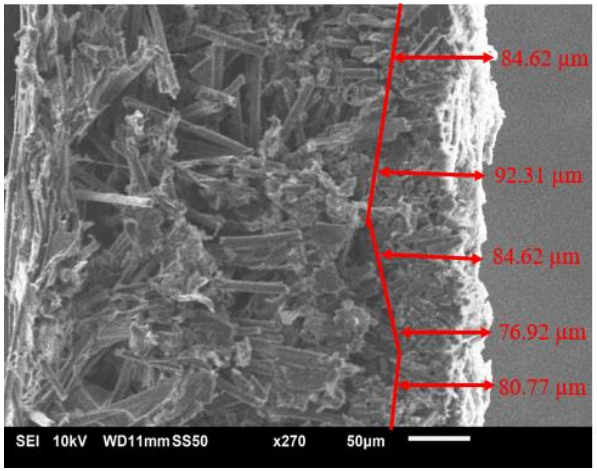

(a) 0.5 mgcm^{-2}

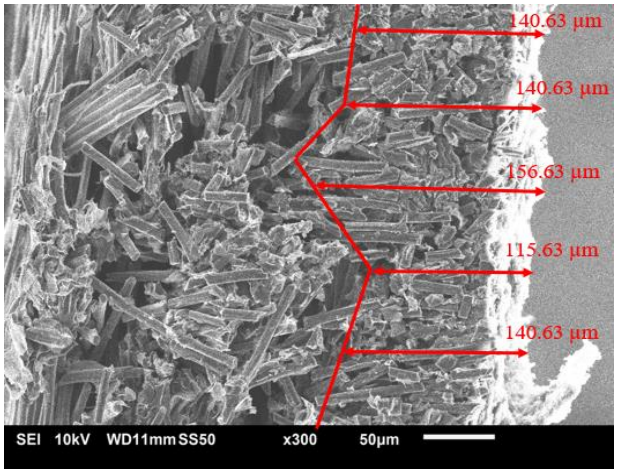

(b) 1.0 mgcm^{-2}

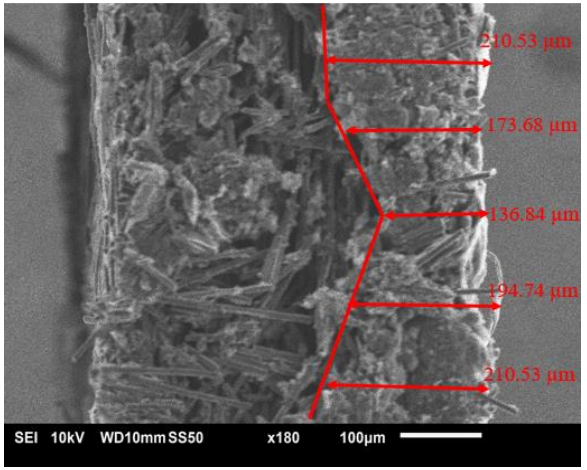

(c) 2.0 mgcm^{-2}

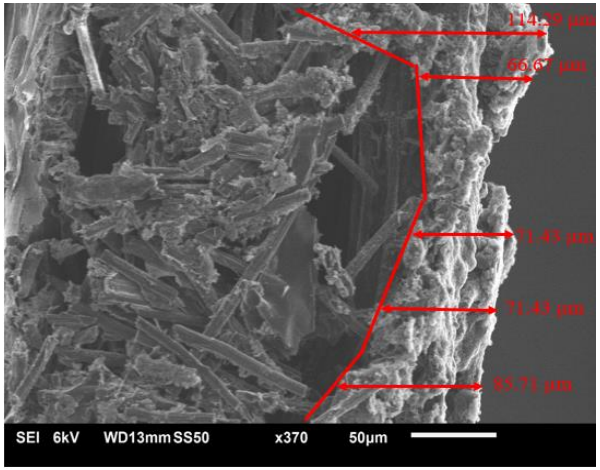

(d) 0.5 mgcm^{-2}

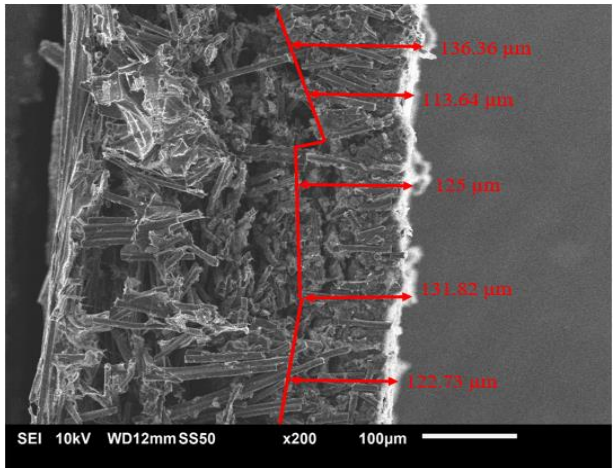

(e) 1.0 mgcm^{-2}

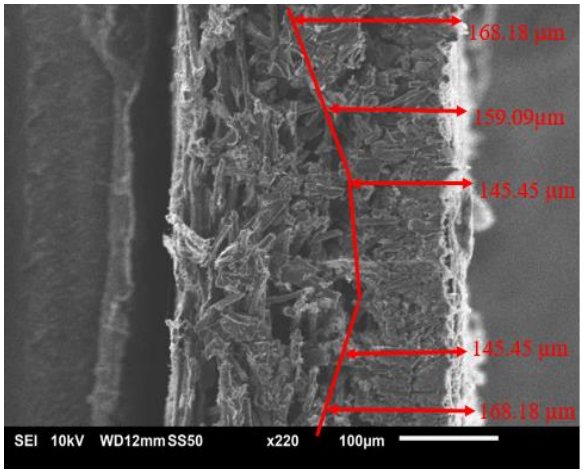

(f) 2.0 mgcm^{-2}

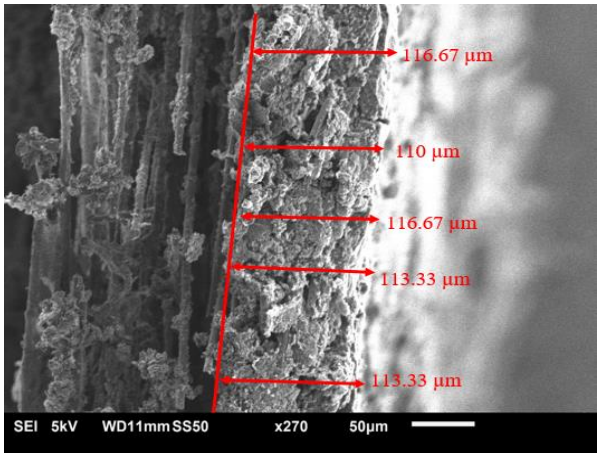

(g) 0.5 mgcm^{-2}

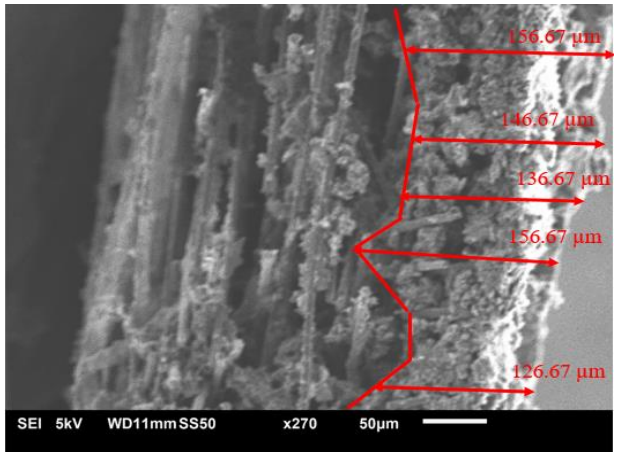

(h) 1.0 mgcm^{-2}

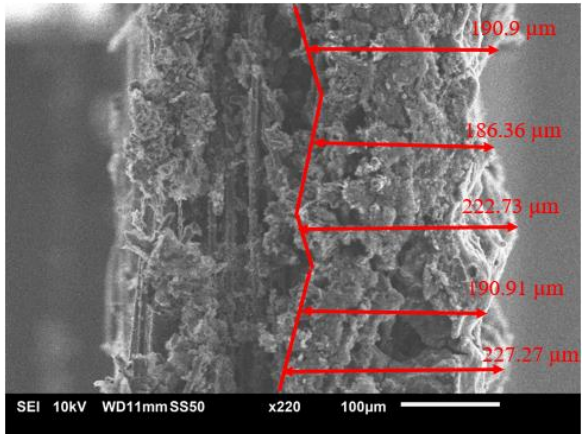

(i) 2.0 mgcm^{-2}

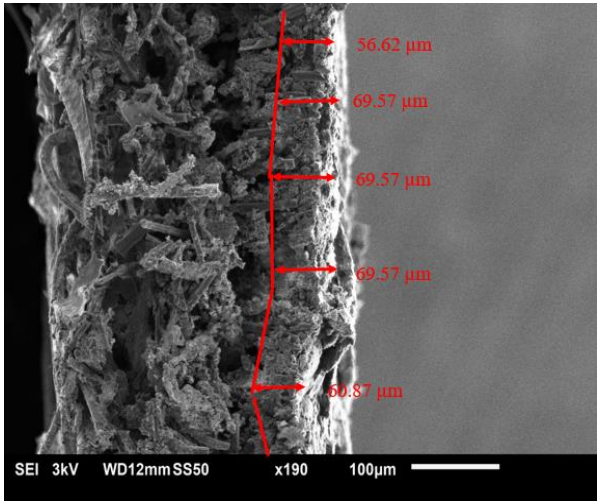

(j) 0.5 mgcm^{-2}

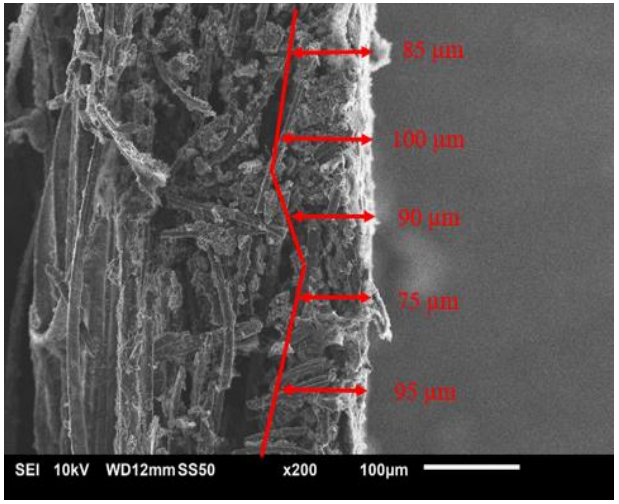

(k) 1.0 mgcm^{-2}

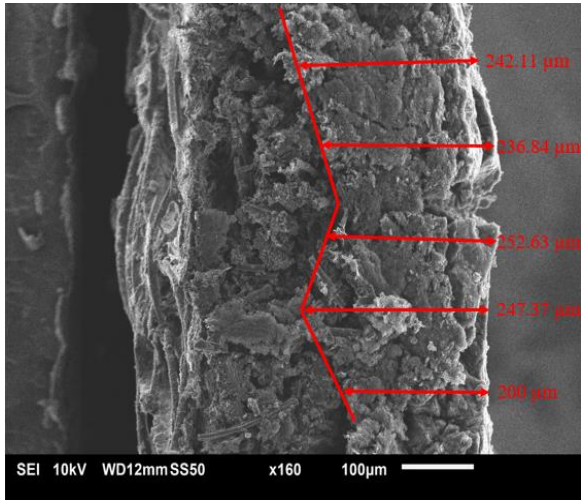

(l) 2.0 mgcm^{-2}

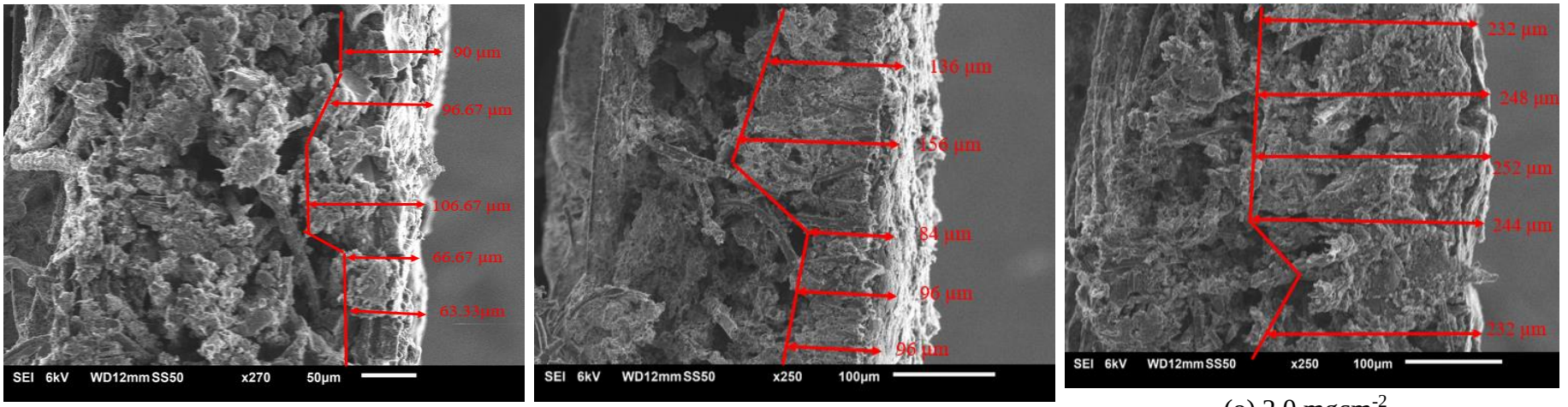

(m) 0.5 mgcm^{-2} (n) 1.0 mgcm^{-2} (o) 2.0 mgcm^{-2}

Figure 4. 14 Cross-section SEM images of substrates coated with Ketjenblack EC-300J (a-c) Toray TGP-H-120, (d-f) Toray TGP-H-90, (g-i) SGL 35BA, (j-l) SGL 10CA and (m-0) SGL 10EA.

4.4 Conclusions

This chapter contains the results of the investigations into the effect of carbon type and carbon loading on GDM through-plane permeability and considers the structural differences in the GDL for two types of carbon fibre papers: non-woven straight and felt/spaghetti. The effect of carbon type and carbon loading for MPLs coated onto these different structured GDLs was carried for three different carbon loadings and two carbon powder types for a constant MPL composition of 80 wt.% carbon powder and 20 wt.% PTFE. The impact of increased PTFE loading in the GDL on the through-plane gas permeability and thickness of the GDM was also explored. SEM images were used investigate the surface morphology of the MPL with different carbon loading and types and to determine the thickness of the MPL which penetrates the GDL. The following conclusions were obtained as follow:

- GDM through-plane permeability does not necessarily decrease with increased carbon loading. The type of carbon powder and loading used in conjunction with the type of GDL substrate was shown to influence the overall GDM through-plane permeability such that carbon powders with a large surface area (Ketjenblack EC-300J) showed the greatest reduction in permeability for low carbon loadings when coated onto non-woven straight carbon fibre papers.
- Surface morphology of the MPLs composed of a carbon powder with a low surface area showed (Vulcan XC-72R) smoother surfaces with smaller crack formation when compared to MPLs composed of a large surface area which showed significantly larger cracks. Furthermore, the combination of non-woven straight carbon fibre papers with a large surface area revealed larger surface crack formations with increased carbon loading when compared to the felt/spaghetti type fibre papers which showed incomplete coating of the surface for low carbon loadings with cracks being

formed as the carbon loadings was increased; however, the permeability of the GDMs utilising felt/spaghetti type fibre papers, decreased with increasing carbon loading independent of the carbon type.

- GDM through-plane permeability was shown to be higher with compositions containing powders with a large surface area. The permeability of the substrates coated with Ketjenblack EC-300J was higher than those that contained Vulcan XC-72R due to less dense, compact structures with increased surface cracks.
- The through-plane permeability of the MPL showed no distinct trend with increased carbon loading and was independent of carbon type despite the MPL composition being kept constant at 80wt.% carbon and 20wt.% PTFE. This was attributed to significant variations of MPL thickness as determined from SEM cross-sectional images.
- GDLs sharing a similar type structure resulted in similar percentage reductions in through-plane permeability from the original substrate when an MPL was applied to it regardless of carbon type and loading. This was predictable given that the MPL composition was kept constant.
- The impact of PTFE in the GDL showed larger percentage reductions from the original GDL substrate permeability with increasing PTFE in the GDL for increasing carbon loadings with lower surface area carbon powders. The increase in PTFE in the GDL also lead to thickness increases in the MPL. For a large surface carbon powder, the percentage reduction in GDM permeability from the original GDL substrate permeability, showed very little impact with increased carbon loading.
- Ignoring the effects of penetration of the MPL into the GDL results in significantly lower values of the of the GDM through-plane permeability by at least an order of magnitude.

The following chapter highlights the impact of GDL structure and composition on the overall through-plane permeability, thickness and surface morphology of the GDM. The effect of carbon powders with different physical properties in conjunction with different structured GDLs was discussed and has led to some insight of how to optimize the GDM to achieve a more desirable structure depending on operating conditions of the fuel cell.

Chapter 5

Effect of Sintering time and Composite Carbon Mixtures on the through-plane gas permeability of PEFC porous Media

5.1 Introduction

There have been several techniques explored in the literature aimed at optimization of the gas diffusion layer (GDL) which differ from the conventional GDL improvements such as infusing it with a hydrophobic agent (PTFE) or the addition of a microporous layer (MPL) to aid in water management [35]. Sintering of the gas diffusion media (GDM) essentially involves the heat treatment of the GDM in an effort to homogenize the distribution of PTFE throughout the layer to render it more hydrophobic[82], [148]. Heat treatment of the GDM is usually carried out at 350 °C in order to allow the PTFE to melt.

Rohendi et al. [131] investigated the effect of sintering temperature on hydrophobicity, surface morphology and electrical conductivity. The results presented in [131] showed maximum hydrophobicity at 350 °C with decreased electrical conductivity for increased sintering temperature below the melting point of PTFE. The effect of sintering is usually discussed by considering the amount of PTFE in relation to electrical conductivity, mass transport and hydrophobicity [100], [131]. Jordan et al. [82] investigated the effect of sintering on fuel cell performance for various carbon loadings between 0.7-2.5 $mgcm^{-2}$ and 10% PTFE, with the use of two different carbon black types in the MPL: Acetylene black and Vulcan XC-72R. The sintering time remained constant in their investigations at 30 minutes. The results indicated improved cell performance at high current densities for carbon

loadings between 1.25-1.9 $mgcm^{-2}$ with acetylene black showing more desirable performance due to a more hydrophobic GDM which allowed for improved water management.

The influence of PTFE content in the GDL on sintering time and temperature was investigated by Bevers et al. [100]. A constant temperature of 390 °C and sintering time of 20 minutes for varying PTFE loadings and varying temperatures with a constant PTFE loading of 180 wt.% with a sintering time of 15 minutes was investigated. The results indicated a decrease in pressure drop of gas flow across the samples (that is, increased gas permeability) with increasing temperatures. It was suggested that this was due to the PTFE being dispersed thoroughly from the voids between fibres to the fibres themselves which allowed improved gas flow through the samples.

Aslam [132] explored the heat treatment of commercial GDMs for varying temperatures between 200-1000 °C in terms of through-plane gas permeability. Through-plane permeability increased with increasing temperatures up to 800 °C due to reduced PTFE content. Bevers et al. [100] reported a 8 wt.% loss and a 10 wt.% loss of PTFE at 360 °C and 420 °C respectively due to evaporation. Undoubtedly, the increase permeability of the samples in [132] was due to evaporation of the PTFE within the GDMs. The through-plane permeability of SGL 10BC (MPL coated GDL) was reported to increase up to 500 °C; however, at temperatures about 800 °C a significant reduction was witnessed. SEM images revealed structural surface degradation of the GDM at 1000 °C with the surface cracks reducing in size.

Orogbemi et al. [128] investigated through-plane gas permeability of GDMs before and after sintering for five different carbon loadings between 0.5-2.5 $mgcm^{-2}$ for MPL composed of two different carbon black types (Vulcan XC-72R and Ketjenblack EC-300J) with a constant

PTFE loading of 20%. The MPL was applied to an SGL 10BA carbon substrate using a spray coating technique. Sintering time was held constant at 30 minutes for a temperature of 350 °C. The results indicated a reduction in through-plane permeability due to a "spreading effect" which allowed the narrowing of cracks on the surface of the MPL. The effect of the carbon type was also highlighted with the MPLs composed of Ketjenblack EC-300J showing a greater reduction in permeability.

Lo et al. [133] and associates [134] investigated the effect of sintering time on gas permeability by considering times at one, five, nine and thirteen hours for a sintering temperature of 350 °C. The results showed increase through-plane permeability and cell performance with increasing sintering time; a sintering time of nine hours showed the most desirable fuel cell performance. The GDM investigated consisted of a Toray TGP-H-120 carbon fibre paper substrate with 20% PTFE in the GDL and 40% PTFE loading in the MPL with the MPL being applied to the GDL via brushing. The MPL consisted of Triton carbon powder; no indication of the carbon loading in the MPL was given. The results presented in [133], [134] contradicts the conclusion by Orogbemi et al. [128] such that the later indicated a decrease in permeability for a sintering time of 30 minutes. It is, however, difficult to compare results due to the fact that different carbon powder types, MPL application technique and PTFE loading in the MPL varied. Orogbemi [136] extended the work on sintering conducted in [128] to include the effect PTFE loading in the MPL for a constant carbon loading of 1.5 $mgcm^{-2}$ utilising Vulcan XC-72R and Ketjenblack EC-300J as the carbon powders. The results indicated a decrease in through-plane permeability for PTFE loadings of 10, 20 and 30% after sintering for MPLs consisting of Vulcan XC-72R and Ketjenblack EC-300J; however, there was an increase in through-plane permeability for both carbon powders with a PTFE loading of 40 wt.% and 50 wt.% which seems in agreement with the results in [133],[134].

Many of the investigations discussed in the literature focused on MPLs composed of only one type of carbon powder with investigations being discussed and compared with other manufactured materials as in [55], [82], [108], [115], [116], [122], [127], [128]. The use of composite carbon mixtures, that is, a combination of at least two carbon-based materials used in the composition has shown promise in improving cell performance.

Stampino et al. [109] investigated a composite mixture of Vulcan XC-72R and carbon nanotubes (CNTs) in a ratio of 90:10 wt.% respectively for a 14 wt.% PTFE loading. The mixture was coated on commercial carbon cloth using the doctor blade technique. Results indicated a thicker MPL when compared to one containing only Vulcan XC-72R, improved cell performance and surprisingly a far lower ohmic resistance even though the thickness of the MPL was doubled. Gharibi et al. [118] also investigated a composite mixture using Vulcan XC-72R and multi-walled carbon nanotubes (MWCNTs) for an optimized PTFE loading of 30 wt.% and carbon content of 70 wt.% for different ratios of MWCNTs to Vulcan XC-72R and an overall carbon loading of 1.0 $mgcm^{-2}$. It was determined that an 80 wt.% MWCNTs showed the highest cell performance and permeability due to MPL structure allowing higher surface concentration of reactants at the catalyst layer because of MWCNTs ability to adsorb oxygen to their surfaces.

Wang et al. [113] combined two carbon blacks: acetylene black (AB) and black pearls 2000 (BP) in a composite mixture to investigate the effect on fuel cell performance. The ratio of AB to BP in the MPL was 80:20 wt.% respectively for a constant carbon loading of 1.0 $mgcm^{-2}$ and a PTFE loading of 30 wt.%. The MPL was applied to a carbon fibre paper, Toray TGP-H-30, using a doctor blade technique. Physical properties such as surface area, pore volume and contact angle of the composite mixture showed similar trends such that, the mixture lay in-between the bounds of the two separate carbon powders. The permeability of

the composite mixture also followed a similar trend for the AB to BP ratio 80:20 wt.% such that numerically it was closer to that of the permeability of a GDL coated with a MPL composed of 100% AB. Lastly, Wang et al. [113] determined an optimum ratio of 10wt% resulted in the highest fuel cell performance.

The effect of sintering time on through-plane permeability of GDMs is still unclear as reported above. Further experiments are therefore necessary to elaborate the impact of sintering time on gas permeability. This chapter reports the investigations conducted on several different sintering time utilising different carbon powder types and varying PTFE loading in the MPL. Also, a more detailed look at the effect of composite mixtures on through-plane permeability and surface morphology is investigated for different carbon loadings and carbon types in the MPL with a constant PTFE loading.

5.2 Materials and Methods

An in-house gas permeability setup was used to determine the through-plane permeability as discussed in Section 3.3.4 and preparation of the samples and data analysis involved in this chapter was described previously in Section 3.3.3 and 3.3.5 respectively. The experiments involving the sintering of samples were carried out with the cylindrical furnace described in Section 3.3.7. GDM samples were prepared using two types of carbon powders (Vulcan XC-72R and Ketjenblack EC-300J). The GDLs used in the sintering experiments were Toray TGP-H-60 and SGL 35BA carbon fibre papers. Four (4) samples each of Toray TGP-H-60 and SGL 35BA were coated with a MPL composed of 80 wt.% carbon powder and 20 wt.% PTFE for a constant carbon loading of 1.0 $mgcm^{-2}$ and for each carbon powder type (a total of eight of each GDL substrates were used, four for each carbon powder type). Two (2) commercial GDMs were using in the investigation of sintering with varying PTFE content in the MPL. Four (4) samples of SGL 10BC and SGL 10BE were used to investigate

the effect of PTFE loading on GDM through-plane permeability for varying sintering times. The sintering times for the above samples were held at 30 minutes, 2 hours, 4 hours, 6 hours and 8 hours at 350 °C. A pre-processing heat treatment was carried out for the in-house prepared samples on Toray TGP-H-60 and SGL 35BA such that they were treated at 120 °C for 1 hour and 280 °C for 30 minutes before proceeding to the variable timed stage at 350 °C. It should be noted that before inserting the samples into the furnace, samples were positioned in a glass crucible with the MPL side facing upwards. Samples were removed from the furnace upon completion of the variable timed stage and were not left for the furnace temperature to return to the ambient temperature.

The MPL containing composite mixtures involved different ratios of Vulcan XC-72R to Ketjenblack EC-300J coated onto an SGL 10EA substrate. Six (6) samples were prepared for each of the carbon loadings (1.0 $mgcm^{-2}$ and 2.0 $mgcm^{-2}$) and for each carbon powder ratio of 80:20, 50:50 and 20:80 wt.% Vulcan XC-72R to Ketjenblack EC-300J respectively. The total MPL composition was held constant for 80 wt.% carbon powder and 20 wt.% PTFE.

5.3 Results and discussion

5.3.1 Through-plane permeability of the gas diffusion layer substrates.

The through-plane gas permeability of the GDL substrates used in these investigations are listed in Table 5.1 below, before application of the MPL onto the substrates. Gas permeability was estimated experimentally by fitting the data, determined from the dependence of fluid velocity on pressure drop, to Equation 3.4. The listed values presented in Table 5.1 represent the mean and 95% confidence interval limits for the through-plane gas permeability and thickness for the eight (8) samples each of Toray TGP-H-60 and SGL

35BA and thirty-six (36) samples of SGL 10EA. Figure 5.1 illustrates the relationship between the pressure gradient across the substrates to the fluid velocity used in estimation of the gas permeability of the samples. Figure 5.2 shows the relationship of the pressure gradient versus fluid velocity for each GDL with the error bars representing the 95% confidence interval about the mean. The linearity of the pressure gradient to fluid velocity relationship for the samples investigated, justifies the use of Darcy's law.

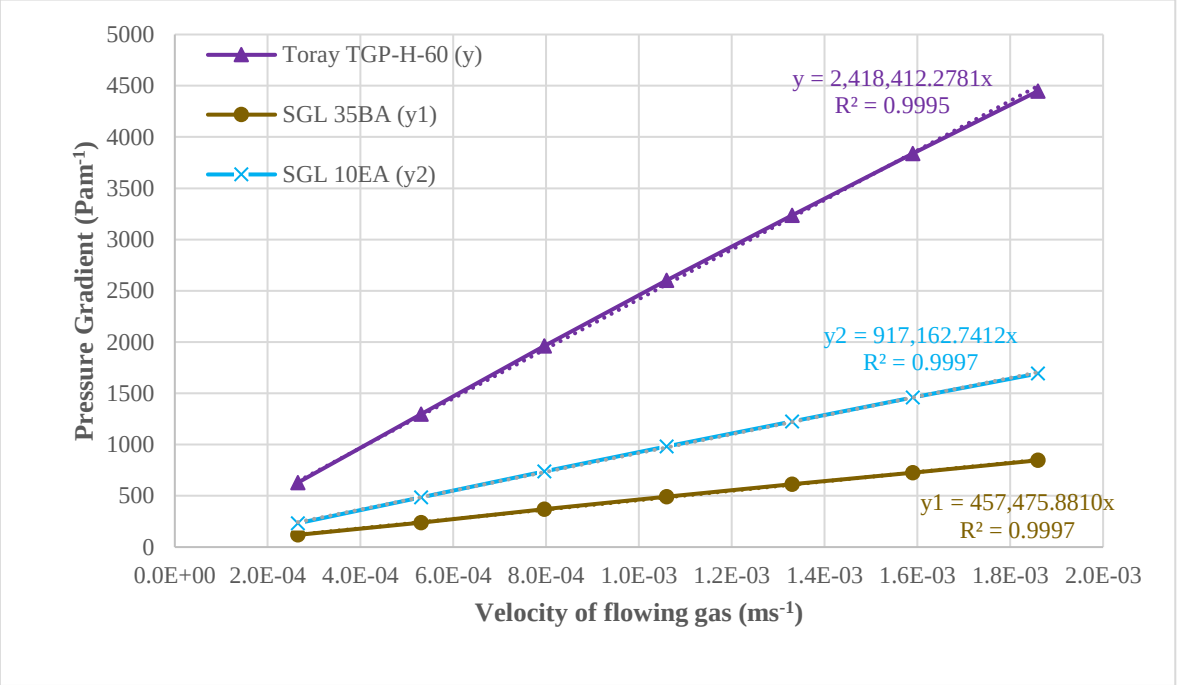

Figure 5. 1 Experimental data for the pressure gradient as a function of fluid velocity for the GDL substrates used.

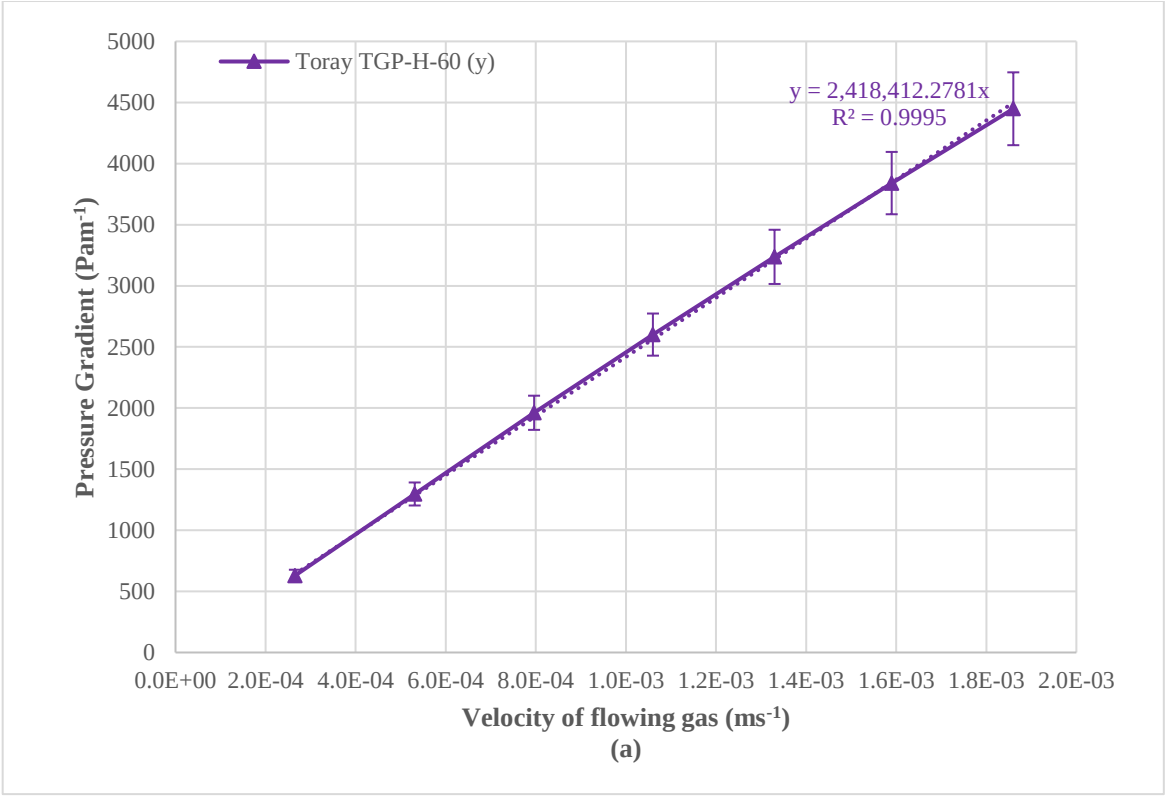
Toray TGP-H-60 (y)
y = 2,418,412.2781x
R² = 0.9995
Pressure Gradient (Pam-1)
5000
4500
4000
3500
3000
2500
2000
1500
1000
500
0
0.0E+00 2.0E-04 4.0E-04 6.0E-04 8.0E-04 1.0E-03 1.2E-03 1.4E-03 1.6E-03 1.8E-03 2.0E-03
Velocity of flowing gas (ms-1)

(a)

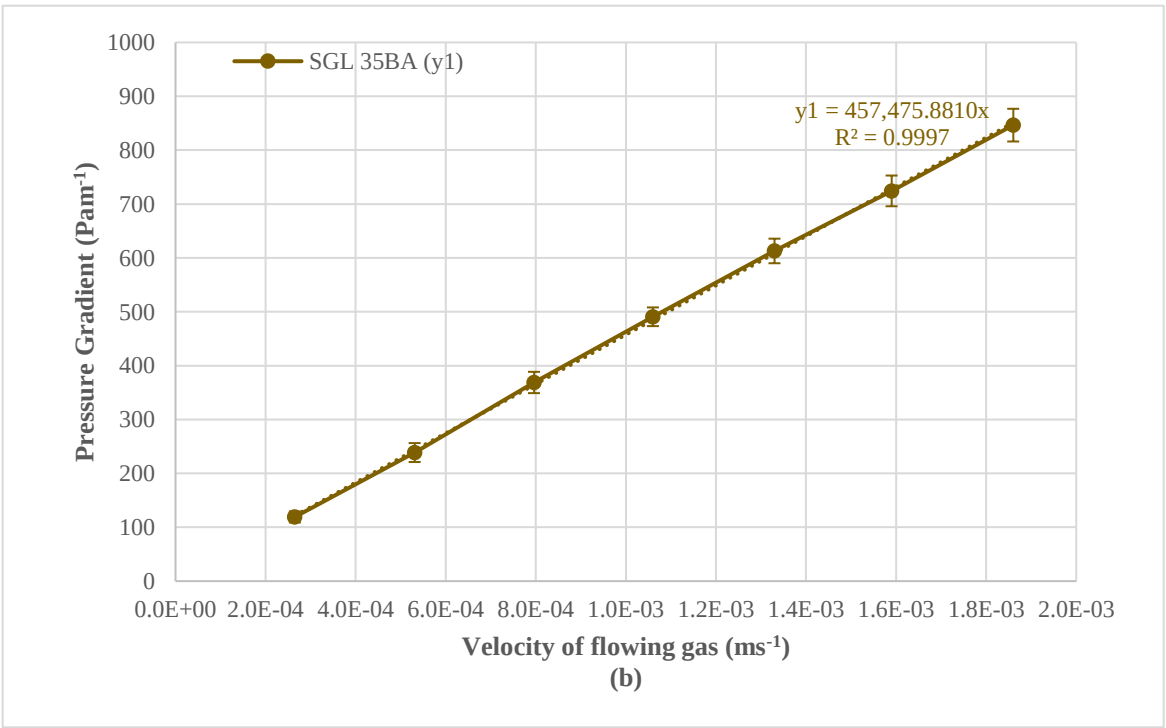
SGL 35BA (y1)
y1 = 457,475.8810x
R² = 0.9997
Pressure Gradient (Pam-1)
1000
900
800
700
600
500
400
300
200
100
0
0.0E+00 2.0E-04 4.0E-04 6.0E-04 8.0E-04 1.0E-03 1.2E-03 1.4E-03 1.6E-03 1.8E-03 2.0E-03
Velocity of flowing gas (ms-1)

(b)

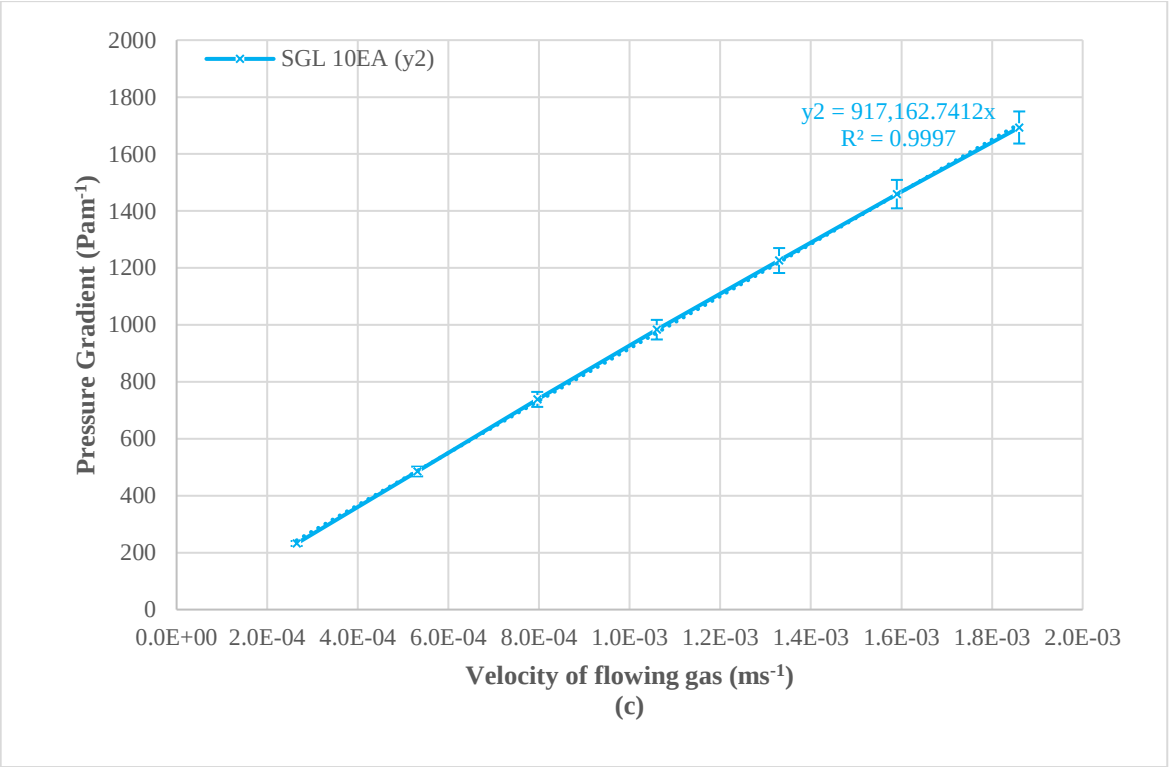

Figure 5. 2 Experimental data for pressure gradient as a function of fluid velocity for (a) Toray TGP-H-60, (b) SGL 35BA and (c) SGL 10EA showing the 95% confidence interval about the mean.

Table 5. 1 Through-plane permeability of tested GDL substrates.

GDL substrates	**Permeability** $k \times 10^{-12}(\mathrm{m}^2)$	**Thickness** $(\mu\mathrm{m})$
Toray TGP-H-060	7.482 ± 0.464	193.281 ± 3.302
SGL 35BA	39.448 ± 1.789	292.188 ± 4.564
SGL 10EA	19.818 ± 0.662	383.611 ± 6.852

The results presented here are compared with those of Chapter 4. The through-plane permeability of SGL 10EA was slightly higher than the value obtained previously (18.772×10^{-12} m^2); however, it was established previously that there is variability of samples between sheets as a result of fabrication uncertainties [31] Toray TGP-H-60 shows structural similarity to that of Toray TGP-H-90 (6.906×10^{-12} m^2) and Toray TGP-H-120 (5.701×10^{-12} m^2) and as such should show a higher permeability due to its reduced thickness [33]. Figure 5.3 shows the SEM images of the bare carbon substrates used in these investigations.

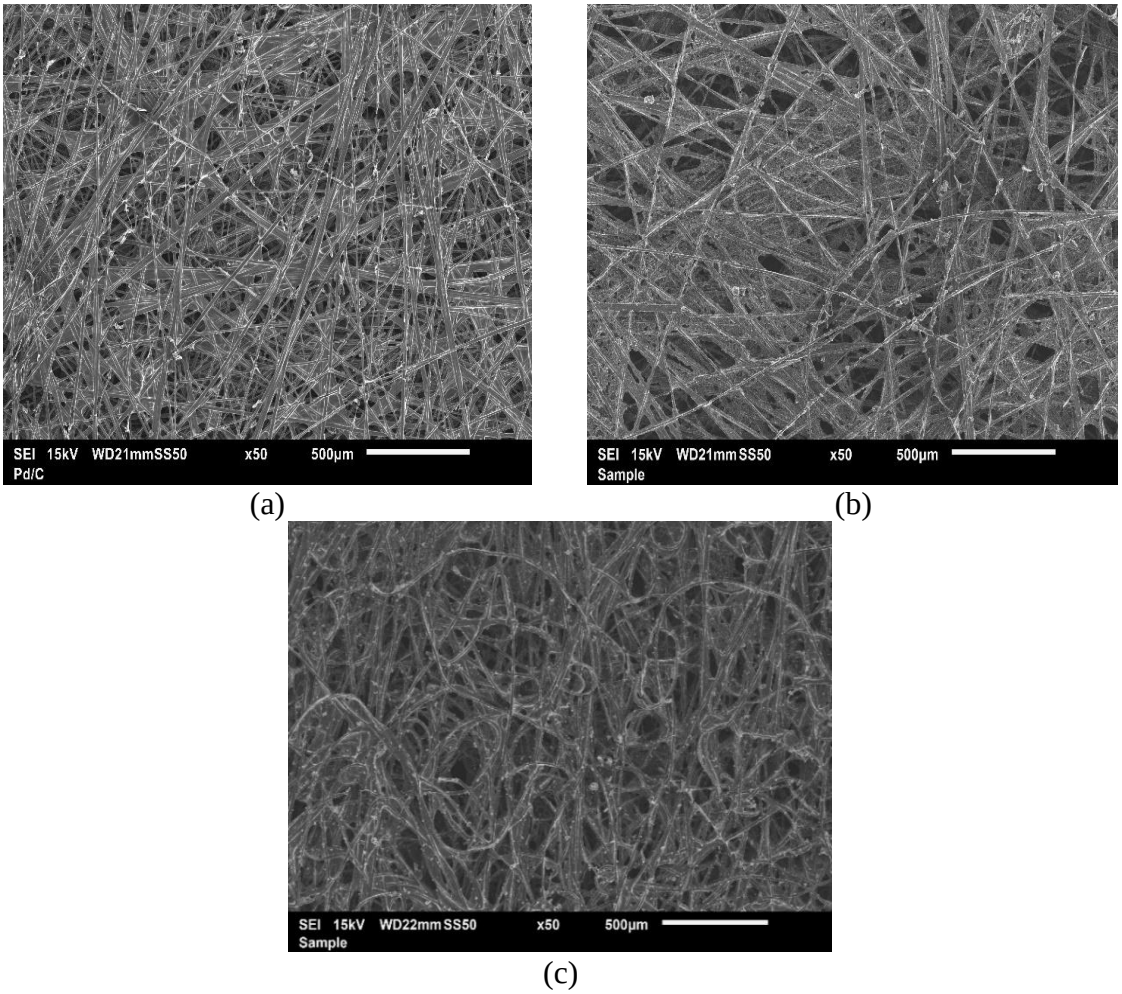

(a) (b)

(c)

Figure 5. 3 SEM micrographs for (a) Toray TGP-H-60, (b) SGL 35BA and (c) SGL 10EA.

5.3.2 Through-plane permeability of the gas diffusion media

The through-plane gas permeability of the GDMs used in the two investigations are listed in Table 5.2 below. Gas permeability was estimated in a similar manner as described above in Section 5.3.1. The listed values presented in Table 5.2 represent the mean and 95% confidence interval limits for the through-plane gas permeability and thickness of the GDMs. Figure 5.4 (a-d) illustrates the relationship between the pressure gradient across the GDM substrates to the fluid velocity used in estimation of the gas permeability of the samples GDL with the error bars representing the 95% confidence interval about the mean. It should be noted that, the SGL 10BC samples exceeded the range of the pressure sensor used and as a result eight (8) lower, equally spaced flow rates were used.

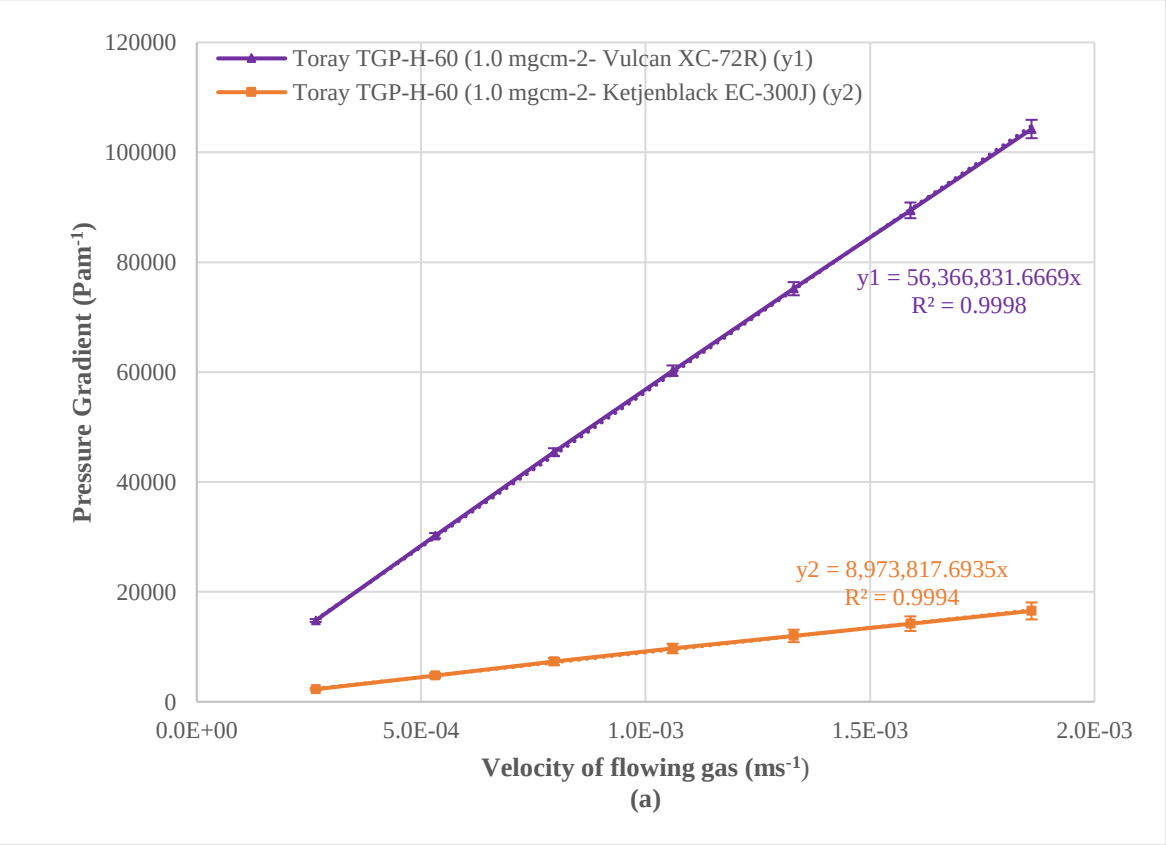

(a)

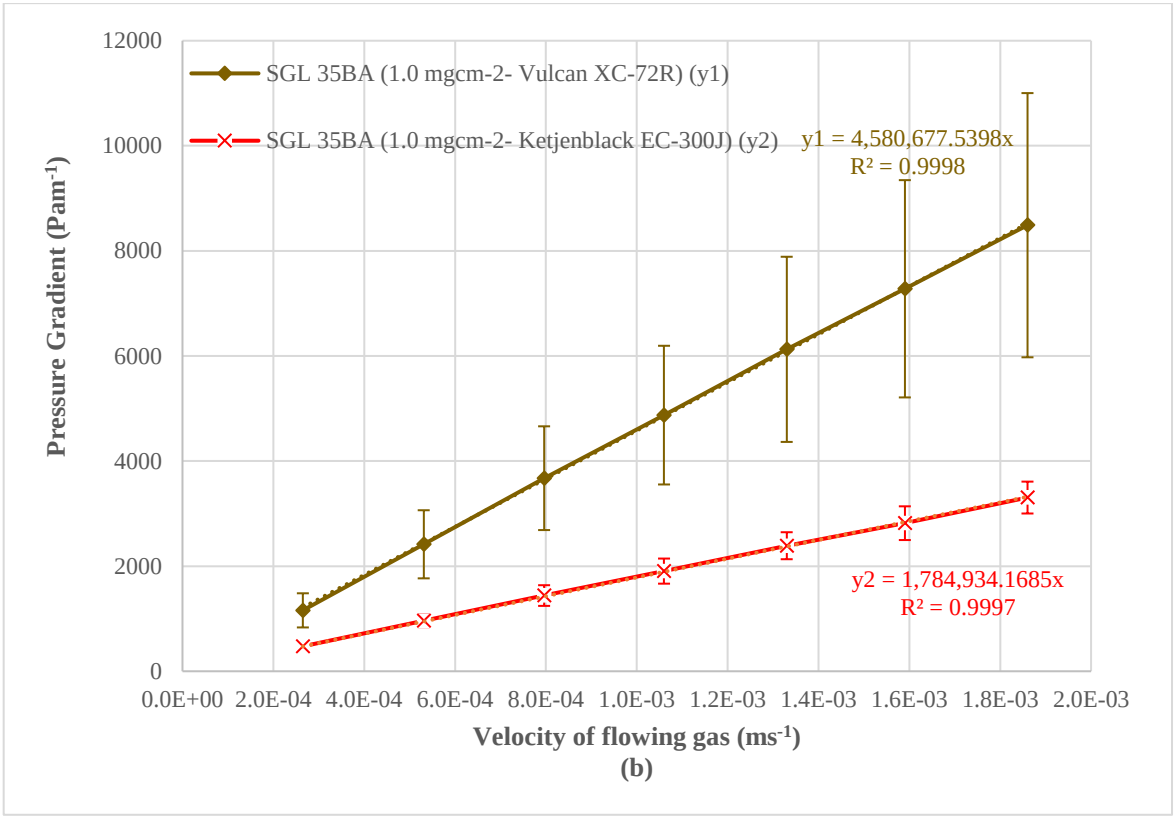
SGL 35BA (1.0 mgcm-2- Vulcan XC-72R) (y1)
SGL 35BA (1.0 mgcm-2- Ketjenblack EC-300J) (y2)
y1 = 4,580,677.5398x
R² = 0.9998
y2 = 1,784,934.1685x
R² = 0.9997
Pressure Gradient (Pam-1)
Velocity of flowing gas (ms-1)
0
2000
4000
6000
8000
10000
12000
0.0E+00
2.0E-04
4.0E-04
6.0E-04
8.0E-04
1.0E-03
1.2E-03
1.4E-03
1.6E-03
1.8E-03
2.0E-03

(b)

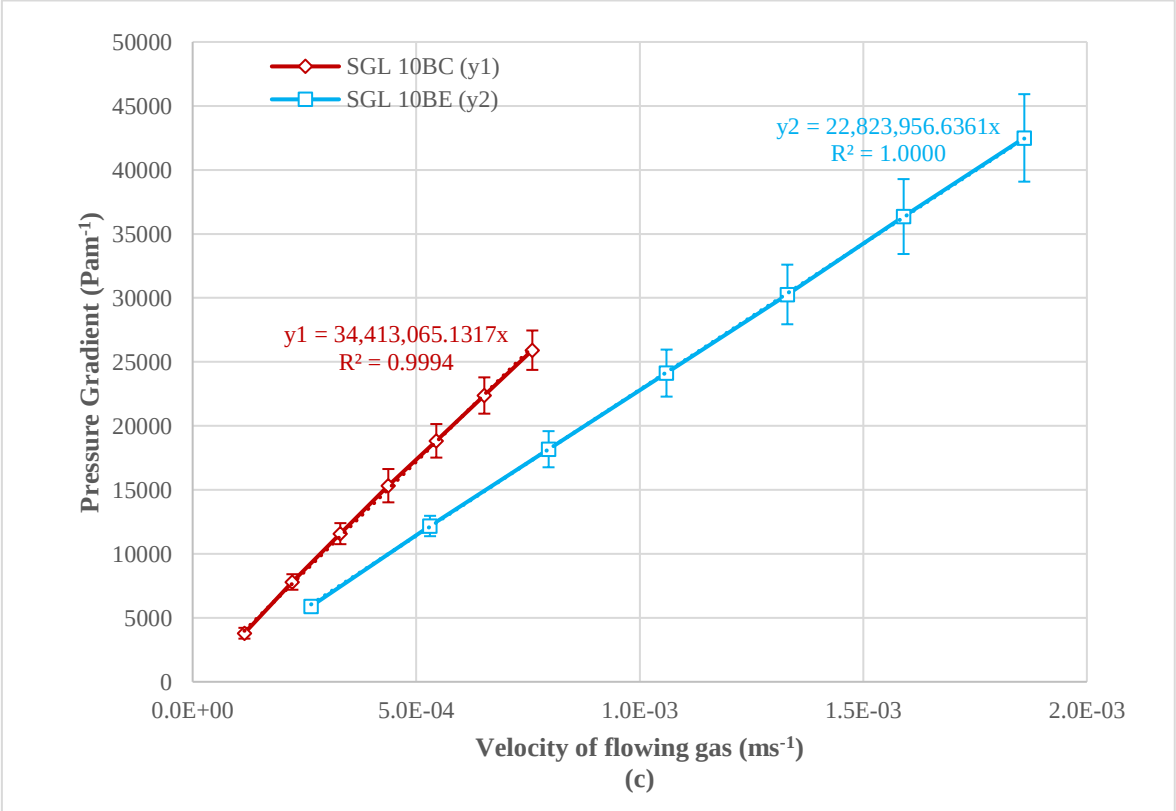
SGL 10BC (y1)
SGL 10BE (y2)
y1 = 34,413,065.1317x
R² = 0.9994
y2 = 22,823,956.6361x
R² = 1.0000
Pressure Gradient (Pam-1)
Velocity of flowing gas (ms-1)
0
5000
10000
15000
20000
25000
30000
35000
40000
45000
50000
0.0E+00
5.0E-04
1.0E-03
1.5E-03
2.0E-03

(c)

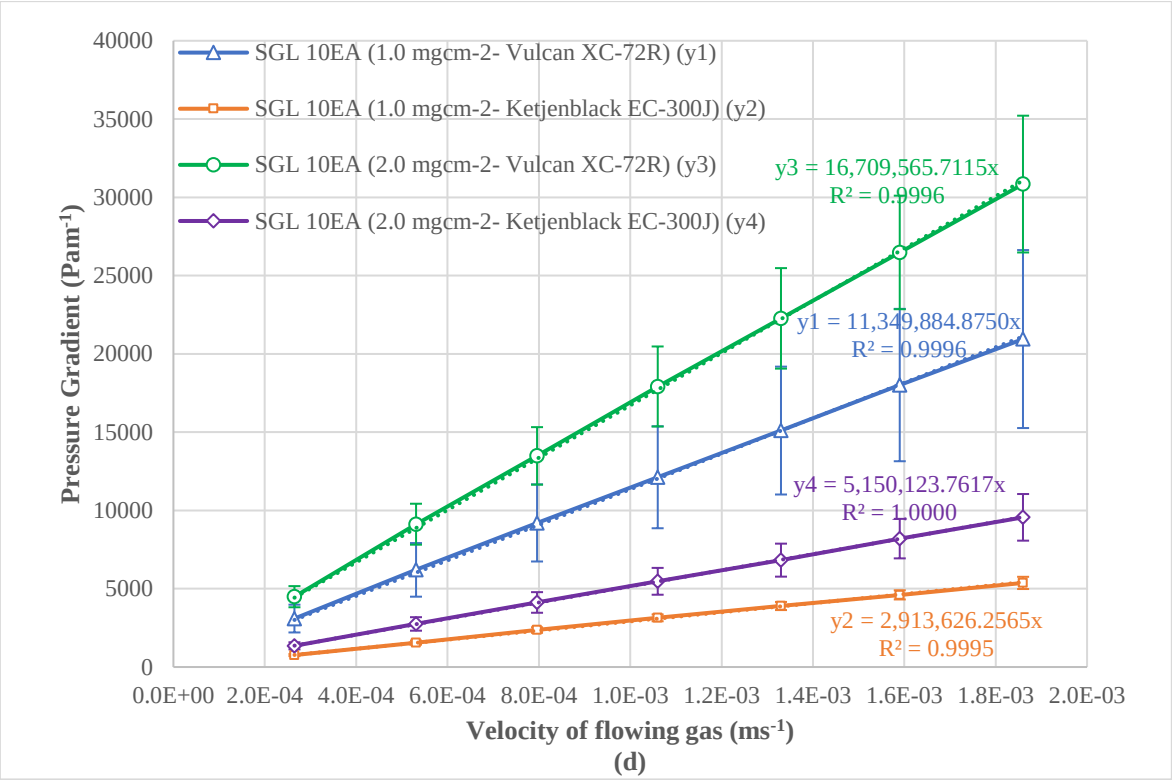

(d)

Figure 5. 4 Experimental data for pressure gradient as a function of fluid velocity for the GDMs (a) Toray TGP-H-60 (1.0 mgcm^{-2} Vulcan XC-72R and Ketjenblack EC-300J), (b) SGL 35BA (1.0 mgcm^{-2} Vulcan XC-72R and Ketjenblack EC-300J), (c) SGL 10BC and SGL 10BE (d) SGL 10EA (1.0 mgcm^{-2} and 2.0 mgcm^{-2} Vulcan XC-72R and Ketjenblack EC-300J) showing the 95% confidence interval about the mean.

Table 5. 2 Through-plane permeability of base GDMs used before sintering and applying an MPL coating.

Investigation	**GDM substrates**	**Permeability** $k \times 10^{-12}(m^2)$	**Thickness** (μm)
Sintering (base GDMs)	Toray TGP-H-060 (Vulcan XC-72R - 1.0 mgcm^{-2})	0.319 ± 0.005	206.563 ± 3.396
	Toray TGP-H-060 (Ketjenblack EC-300J - 1.0 mgcm^{-2})	2.012 ± 0.185	231.250 ± 3.248
	SGL 35BA (Vulcan XC-72R - 1.0 mgcm^{-2})	4.043 ± 1.344	296.875 ± 10.832

	SGL 35BA (Ketjenblack EC-300J- 1.0 mgcm^{-2})	10.120 ± 1.111	343.438 ± 8.180
	SGL 10BC	0.524 ± 0.035	342.188 ± 5.230
	SGL 10BE	0.790 ± 0.062	387.813 ± 15.607
Composite mixtures (base GDMs)	SGL 10EA (Vulcan XC-72R – 1.0 mgcm^{-2})	1.667 ± 0.040	375.625 ± 6.521
	SGL 10EA (Vulcan XC-72R – 2.0 mgcm^{-2})	1.093 ± 0.015	426.042 ± 9.620
	SGL 10EA (Ketjenblack EC-300J – 1.0 mgcm^{-2})	6.200 ± 0.043	417.083 ± 16.040
	SGL 10EA (Ketjenblack EC-300J – 2.0 mgcm^{-2})	3.573 ± 0.067	512.083 ± 16.733

The percentage reduction from the original substrate for GDLs Toray TGP-H-90 and Toray TGP-H-120 when coated with Vulcan XC-72R and Ketjenblack EC-300J for a carbon loading of 1.0 mgcm^{-2} was approximately 94-95% and 65-68% respectively as shown in Chapter 4. Toray TGP-H-60 is similar in structure [33]. The results shown in Table 5.2 for the coated Toray TGP-H-60 GDMs showed a reduction in permeability of 95.8% and 72.3% for 1.0 mgcm^{-2} Vulcan XC-72R and Ketjenblack EC-300J respectively. Ismail et al. [32] reported through-plane permeability values for SGL 10BC and SGL 10BE to be 0.497×10^{-12} m^2 and 0.946×10^{-12} m^2 respectively. Aslam [132] reported a value of 0.487×10^{-12} m^2 for SGL 10BC. Ihonen et al. [105] reported the through-plane permeability SGL 10BC to be 0.33×10^{-12} m^2. The variations in the through-plane

permeability are the result of fabrication uncertainties as discussed in Chapter 4. The SGL 35BA and SGL 10EA GDMs were from the investigations conducted and reported in Chapter 4.

5.3.3 Effect of sintering time on through-plane gas permeability of the GDMs.

5.3.3.1 Effect of sintering time on through-plane gas permeability using different carbon powder types

The effect of sintering time on the through-plane gas permeability of the GDMs outlined in Section 5.2 was investigated for different carbon powder types, namely, Vulcan XC-72R and Ketjenblack EC-300J. Figure 5.5 and 5.6 illustrates the through-plane gas permeability as a function of sintering time for the two carbon powder types. The error bars represent the 95% confidence interval about the mean. Figure 5.7 and Figure 5.8 show the SEM images before sintering and after eight (8) hours of sintering for the GDMs coated with Vulcan XC-72R and Ketjenblack EC-300J respectively.

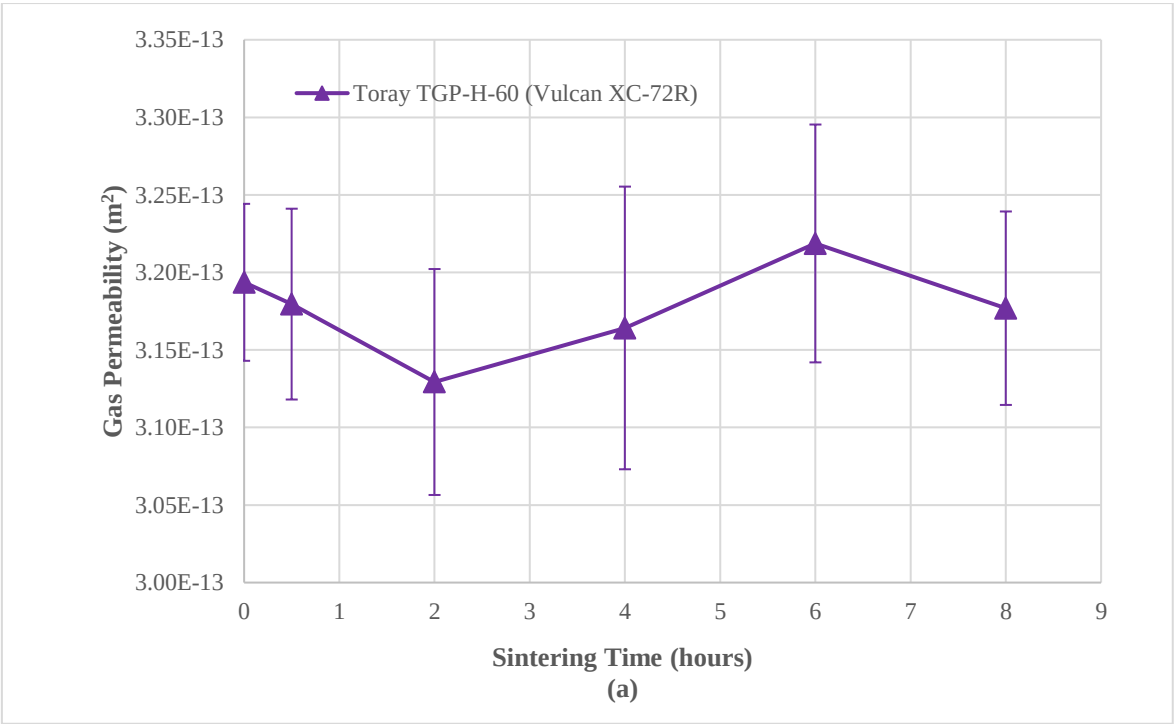

(a)

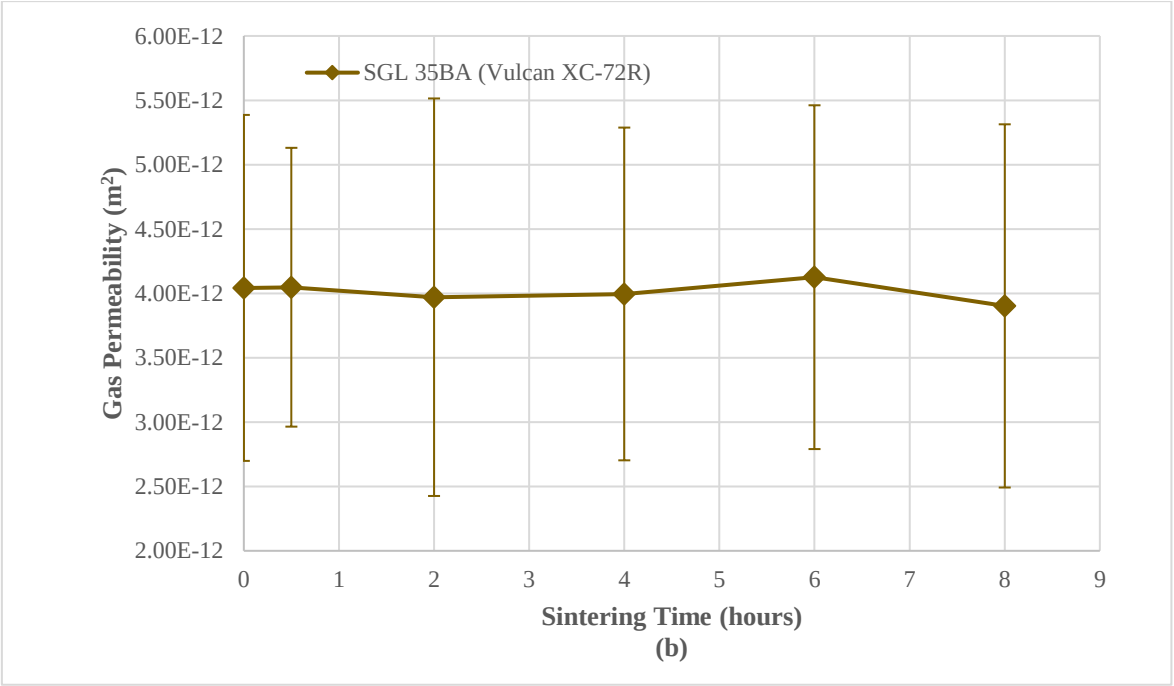

Figure 5. 5 Through-plane permeability of the GDM for a constant carbon loading of 1.0 $mgcm^{-2}$ using Vulcan XC-72R carbon powder as a function of sintering time for (a) Toray TGP-H-60 and (b) SGL 35BA.

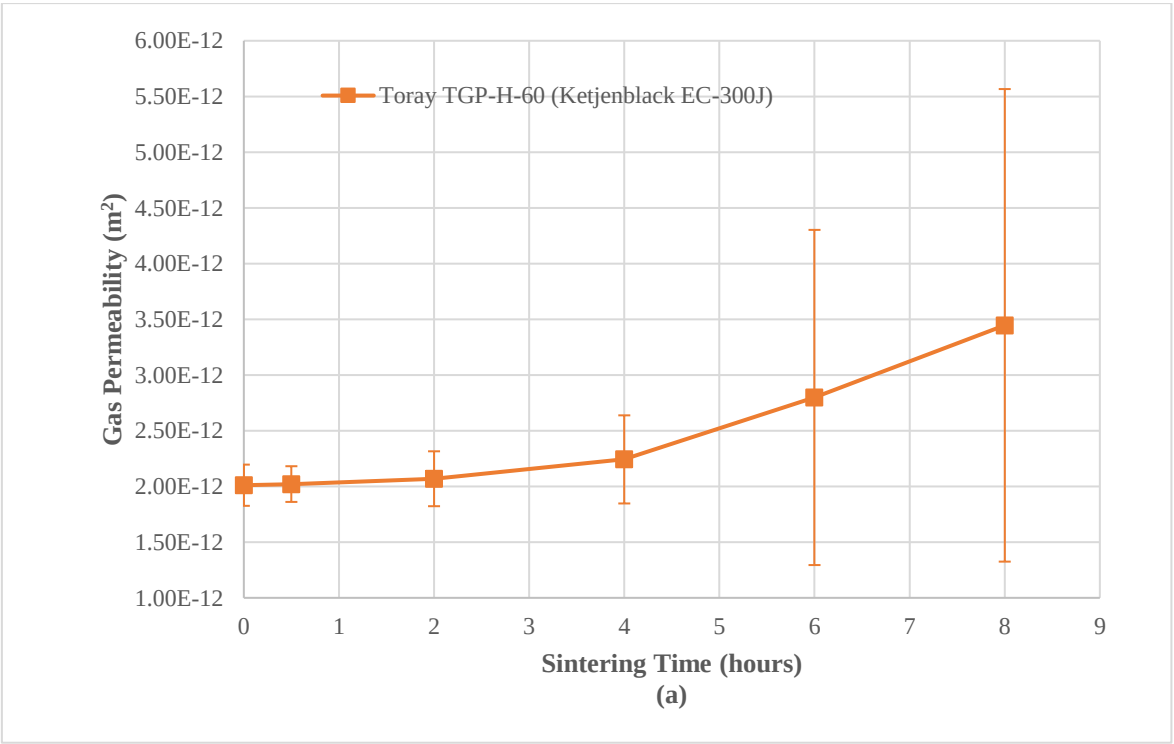

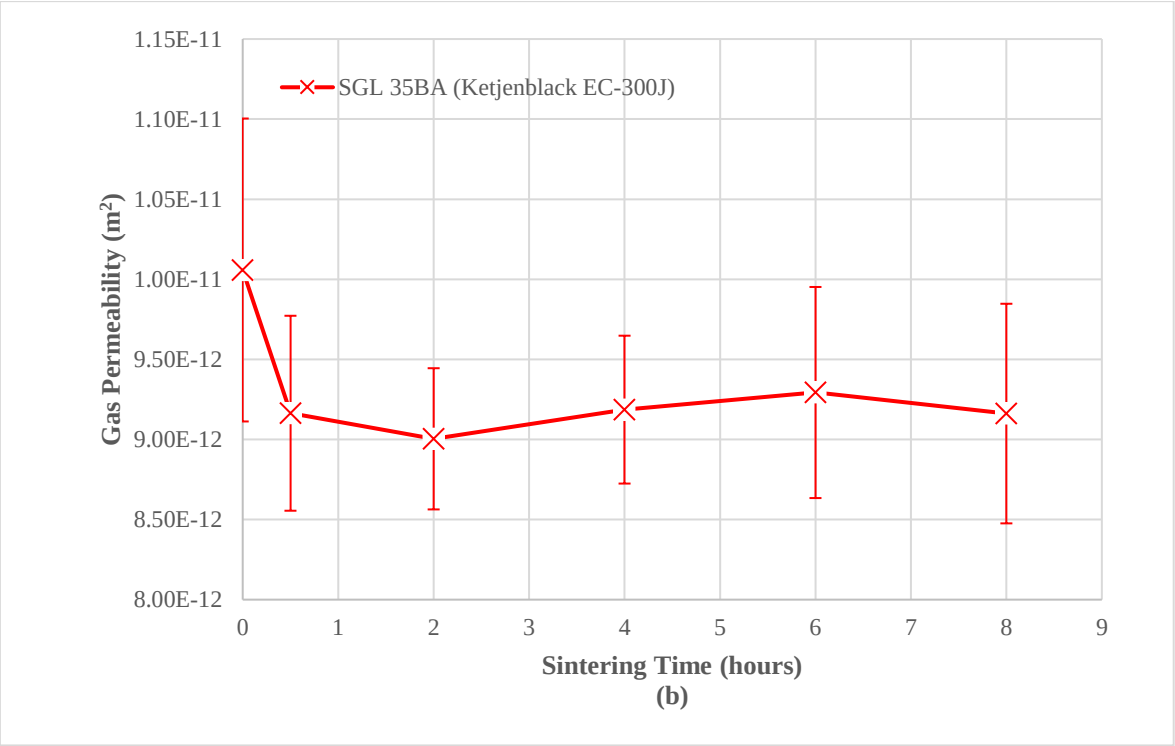

Figure 5. 6 Through-plane permeability of the GDM for a constant carbon loading of 1.0 $mgcm^{-2}$ using Ketjenblack EC-300J carbon powder as a function of sintering time for (a) Toray TGP-H-60 and (b) SGL 35BA.

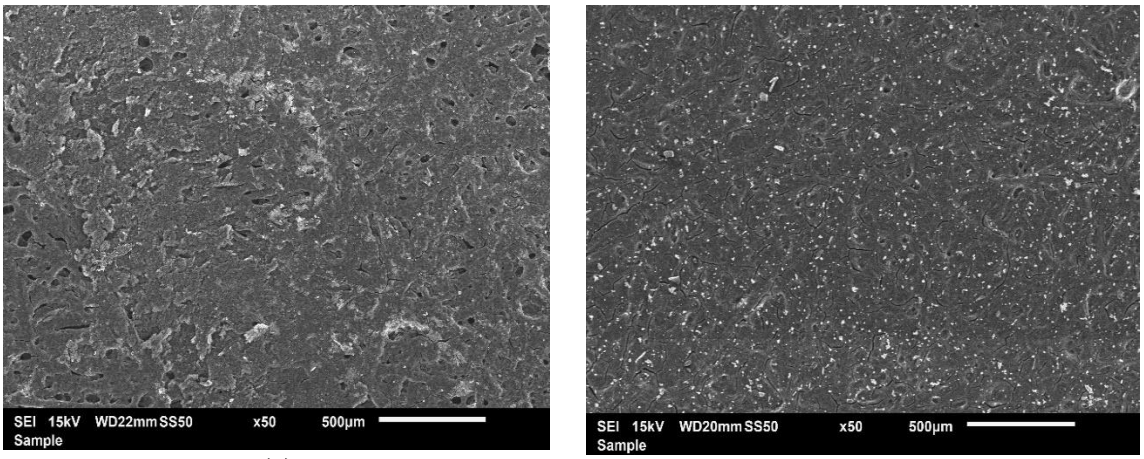

(a) (b)

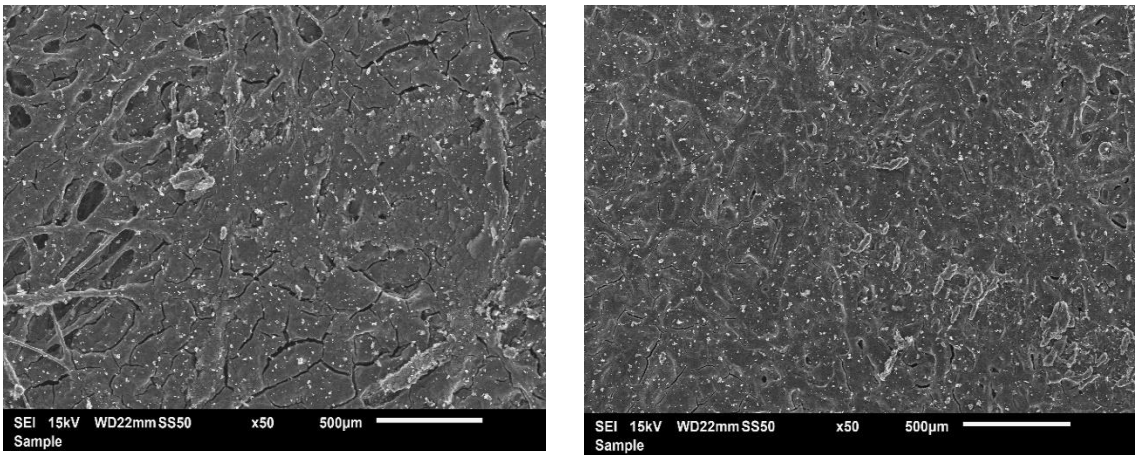

(c) (d)

Figure 5. 7 SEM micrographs showing the surface of the MPL composed of Vulcan XC-72R before sintering (L) and after eight (8) hours of sintering (R) for (a-b) Toray TGP-H-60 and (c-d) SGL 35BA.

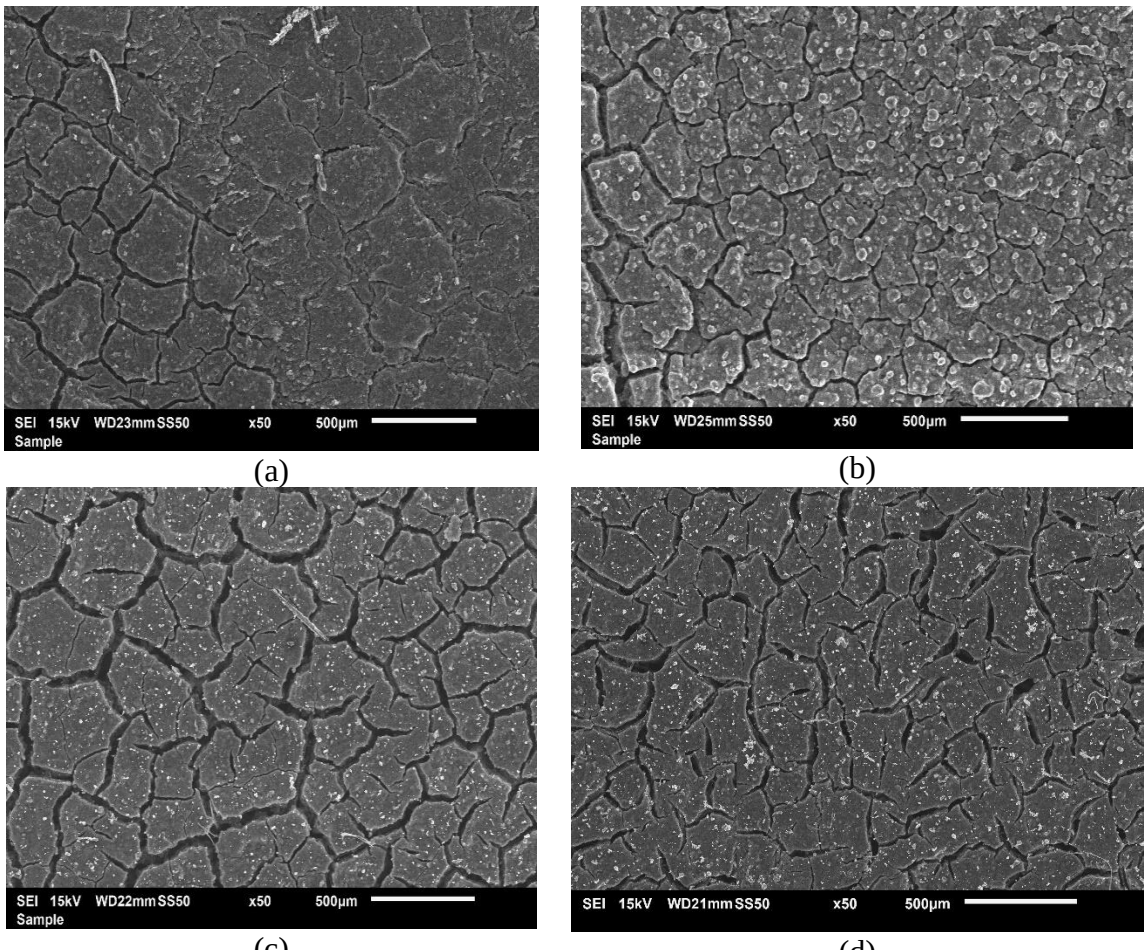

(a) (b)

(c) (d)

Figure 5. 8 SEM micrographs showing the surface of the MPL composed of Ketjenblack before sintering (L) and after eight (8) hours of sintering (R) for (a-b) Toray TGP-H-60 and (c-d) SGL 35BA.

Figures 5.5 and 5.6 illustrated that the through-plane permeability as a function of sintering time shows no conclusion and no trend in the permeability could be discerned. Toray TGP-H-60 and SGL 35BA are similar structured GDLs (non-woven straight fibre carbon papers); however, as the sintering time was increased three out of the four cases, that is, the three cases in Figure 5.5 (a) and (b) and Figure 5.6 (b) all illustrate a reduction in permeability after two (2) hours and this as explained by Orogbemi et al. [128] was due to the "spreading effect" whereby the cracks begin to become narrower. The period between two (2) to six (6) hours resulted in a general increase in the permeability in all three cases followed by a decrease at the eight (8) hour stage. The micrographs in Figure 5.7 (b) and (d) and Figure 5.8 (d) illustrate the narrowing of the cracks when compared to the GDM before sintering. The case shown in Figure 5.6 (a) showed a general increase in the permeability as the sintering time increased; however, when compared to Figure 5.6 (b) which was coated with the same carbon powder the trend was the exact opposite where the former showed a constant increase and the latter a constant decrease. The micrograph in Figure 5.8 (b) indicated a widening of the cracks on the surface which corroborated the increase in permeability after the eight (8) hours. It can be concluded that sintering time has a very small effect on the through-plane permeability; however, there is a visible effect on the surface morphology. Furthermore, effect of carbon powder type for a constant PTFE loading of 20 wt.% had no discernible effect on the through-plane permeability with increasing sintering time.

5.3.3.2 Effect of sintering time on the through-plane gas permeability for different PTFE loadings in the MPL.

Commercial samples, SGL 10BC and SGL 10BE were used to investigate the effect of sintering on GDMs with different PTFE loadings in the MPL; 20-25 and ~50 wt.% PTFE for SGL 10BC and SGL 10BE respectively. Figure 5.9 (a) and (b) illustrates the through-plane gas permeability as a function of sintering time for SGL 10BC and SGL 10BE

respectively. Figure 5.10 shows the SEM micrographs before and after eight (8) hours sintering for the two samples.

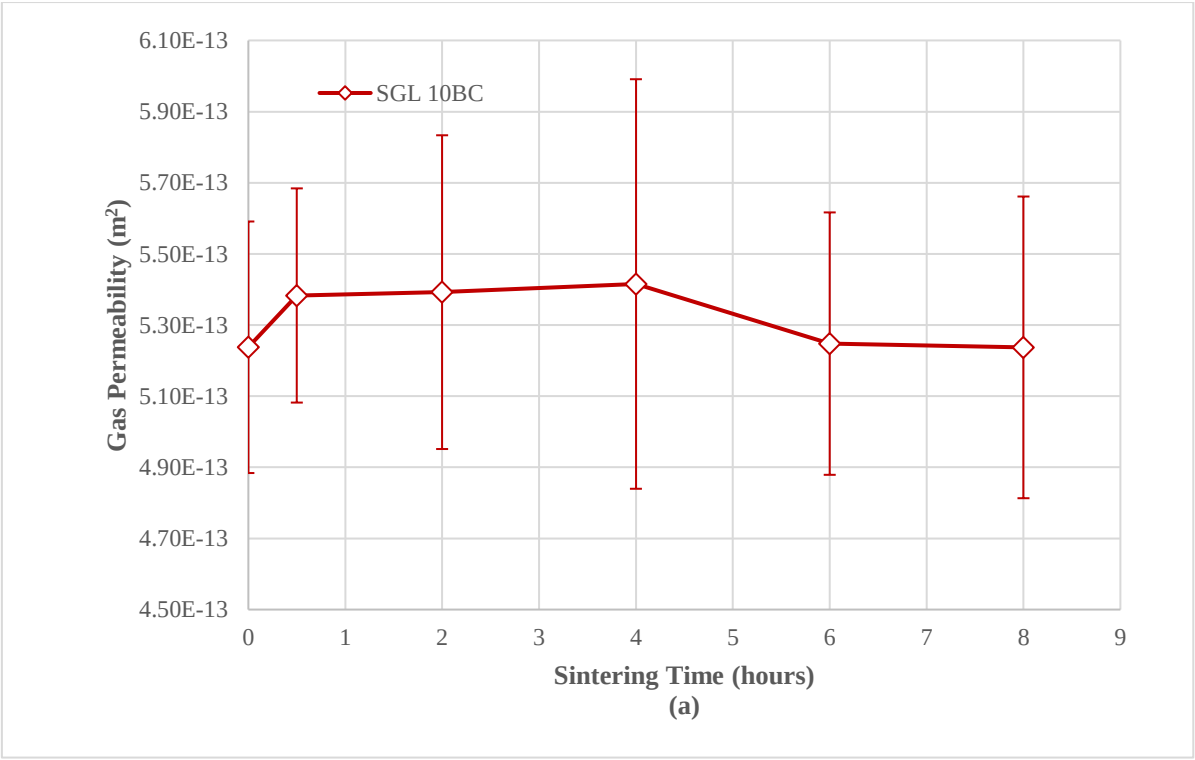

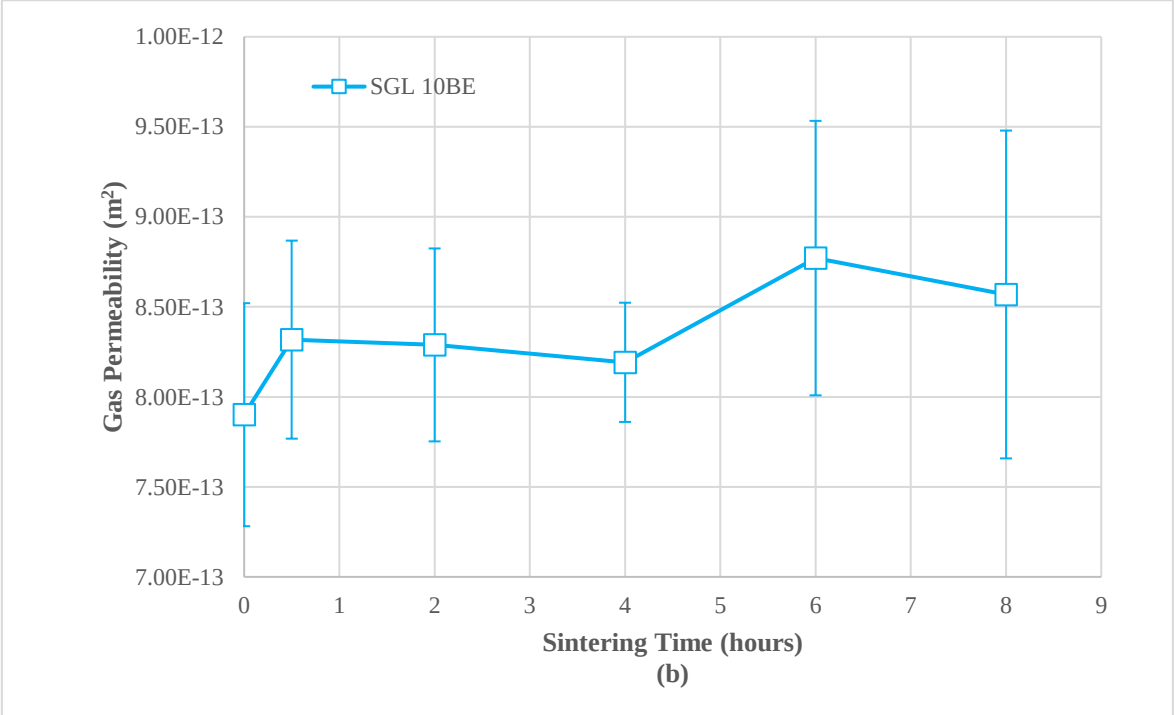

Figure 5. 9 Through-plane permeability as a function of sintering time for (a) SGL 10BC and (b) SGL 10BE.

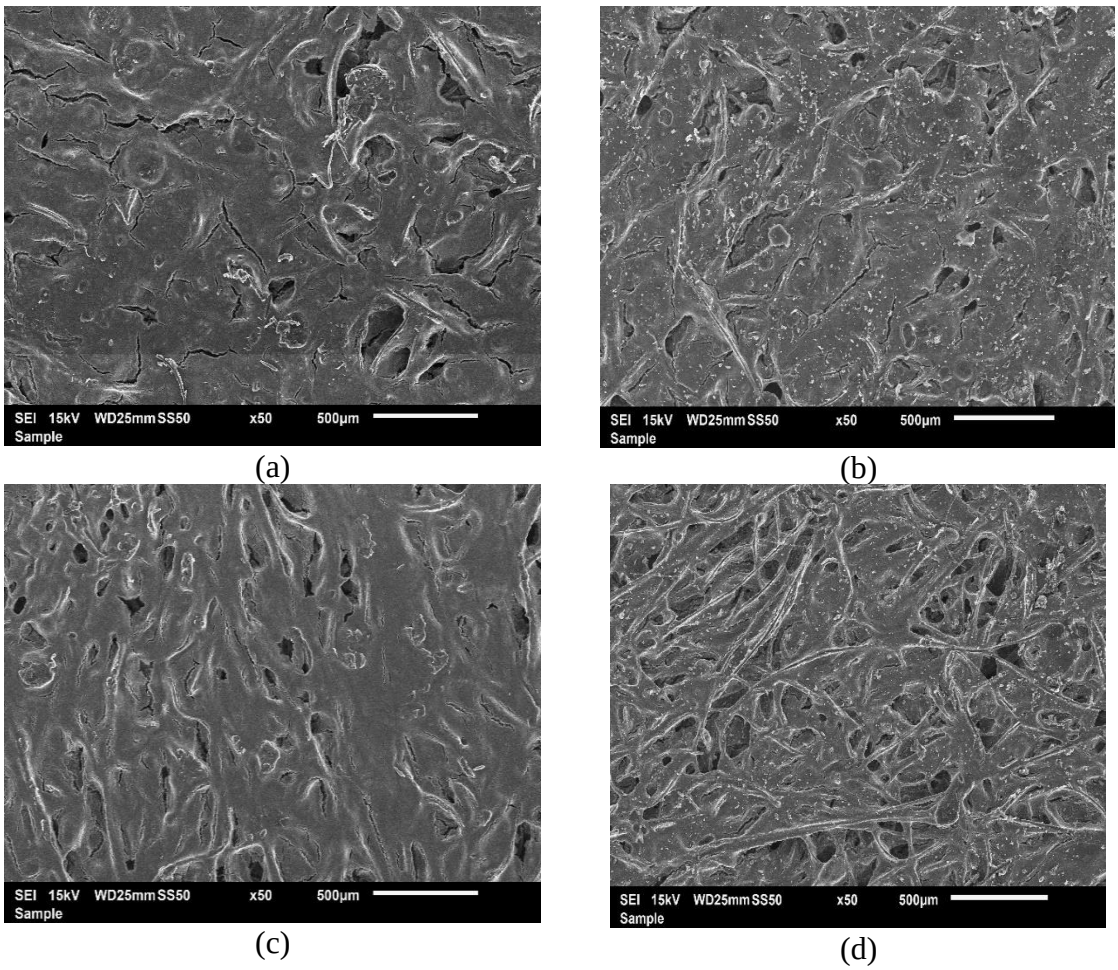

Figure 5. 10 SEM micrographs showing the surface of the MPL before sintering (L) and after eight (8) hours of sintering (R) for (a-b) SGL 10BC and (c-d) SGL 10BE.

Figure 5.9 (a) indicated that the through-plane permeability as a function of sintering time for SGL 10BC was variable with almost insignificant change to the through-plane permeability before and after eight (8) hours , similar to the results in Section 5.2.3.1 in which the MPLs had a similar amount of PTFE in the MPL. The micrograph in Figure 5.10 (a) and (b) showed a small variation after sintering for eight (8) hours. Figure 5.9 (b) also showed a variable trend for SGL 10BE; however, for all the sintering times, there was an increase in through-plane permeability from the original sample which is in agreement with the results in [133], [134], [136]. The micrograph in Figure 5.10 (d) illustrated larger voids

being exposed on the surface after the eight (8) hour period. As such, it can be concluded that for low PTFE loadings in the MPL, there is no discernible effect with increasing sintering time; however, for high PTFE loadings in the MPL, there is a general increase in through-plane permeability.

5.3.4 Effect of composite mixtures on through-plane gas permeability of the GDM

The effect of composite mixtures, that is, a combination of two carbon powders in the MPL was investigated and its impact on the through-plane permeability compared with the base cases for the SGL 10EA which consisted of 100% Vulcan XC-72R and 100% Ketjenblack EC-300J. Two (2) carbon loadings were considered 1.0 $mgcm^{-2}$ and 2.0 $mgcm^{-2}$ for an overall constant composition of 80 wt.% carbon powder and 20 wt.% PTFE in the MPL. Figure 5.11 shows the pressure gradient as a function of fluid velocity for the various ratio combinations of Vulcan XC-72R and Ketjenblack EC-300J with the error bars representing a 95% confidence interval. Linearity is observed which justified the use of Darcy's law. Figure 5.12 shows the through-plane permeability of GDMs with respect to the different ratios. It should be noted that 20% Ketjenblack EC-300J corresponds to a ratio of 80% Vulcan XC-72R and 20% Ketjenblack EC-300J and 0% Ketjenblack EC-300J indicates the case with 100% Vulcan XC-72R.

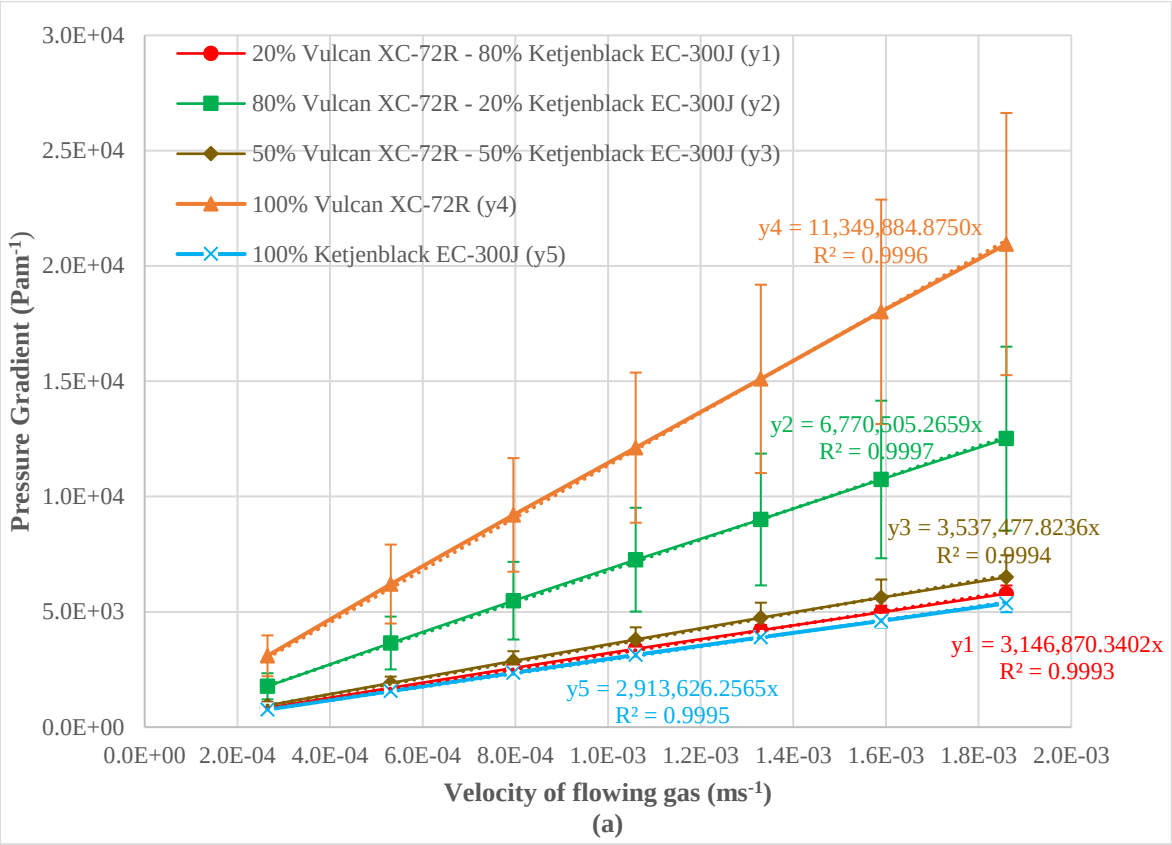

(a)

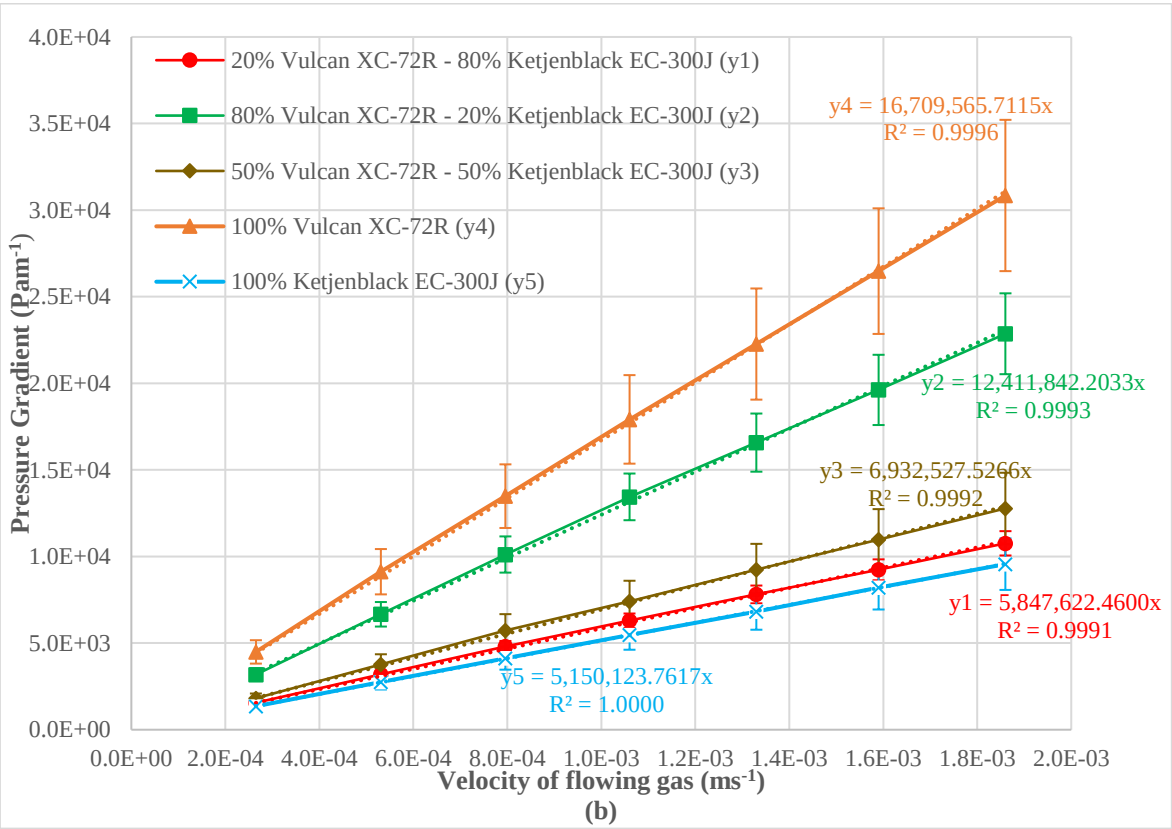

(b)

Figure 5. 11 Experimental data for the pressure gradient as a function of fluid velocity for carbon loadings of (a) 1.0 mgcm^{-2} and (b) 2.0 mgcm^{-2}.

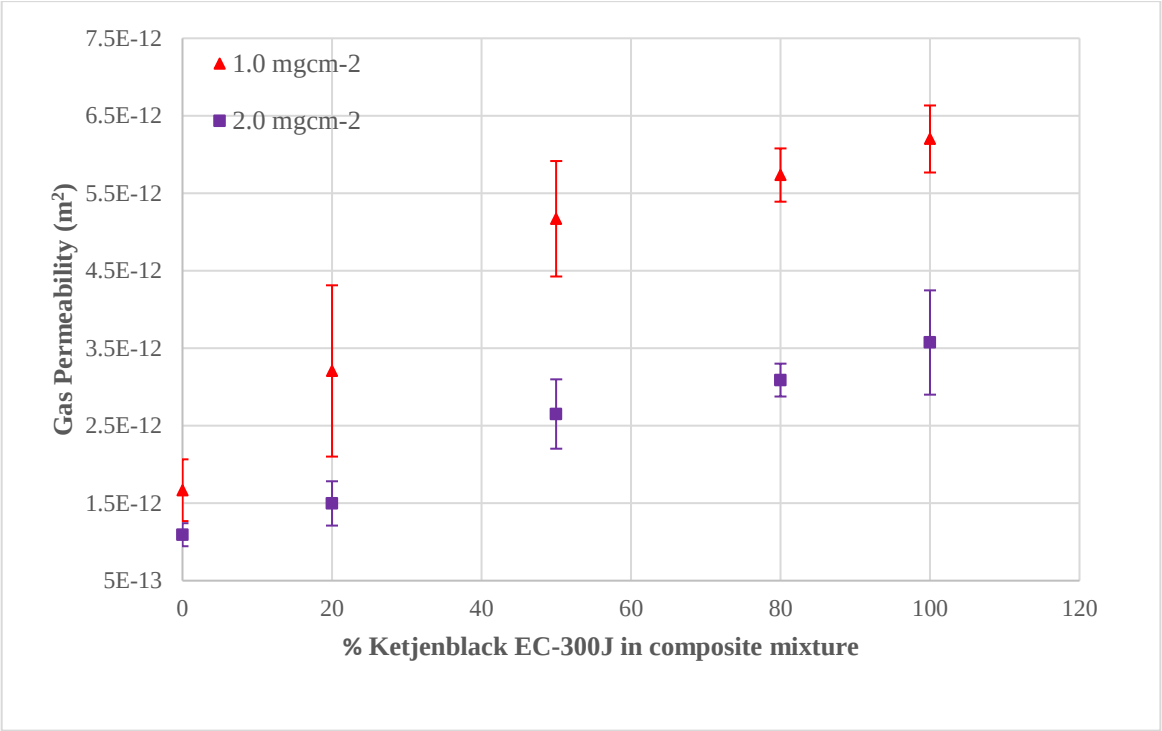

Figure 5. 12 Through-plane permeability of the composite mixtures for the two carbon loadings under investigation.

As shown in Figure 5.12, the through-plane permeability of the various composite mixtures lied within the bounds of the 100% Vulcan XC-72R and 100% Ketjenblack EC-300J regardless of the carbon loadings of 1.0 $mgcm^{-2}$ and 2.0 $mgcm^{-2}$. This was in agreement with the results presented by Wang et al. [113].

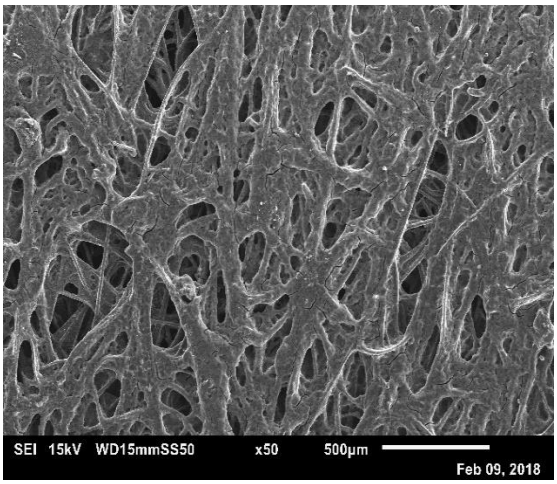

(a)

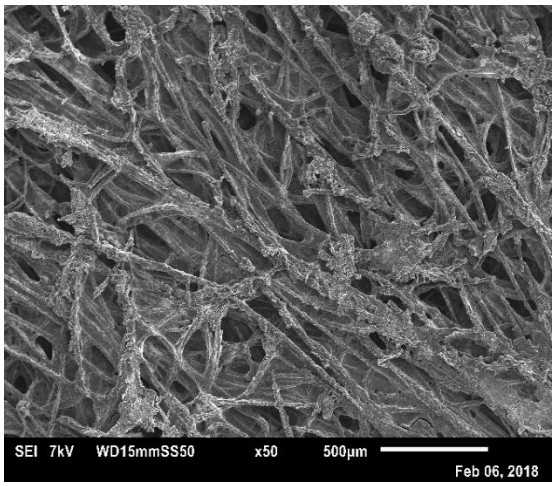

(b)

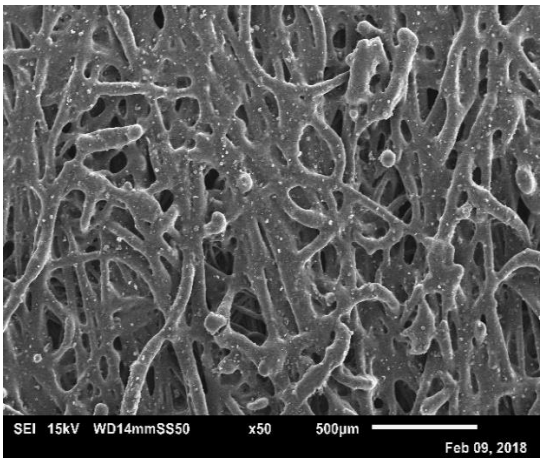

(c)

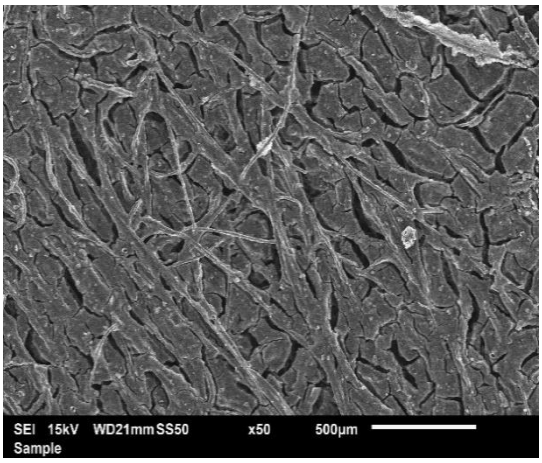

(d)

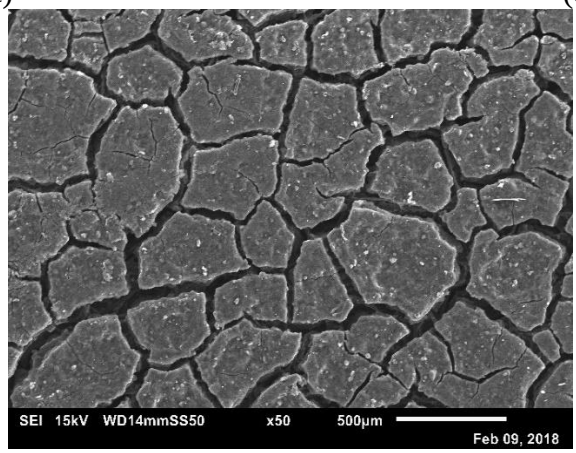

(e)

Figure 5. 13 SEM images for 1.0 mgcm^{-2} composite mixtures showing (a) 100% Vulcan XC-72R, (b) 80% Vulcan XC-72R – 20% Ketjenblack EC-300J, (c) 50% Vulcan XC-72R – 50% Ketjenblack EC-300J, (d) 20% Vulcan XC-72R – 80% Ketjenblack EC-300J and (e) 100% Ketjenblack EC-300J.

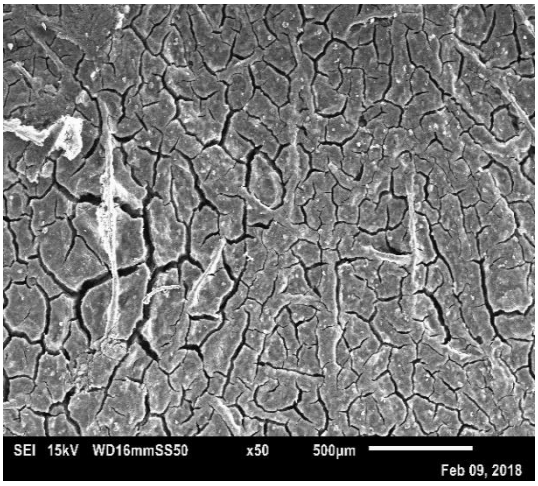

(a)

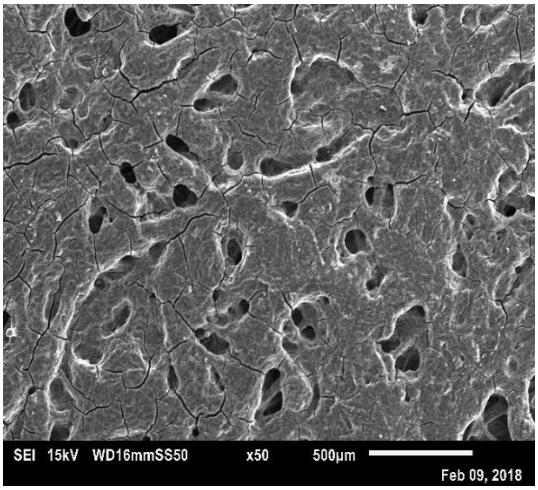

(b)

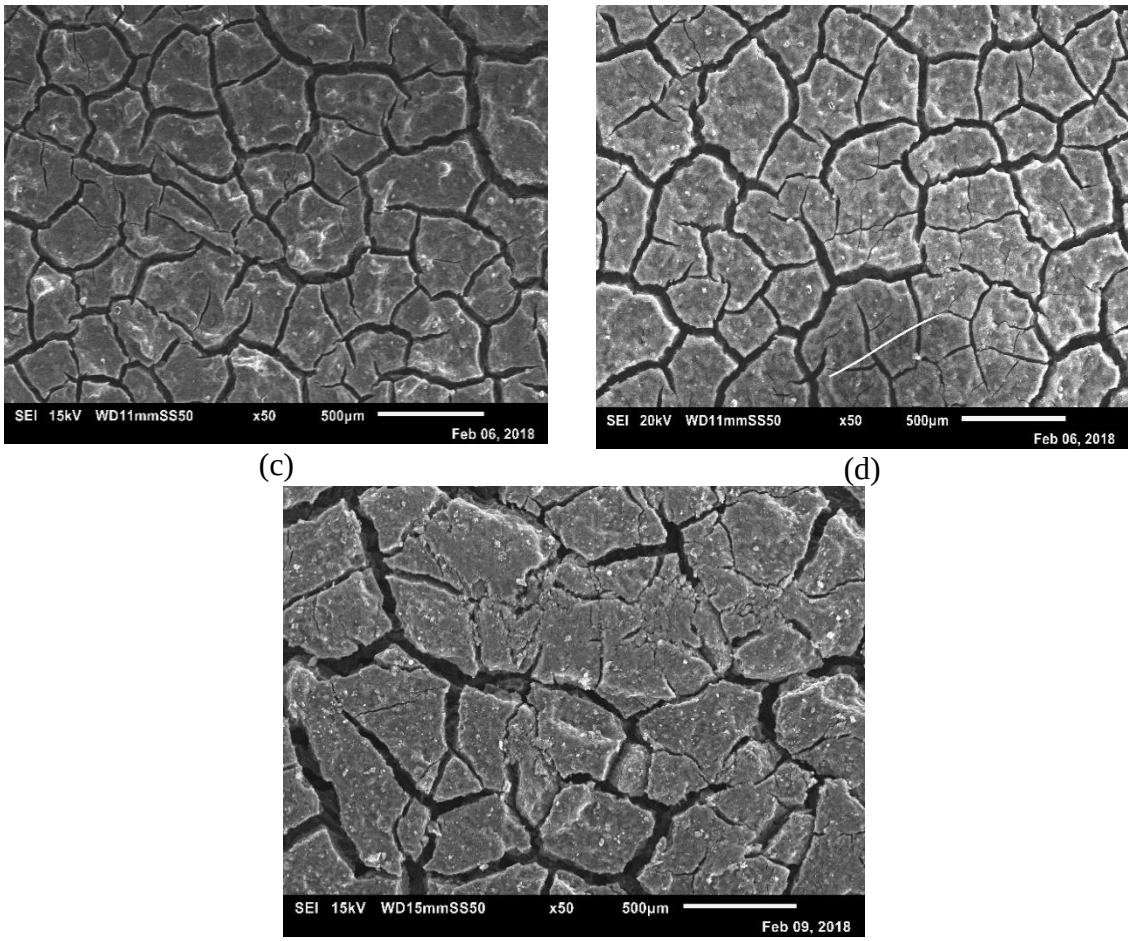

Figure 5. 14 SEM images for 2.0 mgcm^{-2} composite mixtures showing (a) 100% Vulcan XC-72R, (b) 80% Vulcan XC-72R – 20% Ketjenblack EC-300J, (c) 50% Vulcan XC-72R – 50% Ketjenblack EC-300J, (d) 20% Vulcan XC-72R – 80% Ketjenblack EC-300J and (e) 100% Ketjenblack EC-300J.

Figures 5.13 and 5.14 show the SEM micrographs for the composite mixtures with the carbon loadings of 1.0 mgcm^{-2} and 2.0 mgcm^{-2} respectively. The surface morphology tends to differ from the base cases of 100% of either carbon powder; however, the images do corroborate the findings of the through-plane permeability data shown in Figure 5.12. Investigations into the thickness changes with regard to each composition do reveal a similar trend to that of the through-plane permeability, that is, the thicknesses of the GDMs for the various percentage ratios of carbon powders also lie within the bounds of the 100% cases as shown in Figure 5.15 below.

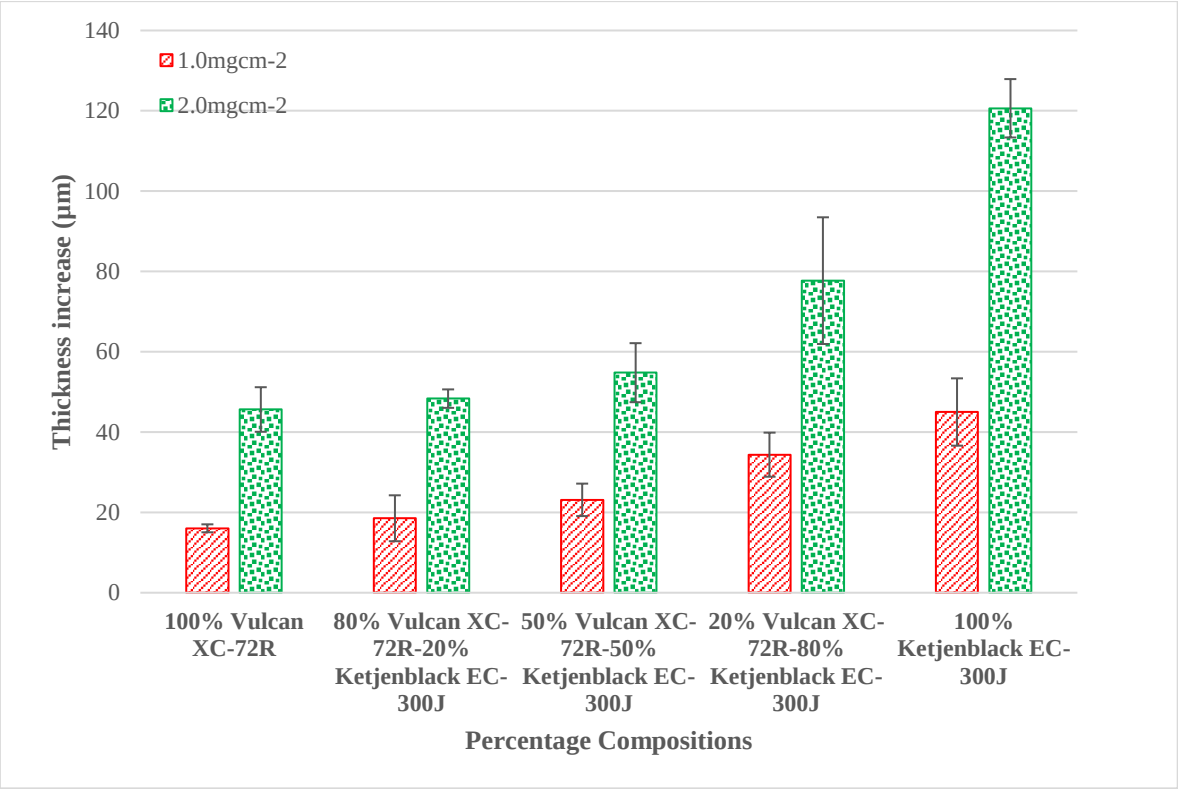

Figure 5. 15 Thickness increases in the GDMs for the various ratios of Vulcan XC-72R and Ketjenblack EC-300J for the two carbon loadings.

5.4 Conclusion

This chapter contains the results of the investigation conducted on the effect of sintering time and composite mixture of carbon powders on the through-plane permeability of the GDM. The effect of sintering time with regard to carbon type for a constant carbon loading of 1.0 $mgcm^{-2}$ on the through-plane permeability of the GDM was explored as well as the effect of varying PTFE in the MPL. The impact carbon loading with regard to various composition ratios of the MPL considering two types of carbon powders was investigated on the through-plane permeability and thickness of the GDM. Surface morphology was used to validate the findings for both the investigations of sintering time and composite mixtures. The following conclusions were obtained as follows:

- Low PTFE loading (~20-25%) in the MPL resulted in variable trends in through-plane permeability of the GDM with regard to increasing sintering time regardless of the carbon powder used. SEM micrographs did indicate a difference in the surface morphology before and after sintering which varied for the two carbon powders used.
- High PTFE loading (~50%) in the MPL did show an increase in the through-plane permeability of the GDM with increasing sintering time. SEM images did indicate increase pores/gaseous paths on the MPL surface, and this result was consistent with the literature.
- Various composition ratios of two different carbon powders used in the MPL showed that the through-plane permeability of the GDM can be controlled between two bounds regardless of the carbon loading in the MPL. Surface morphology of the composite mixtures was shown to be different from that of the MPLs which composed of only one carbon powder.
- The thickness of the composite mixtures also followed a similar trend to that of the through-plane permeability which also indicated that the thickness of the MPL can be controlled with the mixture of two carbon powders.

The two investigations conducted in this chapter revealed two simple techniques which can be used to improve properties such as gas permeability and thickness of the GDM

Chapter 6

Influence of ink slurry homogenization on through-plane gas permeability of gas diffusion media in polymer electrolyte fuel cells

6.1 Introduction

There have been numerous studies aimed at improving MPL characteristics through its composition. MPL composition focuses on the type of carbon powder and carbon loading [55], [109], [113], [115]–[122] used as well as the type and loading of the hydrophobic agent [61], [63], [123]–[125], [127], [128] used in its preparation. Most of these investigations, however, have never focused on the homogenization technique used in the preparation of the MPL ink slurry. The techniques used in homogenization of the ink have varied widely in the literature.

Zhiani et al. [129] investigated the effect of ink homogenization of the MPL using four different techniques: (i) Pulse probe sonication, (ii) continuous probe sonication, (iii) bath sonication and (iv) magnetic stirring. The in-plane permeability and through-plane resistivity of the GDM were investigated for MPLs prepared with Vulcan XC-72R carbon powder onto a Toray TGP-H-60 carbon paper for a constant loading of 1.4 $mgcm^{-2}$ and a PTFE loading of 20% by weight. Zhiani et al. [129] concluded that bath sonication was the most desirable technique for ink homogenization as it yielded the highest in-plane permeability and lowest through-plane resistivity for a compression ratio of 20%. Furthermore, the surface morphology of the MPLs prepared indicated that bath sonication resulted in a uniform

distribution on the surface without any large cracks being formed. Zhiani et al. [129], however, did not consider the effect of different structured GDLs onto which the MPL was coated and held the time constant at ten (10) minutes for pulse and continuous probe sonication and two (2) hours for bath sonication and magnetic stirring. The effect of the different homogenization techniques was also only investigated for Vulcan XC-72R carbon powder.

In the present study, effect of two homogenization techniques are investigated with regard to preparation of the MPL ink and its effect on through-plane permeability and surface morphology of the GDM. The time for the ink mixture to homogenization was held constant at two (2) hours for both techniques: (i) bath sonication and (ii) magnetic stirring. In order to investigate the effect of homogenization time, the results from Chapter 5 are compared with those discussed here. MPLs were coated onto two (2) different structured carbon fibre paper GDLs to investigate the effect of the homogenization techniques on the through-plane permeability for GDMs with different GDLs. Furthermore, the effect of homogenization techniques was investigated using different carbon powder types for a constant carbon loading of 1.0 $mgcm^{-2}$.

6.2 Materials and Methods

The in-house gas permeability setup, preparation of the samples and data analysis used in this investigation was described previously in Section 3.3. The through-plane permeability was investigated for sixteen (16) samples (four samples of each substrate were used for each homogenization technique for two different types of carbon powders, namely, Vulcan XC-72R and Ketjenblack EC-300J) of each GDL substrate which were coated with an MPL onto two different structured GDLs: Toray TGP-H-60 and SGL 10DA. The manufacturer's data for these substrates can be found in Table 3.1. The carbon loading used in these

investigations was 1.0 $mgcm^{-2}$. For this carbon loading, the MPL composition by weight is kept constant at 80 wt.% carbon powder and 20 wt.% PTFE for two carbon powders used: Vulcan XC-72R and Ketjenblack EC-300J. The manufacturer's data on the two carbon powders can be found in Table 3.2. Two methods were used to homogenize the ink slurry prepared for the MPL: (i) Ultrasonic bath sonication and (ii) magnetic stirring. The homogenization time for the ink slurry remained constant at two (2) hours for both techniques. The MPL ink slurry was sonicated using an ultrasonic bath (Ultrawave U-300H, Ultrawave, UK) for an operating frequency of 44 kHz and an isothermal bath temperature of 40 ℃. Magnetic stirring of the ink slurry was carried out using a magnetic stirrer (IKA, USA) at a room temperature of 23 ℃ and a stirring speed of 1200 rpm. The experiments involving bath sonication in this chapter were compared with those of Chapter 5 (three-hour bath sonication) to investigate effect of homogenization time on through-plane gas permeability and MPL thickness. The surface morphology of the MPL was studied using scanning electron microscopy (SEM).

6.3 Results and discussion

6.3.1 Through-plane gas permeability of the gas diffusion layer substrates.

The through-plane gas permeability of the GDL substrates used in these investigations are listed in Table 6.1 were determined initially, before application of a microporous layer onto the substrate. Gas permeability was estimated experimentally by fitting the data, determined from the dependence of fluid velocity on pressure drop, to Eq. 3.4. The through-plane permeability and thickness of all uncoated GDL substrates under investigation are presented in Table 6.1. The listed values represent the mean and 95% confidence interval limits for the gas permeability and thickness of sixteen samples of each GDL substrate. Figure 6.1 illustrates the relationship between the pressure gradient across the substrates to the fluid

velocity used in the estimation of the gas permeability of the samples. Figure 6.2 shows the pressure gradient as a function of fluid velocity for each individual GDL with the error bars representing the 95% confidence interval for the samples used. The linearity of the pressure gradient to fluid velocity relationship for the samples investigated, justifies the use of Darcy's law.

Table 6. 1 Through-plane permeability of tested GDL substrates.

GDL substrates	**Permeability** $k \times 10^{-12}(m^2)$	**Thickness** (µm)
Toray TGP-H-060	7.388 ± 0.154	196.875 ± 2.092
SGL 10DA	19.639 ± 0.847	350.938 ± 6.776

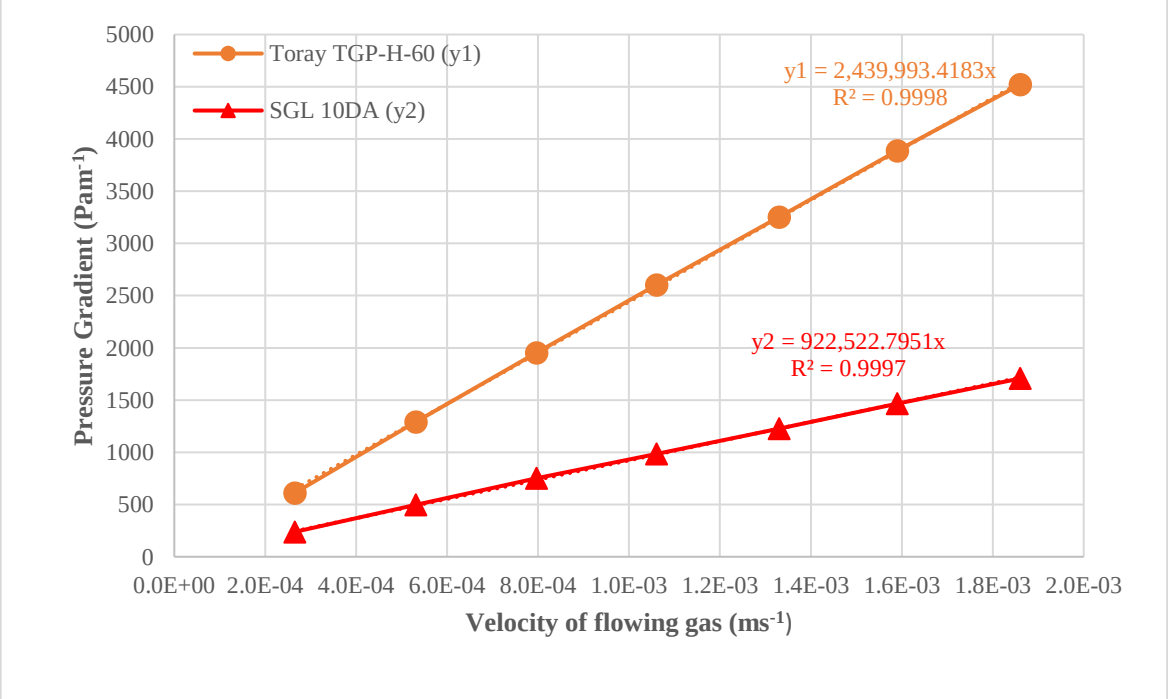

Figure 6. 1 Experimental data for the pressure gradient as a function of fluid velocity for the GDL substrates used.

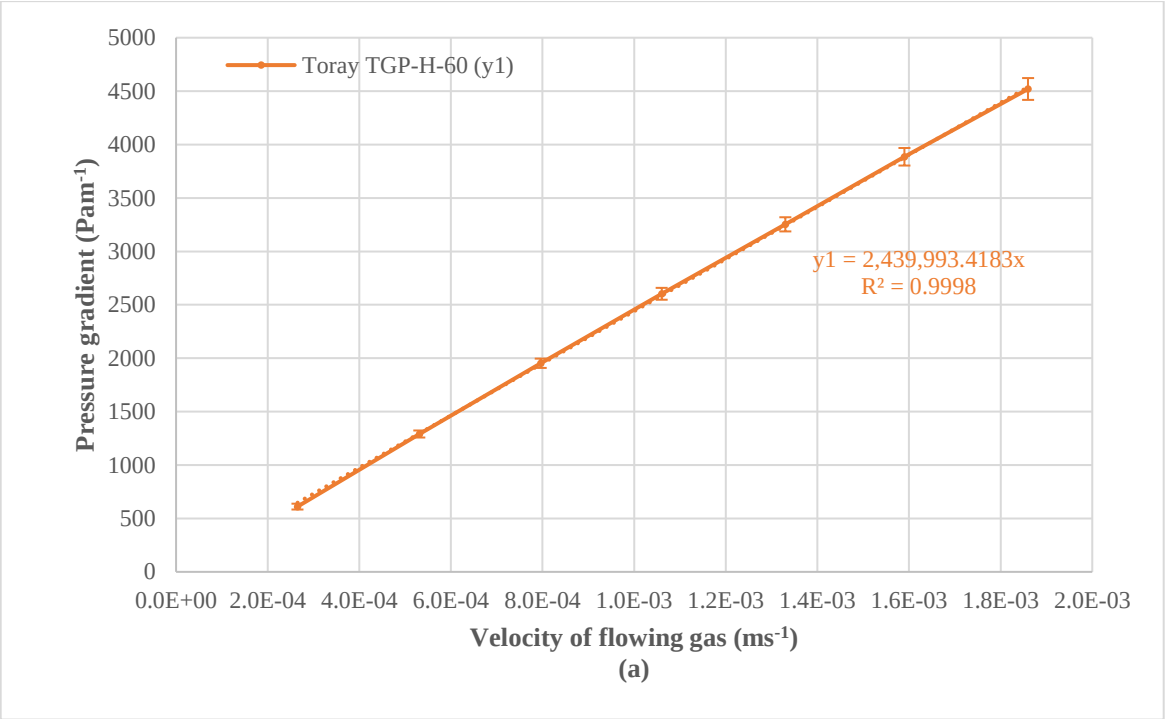

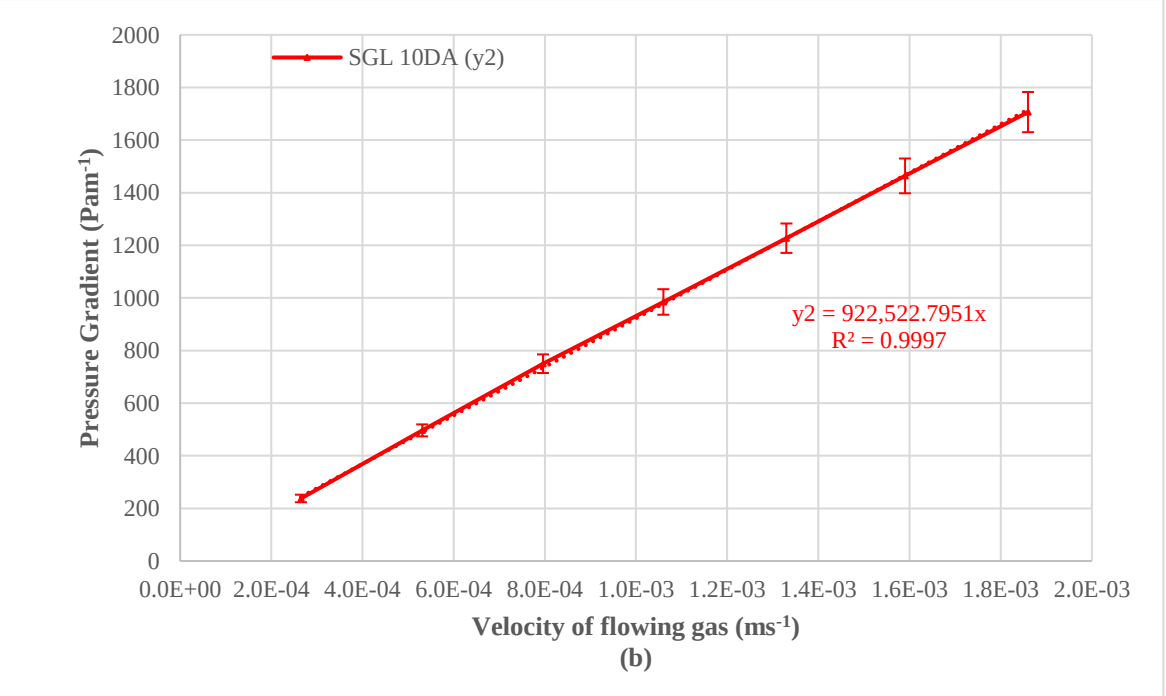

Figure 6. 2 Experimental data for pressure gradient as a function of fluid velocity for (a) Toray TGP-H-60 and (b) SGL 10DA showing the 95% confidence interval for each sample.

Comparison of the through-plane permeability of the GDL substrates used show good agreement with the literature. Ismail et al. [99] reported the through-plane permeability of SGL 10DA as 2.19×10^{-11} m^2 which is comparable to the results shown in Table 6.1.

Mathias [79] measured the through-plane permeability of uncompressed Toray TGP-H-60 to be between 5-10 Darcy's which is comparable to results shown in Table 6.1. Furthermore, the pressure gradients versus the velocity of the fluid flow are compared for the GDLs used here with the previous results of Chapter 4 as illustrated in Figure 6.3.

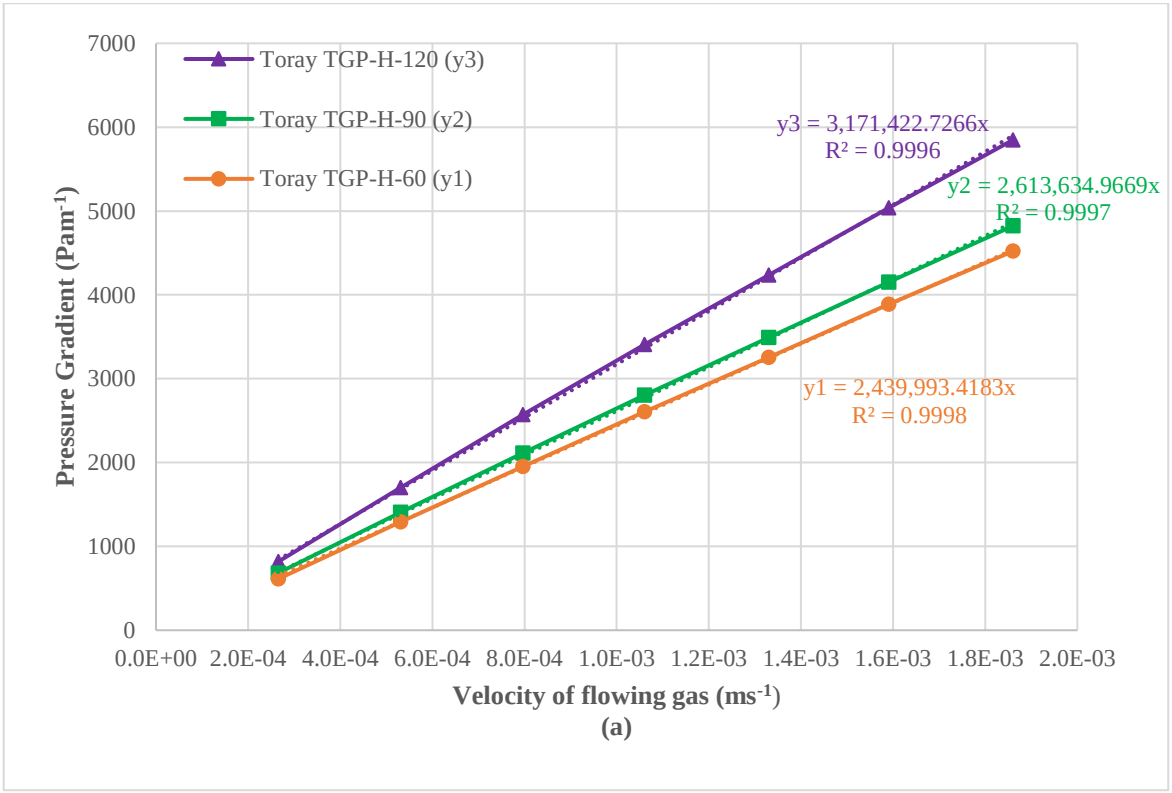

(a)

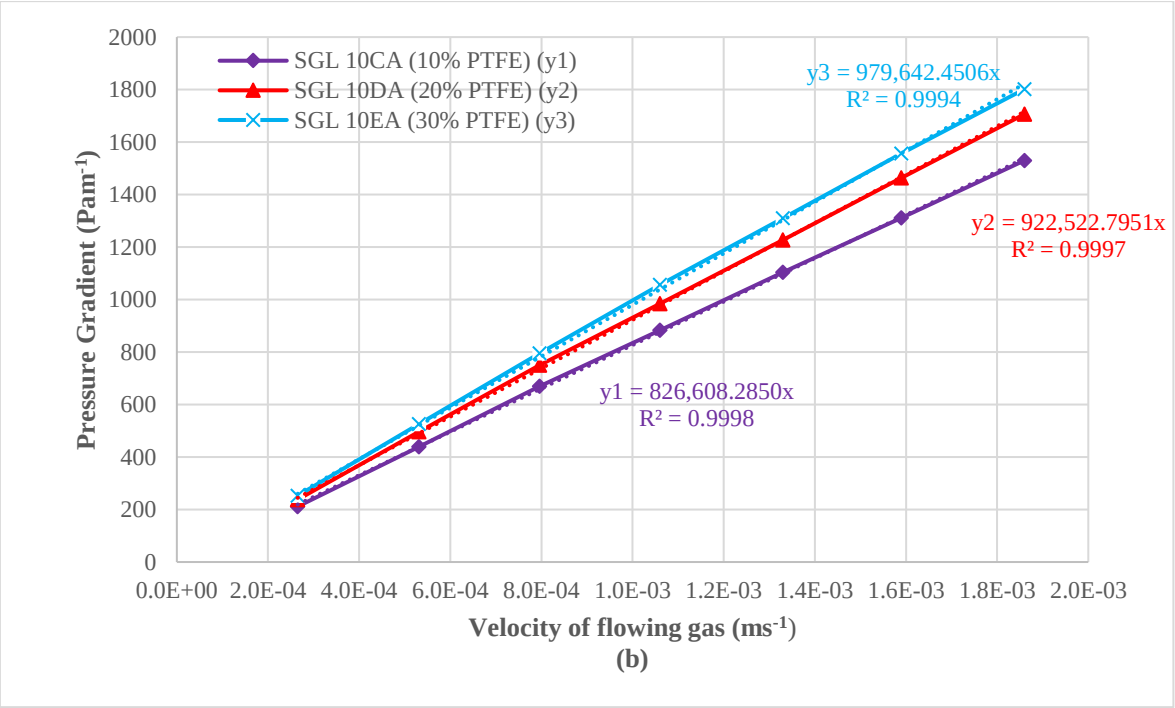

Figure 6. 3 Comparison of the pressure gradient as a function of fluid velocity for (a) non-woven carbon fibre paper substrates- Toray TGP-H-120/90/60 and (b) felt-like/spaghetti carbon fibre substrates- SGL 10CA, DA and EA.

As expected, the pressure drops of the Toray carbon fibre papers (Figure 6.3 a) increase (permeability decreases) with increasing thickness (Toray TGP-H-120 has the highest thickness as compared to Toray TGP-H-60 having the lowest). El-Kharouf et al. [33] reported similar findings for the Toray- carbon fibre papers such that the permeability decreases with increasing thickness. The pressure drop also increases with increasing PTFE content as shown in Figure 6.3b. This is in agreement with the findings in [94], [100], [101]. The SEM images for the two (2) GDLs used are shown in Figure 6.4.

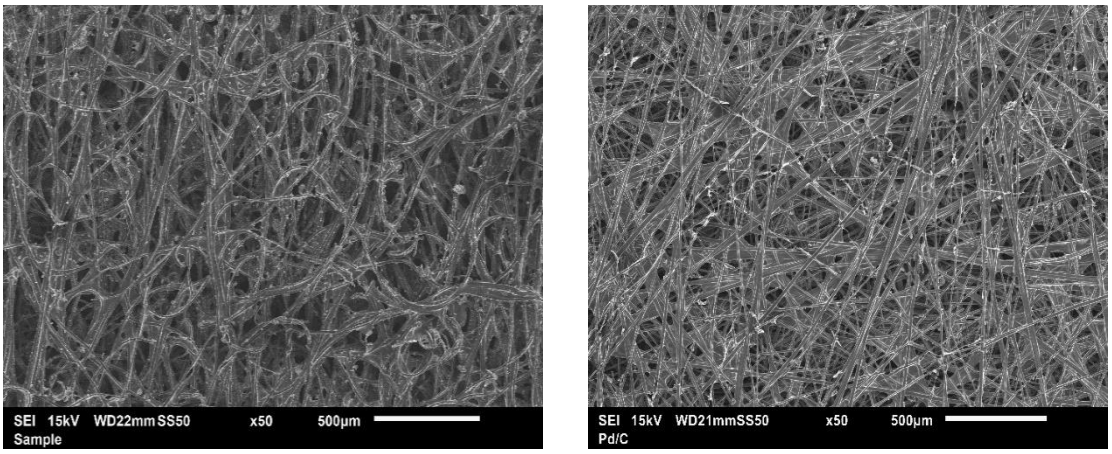

(a) (b)

Figure 6. 4 SEM images of the bare GDL substrates for (a) SGL 10DA (b) Toray TGP-H-60.

6.3.2 Through-plane permeability of the MPL coated GDLs (GDM)

6.3.2.1 Effect of homogenization techniques on through-plane permeability of gas diffusion media

The through-plane gas permeability of the GDMs was investigated in this section using two carbon blacks (Vulcan XC-72R and Ketjenblack EC-300J) for two different ink homogenization techniques: (i) bath sonication and (ii) magnetic stirring for a constant homogenization time for two (2) hours. Two different structured GDL substrates are used to investigate the impact of the homogenization techniques. Lastly, the surface morphology is compared as well as the impact of MPL thickness utilising both techniques. Figure 6.5 (a) and (b) demonstrates the relationship between the pressure gradient across the substrates to the fluid velocity used in the estimation of the gas permeability of the samples. The linearity of the relationship justifies the use of Darcy's law.

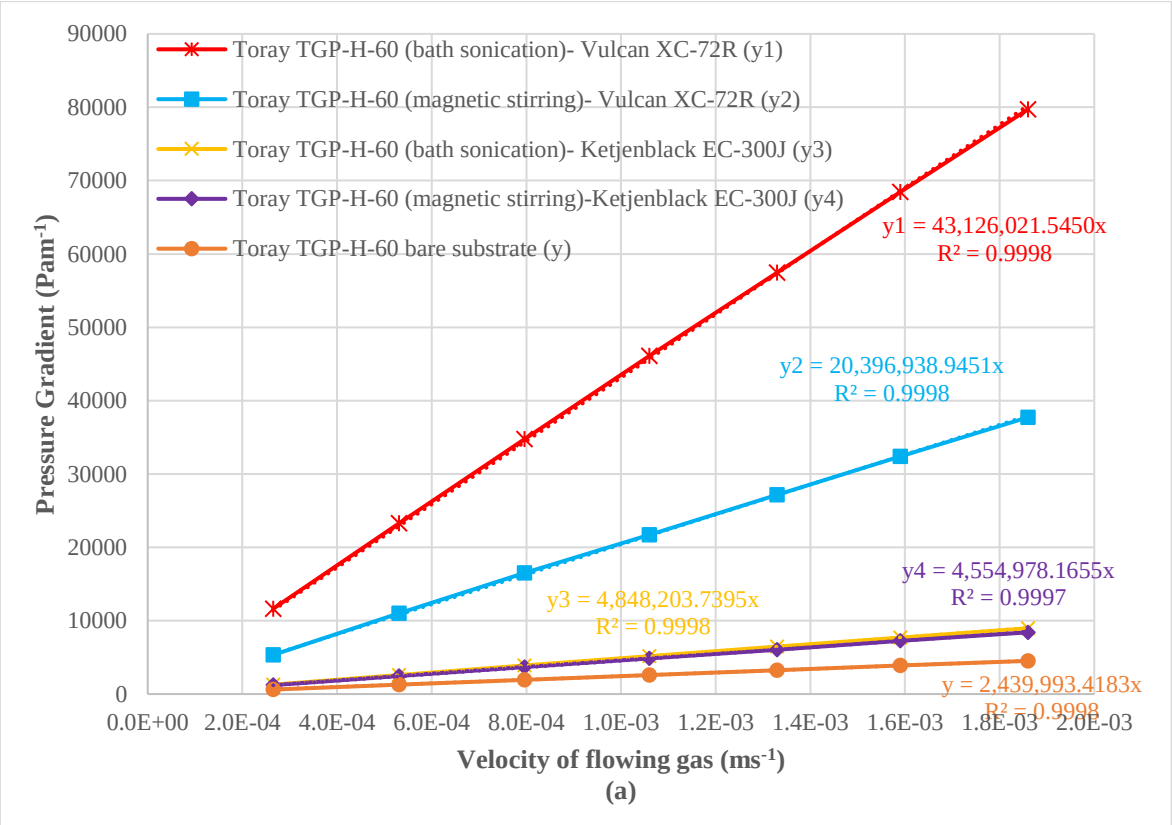

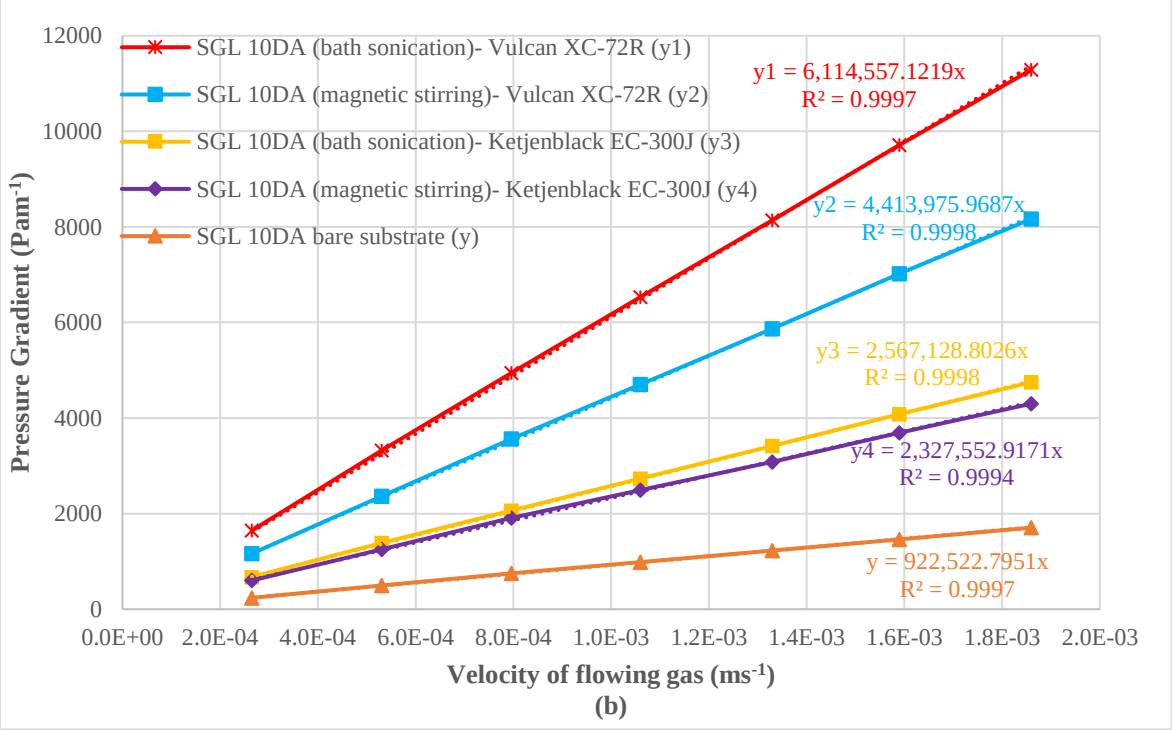

Figure 6. 5 Pressure gradient as a function of fluid velocity using two different ink homogenization techniques for (a) Toray TGP-H-60 and (b) SGL 10DA

Figure 6.6 (a) and (b) illustrate the through-plane permeability of the GDMs for the two (2) techniques indicated and for the two (2) carbon black types: (a) Vulcan XC-72R and (b) Ketjenblack EC-300J. The error bars represent a 95% confidence interval about the mean.

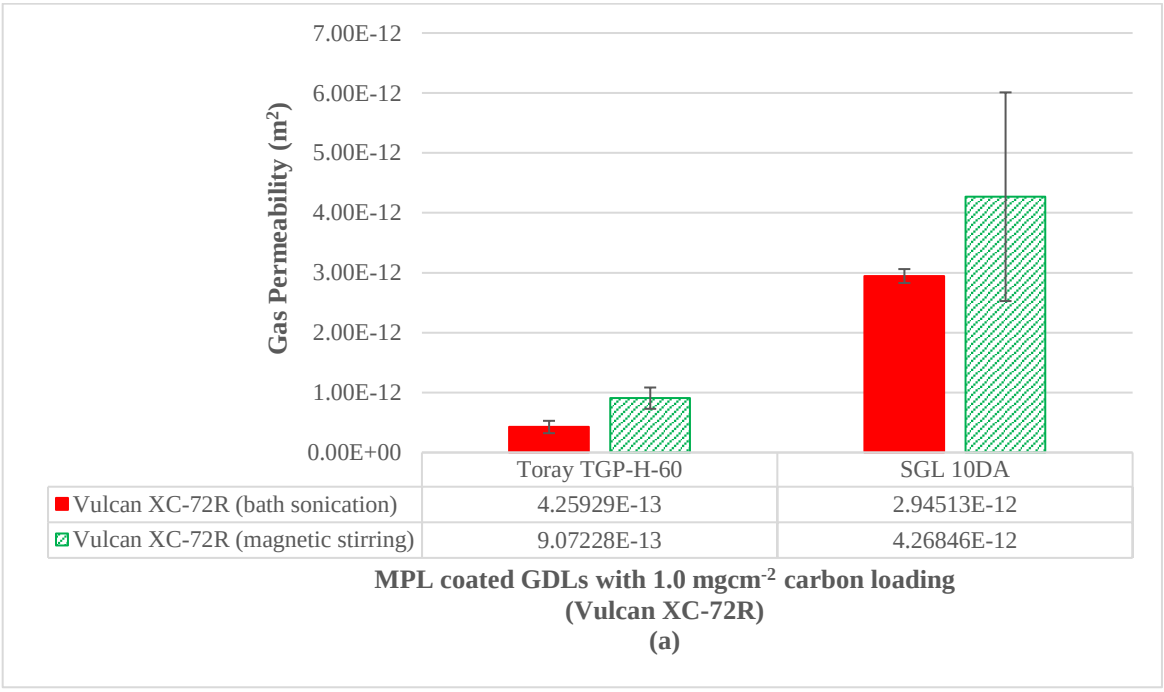

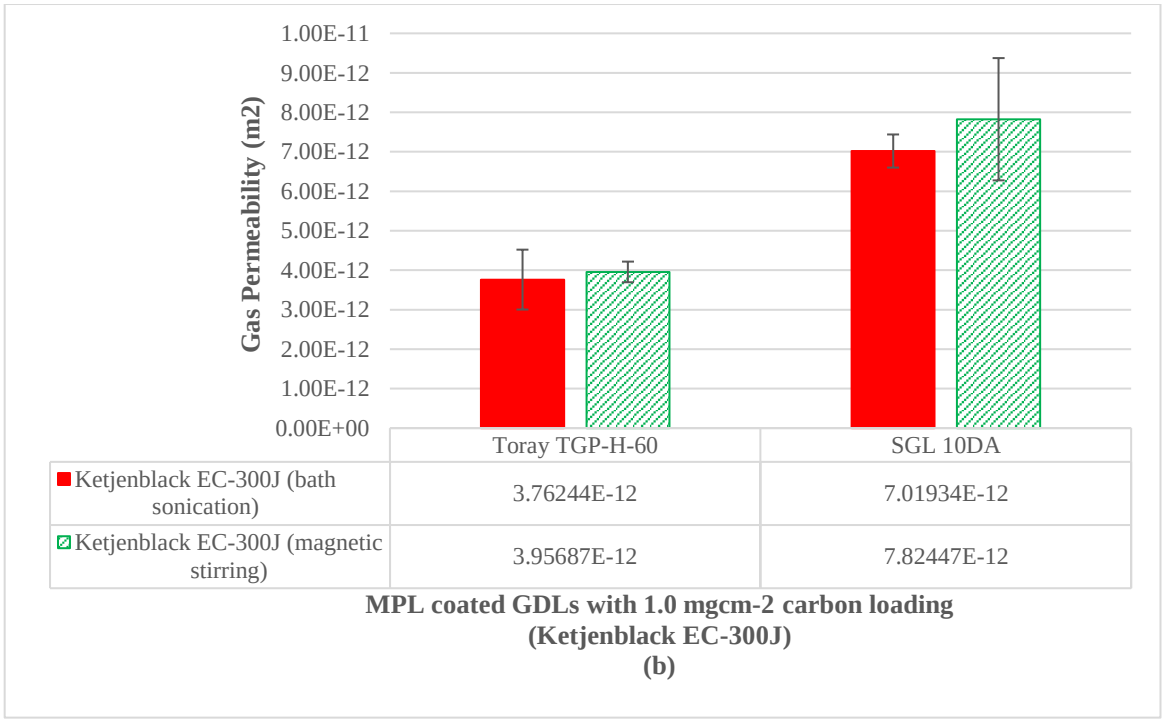

Figure 6. 6 Through-plane gas permeability for substrates coated with (a) Vulcan XC-72R and (b) Ketjenblack EC-300J comparing the effects of bath sonication and magnetic stirring.

Figure 6.6 (a) emphasizes the effect of the two (2) homogenization techniques on the through-plane permeability of the GDMs. The permeability of the GDMs created from magnetic stirring of the ink slurry increased by a factor of 1.5 and 2 for the MPLs composed of Vulcan XC-72R when coated onto SGL 10DA and Toray TGP-H-60 respectively. In all cases, the through-plane permeability increased while utilising magnetic stirring as the homogenization technique and this was independent of the carbon black type; however, the effect was more pronounced for Vulcan XC-72R which had a smaller surface area. Zhiani et al. [129] reported a decrease in in-plane permeability with magnetic stirring when compared to bath sonication; however, this was not the case for through-plane permeability which showed an increase with homogenization using magnetic stirring. Zhiani et al. [129] did indicate that magnetic stirring required a longer period for homogenization. This is quite evident in the results presented here which illustrates the dependency of the period required for homogenization on the carbon powder type. Furthermore, the dispersion of the carbon and PTFE in the ink slurry can explain the results represented here, such that, the utilization of magnetic stirring to homogenize the solution containing Vulcan XC-72R was not as effective as bath sonication and most likely formed larger aggregates of carbon and PTFE creating a less dense, compact MPL containing larger pores which subsequently lead to an increase in through-plane permeability. In order to further investigate the effect of the techniques, the GDM thickness are compared as shown in Figure 6.7 (a) and (b).

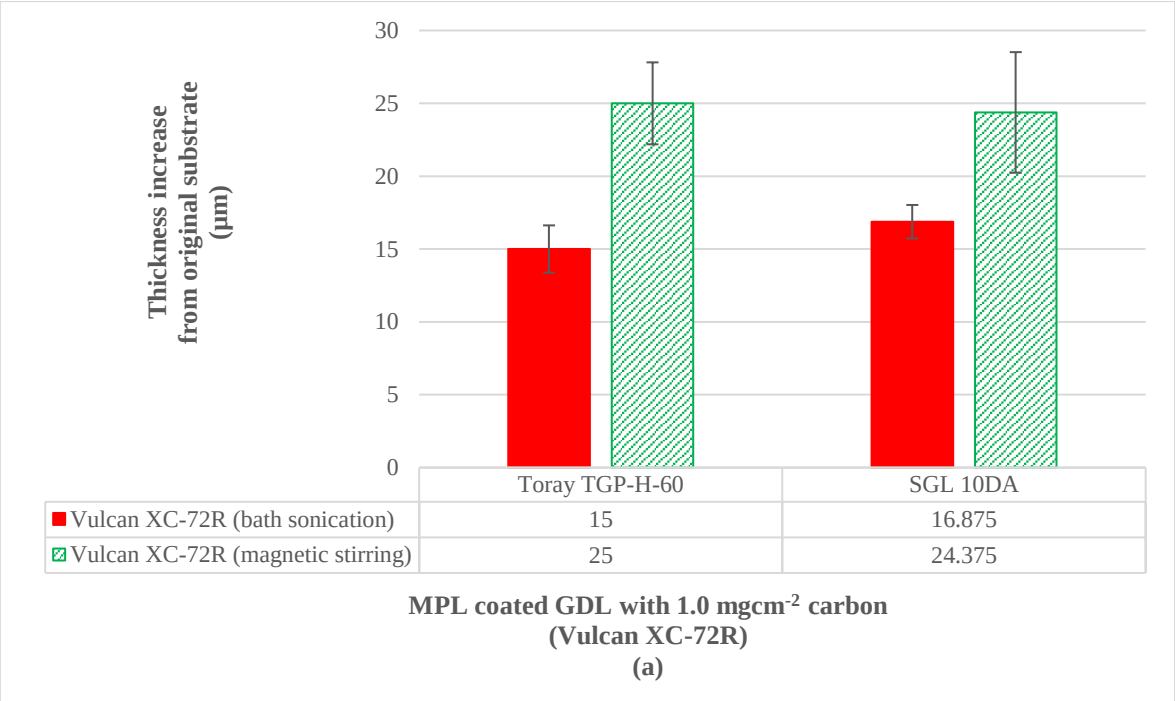

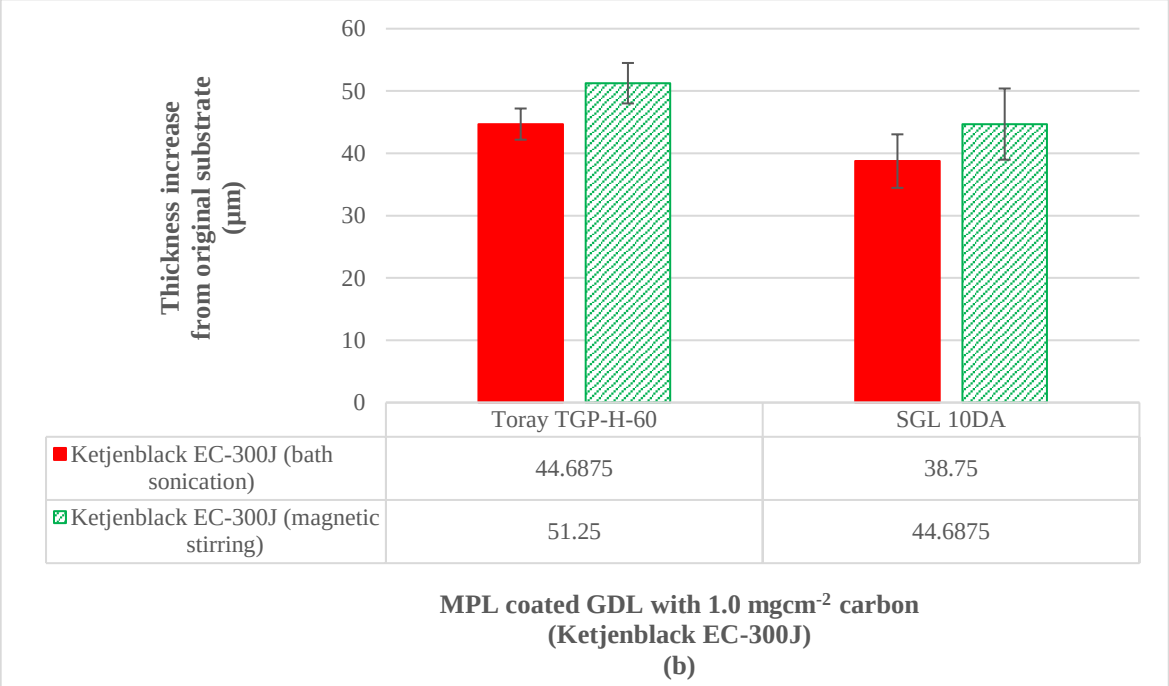

Figure 6. 7 Comparison between the thickness increases of the GDMs from the bare GDL substrate for the two homogenization techniques coated with (a) Vulcan XC-72R and (b) Ketjenblack EC-300J.

As illustrated in Figure 6.7, all cases showed a higher increase in thickness when magnetic stirring was used as the homogenization technique. This further lends weight to the argument that the MPLs created formed larger aggregates which are unable to penetrate the pores of

the GDL, thus resulting in an increase in thickness of the MPL. Figure 6.8 shows the SEM micrographs of the two GDMs coated with each technique discussed for each carbon powder used. The surface morphology of substrates coated using magnetic stirring for the homogenization of the MPL ink show large cracks and many open pores when compared to those which were coated using bath sonication. The micrographs are in agreement with those produced in [129].

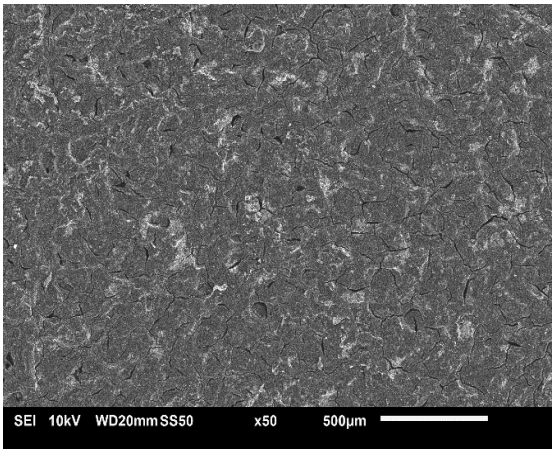

(a)

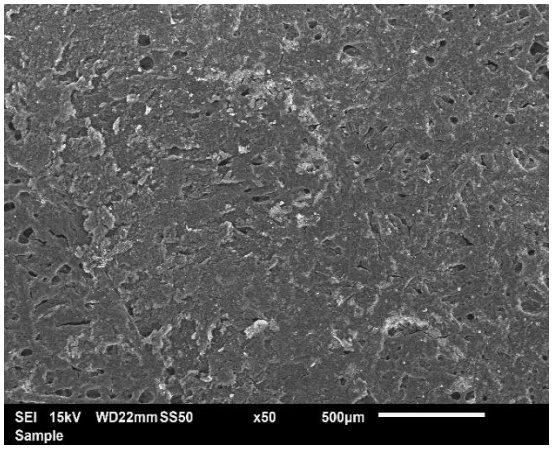

(b)

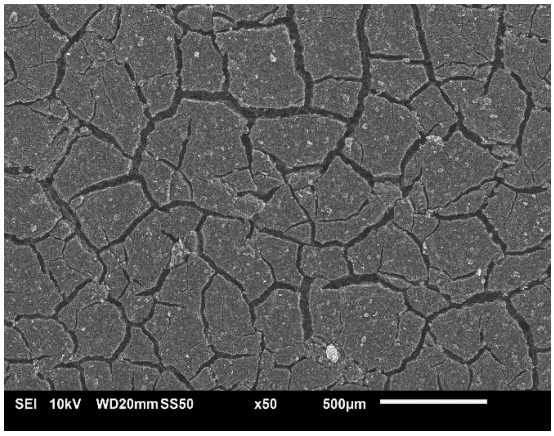

(c)

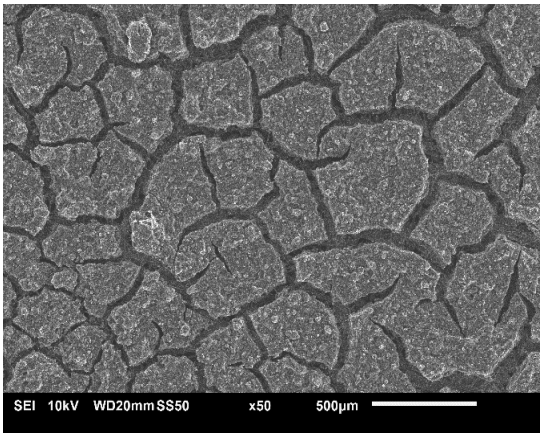

(d)

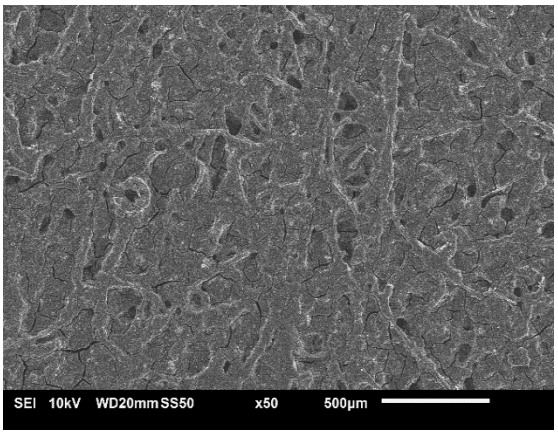

(e)

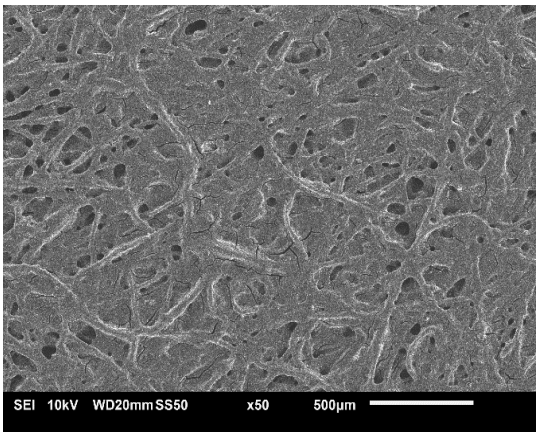

(f)

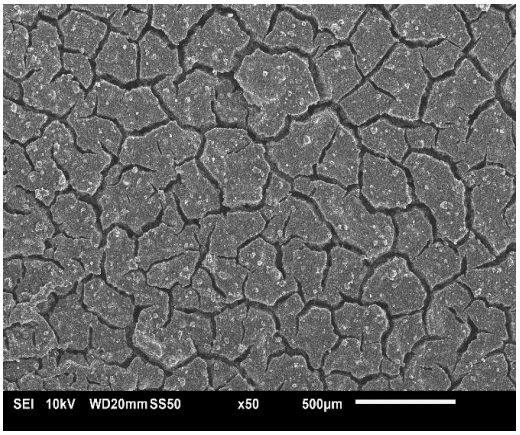

(g)

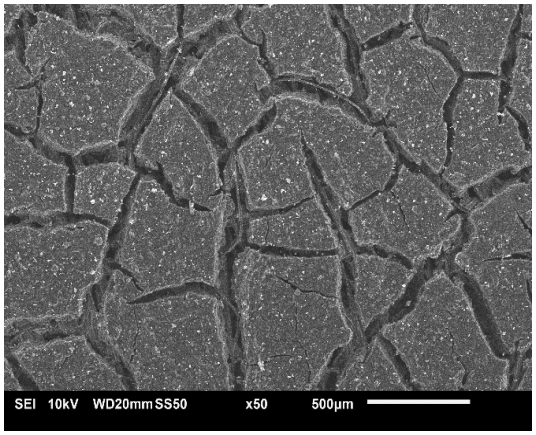

(h)

Figure 6. 8 SEM micrographs showing the surface morphology of the coated substrates using (L) bath sonication and (R) magnetic stirring for (a-b) Toray TGP-H-60 (Vulcan XC-72R), (c-d) Toray TGP-H-60 (Ketjenblack EC-300J, (e-f) SGL 10DA (Vulcan XC-72R) and (g-h) SGL 10DA (Ketjenblack EC-300J).

6.3.2.2 Effect of homogenization time on bath sonication on the through-plane gas permeability of the GDM

This section compares the results of the previous chapters (4 and 5) to understand the effect of homogenization time on through-plane permeability of the GDMs. The through-plane gas permeability and the percentage reduction in permeability from the original substrate for the coated GDLs using Toray TGP-H-60 and SGL 10DA were compared with previous results of Chapter 4 in which MPLs of a similar composition, carbon loading and carbon types were

coated onto similar types of substrates using bath sonication as the homogenization technique for the MPL ink slurry as shown in Figure 6.9 (a) and (b) respectively. It should be noted that the results from Chapter 4 were produced for a three (3) hour sonication time.

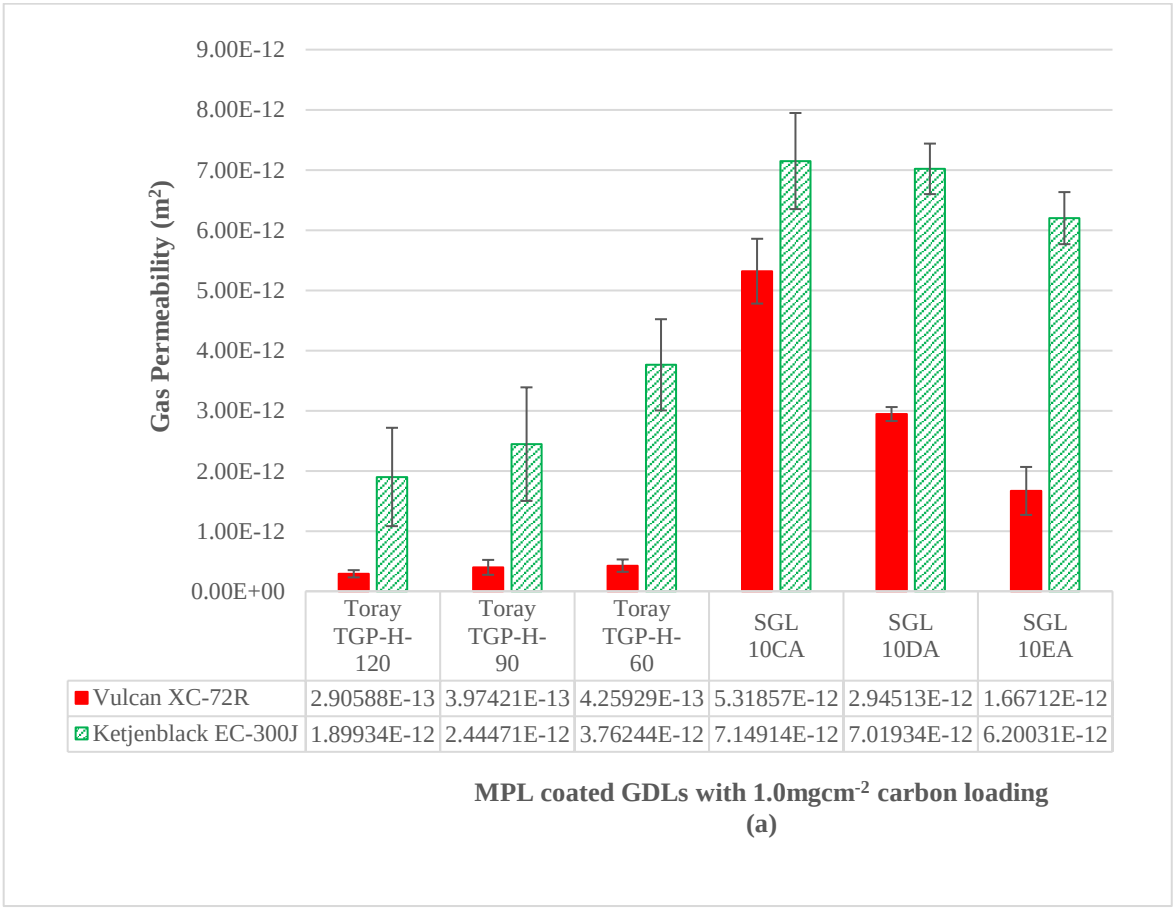

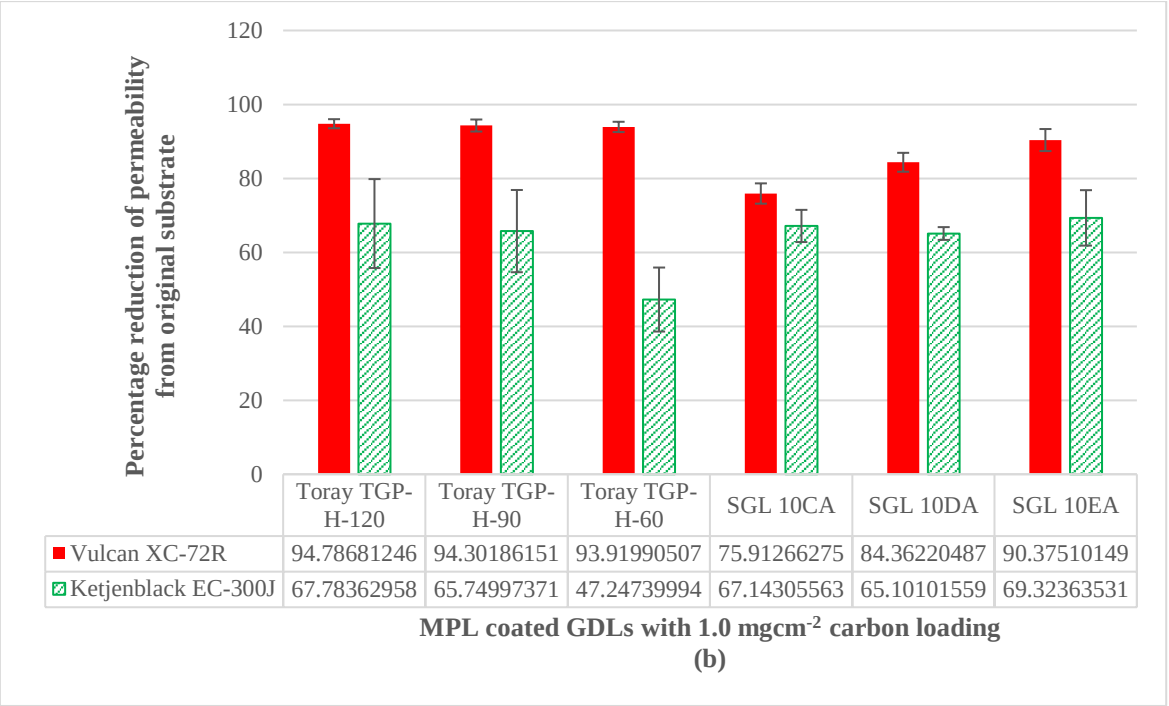

Figure 6. 9 Comparison with previous results (three-hour sonication time) for the (a) Gas permeability and (b) Percentage reduction in permeability of the coated GDLs from the original substrates using bath sonication (two-hour sonication time) as the homogenization technique.

There was a significantly lower difference in the reduction of through-plane gas permeability of Toray TGP-H-60 coated with Ketjenblack EC-300J when compared to similar type GDMs coated with the same carbon black type on Toray TGP-H-120 and Toray TGP-H-90. This can be attributed to the difference in sonication time; however, from Figure 6.9 (b) it can be seen that a one-hour difference in sonication time for the Toray TGP-H-60 GDMs coated with Vulcan XC-72R did not show any significant change. The MPLs coated on SGL 10DA show an 84.36% reduction in permeability for the MPLs composed of Vulcan XC-72R and a 65.1% reduction for those composed of Ketjenblack EC-300J. The results presented in Chapter 4 and shown in Figure 6.9 (b) indicated that there was an increase reduction in permeability from the original substrates with an increase in PTFE loading in the GDL; as such, the results shown for the MPLs coated on SGL 10DA are reasonable and were expected to lie within the bounds of SGL 10CA and SGL 10EA. This was not the case for MPLs composed of Ketjenblack EC-300J coated onto SGL 10DA which should have been within

the range 67.14-69.32% reduction. The small variation outside of this range is attributed to variation in homogenization time. As such, one can deduce that the effect of sonication time significantly affects the through-plane permeability of MPL coated GDLs based on the carbon powder type and also the structure of the GDL substrate, that is, the case of non-woven straight carbon fibre paper GDLs (Toray TGP-H-60) coated with a carbon powder of a larger surface area (Ketjenblack EC-300J) showed the greatest variation.

In order to further investigate the effect of homogenization time the results from this Chapter are compared with those of Chapter 5 in which Toray TGP-H-60 was coated with the same carbon black types, however, the sonication time was increased to three (3) hours. The comparison between the results are shown below in Figure 6.10 (a) and (b). The effect of homogenization time was not discussed for GDMs using SGL 10DA as the GDL substrate since the percentage reduction in gas permeability showed reasonable variation to SGL 10CA and SGL 10EA.

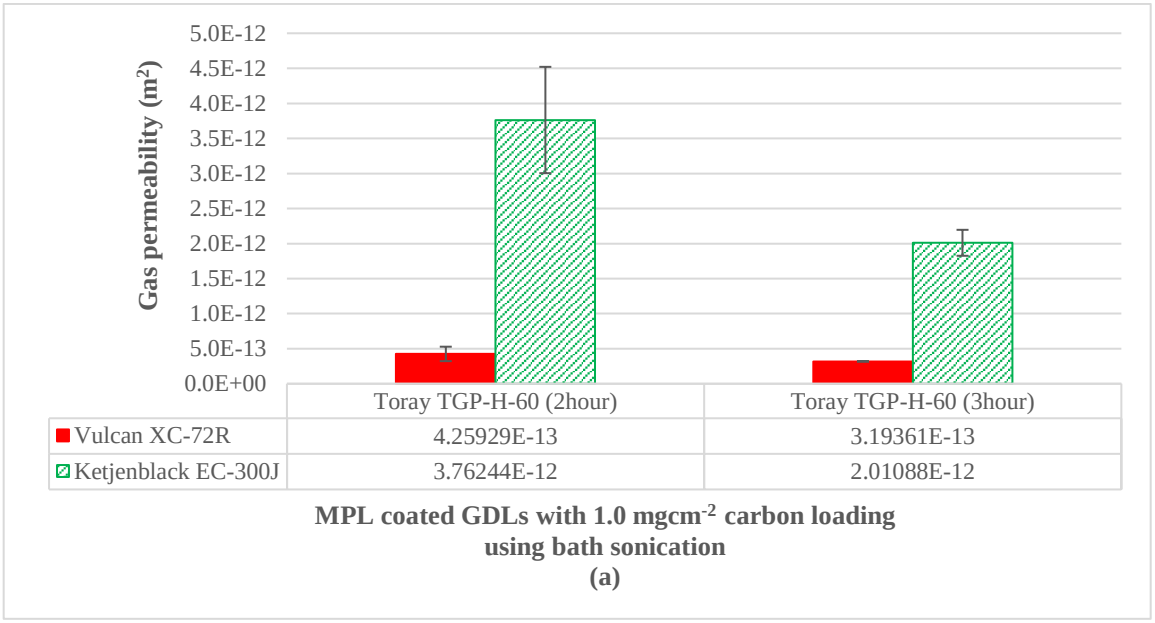

	Toray TGP-H-60 (2hour)	Toray TGP-H-60 (3hour)
Vulcan XC-72R	4.25929E-13	3.19361E-13
Ketjenblack EC-300J	3.76244E-12	2.01088E-12

MPL coated GDLs with 1.0 mgcm^{-2} carbon loading using bath sonication
(a)

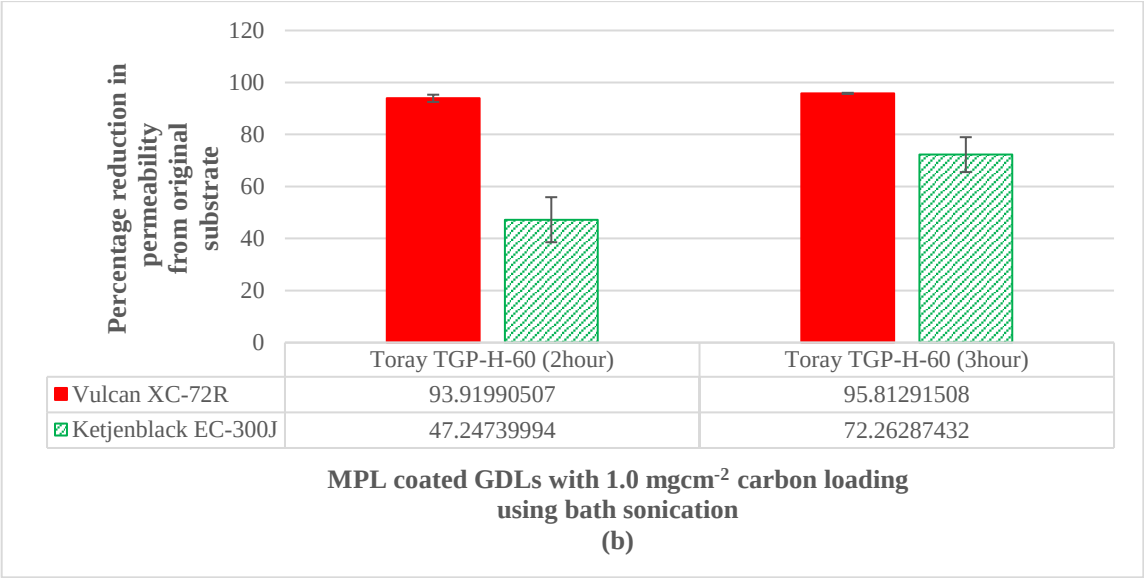

Figure 6. 10 Comparison of the effect of homogenization time using bath sonication on (a) Gas permeability and (b) Percentage reduction in permeability of the coated GDLs from the original substrates.

The GDL substrates coated with Vulcan XC-72R and Ketjenblack EC-300J showed a percentage decrease in terms of gas permeability by 25% and 46.6% respectively with a one hour increase in sonication time; however, the percentage reduction from the original substrates, shown in Figure 6.10 (b) indicated that there was almost an insignificant difference in the reduction of through-plane permeability when compared with the original substrates for the GDLs coated with Vulcan XC-72R. The GDLs coated with Ketjenblack EC-300J does, however, show a considerable difference in percentage reduction. This change is also directly observed in the following SEM images shown in Figure 6.11 (c-d) below with the increase in sonication time showing a smoother, less cracked surface which is an indication of the lower gas permeability. The large variation in the percentage reduction between the two- and three-hour sonication times for MPLs composed of Ketjenblack EC-300J gives an indication of how sensitive carbon powders with larger surface areas are to the period of homogenization of the ink mixture. As such, larger aggregates of carbon and PTFE are most likely present due to a reduced homogenization time.

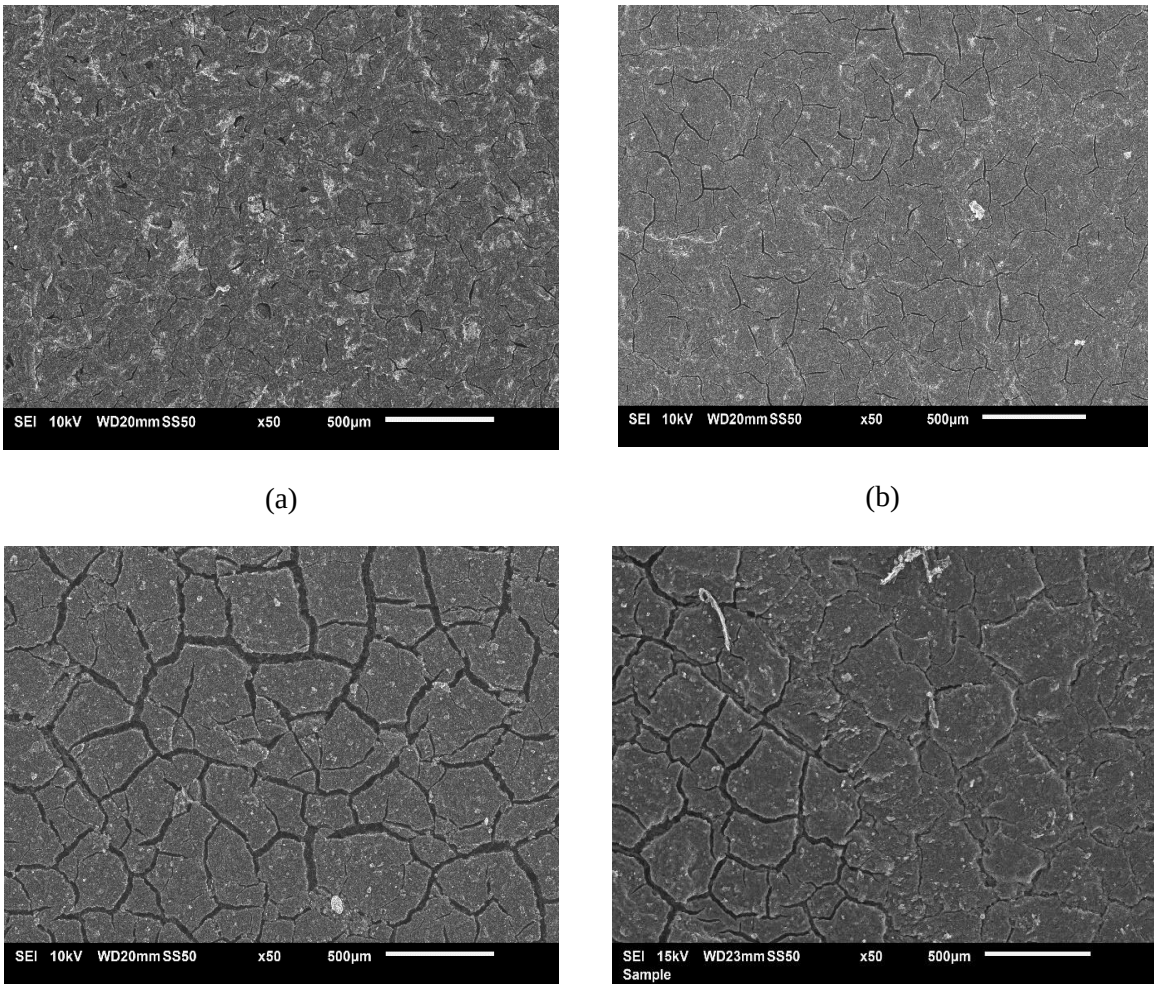

(a) (b)

(c) (d)

Figure 6. 11 SEM images showing the effect of homogenization time for GDLs coated with (a-b) Vulcan XC-72R for 2 and 3 hours sonication time respectively and (c-d) Ketjenblack EC-300J for 2 and 3 hours sonication time respectively.

6.4 Conclusion

This chapter highlights the investigations into two (2) techniques: (i) Bath sonication and (ii) magnetic stirring used in the homogenization of the ink slurry used for preparation of a MPL. The focus of the investigations was on the technique and carbon powder used and their impact on the through-plane permeability and surface morphology of the GDM for a constant carbon loading of 1.0 mgcm^{-2} and constant PTFE loading of 20%. The results in this chapter were compared with previous results described in the earlier chapters of this thesis. The following conclusions obtained are as follows:

- Bath sonication produced MPLs with a smoother surface and less cracks when compared with the surface morphology produced with magnetic stirring.
- Magnetic stirring resulted in an increase in through-plane permeability by a factor of 1.5 to 2 for MPLs composed of Vulcan XC-72R when coated on SGL 10DA and Toray TGP-H-60 respectively. The resulting increase in permeability was attributed to larger aggregates of carbon and PTFE being formed due to the technique used, that is, magnetic stirring requires a longer time to produce a more dispersed homogenized ink mixture as compared to bath sonication. The homogenization technique also influenced the thickness of the MPL where magnetic stirring resulted in thicker structures independent of the GDL substrate. Furthermore, the impact of the felt/spaghetti carbon fibre paper (SGL 10DA) did not show significant influence when both techniques were used to homogenize the ink slurry. Based on the three-hour sonication time used in previous chapters, the through-plane permeability of the GDM containing SGL 10DA as the substrate appeared to be close to the predicted permeability for the two carbon powders when compared to SGL 10CA and SGL 10EA.
- For the two carbon types investigated, the impact of the technique used in the homogenization of the ink mixture was more pronounced for carbon powders with a smaller surface area, that is, Vulcan XC-72R.
- The impact of bath sonication time revealed a significant difference in through-plane permeability with simply a one hour increase in ink homogenization time. The results revealed that carbon powders with a larger surface area (Ketjenblack EC-300J) showed a larger decrease in through-plane permeability by approximately 46% as compared to a carbon powder with a smaller surface area (Vulcan XC-72R) which showed a 25% decrease in through-plane permeability.

The results of the investigations in this study revealed how significant MPL properties are influenced by the type of carbon powder, homogenization technique and time required to produce a well dispersed ink mixture and structure of the substrate onto which an MPL is coated.

Chapter 7

Conclusions and Future Work

Gas permeability is a crucial aspect which can affect the performance of the PEFC as it relates to mass transport losses encountered during PEFC operation. This thesis has focused on experimentally determining the through-plane gas permeability of the PEFC porous media, namely, the gas diffusion layer (GDL) and microporous layer (MPL). In-house experimental apparatus was used to accomplish investigations tailored to focus on the impact of different structured GDLs used in the GDM in order to explore the effects of carbon powder type, carbon loading which directly relates to MPL thickness, sintering time, composite mixtures of combined carbon powders and preparation techniques of the MPL on the through-plane permeability and surface morphology of the GDM. The conclusions described in this chapter were the culmination of all the results attained from the experimental investigations.

7.1 Conclusions

The following conclusions and main findings are discussed as follows:

- Chapter 4 focused on the structural differences of various commercial GDLs and its impact on through-plane permeability of the GDM with attention being paid to carbon type, carbon loading and surface morphology. All investigations were performed for a single MPL composition of 80 wt.% carbon powder and 20 wt.% PTFE and for three (3) different carbon loadings. The impact of PTFE in the GDL

was also investigated. SEM micrographs were used to explore not only surface morphology but also MPL thickness.

Past investigations reported that through-plane permeability of the GDM decreased with increasing carbon loading which directly relates to the MPL thickness; however, it was shown that this conclusion from past research is not necessarily true. Results obtain in Chapter 4 showed that the type of GDL substrate used in conjunction with the type of carbon powder influenced the trend in through-plane permeability of the GDM. Large surface area carbon powder (Ketjenblack EC-300J) used to create an MPL onto a non-woven straight fibre carbon paper showed lower gas permeability for low carbon loadings and higher permeability when the carbon loading increased. Furthermore, the surface morphology of the MPL composed of a low surface area carbon powder (Vulcan XC-72R) resulted in smoother surfaces and lower through-plane permeability when compared to that of the MPL composed of the high surface area which resulted in increased crack sizes and higher gas permeability. This was not the case reported in the literature previously, where the GDM through-plane permeability was found to be lower with Ketjenblack EC-300J. It should also be pointed out that independent of the carbon powder used in the MPL when coated onto a felt/spaghetti type carbon fibre paper, the through-plane permeability decreased with increasing carbon loading.

The MPL permeability was shown to have no distinct trend with increasing carbon loading and was independent of the carbon powder used even when the MPL thickness was determined from SEM images. These further highlight the inaccuracy of determining the MPL penetration into the GDL substrate. MPL permeability was

to be significantly lower, by at least an order of magnitude if the penetration into the GDL was ignored.

The impact of PTFE in the GDL on GDM through-plane permeability also showed larger percentage reductions from the permeability of the original substrate with increasing PTFE in the GDL for increased carbon loadings with a low surface area carbon powder and resulted in thicker MPL thicknesses. High surface area carbon powders showed negligible impact in terms of percentage reduction of GDM through-plane permeability from the original substrate with increased carbon loading.

- Chapter 5 focused on the effect of sintering time and composite mixtures of two carbon powders on the through-plane permeability of the GDM. Investigations were conducted for a constant carbon loading of 1.0 $mgcm^{-2}$ for the former and for 1.0 $mgcm^{-2}$ and 2.0 $mgcm^{-2}$ for the later. The effect of PTFE in the MPL was also assessed with regard to variable sintering times. SEM images were used to explore the effects of both investigations on surface morphology.

  Low PTFE loadings in the MPL (~20-25%) resulted in variable trends in through-plane permeability with increasing sintering times. High PTFE loading (~50%) in the MPL resulted in an increase in through-plane permeability which was validated with SEM images indicating increased pores/gaseous paths on the MPL surface.

  Composite mixtures of two carbon blacks in different ratios was investigated in relation to GDM permeability. The results indicated that the various percentage ratio

combinations were found to lie within the bounds of the single powders used regardless of the carbon loadings. The through-plane permeability and thickness increase were both found to lie within the limits of the GDMs constructed of single carbon powders.

- Chapter 6 focused on the impact of two (2) homogenization techniques used to create the MPL ink slurry before its application to the GDL. Bath sonication and magnetic stirring were two methods explored; two different carbon powders were explored for a constant carbon loading of 1.0 $mgcm^{-2}$ and constant MPL composition of 80 wt.% carbon powder and 20 wt.% PTFE. The impact of different structured GDLs was also investigated in order to ascertain if the homogenization techniques would be impacted by structural differences in the GDL.

  Bath sonication was found to produce MPLs with a smoother surface which formed less cracks when compared with the surface morphology of magnetic stirring. Magnetic stirring resulted in the through-plane permeability of the GDM being increased by a factor of 1.5 to 2 for MPLs composed of Vulcan XC-72R when coated onto SGL 10DA and Toray TGP-H-60 respectively. This increase was attributed to larger aggregates of carbon and PTFE being formed due to the technique, that is, magnetic stirring required a longer time to produce a more dispersed mixture. The impact of the technique used in the homogenization was shown to be more pronounced with small surface area carbon powders. The homogenization technique also influenced the thickness of the MPL where magnetic stirring resulted in thicker structures independent of the GDL substrate. Furthermore, the impact of the felt/spaghetti carbon fibre paper (SGL 10DA) did not show significant influence when both techniques were used to homogenize the ink slurry. Based on the 3 hour

sonication time used in previous chapters, the through-plane permeability of the GDM containing SGL 10DA as the substrate appeared to be close to the predicted permeability for the two carbon powders when compared to SGL 10CA and SGL 10EA.

The impact of bath sonication time was investigated and its impact was significant. There was a significant difference in the through-plane permeability with only a one hour increase in sonication time. The reduction in through-plane permeability for the larger surface area carbon powder was approximately 46% as compared to that of the smaller surface area carbon powder which showed a 25% decrease. The percentage decrease in permeability from the original substrate was ~47% for the large surface area carbon powder with a two-hour sonication time as compared with ~72% for a three-hour sonication time.

The results revealed how significant MPL properties are influences by the type of powder, homogenization technique, the time required to obtain a well dispersed ink solution and the type of substrate.

7.2 Possible future work

Several GDM structures were discussed in this thesis which varied in thickness, morphology and gas permeability. Various techniques were used to ascertain the impact on the above; however, the knowledge gained from the experimental work still leaves several aspects of the research unanswered in the optimization of the GDM. As such, several key issues require further investigation in order to further tailor the GDM to achieve the desirable fuel cell performance under certain conditions:

- Non-woven straight carbon fibre papers were investigated in Chapter 4 for a single MPL composition of 80 wt.% carbon powder and 20 wt.% PTFE. In more thorough look into various MPL compositions, for example different ratios of carbon powder to PTFE, using this structured GDL would be beneficial since its showed significant variation from the accepted literature in terms of increase carbon loadings in conjunction with the type of carbon powder used. Furthermore, the impact of PTFE in the GDL was only conducted for felt/spaghetti carbon fibre paper. As such, investigations into different PTFE loadings in the GDL for non-woven straight fibre GDLs still remains unanswered.
- The impact of sintering time for varying PTFE in the MPL was conducted for commercial samples whose GDL substrate is a felt/spaghetti carbon fibre paper. The impact of varying levels of PTFE in the MPL utilising a non-woven straight carbon fibre paper requires further investigation.
- Composite mixtures were conducted using two carbon powders with varied physical characteristics. The investigations conducted in this thesis highlighted that regardless of the carbon loading for a given MPL composition, the GDM can be engineering to possess certain characters such as gas permeability, thickness and surface morphology. However, other characteristics such as contact angle, electrical conductivity, porosity, contact resistance, bulk density and tortuosity still require further investigations.

  The above quantities are needed for a complete investigation of the impact of carbon loading and carbon powder type on the GDM. Contact angle is typically investigated with a drop shape analyser which utilises the Sessile Drop Method to determine the angle at which a water droplet interfaces with the surface of the GDM. Electrical properties such as conductivity and contact resistance are usually measured with in-

house based experimental setup. A four-point/plate method is employed whereby a DC current is supplied across the GDM and the voltage drop measured across two different points/plates. Bulk density, tortuosity, porosity and pore-size distribution can be obtained with the use of a Mercury Intrusion Porosimeter (MIP) whereby mercury is forced into the larger pores at low pressures and smaller pores at high pressures within a specified range. Furthermore, the absolute permeability of the GDM can be obtained with MIP which can then be used to determine the tortuosity. The absolute density of the GDM can be measured with the use of a pycnometer. The sample GDM is placed in a chamber of known volume; after evacuation of the air in the chamber, a gas such as helium is pumped into the sample to measure the void volume. The density is then determined from the division of the sample mass by the subtraction of the chamber volume from the void volume. Further information on these techniques can be found in [78]. Surface area measurements can be determined with the use of a surface area analyser. Surface area analysers utilise Brunauer-Emmett-Teller (BET) theory which determines how a surface (solid or porous) interfaces with its surroundings such as a fluid. Gas adsorption is used to determine the surface area through consideration of the adsorption capacity of the sample. Further information about BET theory can be found in [149].

- The technique used to homogenize the ink slurry in MPL preparation was investigated for through-plane permeability. Homogenization time in conjunction with the type of carbon powders still needs further investigation. A more standardized approach needs to be adopted in order to determine the time needed to produce a well dispersed and homogenized solution.
- Experimental application of the MPL in this thesis involved a single technique, that is, spray coating. There are several techniques used in the application of the MPL ink

slurry to the GDL. Undoubtedly, the morphology and characteristics of the GDM would differ for the type of application. Moreover, spray coating performed during this thesis was done manually and as such, in order to improved reproducibility an automated coating system would be an improvement and something to consider for future work.

- This thesis focused on the through-plane permeability of the GDM. The GDL is considered anisotropic and the experimental work conducted here can be extended to focus on how these investigated parameters can affect the in-plane permeability.

Bibliography

[1] X. Li, “Diversification and localization of energy systems for sustainable development and energy security,” *Energy Policy*, vol. 33, no. 17, pp. 2237–2243, 2005, doi: 10.1016/j.enpol.2004.05.002.

[2] I. E. Agency, “Energy and Climate Change World Energy Outlook Special Report,” 2015.

[3] BP, “Statistical Review of World Energy,” 2015. [Online]. Available: https://www.bp.com/en/global/corporate/energy-economics/statistical-review-of-world-energy.html.

[4] J. Bielecki, “Energy security: Is the wolf at the door?,” *Q. Rev. Econ. Financ.*, vol. 42, no. 2, pp. 235–250, 2002, doi: 10.1016/S1062-9769(02)00137-0.

[5] K. Sopian and W. R. Wan Daud, “Challenges and future developments in proton exchange membrane fuel cells,” *Renew. Energy*, vol. 31, no. 5, pp. 719–727, 2006, doi: 10.1016/j.renene.2005.09.003.

[6] H. Lund, “Renewable energy strategies for sustainable development,” *Energy*, vol. 32, no. 6, pp. 912–919, 2007, doi: 10.1016/j.energy.2006.10.017.

[7] IEA, “Tracking Clean Energy Progress 2016,” *Energy Technol. Perspect. 2016 Excerpt*, p. 84, 2016.

[8] F. Barbir, *PEM Fuel Cells: Theory and Practice*, Second Edi. Elsevier Science, 2012.

[9] N. H. Behling, *Fuel Cells: Current Technology Challenges and Future Research*

Needs, First. Elsevier Science, 2012.

[10] Y. Wang, K. S. Chen, J. Mishler, S. C. Cho, and X. C. Adroher, "A review of polymer electrolyte membrane fuel cells: Technology, applications, and needs on fundamental research," *Appl. Energy*, vol. 88, no. 4, pp. 981–1007, 2011, doi: 10.1016/j.apenergy.2010.09.030.

[11] O. Z. Sharaf and M. F. Orhan, "An overview of fuel cell technology: Fundamentals and applications," *Renew. Sustain. Energy Rev.*, vol. 32, pp. 810–853, 2014, doi: 10.1016/j.rser.2014.01.012.

[12] D. Bruggeman, "Calculation of Various Physics Constants in Heterogeneous Substances I Dielectricity Constants and Conductivity of Mixed Bodies from Isotropic Substances," *Ann. Phys.*, vol. 24, no. 7, pp. 636–664, 1935.

[13] G. H. Neale and W. K. Nader, "Prediction of transport processes within porous media: Diffusive flow processes within an homogeneous swarm of spherical particles," *AIChE J.*, vol. 19, no. 1, pp. 112–119, 1973, doi: 10.1002/aic.690190116.

[14] P. K. Das, X. Li, and Z. S. Liu, "Effective transport coefficients in PEM fuel cell catalyst and gas diffusion layers: Beyond Bruggeman approximation," *Appl. Energy*, vol. 87, no. 9, pp. 2785–2796, 2010, doi: 10.1016/j.apenergy.2009.05.006.

[15] M. M. Tomadakis and S. V. Sotirchos, "Ordinary, transition, and Knudsen regime diffusion in random capillary structures," *Chem. Eng. Sci.*, vol. 48, no. 19, pp. 3323–3333, 1993, doi: 10.1016/0009-2509(93)80149-K.

[16] J. H. Nam and M. Kaviany, "Effective diffusivity and water-saturation distribution in single- and two-layer PEMFC diffusion medium," *Int. J. Heat Mass Transf.*, vol. 46, no. 24, pp. 4595–4611, 2003, doi: 10.1016/S0017-9310(03)00305-3.

[17] N. Zamel, X. Li, and J. Shen, “Correlation for the effective gas diffusion coefficient in carbon paper diffusion media,” *Energy and Fuels*, vol. 23, no. 12, pp. 6070–6078, 2009, doi: 10.1021/ef900653x.

[18] N. Zamel, X. Li, J. Becker, and A. Wiegmann, “Effect of liquid water on transport properties of the gas diffusion layer of polymer electrolyte membrane fuel cells,” *Int. J. Hydrogen Energy*, vol. 36, no. 9, pp. 5466–5478, 2011, doi: 10.1016/j.ijhydene.2011.01.146.

[19] G. Unsworth, L. Dong, and X. Li, “Improved experimental method for measuring gas diffusivity through thin porous media,” *AlChe*, vol. 59, no. 4, pp. 1409–1419, 2013.

[20] M. J. Martínez, S. Shimpalee, and J. W. Van Zee, “Measurement of MacMullin numbers for PEMFC gas-diffusion media,” *J. Electrochem. Soc.*, vol. 156, no. 1, pp. 25–27, 2009, doi: 10.1149/1.3005564.

[21] R. Flückiger, S. A. Freunberger, D. Kramer, A. Wokaun, G. G. Scherer, and F. N. Büchi, “Anisotropic, effective diffusivity of porous gas diffusion layer materials for PEFC,” *Electrochim. Acta*, vol. 54, no. 2, pp. 551–559, 2008, doi: 10.1016/j.electacta.2008.07.034.

[22] J. M. Lamanna and S. G. Kandlikar, “Determination of effective water vapor diffusion coefficient in pemfc gas diffusion layers,” *Int. J. Hydrogen Energy*, vol. 36, no. 8, pp. 5021–5029, 2011, doi: 10.1016/j.ijhydene.2011.01.036.

[23] N. Zamel *et al.*, “Experimental measurements of effective diffusion coefficient of oxygen-nitrogen mixture in PEM fuel cell diffusion media,” *Chem. Eng. Sci.*, vol. 65, no. 2, pp. 931–937, 2010, doi: 10.1016/j.ces.2009.09.044.

[24] C. Chan, N. Zamel, X. Li, and J. Shen, “Experimental measurement of effective diffusion coefficient of gas diffusion layer/microporous layer in PEM fuel cells,” *Electrochim. Acta*, vol. 65, pp. 13–21, 2012, doi: 10.1016/j.electacta.2011.12.110.

[25] N. Zamel and X. Li, “Effective transport properties for polymer electrolyte membrane fuel cells - With a focus on the gas diffusion layer,” *Prog. Energy Combust. Sci.*, vol. 39, no. 1, pp. 111–146, 2013, doi: 10.1016/j.pecs.2012.07.002.

[26] D. Baker, C. Wieser, K. C. Neyerlin, and M. W. Murphy, “The use of limiting current to determine transport resistance in PEM fuel cells,” *ECS Trans.*, vol. 3, no. 1, pp. 989–999, 2006, doi: 10.1149/1.2356218.

[27] D. R. Baker, D. A. Caulk, K. C. Neyerlin, and M. W. Murphy, “Measurement of oxygen transport resistance in PEM fuel cells by limiting current methods,” *J. Electrochem. Soc.*, vol. 156, no. 9, 2009, doi: 10.1149/1.3152226.

[28] J. Stumper, H. Haas, and A. Granados, “In situ determination of MEA resistance and electrode diffusivity of a fuel cell,” *J. Electrochem. Soc.*, vol. 152, no. 4, 2005, doi: 10.1149/1.1867673.

[29] U. Beuscher, “Experimental method to determine the mass transport resistance of a polymer electrolyte fuel cell,” *J. Electrochem. Soc.*, vol. 153, no. 9, pp. 1788–1793, 2006, doi: 10.1149/1.2218760.

[30] D. Kramer *et al.*, “Electrochemical diffusimetry of fuel cell gas diffusion layers,” *J. Electroanal. Chem.*, vol. 612, no. 1, pp. 63–77, 2008, doi: 10.1016/j.jelechem.2007.09.014.

[31] N. B. Carrigy, L. M. Pant, S. Mitra, and M. Secanell, “Knudsen Diffusivity and Permeability of PEMFC Microporous Coated Gas Diffusion Layers for Different

Polytetrafluoroethylene Loadings," *J. Electrochem. Soc.*, vol. 160, no. 2, pp. F81–F89, 2012, doi: 10.1149/2.036302jes.

[32] M. S. Ismail, D. Borman, T. Damjanovic, D. B. Ingham, and M. Pourkashanian, "On the through-plane permeability of microporous layer-coated gas diffusion layers used in proton exchange membrane fuel cells," *Int. J. Hydrogen Energy*, vol. 36, no. 16, pp. 10392–10402, 2011, doi: 10.1016/j.ijhydene.2010.09.012.

[33] A. El-Kharouf, T. J. Mason, D. J. L. Brett, and B. G. Pollet, "Ex-situ characterisation of gas diffusion layers for proton exchange membrane fuel cells," *J. Power Sources*, vol. 218, pp. 393–404, 2012, doi: 10.1016/j.jpowsour.2012.06.099.

[34] C. K. Dyer, "Fuel cells for portable applications," *J. Power Sources*, vol. 106, no. 1–2, pp. 31–34, 2002, doi: 10.1016/S0378-7753(01)01069-2.

[35] S. Park, J. W. Lee, and B. N. Popov, "A review of gas diffusion layer in PEM fuel cells: Materials and designs," *Int. J. Hydrogen Energy*, vol. 37, no. 7, pp. 5850–5865, 2012, doi: 10.1016/j.ijhydene.2011.12.148.

[36] H. K. Atiyeh, K. Karan, B. Peppley, A. Phoenix, E. Halliop, and J. Pharoah, "Experimental investigation of the role of a microporous layer on the water transport and performance of a PEM fuel cell," *J. Power Sources*, vol. 170, no. 1, pp. 111–121, 2007, doi: 10.1016/j.jpowsour.2007.04.016.

[37] W. Dai *et al.*, "A review on water balance in the membrane electrode assembly of proton exchange membrane fuel cells," *Int. J. Hydrogen Energy*, vol. 34, no. 23, pp. 9461–9478, 2009, doi: 10.1016/j.ijhydene.2009.09.017.

[38] S. G. Kandlikar and Z. Lu, "Thermal management issues in a PEMFC stack - A brief review of current status," *Appl. Therm. Eng.*, vol. 29, no. 7, pp. 1276–1280,

2009, doi: 10.1016/j.applthermaleng.2008.05.009.

[39] S. G. Goebel, “Evaporative Cooled Fuel Cell,” US 6,960,404 B2, 2005.

[40] A. Hakenjos, H. Muenter, U. Wittstadt, and C. Hebling, “A PEM fuel cell for combined measurement of current and temperature distribution, and flow field flooding,” *J. Power Sources*, vol. 131, no. 1–2, pp. 213–216, 2004, doi: 10.1016/j.jpowsour.2003.11.081.

[41] J. G. Pharoah and O. S. Burheim, “On the temperature distribution in polymer electrolyte fuel cells,” *J. Power Sources*, vol. 195, no. 16, pp. 5235–5245, 2010, doi: 10.1016/j.jpowsour.2010.03.024.

[42] R. M. Aslam, D. B. Ingham, M. S. Ismail, K. J. Hughes, L. Ma, and M. Pourkashanian, “Simultaneous thermal and visual imaging of liquid water of the PEM fuel cell flow channels,” *J. Energy Inst.*, vol. 92, no. 2, pp. 311–318, 2019, doi: 10.1016/j.joei.2018.01.005.

[43] M. S. Ismail, D. B. Ingham, K. J. Hughes, L. Ma, and M. Pourkashanian, “An efficient mathematical model for air-breathing PEM fuel cells,” *Appl. Energy*, vol. 135, pp. 490–503, 2014, doi: 10.1016/j.apenergy.2014.08.113.

[44] W. T. Grubb and L. W. Niedrach, “Batteries with Solid Ion-Exchange Membrane Electrolytes II. Low-Temperature Hydrogen-Oxygen Fuel Cells,” *J. Electrochem. Soc.*, vol. 107, no. 2, pp. 131–135, 1960.

[45] L. W. Niedrach, “The Performance of Hydrocarbons in Ion Exchange Membrane Fuel Cells,” *J. Electrochem. Soc.*, vol. 109, no. 11, p. 1092, 1962, doi: 10.1149/1.2425244.

[46] G. A. Eisman, “The application of Dow Chemical’s perfluorinated membranes in proton-exchange membrane fuel cells,” *J. Power Sources*, vol. 29, no. 3–4, pp. 389–398, 1990, doi: 10.1016/0378-7753(90)85012-2.

[47] K. Prater, “The renaissance of the solid polymer fuel cell,” *J. Power Sources*, vol. 29, no. 1–2, pp. 239–250, 1990, doi: 10.1016/0378-7753(90)80023-7.

[48] S. Srinivasan, E. A. Ticianelli, C. R. Derouin, and A. Redondo, “Advances in solid polymer electrolyte fuel cell technology with low platinum loading electrodes,” *J. Power Sources*, vol. 22, no. 3–4, pp. 359–375, 1988, doi: 10.1016/0378-7753(88)80030-2.

[49] I. D. Raistrick, “Electrode Assembly For Use In A Solid Polymer Electrolyte Fuel Cell,” 4,876,115, 1989.

[50] R. W. Lindstrom, “Electrocatalytic Gas Diffusion Electrode Employing Then Carbon Cloth Layer,” 4,647,359, 1987.

[51] G. Hoogers, “Fuel cell Technology Handbook,” First., G. Hoogers, Ed. Boca Raton, Florida: CRC Press, 2003.

[52] D. S. Cameron, “World Development of Fuel Cells,” *Int. J. Hydrogen Energy*, vol. 15, no. 9, pp. 669–675, 1990.

[53] H. Kato, “Gas Diffusion Layer For Solid Polymer Electrolyte Fuel Cell,” 6,127,059, 2000.

[54] M. S. Wilson, “Fuel Cell With Interdigitated Porous Flow-Field,” 5,641,586, 1997.

[55] E. Passalacqua, G. Squadrito, F. Lufrano, A. Patti, and L. Giorgi, “Effects of the diffusion layer characteristics on the performance of polymer electrolyte fuel cell

electrodes," *J. Appl. Electrochem.*, vol. 31, no. 4, pp. 449–454, 2001, doi: 10.1023/A:1017547112282.

[56] J. H. Chun *et al.*, "Development of a novel hydrophobic/hydrophilic double micro porous layer for use in a cathode gas diffusion layer in PEMFC," *Int. J. Hydrogen Energy*, vol. 36, no. 14, pp. 8422–8428, 2011, doi: 10.1016/j.ijhydene.2011.04.038.

[57] C. S. Kong, D. Y. Kim, H. K. Lee, Y. G. Shul, and T. H. Lee, "Influence of pore-size distribution of diffusion layer on mass-transport problems of proton exchange membrane fuel cells," *J. Power Sources*, vol. 108, no. 1–2, pp. 185–191, 2002, doi: 10.1016/S0378-7753(02)00028-9.

[58] J. Zhang, *PEM Fuel Cell Electrocatalysts and Catalyst Layers: Fundamentals and Applications*, First. Springer London, 2008.

[59] C. Spiegel, *PEM Fuel Cell Modeling and Simulation Using Matlab*. Elsevier Science, 2011.

[60] M. S. Ismail, "On the Transport Properties of Gas Diffusion Layers used in Proton Exchange Membrane Fuel Cells," University of Leeds, 2011.

[61] C. Lim and C. Y. Wang, "Effects of hydrophobic polymer content in GDL on power performance of a PEM fuel cell," *Electrochim. Acta*, vol. 49, no. 24, pp. 4149–4156, 2004, doi: 10.1016/j.electacta.2004.04.009.

[62] M. Ji and Z. Wei, "A review of water management in polymer electrolyte membrane fuel cells," *Energies*, vol. 2, no. 4, pp. 1057–1106, 2009, doi: 10.3390/en20401057.

[63] S. Park, J. W. Lee, and B. N. Popov, "Effect of carbon loading in microporous layer on PEM fuel cell performance," *J. Power Sources*, vol. 163, no. 1 SPEC. ISS., pp.

357–363, 2006, doi: 10.1016/j.jpowsour.2006.09.020.

[64] R. P. Ramasamy, E. C. Kumbur, M. M. Mench, W. Liu, D. Moore, and M. Murthy, "Investigation of macro- and micro-porous layer interaction in polymer electrolyte fuel cells," *Int. J. Hydrogen Energy*, vol. 33, no. 13, pp. 3351–3367, 2008, doi: 10.1016/j.ijhydene.2008.03.053.

[65] A. Fischer, J. Jindra, and H. Wendt, "Porosity and catalyst utilization of thin layer cathodes in air operated PEM-fuel cells," *J. Appl. Electrochem.*, vol. 28, no. 3, pp. 277–282, 1998, doi: 10.1023/A:1003259531775.

[66] R. Chen and T. S. Zhao, "A novel electrode architecture for passive direct methanol fuel cells," *Electrochem. commun.*, vol. 9, no. 4, pp. 718–724, 2007, doi: 10.1016/j.elecom.2006.11.004.

[67] C. C. Yang, S. J. Chiu, and C. T. Lin, "Electrochemical performance of an air-breathing direct methanol fuel cell using poly(vinyl alcohol)/hydroxyapatite composite polymer membrane," *J. Power Sources*, vol. 177, no. 1, pp. 40–49, 2008, doi: 10.1016/j.jpowsour.2007.11.010.

[68] F. Y. Zhang, S. G. Advani, and A. K. Prasad, "Performance of a metallic gas diffusion layer for PEM fuel cells," *J. Power Sources*, vol. 176, no. 1, pp. 293–298, 2008, doi: 10.1016/j.jpowsour.2007.10.055.

[69] Y. Tang, W. Zhou, M. Pan, H. Chen, W. Liu, and H. Yu, "Porous copper fiber sintered felts: An innovative catalyst support of methanol steam reformer for hydrogen production," *Int. J. Hydrogen Energy*, vol. 33, no. 12, pp. 2950–2956, 2008, doi: 10.1016/j.ijhydene.2008.04.006.

[70] W. Zhou, Y. Tang, M. Pan, X. Wei, H. Chen, and J. Xiang, "A performance study of

methanol steam reforming microreactor with porous copper fiber sintered felt as catalyst support for fuel cells," *Int. J. Hydrogen Energy*, vol. 34, no. 24, pp. 9745–9753, 2009, doi: 10.1016/j.ijhydene.2009.10.009.

[71] E. H. Yu and K. Scott, "Direct methanol alkaline fuel cell with catalysed metal mesh anodes," *Electrochem. commun.*, vol. 6, no. 4, pp. 361–365, 2004, doi: 10.1016/j.elecom.2004.02.002.

[72] Z. G. Shao, W. F. Lin, F. Zhu, P. A. Christensen, H. Zhang, and B. Yi, "A tubular direct methanol fuel cell with Ti mesh anode," *J. Power Sources*, vol. 160, no. 2 SPEC. ISS., pp. 1003–1008, 2006, doi: 10.1016/j.jpowsour.2006.02.047.

[73] T. Hottinen, M. Mikkola, T. Mennola, and P. Lund, "Titanium sinter as gas diffusion backing in PEMFC," *J. Power Sources*, vol. 118, no. 1–2, pp. 183–188, 2003, doi: 10.1016/S0378-7753(03)00087-9.

[74] P. Yi, L. Peng, X. Lai, M. Li, and J. Ni, "Investigation of sintered stainless steel fiber felt as gas diffusion layer in proton exchange membrane fuel cells," *Int. J. Hydrogen Energy*, vol. 37, no. 15, pp. 11334–11344, 2012, doi: 10.1016/j.ijhydene.2012.04.161.

[75] A. Oedegaard, C. Hebling, A. Schmitz, S. Møller-Holst, and R. Tunold, "Influence of diffusion layer properties on low temperature DMFC," *J. Power Sources*, vol. 127, no. 1–2, pp. 187–196, 2004, doi: 10.1016/j.jpowsour.2003.09.015.

[76] P. J. Hamilton and B. G. Pollet, "Polymer electrolyte membrane fuel cell (PEMFC) flow field plate: Design, materials and characterisation," *Fuel Cells*, vol. 10, no. 4, pp. 489–509, 2010, doi: 10.1002/fuce.201000033.

[77] R. A. Antunes, M. C. L. Oliveira, G. Ett, and V. Ett, "Corrosion of metal bipolar

plates for PEM fuel cells: A review," *Int. J. Hydrogen Energy*, vol. 35, no. 8, pp. 3632–3647, 2010, doi: 10.1016/j.ijhydene.2010.01.059.

[78] A. El-Kharouf, "Understanding GDL Properties and Performance in Polymer Electrolyte Fuel Cells," University of Birmingham, 2014.

[79] M. F. Mathias, J. Roth, J. Fleming, and W. Lehnert, "Diffusion media materials and characterisation," *Handb. Fuel Cells*, vol. 3, pp. 517–537, 2010, doi: 10.1002/9780470974001.f303046.

[80] A. El-Kharouf and B. G. Pollet, "Gas Diffusion Media and their Degradation," in *Polymer Electrolyte Fuel Cell Degradation*, First Edit., M. M. Mench, E. C. Kumbur, and T. N. Veziroglu, Eds. Academic Press, 2012.

[81] W. M. Yan, C. Y. Hsueh, C. Y. Soong, F. Chen, C. H. Cheng, and S. C. Mei, "Effects of fabrication processes and material parameters of GDL on cell performance of PEM fuel cell," *Int. J. Hydrogen Energy*, vol. 32, no. 17, pp. 4452–4458, 2007, doi: 10.1016/j.ijhydene.2007.02.003.

[82] L. . Jordan, a. . Shukla, T. Behrsing, N. . Avery, B. . Muddle, and M. Forsyth, "Diffusion layer parameters influencing optimal fuel cell performance," *J. Power Sources*, vol. 86, no. 1–2, pp. 250–254, 2000, doi: 10.1016/S0378-7753(99)00489-9.

[83] F. A. L. Dullien, *Porous Media: Fluid Transport and Pore Structure*, 2nd Editio. Academic Press, 2012.

[84] K. Malek and M. O. Coppens, "Knudsen self- and Fickian diffusion in rough nanoporous media," *J. Chem. Phys.*, vol. 119, no. 5, pp. 2801–2811, 2003, doi: 10.1063/1.1584652.

[85] J. Becker, R. Flückiger, M. Reum, F. N. Büchi, F. Marone, and M. Stampanoni, "Determination of Material Properties of Gas Diffusion Layers: Experiments and Simulations Using Phase Contrast Tomographic Microscopy," *J. Electrochem. Soc.*, vol. 156, no. 10, p. B1175, 2009, doi: 10.1149/1.3176876.

[86] T. Rosen, J. Eller, J. Kang, N. I. Prasianakis, J. Mantzaras, and F. N. Buchi, "Saturation Dependent Effective Transport Properties of PEFC Gas Diffusion Layers," *J. Electrochem. Soc.*, vol. 159, no. 9, pp. F536–F544, 2012, doi: 10.1149/2.005209jes.

[87] J. P. James, H.-W. Choi, and J. G. Pharoah, "X-ray computed tomography reconstruction and analysis of polymer electrolyte membrane fuel cell porous transport layers," *Int. J. Hydrogen Energy*, vol. 37, no. 23, pp. 18216–18230, 2012, doi: 10.1016/j.ijhydene.2012.08.077.

[88] X. M. Zhang and X. X. Zhang, "Impact of compression on effective thermal conductivity and diffusion coefficient of woven gas diffusion layers in polymer electrolyte fuel cells," *Fuel Cells*, vol. 14, no. 2, pp. 303–311, 2014, doi: 10.1002/fuce.201200233.

[89] S. Didari, A. Asadi, Y. Wang, and T. a L. Harris, "Modeling of composite fibrous porous diffusion media," *Int. J. Hydrogen Energy*, vol. 39, no. 17, pp. 9375–9386, 2014, doi: 10.1016/j.ijhydene.2014.04.011.

[90] H. Ostadi, P. Rama, Y. Liu, R. Chen, X. X. Zhang, and K. Jiang, "3D reconstruction of a gas diffusion layer and a microporous layer," *J. Memb. Sci.*, vol. 351, no. 1–2, pp. 69–74, 2010, doi: 10.1016/j.memsci.2010.01.031.

[91] E. A. Wargo, V. P. Schulz, A. Çeçen, S. R. Kalidindi, and E. C. Kumbur,

"Resolving macro- and micro-porous layer interaction in polymer electrolyte fuel cells using focused ion beam and X-ray computed tomography," *Electrochim. Acta*, vol. 87, pp. 201–212, 2013, doi: 10.1016/j.electacta.2012.09.008.

[92] M. V. Williams, H. Russell Kunz, and J. M. Fenton, "Influence of convection through gas-diffusion layers on limiting current in PEM FCs using a serpentine flow field," *J. Electrochem. Soc.*, vol. 151, no. 10, 2004, doi: 10.1149/1.1789791.

[93] M. S. Ismail, T. Damjanovic, D. B. Ingham, L. Ma, and M. Pourkashanian, "Effect of polytetrafluoroethylene-treatment and microporous layer-coating on the in-plane permeability of gas diffusion layers used in proton exchange membrane fuel cells," *J. Power Sources*, vol. 195, no. 19, pp. 6619–6628, 2010, doi: 10.1016/j.jpowsour.2010.04.036.

[94] V. Gurau, M. J. Bluemle, E. S. De Castro, Y. M. Tsou, T. A. Zawodzinski, and J. A. Mann, "Characterization of transport properties in gas diffusion layers for proton exchange membrane fuel cells. 2. Absolute permeability," *J. Power Sources*, vol. 165, no. 2, pp. 793–802, 2007, doi: 10.1016/j.jpowsour.2006.12.068.

[95] H. Dohle, R. Jung, N. Kimiaie, J. Mergel, and M. Müller, "Interaction between the diffusion layer and the flow field of polymer electrolyte fuel cells - Experiments and simulation studies," *J. Power Sources*, vol. 124, no. 2, pp. 371–384, 2003, doi: 10.1016/S0378-7753(03)00800-0.

[96] J. G. Pharoah, "On the permeability of gas diffusion media used in PEM fuel cells," *J. Power Sources*, vol. 144, no. 1, pp. 77–82, 2005, doi: 10.1016/j.jpowsour.2004.11.069.

[97] D. Tehlar, R. Flückiger, A. Wokaun, and F. N. Büchi, "Investigation of channel-to-

channel cross convection in serpentine flow fields," *Fuel Cells*, vol. 10, no. 6, pp. 1040–1049, 2010, doi: 10.1002/fuce.201000034.

[98] J. P. Feser, A. K. Prasad, and S. G. Advani, "Experimental characterization of in-plane permeability of gas diffusion layers," *J. Power Sources*, vol. 162, no. 2 SPEC. ISS., pp. 1226–1231, 2006, doi: 10.1016/j.jpowsour.2006.07.058.

[99] M. S. Ismail *et al.*, "Through-Plane Permeability for Untreated and PTFE-Treated Gas Diffusion Layers in Proton Exchange Membrane Fuel Cells," *J. Fuel Cell Sci. Technol.*, vol. 7, no. 5, p. 051016, 2010, doi: 10.1115/1.4000685.

[100] D. Bevers, R. Rogers, and M. Von Bradke, "Examination of the influence of PTFE coating on the properties of carbon paper in polymer electrolyte fuel cells," *J. Power Sources*, vol. 63, no. 2, pp. 193–201, 1996, doi: 10.1016/S0378-7753(96)02465-2.

[101] G. G. Park, Y. J. Sohn, T. H. Yang, Y. G. Yoon, W. Y. Lee, and C. S. Kim, "Effect of PTFE contents in the gas diffusion media on the performance of PEMFC," *J. Power Sources*, vol. 131, no. 1–2, pp. 182–187, 2004, doi: 10.1016/j.jpowsour.2003.12.037.

[102] J. T. Gostick, M. W. Fowler, M. D. Pritzker, M. A. Ioannidis, and L. M. Behra, "In-plane and through-plane gas permeability of carbon fiber electrode backing layers," *J. Power Sources*, vol. 162, no. 1, pp. 228–238, 2006, doi: 10.1016/j.jpowsour.2006.06.096.

[103] A. Tamayol, F. McGregor, and M. Bahrami, "Single phase through-plane permeability of carbon paper gas diffusion layers," *J. Power Sources*, vol. 204, pp. 94–99, 2012, doi: 10.1016/j.jpowsour.2011.11.084.

[104] M. V Williams, E. Begg, L. Bonville, H. R. Kunz, and J. M. Fenton,

"Characterization of gas diffusion layers for PEMFC," *J. Electrochem. Soc.*, vol. 151, no. 8, pp. A1173–A1180, 2004, doi: Doi 10.1149/1.1764779.

[105] J. Ihonen, M. Mikkola, and G. Lindbergh, "Flooding of gas diffusion backing in PEFCs: Physical and electrochemical characterization," *J. Electrochem. Soc.*, vol. 151, no. 8, pp. 1152–1161, 2004, doi: 10.1149/1.1763138.

[106] V. Gurau, M. J. Bluemle, E. S. De Castro, Y. M. Tsou, J. A. Mann, and T. A. Zawodzinski, "Characterization of transport properties in gas diffusion layers for proton exchange membrane fuel cells. 1. Wettability (internal contact angle to water and surface energy of GDL fibers)," *J. Power Sources*, vol. 160, no. 2 SPEC. ISS., pp. 1156–1162, 2006, doi: 10.1016/j.jpowsour.2006.03.016.

[107] P. Mangal *et al.*, "Experimental study of mass transport in PEMFCs: Through plane permeability and molecular diffusivity in GDLs," *Electrochim. Acta*, vol. 167, pp. 160–171, 2015, doi: 10.1016/j.electacta.2015.03.100.

[108] J. Yu, Y. Yoshikawa, T. Matsuura, M. N. Islam, and M. Hori, "Preparing gas-diffusion layers of PEMFCs with a dry deposition technique," *Electrochem. Solid-State Lett.*, vol. 8, no. 3, pp. 152–155, 2005, doi: 10.1149/1.1854119.

[109] P. Gallo Stampino, L. Omati, C. Cristiani, and G. Dotelli, "Characterisation of nanocarbon-based gas diffusion media by electrochemical impedance spectroscopy," *Fuel Cells*, vol. 10, no. 2, pp. 270–277, 2010, doi: 10.1002/fuce.200900126.

[110] P. Gallo Stampino *et al.*, "Effect of different substrates, inks composition and rheology on coating deposition of microporous layer (MPL) for PEM-FCs," *Catal. Today*, vol. 147, no. SUPPL., pp. 30–35, 2009, doi: 10.1016/j.cattod.2009.07.023.

[111] R. Sitanggang, A. B. Mohamad, W. R. W. Daud, A. A. H. Kadhum, and S. E. Iyuke, "Fabrication of gas diffusion layer based on x-y robotic spraying technique for proton exchange membrane fuel cell application," *Energy Convers. Manag.*, vol. 50, no. 6, pp. 1419–1425, 2009, doi: 10.1016/j.enconman.2009.03.006.

[112] Z. Y. Xie *et al.*, "Improved properties of carbon fiber paper as electrode for fuel cell by coating pyrocarbon via CVD method," *Trans. Nonferrous Met. Soc. China (English Ed.*, vol. 20, no. 8, pp. 1412–1417, 2010, doi: 10.1016/S1003-6326(09)60313-7.

[113] X. Wang *et al.*, "A bi-functional micro-porous layer with composite carbon black for PEM fuel cells," *J. Power Sources*, vol. 162, no. 1, pp. 474–479, 2006, doi: 10.1016/j.jpowsour.2006.06.064.

[114] A. Pozio, A. Cemmi, M. Carewska, C. Paoletti, and F. Zaza, "Characterization of gas diffusion electrodes for polymer electrolyte fuel cells," *J. Fuel Cell Sci. Technol.*, vol. 7, no. 4, pp. 0410031–0410037, 2010, doi: 10.1115/1.3119061.

[115] E. Antolini, R. . Passos, and E. . Ticianelli, "Effects of the carbon powder characteristics in the cathode gas diffusion layer on the performance of polymer electrolyte fuel cells," *J. Power Sources*, vol. 109, no. 2, pp. 477–482, 2002, doi: 10.1016/S0378-7753(02)00112-X.

[116] J. Chen, T. Matsuura, and M. Hori, "Novel gas diffusion layer with water management function for PEMFC," *J. Power Sources*, vol. 131, no. 1–2, pp. 155–161, 2004, doi: 10.1016/j.jpowsour.2004.01.007.

[117] M. Han, S. H. Chan, and S. P. Jiang, "Development of carbon-filled gas diffusion layer for polymer electrolyte fuel cells," *J. Power Sources*, vol. 159, no. 2, pp.

1005–1014, 2006, doi: 10.1016/j.jpowsour.2005.12.003.

[118] H. Gharibi, M. Javaheri, and R. A. Mirzaie, “The synergy between multi-wall carbon nanotubes and Vulcan XC72R in microporous layers,” *Int. J. Hydrogen Energy*, vol. 35, no. 17, pp. 9241–9251, 2010, doi: 10.1016/j.ijhydene.2009.08.092.

[119] A. M. Kannan and L. Munukutla, “Carbon nano-chain and carbon nano-fibers based gas diffusion layers for proton exchange membrane fuel cells,” *J. Power Sources*, vol. 167, no. 2, pp. 330–335, 2007, doi: 10.1016/j.jpowsour.2007.02.064.

[120] J. F. Lin, J. Wertz, R. Ahmad, M. Thommes, and A. M. Kannan, “Effect of carbon paper substrate of the gas diffusion layer on the performance of proton exchange membrane fuel cell,” *Electrochim. Acta*, vol. 55, no. 8, pp. 2746–2751, 2010, doi: 10.1016/j.electacta.2009.12.056.

[121] A. M. Kannan, A. Menghal, and I. V. Barsukov, “Gas diffusion layer using a new type of graphitized nano-carbon PUREBLACK® for proton exchange membrane fuel cells,” *Electrochem. commun.*, vol. 8, no. 5, pp. 887–891, 2006, doi: 10.1016/j.elecom.2006.03.041.

[122] A. Ozden, S. Shahgaldi, J. Zhao, X. Li, and F. Hamdullahpur, “Assessment of graphene as an alternative microporous layer material for proton exchange membrane fuel cells,” *Fuel*, vol. 215, no. November 2017, pp. 726–734, 2018, doi: 10.1016/j.fuel.2017.11.109.

[123] S. B. Park, S. Kim, Y. Il Park, and M. H. Oh, “Fabrication of GDL microporous layer using PVDF for PEMFCs,” *J. Phys. Conf. Ser.*, vol. 165, 2009, doi: 10.1088/1742-6596/165/1/012046.

[124] A. L. Ong, A. Bottino, G. Capannelli, and A. Comite, “Effect of preparative

parameters on the characteristic of poly(vinylidene fluoride)-based microporous layer for proton exchange membrane fuel cells," *J. Power Sources*, vol. 183, no. 1, pp. 62–68, 2008, doi: 10.1016/j.jpowsour.2008.04.064.

[125] S. B. Park and Y. il Park, "Fabrication of gas diffusion layer (GDL) containing microporous layer using flourinated ethylene prophylene (FEP) for proton exchange membrane fuel cell (PEMFC)," *Int. J. Precis. Eng. Manuf.*, vol. 13, no. 7, pp. 1145–1151, 2012, doi: 10.1007/s12541-012-0152-x.

[126] A. Z. Weber and J. Newman, "Effects of Microporous Layers in Polymer Electrolyte Fuel Cells," *J. Electrochem. Soc.*, vol. 152, no. 4, p. A677, 2005, doi: 10.1149/1.1861194.

[127] O. M. Orogbemi, D. B. Ingham, M. S. Ismail, K. J. Hughes, L. Ma, and M. Pourkashanian, "The effects of the composition of microporous layers on the permeability of gas diffusion layers used in polymer electrolyte fuel cells," *Int. J. Hydrogen Energy*, vol. 41, no. 46, pp. 21345–21351, 2016, doi: 10.1016/j.ijhydene.2016.09.160.

[128] O. M. Orogbemi, D. B. Ingham, M. S. Ismail, K. J. Hughes, L. Ma, and M. Pourkashanian, "Through-plane gas permeability of gas diffusion layers and microporous layer: Effects of carbon loading and sintering," *J. Energy Inst.*, vol. 91, no. 2, pp. 270–278, 2018, doi: 10.1016/j.joei.2016.11.008.

[129] M. Zhiani, S. Kamali, and S. Majidi, "In-plane gas permeability and thought-plane resistivity of the gas diffusion layer influenced by homogenization technique and its effect on the proton exchange membrane fuel cell cathode performance," *Int. J. Hydrogen Energy*, vol. 41, no. 2, pp. 1112–1119, 2016, doi: 10.1016/j.ijhydene.2015.10.052.

[130] S. Park, J. W. Lee, and B. N. Popov, “Effect of PTFE content in microporous layer on water management,” *ECS Trans.*, vol. 11, no. 1 PART 1, pp. 623–628, 2007, doi: 10.1149/1.2780975.

[131] D. Rohendi, E. H. Majlan, A. B. Mohamad, W. R. W. Daud, A. A. H. Kadhum, and L. K. Shyuan, “Effect of PTFE content and sintering temperature on the properties of a fuel cell electrode backing layer,” *J. Fuel Cell Sci. Technol.*, vol. 11, no. 4, pp. 1–6, 2014, doi: 10.1115/1.4026932.

[132] R. M. Aslam, “Water and Thermal Management of PEM Fuel Cells,” University of Sheffield, 2018.

[133] S. K. Lo, C. J. Tseng, L. D. Tsai, and J. N. Lin, “Fractal permeability models for the microporous layer and gas diffusion layer of PEM fuel cell,” *J. Chinese Inst. Eng. Trans. Chinese Inst. Eng. A/Chung-kuo K. Ch’eng Hsuch K’an*, vol. 34, no. 1, pp. 39–47, 2011, doi: 10.1080/02533839.2011.552964.

[134] C. J. Tseng and S. K. Lo, “Effects of microstructure characteristics of gas diffusion layer and microporous layer on the performance of PEMFC,” *Energy Convers. Manag.*, vol. 51, no. 4, pp. 677–684, 2010, doi: 10.1016/j.enconman.2009.11.011.

[135] S. Litster and G. McLean, “PEM fuel cell electrodes,” *J. Power Sources*, vol. 130, no. 1–2, pp. 61–76, 2004, doi: 10.1016/j.jpowsour.2003.12.055.

[136] O. M. Orogbemi, “Gas Permeability of Gas Diffusion Media Used in Polymer Electrolyte Fuel Cells,” University of Sheffield, 2017.

[137] D. P. Wilkinson, J. Zhang, R. Hui, J. Fergus, and X. Li, *Proton exchange membrane fuel cells : materials properties and performance*. 2010.

[138] D. a Nield and A. Bejan, *Convection in Porous Media Third Edition*, vol. 24. 2006.

[139] D. Shou, J. Fan, and F. Ding, "Effective Diffusivity of Gas Diffusion Layer in Proton Exchange Membrane Fuel Cells," *J. Power Sources*, vol. 225, pp. 179–186, 2012, doi: 10.1016/j.jpowsour.2012.10.039.

[140] R. J. Moffat, "Describing the uncertainties in experimental results," *Exp. Therm. Fluid Sci.*, vol. 1, no. 1, pp. 3–17, 1988, doi: 10.1016/0894-1777(88)90043-X.

[141] J. White, A. Yeats, and G. Skipworth, *Tables for Statisticians*, 3rd Ed. Stanley Thornes Ltd., 1979.

[142] J. Ihonen, M. Mikkola, and G. Lindbergh, "Flooding of Gas Diffusion Backing in PEFCs," *J. Electrochem. Soc.*, vol. 151, no. 8, p. A1152, 2004, doi: 10.1149/1.1763138.

[143] M. Uchida, "Investigation of the Microstructure in the Catalyst Layer and Effects of Both Perfluorosulfonate Ionomer and PTFE-Loaded Carbon on the Catalyst Layer of Polymer Electrolyte Fuel Cells," *J. Electrochem. Soc.*, vol. 142, no. 12, p. 4143, 1995, doi: 10.1149/1.2048477.

[144] T. Kitahara, T. Konomi, and H. Nakajima, "Microporous layer coated gas diffusion layers for enhanced performance of polymer electrolyte fuel cells," *J. Power Sources*, vol. 195, no. 8, pp. 2202–2211, 2010, doi: 10.1016/j.jpowsour.2009.10.089.

[145] T.-H. Ko, J.-H. Lin, W.-S. Kuo, W.-H. Chen, S.-H. Su, and W.-C. Chen, "Effect of Multi Micro Porous Layer in Proton Exchange Membrane Fuel Cell," *2010 Asia-Pacific Power Energy Eng. Conf.*, pp. 1–4, 2010, doi: 10.1109/APPEEC.2010.5449417.

[146] H. H. Chen and M. H. Chang, “Effect of cathode microporous layer composition on proton exchange membrane fuel cell performance under different air inlet relative humidity,” *J. Power Sources*, vol. 232, pp. 306–309, 2013, doi: 10.1016/j.jpowsour.2013.01.079.

[147] M. Prasanna, H. Y. Ha, E. A. Cho, S. A. Hong, and I. H. Oh, “Influence of cathode gas diffusion media on the performance of the PEMFCs,” *J. Power Sources*, vol. 131, no. 1–2, pp. 147–154, 2004, doi: 10.1016/j.jpowsour.2004.01.030.

[148] S. Park, J. W. Lee, and B. N. Popov, “Effect of PTFE content in microporous layer on water management in PEM fuel cells,” *J. Power Sources*, vol. 177, no. 2, pp. 457–463, 2008, doi: 10.1016/j.jpowsour.2007.11.055.

[149] M. Naderi, “Progress in Filtration and Separation,” 1st Ed., E. S. Tareleton, Ed. Academic Press, 2014.

Appendices

Appendix A

Chapter 4 Results

Table A- 1 Toray TGP-H-120 (0.5 $mgcm^{-2}$) Vulcan XC-72R.

Toray TGP-H-120										
0.5 $mgcm^{-2}$ (Vulcan XC-72R)										
Sample Number	**Permeability $k\ (m^2)$**		**Thickness (μm)**		**Thickness change (L_{MPL}) (μm)**	**Percentage reduction in permeability (%)**	**MPL permeability (k_{MPL}) (m^2)**	**Mass of samples (mg)**		**Actual carbon loading $(mgcm^{-2})$**
	Uncoated (k_{GDL})	**Coated (k_{GDM})**	**Uncoated (L_{GDL})**	**Coated (L_{GDM})**				**Uncoated**	**Coated**	
1	6.25E-12	2.70E-12	366.25	372.50	6.25	56.89	7.85E-14	84.90	88.08	0.51
2	6.35E-12	2.93E-12	363.75	366.25	2.50	53.85	3.69E-14	84.82	88.00	0.52
3	5.64E-12	2.66E-12	345.00	351.25	6.25	52.89	8.79E-14	83.16	86.34	0.50
4	6.10E-12	2.77E-12	362.50	367.50	5.00	54.57	6.83E-14	85.92	89.10	0.51
5	5.94E-12	1.49E-12	356.25	358.75	2.50	74.85	1.39E-14	86.09	89.27	0.52
6	6.12E-12	2.03E-12	368.75	373.75	5.00	66.78	4.04E-14	87.11	90.29	0.50
Mean	6.07E-12	2.43E-12	360.42	365.00	4.58	59.97	5.43E-14	**Mean**		0.51
Std. Dev	2.52E-13	5.52E-13	8.65	8.59	1.71	8.88	2.84E-14	**Std. Dev**		0.01
95 % CI	2.65E-13	5.79E-13	9.08	9.01	1.79	9.32	2.98E-14	**95 % CI**		0.01

Table A- 2 Toray TGP-H-120 (1.0 $mgcm^{-2}$) Vulcan XC-72R.

Toray TGP-H-120										
1.0 $mgcm^{-2}$ (Vulcan XC-72R)										
Sample Number	**Permeability $k\ (m^2)$**		**Thickness (μm)**		**Thickness change (μm) (L_{MPL})**	**Percentage reduction in permeability (%)**	**MPL permeability (k_{MPL}) (m^2)**	**Mass of samples (mg)**		**Actual carbon loading $(mgcm^{-2})$**
	Uncoated (k_{GDL})	**Coated (k_{GDM})**	**Uncoated (L_{GDL})**	**Coated (L_{GDM})**				**Uncoated**	**Coated**	
1	5.50E-12	3.12E-13	355.00	370.00	15.00	94.32	1.34E-14	84.33	90.67	1.04
2	5.54E-12	2.71E-13	358.75	370.00	11.25	95.10	8.66E-15	85.46	91.80	1.08
3	5.72E-12	2.66E-13	360.00	365.00	5.00	95.35	3.82E-15	82.04	88.38	1.08
4	5.39E-12	3.96E-13	358.75	370.00	11.25	92.65	1.30E-14	88.27	94.61	1.00
5	5.68E-12	2.63E-13	363.75	370.00	6.25	95.37	4.66E-15	86.55	92.89	0.99
6	5.77E-12	2.35E-13	355.00	365.00	10.00	95.93	6.70E-15	85.15	91.49	1.00
Mean	5.60E-12	2.91E-13	358.54	368.33	9.79	94.79	8.36E-15	**Mean**		1.03
Std. Dev	1.46E-13	5.73E-14	3.30	2.58	3.66	1.17	4.09E-15	**Std. Dev**		0.04
95 % CI	1.53E-13	6.01E-14	3.46	2.71	3.84	1.23	4.29E-15	**95 % CI**		0.04

Table A- 3 Toray TGP-H-120 (2.0 $mgcm^{-2}$) Vulcan XC-72R.

Toray TGP-H-120										
2.0 $mgcm^{-2}$ (Vulcan XC-72R)										
Sample Number	**Permeability $k\ (m^2)$**		**Thickness (μm)**		**Thickness change (L_{MPL}) (μm)**	**Percentage reduction in permeability (%)**	**MPL permeability (k_{MPL}) (m^2)**	**Mass of samples (mg)**		**Actual carbon loading $(mgcm^{-2})$**
	Uncoated (k_{GDL})	**Coated (k_{GDM})**	**Uncoated (L_{GDL})**	**Coated (L_{GDM})**				**Uncoated**	**Coated**	
1	5.12E-12	2.32E-13	352.50	395.00	42.50	95.48	2.60E-14	84.98	97.70	2.05
2	5.01E-12	2.31E-13	357.50	397.50	40.00	95.39	2.42E-14	86.27	98.99	2.02
3	5.53E-12	2.22E-13	362.50	403.75	41.25	95.99	2.35E-14	85.65	98.37	2.03
4	5.14E-12	2.16E-13	353.75	392.50	38.75	95.80	2.22E-14	85.59	98.31	2.04
5	4.99E-12	2.18E-13	356.25	396.25	40.00	95.62	2.29E-14	86.13	98.85	2.01
6	5.57E-12	3.23E-13	365.00	406.25	41.25	94.19	3.47E-14	85.89	98.61	2.01
Mean	5.23E-12	2.40E-13	357.92	398.54	40.63	95.41	2.56E-14	**Mean**		2.03
Std. Dev	2.59E-13	4.12E-14	4.92	5.33	1.31	0.63	4.63E-15	**Std. Dev**		0.01
95 % CI	2.72E-13	4.33E-14	5.16	5.59	1.38	0.67	4.86E-15	**95 % CI**		0.01

Table A- 4 Toray TGP-H-120 (0.5 $mgcm^{-2}$) Ketjenblack EC-300J.

Toray TGP-H-120										
0.5 $mgcm^{-2}$ (Ketjenblack EC-300J)										
Sample Number	**Permeability $k\ (m^2)$**		**Thickness (μm)**		**Thickness change (L_{MPL}) (μm)**	**Percentage reduction in permeability (%)**	**MPL permeability (k_{MPL}) (m^2)**	**Mass of samples (mg)**		**Actual carbon loading $(mgcm^{-2})$**
	Uncoated (k_{GDL})	**Coated (k_{GDM})**	**Uncoated (L_{GDL})**	**Coated (L_{GDM})**				**Uncoated**	**Coated**	
1	5.71E-12	1.42E-12	365.00	367.50	2.50	75.18	1.28E-14	83.73	86.91	0.51
2	5.69E-12	1.29E-12	361.25	366.25	5.00	77.42	2.26E-14	85.26	88.44	0.50
3	5.88E-12	1.75E-12	350.00	356.25	6.25	70.14	4.36E-14	84.45	87.63	0.51
4	6.01E-12	1.42E-12	358.75	375.00	16.25	76.42	7.93E-14	85.46	88.64	0.50
5	5.81E-12	1.46E-12	362.50	380.00	17.50	74.87	8.84E-14	86.40	89.58	0.51
6	5.85E-12	1.57E-12	352.50	363.75	11.25	73.13	6.58E-14	85.44	88.62	0.51
Mean	5.83E-12	1.48E-12	358.33	368.13	9.79	74.53	5.21E-14	**Mean**		0.51
Std. Dev	1.17E-13	1.61E-13	5.90	8.39	6.20	2.59	3.08E-14	**Std. Dev**		0.01
95 % CI	1.23E-13	1.69E-13	6.19	8.81	6.50	2.72	3.23E-14	**95 % CI**		0.01

Table A- 5 Toray TGP-H-120 (1.0 mgcm^{-2}) Ketjenblack EC-300J.

Toray TGP-H-120										
1.0 mgcm^{-2} (Ketjenblack EC-300J)										
Sample Number	**Permeability k (m^2)**		**Thickness (μm)**		**Thickness change (L_{MPL}) (μm)**	**Percentage reduction in permeability (%)**	**MPL permeability (k_{MPL}) (m^2)**	**Mass of samples (mg)**		**Actual carbon loading ($mgcm^{-2}$)**
	Uncoated (k_{GDL})	**Coated (k_{GDM})**	**Uncoated (L_{GDL})**	**Coated (L_{GDM})**				**Uncoated**	**Coated**	
1	5.17E-12	1.39E-12	351.25	398.75	47.50	73.10	2.17E-13	82.67	89.01	1.03
2	5.63E-12	1.05E-12	367.50	405.00	37.50	81.43	1.17E-13	83.62	89.96	1.00
3	5.52E-12	1.15E-12	360.00	412.50	52.50	79.12	1.79E-13	81.73	88.07	1.02
4	6.36E-12	2.55E-12	366.25	402.50	36.25	59.92	3.61E-13	84.39	90.73	1.02
5	6.23E-12	2.67E-12	355.00	392.50	37.50	57.15	4.16E-13	84.51	90.85	1.03
6	5.88E-12	2.59E-12	357.50	396.25	38.75	55.99	4.20E-13	84.82	91.16	1.02
Mean	5.80E-12	1.90E-12	359.58	401.25	41.67	67.78	2.85E-13	**Mean**		1.02
Std. Dev	4.47E-13	7.78E-13	6.36	7.07	6.69	11.46	1.31E-13	**Std. Dev**		0.01
95 % CI	4.69E-13	8.17E-13	6.67	7.42	7.02	12.03	1.37E-13	**95 % CI**		0.01

Table A- 6 Toray TGP-H-120 (2.0 $mgcm^{-2}$) Ketjenblack EC-300J.

Toray TGP-H-120										
2.0 $mgcm^{-2}$ (Ketjenblack EC-300J)										
Sample Number	**Permeability $k\ (m^2)$**		**Thickness (μm)**		**Thickness change (L_{MPL}) (μm)**	**Percentage reduction in permeability (%)**	**MPL permeability (k_{MPL}) (m^2)**	**Mass of samples (mg)**		**Actual carbon loading $(mgcm^{-2})$**
	Uncoated (k_{GDL})	**Coated (k_{GDM})**	**Uncoated (L_{GDL})**	**Coated (L_{GDM})**				**Uncoated**	**Coated**	
1	6.12E-12	2.76E-12	355.00	462.50	107.50	54.95	9.80E-13	83.03	95.75	2.00
2	5.00E-12	4.01E-12	353.75	478.75	125.00	19.83	2.57E-12	86.78	99.50	2.04
3	5.49E-12	2.83E-12	356.25	476.25	120.00	48.50	1.16E-12	85.66	98.38	2.03
4	5.93E-12	2.28E-12	355.00	478.75	123.75	61.56	8.24E-13	85.96	98.68	2.02
5	6.12E-12	2.67E-12	355.00	462.50	107.50	56.32	9.35E-13	84.51	97.23	2.03
6	5.49E-12	2.39E-12	356.25	476.25	120.00	56.49	8.92E-13	85.79	98.51	2.02
Mean	5.69E-12	2.82E-12	355.21	472.50	117.29	49.61	1.23E-12	**Mean**		2.02
Std. Dev	4.43E-13	6.19E-13	0.94	7.83	7.84	15.18	6.67E-13	**Std. Dev**		0.01
95 % CI	4.65E-13	6.50E-13	0.99	8.21	8.23	15.93	7.00E-13	**95 % CI**		0.01

Table A- 7 Toray TGP-H-90 (0.5 $mgcm^{-2}$) Vulcan XC-72R.

Toray TGP-H-90										
0.5 $mgcm^{-2}$ (Vulcan XC-72R)										
Sample Number	**Permeability $k\ (m^2)$**		**Thickness (μm)**		**Thickness change (L_{MPL}) (μm)**	**Percentage reduction in permeability (%)**	**MPL permeability (k_{MPL}) (m^2)**	**Mass of samples (mg)**		**Actual carbon loading $(mgcm^{-2})$**
	Uncoated (k_{GDL})	**Coated (k_{GDM})**	**Uncoated (L_{GDL})**	**Coated (L_{GDM})**				**Uncoated**	**Coated**	
1	7.00E-12	4.22E-12	291.25	295.00	3.75	39.61	1.33E-13	64.56	67.74	0.51
2	7.10E-12	3.86E-12	288.75	292.50	3.75	45.68	1.07E-13	64.97	68.15	0.51
3	6.89E-12	3.69E-12	288.75	293.75	5.00	46.44	1.33E-13	64.91	68.09	0.51
4	7.02E-12	2.41E-12	290.00	293.75	3.75	65.62	4.66E-14	65.77	68.95	0.51
5	7.37E-12	2.41E-12	295.00	300.00	5.00	67.31	5.91E-14	64.90	68.08	0.51
6	6.93E-12	2.29E-12	292.50	297.50	5.00	66.92	5.71E-14	65.05	68.23	0.50
Mean	7.05E-12	3.15E-12	291.04	295.42	4.38	55.26	8.92E-14	**Mean**		0.50
Std. Dev	1.72E-13	8.69E-13	2.43	2.81	0.68	12.67	3.96E-14	**Std. Dev**		0.005
95 % CI	1.80E-13	9.12E-13	2.55	2.95	0.72	13.30	4.16E-14	**95 % CI**		0.005

Table A- 8 Toray TGP-H-90 (1.0 $mgcm^{-2}$) Vulcan XC-72R.

Toray TGP-H-90										
1.0 $mgcm^{-2}$ (Vulcan XC-72R)										
Sample Number	**Permeability $k\ (m^2)$**		**Thickness (μm)**		**Thickness change (L_{MPL}) (μm)**	**Percentage reduction in permeability (%)**	**MPL permeability (k_{MPL}) (m^2)**	**Mass of samples (mg)**		**Actual carbon loading $(mgcm^{-2})$**
	Uncoated (k_{GDL})	**Coated (k_{GDM})**	**Uncoated (L_{GDL})**	**Coated (L_{GDM})**				**Uncoated**	**Coated**	
1	6.63E-12	3.38E-13	290.00	298.75	8.75	94.91	1.04E-14	62.49	68.83	1.04
2	6.60E-12	4.46E-13	293.75	301.25	7.50	93.23	1.19E-14	62.74	69.08	1.03
3	7.04E-12	2.42E-13	290.00	303.75	13.75	96.56	1.13E-14	63.51	69.85	1.01
4	7.45E-12	5.82E-13	292.50	297.50	5.00	92.18	1.06E-14	64.12	70.46	1.00
5	7.10E-12	4.40E-13	288.75	298.75	10.00	93.80	1.57E-14	62.20	68.54	1.00
6	6.89E-12	3.35E-13	288.75	296.25	7.50	95.13	8.91E-15	63.00	69.34	1.03
Mean	6.95E-12	3.97E-13	290.63	299.38	8.75	94.30	1.15E-14	**Mean**		1.02
Std. Dev	3.19E-13	1.18E-13	2.05	2.71	2.96	1.55	2.30E-15	**Std. Dev**		0.02
95 % CI	3.35E-13	1.24E-13	2.16	2.84	3.10	1.63	2.41E-15	**95 % CI**		0.02

Table A- 9 Toray TGP-H-90 (2.0 $mgcm^{-2}$) Vulcan XC-72R.

Toray TGP-H-90										
2.0 $mgcm^{-2}$ (Vulcan XC-72R)										
Sample Number	**Permeability $k\ (m^2)$**		**Thickness (μm)**		**Thickness change (L_{MPL}) (μm)**	**Percentage reduction in permeability (%)**	**MPL permeability (k_{MPL}) (m^2)**	**Mass of samples (mg)**		**Actual carbon loading $(mgcm^{-2})$**
	Uncoated (k_{GDL})	**Coated (k_{GDM})**	**Uncoated (L_{GDL})**	**Coated (L_{GDM})**				**Uncoated**	**Coated**	
1	6.42E-12	2.58E-13	291.25	331.25	40.00	95.99	3.23E-14	63.49	76.21	2.01
2	6.45E-12	2.72E-13	293.75	333.75	40.00	95.78	3.39E-14	62.90	75.62	2.02
3	6.66E-12	2.98E-13	290.00	331.25	41.25	95.53	3.86E-14	63.62	76.34	2.06
4	6.60E-12	2.47E-13	290.00	330.00	40.00	96.25	3.10E-14	63.71	76.43	2.00
5	6.56E-12	2.43E-13	293.75	328.75	35.00	96.30	2.68E-14	63.05	75.77	2.02
6	7.00E-12	2.15E-13	290.00	331.25	41.25	96.94	2.75E-14	63.60	76.32	2.04
Mean	6.62E-12	2.55E-13	291.46	331.04	39.58	96.13	3.17E-14	**Mean**		2.02
Std. Dev	2.09E-13	2.81E-14	1.84	1.66	2.33	0.49	4.36E-15	**Std. Dev**		0.02
95 % CI	2.20E-13	2.95E-14	1.93	1.74	2.44	0.51	4.58E-15	**95 % CI**		0.02

Table A- 10 Toray TGP-H-90 (0.5 $mgcm^{-2}$) Ketjenblack EC-300J.

Toray TGP-H-90										
0.5 $mgcm^{-2}$ (Ketjenblack EC-300J)										
Sample Number	**Permeability $k\ (m^2)$**		**Thickness (μm)**		**Thickness change (L_{MPL}) (μm)**	**Percentage reduction in permeability (%)**	**MPL permeability (k_{MPL}) (m^2)**	**Mass of samples (mg)**		**Actual carbon loading $(mgcm^{-2})$**
	Uncoated (k_{GDL})	**Coated (k_{GDM})**	**Uncoated (L_{GDL})**	**Coated (L_{GDM})**				**Uncoated**	**Coated**	
1	6.61E-12	1.57E-12	291.25	297.50	6.25	76.27	4.29E-14	65.01	68.19	0.50
2	7.09E-12	1.23E-12	292.50	297.50	5.00	82.65	2.49E-14	65.85	69.03	0.50
3	6.86E-12	1.99E-12	292.50	306.25	13.75	70.96	1.24E-13	67.01	70.19	0.51
4	7.18E-12	1.46E-12	290.00	302.50	12.50	79.72	7.47E-14	65.06	68.24	0.51
5	7.26E-12	1.60E-12	290.00	301.25	11.25	77.93	7.60E-14	65.29	68.47	0.48
6	7.14E-12	1.22E-12	286.25	297.50	11.25	82.92	5.52E-14	64.21	67.39	0.50
Mean	7.03E-12	1.51E-12	290.42	300.42	10.00	78.41	6.63E-14	**Mean**		0.50
Std. Dev	2.43E-13	2.87E-13	2.33	3.59	3.54	4.48	3.42E-14	**Std. Dev**		0.01
95 % CI	2.55E-13	3.01E-13	2.44	3.77	3.71	4.70	3.59E-14	**95 % CI**		0.01

Table A- 11 Toray TGP-H-90 (1.0 mgcm^{-2}) Ketjenblack EC-300J.

Toray TGP-H-90										
1.0 mgcm^{-2} (Ketjenblack EC-300J)										
Sample Number	**Permeability k (m^2)**		**Thickness (μm)**		**Thickness change (L_{MPL}) (μm)**	**Percentage reduction in permeability (%)**	**MPL permeability (k_{MPL}) (m^2)**	**Mass of samples (mg)**		**Actual carbon loading ($mgcm^{-2}$)**
	Uncoated (k_{GDL})	**Coated (k_{GDM})**	**Uncoated (L_{GDL})**	**Coated (L_{GDM})**				**Uncoated**	**Coated**	
1	6.44E-12	2.23E-12	295.00	331.25	36.25	65.38	3.53E-13	62.74	69.08	1.02
2	6.96E-12	1.07E-12	290.00	327.50	37.50	84.60	1.42E-13	64.45	70.79	0.99
3	6.07E-12	1.79E-12	288.75	327.50	38.75	70.52	2.86E-13	63.51	69.85	1.02
4	7.81E-12	3.27E-12	293.75	330.00	36.25	58.17	5.72E-13	63.28	69.62	1.01
5	7.40E-12	3.20E-12	291.25	330.00	38.75	56.72	6.09E-13	64.50	70.84	0.99
6	7.59E-12	3.10E-12	291.25	331.25	40.00	59.11	5.85E-13	64.68	71.02	1.01
Mean	7.05E-12	2.44E-12	291.67	329.58	37.92	65.75	4.25E-13	**Mean**		1.00
Std. Dev	6.82E-13	8.99E-13	2.33	1.71	1.51	10.59	1.93E-13	**Std. Dev**		0.01
95 % CI	7.15E-13	9.44E-13	2.44	1.79	1.59	11.12	2.02E-13	**95 % CI**		0.01

Table A- 12 Toray TGP-H-90 (2.0 $mgcm^{-2}$) Ketjenblack EC-300J.

Toray TGP-H-90										
2.0 $mgcm^{-2}$ (Ketjenblack EC-300J)										
Sample Number	**Permeability $k\ (m^2)$**		**Thickness (μm)**		**Thickness change (L_{MPL}) (μm)**	**Percentage reduction in permeability (%)**	**MPL permeability (k_{MPL}) (m^2)**	**Mass of samples (mg)**		**Actual carbon loading $(mgcm^{-2})$**
	Uncoated (k_{GDL})	**Coated (k_{GDM})**	**Uncoated (L_{GDL})**	**Coated (L_{GDM})**				**Uncoated**	**Coated**	
1	6.40E-12	3.41E-12	293.75	413.75	120.00	46.69	1.59E-12	62.80	75.52	2.03
2	6.65E-12	2.98E-12	287.50	415.00	127.50	55.24	1.33E-12	62.18	74.90	2.02
3	6.96E-12	3.26E-12	296.25	413.75	117.50	53.09	1.40E-12	62.65	75.37	2.04
4	7.02E-12	2.66E-12	290.00	412.50	122.50	62.17	1.07E-12	64.78	77.50	2.07
5	6.74E-12	2.72E-12	287.50	416.25	128.75	59.56	1.17E-12	62.32	75.04	2.02
6	6.70E-12	2.87E-12	296.25	416.25	120.00	57.16	1.19E-12	62.81	75.53	2.02
Mean	6.74E-12	2.98E-12	291.88	414.58	122.71	55.65	1.29E-12	**Mean**		2.03
Std. Dev	2.24E-13	3.00E-13	4.09	1.51	4.50	5.42	1.87E-13	**Std. Dev**		0.02
95 % CI	2.36E-13	3.15E-13	4.29	1.59	4.72	5.69	1.96E-13	**95 % CI**		0.02

Table A- 13 SGL 35BA (0.5 $mgcm^{-2}$) Vulcan XC-72R.

SGL 35BA										
0.5 $mgcm^{-2}$ (Vulcan XC-72R)										
Sample Number	**Permeability $k\ (m^2)$**		**Thickness (μm)**		**Thickness change (L_{MPL}) (μm)**	**Percentage reduction in permeability (%)**	**MPL permeability (k_{MPL}) (m^2)**	**Mass of samples (mg)**		**Actual carbon loading $(mgcm^{-2})$**
	Uncoated (k_{GDL})	**Coated (k_{GDM})**	**Uncoated (L_{GDL})**	**Coated (L_{GDM})**				**Uncoated**	**Coated**	
1	3.61E-11	1.50E-11	295.00	301.25	6.25	58.33	5.26E-13	29.98	33.16	0.50
2	3.81E-11	1.66E-11	297.50	300.00	2.50	56.37	2.44E-13	29.14	32.32	0.50
3	3.99E-11	1.72E-11	288.75	291.25	2.50	57.03	2.57E-13	29.27	32.45	0.50
4	3.74E-11	1.31E-11	291.25	296.25	5.00	64.95	3.38E-13	28.58	31.76	0.51
5	3.88E-11	1.21E-11	293.75	300.00	6.25	68.84	3.62E-13	29.01	32.19	0.52
6	3.79E-11	1.67E-11	295.00	298.75	3.75	55.95	3.71E-13	29.58	32.76	0.52
Mean	3.80E-11	1.51E-11	293.54	297.92	4.38	60.24	3.50E-13	**Mean**		0.51
Std. Dev	1.30E-12	2.11E-12	3.10	3.68	1.72	5.36	1.02E-13	**Std. Dev**		0.01
95 % CI	1.37E-12	2.21E-12	3.26	3.86	1.81	5.62	1.07E-13	**95 % CI**		0.01

Table A- 14 SGL 35BA (1.0 $mgcm^{-2}$) Vulcan XC-72R.

SGL 35BA										
1.0 $mgcm^{-2}$ (Vulcan XC-72R)										
Sample Number	**Permeability $k\ (m^2)$**		**Thickness (μm)**		**Thickness change (L_{MPL}) (μm)**	**Percentage reduction in permeability (%)**	**MPL permeability (k_{MPL}) (m^2)**	**Mass of samples (mg)**		**Actual carbon loading $(mgcm^{-2})$**
	Uncoated (k_{GDL})	**Coated (k_{GDM})**	**Uncoated (L_{GDL})**	**Coated (L_{GDM})**				**Uncoated**	**Coated**	
1	4.02E-11	3.77E-12	295.00	301.25	6.25	90.63	8.61E-14	28.94	35.28	1.16
2	3.77E-11	3.74E-12	281.25	287.50	6.25	90.06	9.01E-14	28.21	34.55	1.26
3	3.82E-11	5.28E-12	288.75	296.25	7.50	86.19	1.54E-13	28.39	34.73	1.09
4	3.79E-11	3.38E-12	295.00	302.50	7.50	91.09	9.17E-14	28.89	35.23	1.03
5	3.71E-11	3.25E-12	297.50	306.25	8.75	91.24	1.02E-13	29.02	35.36	1.01
6	3.86E-11	3.26E-12	292.50	302.50	10.00	91.55	1.17E-13	28.62	34.96	1.01
Mean	3.83E-11	3.78E-12	291.67	299.38	7.71	90.13	1.07E-13	**Mean**		1.09
Std. Dev	1.07E-12	7.70E-13	5.90	6.65	1.46	2.00	2.59E-14	**Std. Dev**		0.10
95 % CI	1.13E-12	8.08E-13	6.19	6.98	1.53	2.10	2.71E-14	**95 % CI**		0.10

Table A- 15 SGL 35BA (2.0 $mgcm^{-2}$) Vulcan XC-72R.

SGL 35BA										
2.0 $mgcm^{-2}$ (Vulcan XC-72R)										
Sample Number	**Permeability $k\ (m^2)$**		**Thickness (μm)**		**Thickness change (L_{MPL}) (μm)**	**Percentage reduction in permeability (%)**	**MPL permeability (k_{MPL}) (m^2)**	**Mass of samples (mg)**		**Actual carbon loading $(mgcm^{-2})$**
	Uncoated (k_{GDL})	**Coated (k_{GDM})**	**Uncoated (L_{GDL})**	**Coated (L_{GDM})**				**Uncoated**	**Coated**	
1	3.79E-11	1.03E-12	295.00	321.25	26.25	97.29	8.61E-14	29.65	42.37	2.08
2	3.73E-11	9.89E-13	290.00	305.00	15.00	97.34	4.99E-14	29.62	42.34	2.04
3	3.71E-11	5.37E-13	297.50	316.25	18.75	98.55	3.23E-14	29.15	41.87	2.02
4	3.85E-11	9.52E-13	300.00	328.75	28.75	97.53	8.52E-14	29.95	42.67	2.01
5	4.55E-11	9.19E-13	295.00	326.25	31.25	97.98	8.96E-14	29.55	42.27	2.03
6	4.26E-11	9.41E-13	297.50	322.50	25.00	97.79	7.44E-14	29.25	41.97	2.02
Mean	3.98E-11	8.94E-13	295.83	320.00	24.17	97.75	6.96E-14	**Mean**		2.03
Std. Dev	3.43E-12	1.79E-13	3.42	8.51	6.16	0.47	2.33E-14	**Std. Dev**		0.02
95 % CI	3.60E-12	1.88E-13	3.59	8.94	6.46	0.50	2.45E-14	**95 % CI**		0.02

Table A- 16 SGL 35BA (0.5 $mgcm^{-2}$) Ketjenblack EC-300J.

SGL 35BA										
0.5 $mgcm^{-2}$ (Ketjenblack EC-300J)										
Sample Number	**Permeability $k\ (m^2)$**		**Thickness (μm)**		**Thickness change (L_{MPL}) (μm)**	**Percentage reduction in permeability (%)**	**MPL permeability (k_{MPL}) (m^2)**	**Mass of samples (mg)**		**Actual carbon loading $(mgcm^{-2})$**
	Uncoated (k_{GDL})	**Coated (k_{GDM})**	**Uncoated (L_{GDL})**	**Coated (L_{GDM})**				**Uncoated**	**Coated**	
1	3.94E-11	1.29E-11	302.50	313.75	11.25	67.34	6.74E-13	28.46	31.64	0.51
2	4.17E-11	1.31E-11	290.00	310.00	20.00	68.62	1.19E-12	27.76	30.94	0.50
3	3.87E-11	1.00E-11	301.25	311.25	10.00	74.03	4.31E-13	29.15	32.33	0.50
4	4.06E-11	8.85E-12	291.25	302.50	11.25	78.21	4.16E-13	29.94	33.12	0.51
5	4.28E-11	8.31E-12	298.75	311.25	12.50	80.58	4.10E-13	29.46	32.64	0.52
6	4.17E-11	8.18E-12	288.75	298.75	10.00	80.38	3.38E-13	28.89	32.07	0.50
Mean	4.08E-11	1.02E-11	295.42	307.92	12.50	74.86	5.77E-13	**Mean**		0.51
Std. Dev	1.54E-12	2.23E-12	6.11	5.90	3.79	5.84	3.23E-13	**Std. Dev**		0.01
95 % CI	1.61E-12	2.34E-12	6.41	6.19	3.98	6.13	3.39E-13	**95 % CI**		0.01

Table A- 17 SGL 35BA (1.0 $mgcm^{-2}$) Ketjenblack EC-300J.

SGL 35BA										
1.0 $mgcm^{-2}$ (Ketjenblack EC-300J)										
Sample Number	**Permeability $k\ (m^2)$**		**Thickness (μm)**		**Thickness change (L_{MPL}) (μm)**	**Percentage reduction in permeability (%)**	**MPL permeability (k_{MPL}) (m^2)**	**Mass of samples (mg)**		**Actual carbon loading $(mgcm^{-2})$**
	Uncoated (k_{GDL})	**Coated (k_{GDM})**	**Uncoated (L_{GDL})**	**Coated (L_{GDM})**				**Uncoated**	**Coated**	
1	4.26E-11	1.02E-11	297.50	340.00	42.50	76.09	1.61E-12	28.75	35.09	1.01
2	3.90E-11	9.92E-12	290.00	350.00	60.00	74.58	2.15E-12	29.37	35.71	1.05
3	3.73E-11	9.35E-12	292.50	338.75	46.25	74.95	1.63E-12	29.06	35.40	1.03
4	4.02E-11	1.53E-11	302.50	348.75	46.25	61.94	3.03E-12	30.10	36.44	0.99
5	4.17E-11	1.41E-11	290.00	338.75	48.75	66.15	2.86E-12	29.48	35.82	1.01
6	4.26E-11	1.10E-11	297.50	345.00	47.50	74.10	1.96E-12	29.15	35.49	1.02
Mean	4.06E-11	1.16E-11	295.00	343.54	48.54	71.30	2.21E-12	**Mean**		1.02
Std. Dev	2.12E-12	2.46E-12	5.00	5.09	5.99	5.81	6.09E-13	**Std. Dev**		0.02
95 % CI	2.22E-12	2.58E-12	5.25	5.34	6.29	6.10	6.40E-13	**95 % CI**		0.02

Table A- 18 SGL 35BA (2.0 $mgcm^{-2}$) Ketjenblack EC-300J.

SGL 35BA										
2.0 $mgcm^{-2}$ (Ketjenblack EC-300J)										
Sample Number	**Permeability $k\ (m^2)$**		**Thickness (μm)**		**Thickness change (L_{MPL}) (μm)**	**Percentage reduction in permeability (%)**	**MPL permeability (k_{MPL}) (m^2)**	**Mass of samples (mg)**		**Actual carbon loading $(mgcm^{-2})$**
	Uncoated (k_{GDL})	**Coated (k_{GDM})**	**Uncoated (L_{GDL})**	**Coated (L_{GDM})**				**Uncoated**	**Coated**	
1	4.02E-11	2.06E-11	302.50	455.00	152.50	48.83	1.05E-11	28.97	41.69	2.15
2	4.49E-11	1.72E-11	291.25	442.50	151.25	61.80	7.83E-12	27.78	40.50	2.01
3	4.13E-11	2.06E-11	286.25	437.50	151.25	50.17	1.06E-11	28.25	40.97	2.04
4	4.23E-11	1.82E-11	295.00	443.75	148.75	57.07	8.53E-12	28.65	41.37	2.03
5	4.28E-11	1.78E-11	298.75	442.50	143.75	58.28	8.07E-12	29.48	42.20	2.03
6	3.87E-11	1.48E-11	301.25	435.00	133.75	61.65	6.21E-12	29.05	41.77	2.03
Mean	4.17E-11	1.82E-11	295.83	442.71	146.88	56.30	8.61E-12	**Mean**		2.05
Std. Dev	2.17E-12	2.19E-12	6.26	6.91	7.15	5.60	1.67E-12	**Std. Dev**		0.05
95 % CI	2.27E-12	2.30E-12	6.57	7.25	7.50	5.88	1.75E-12	**95 % CI**		0.05

Table A- 19 SGL 10CA (0.5 mgcm^{-2}) Vulcan XC-72R.

SGL 10CA										
0.5 mgcm^{-2} (Vulcan XC-72R)										
Sample Number	**Permeability k (m^2)**		**Thickness (μm)**		**Thickness change (L_{MPL}) (μm)**	**Percentage reduction in permeability (%)**	**MPL permeability (k_{MPL}) (m^2)**	**Mass of samples (mg)**		**Actual carbon loading $(mgcm^{-2})$**
	Uncoated (k_{GDL})	**Coated (k_{GDM})**	**Uncoated (L_{GDL})**	**Coated (L_{GDM})**				**Uncoated**	**Coated**	
1	2.07E-11	8.03E-12	340.00	343.75	3.75	61.15	1.42E-13	42.63	45.81	0.52
2	2.12E-11	5.91E-12	340.00	343.75	3.75	72.11	8.90E-14	43.57	46.75	0.53
3	1.86E-11	8.54E-12	366.25	368.75	2.50	54.06	1.06E-13	48.47	51.65	0.51
4	2.44E-11	8.56E-12	373.75	377.50	3.75	64.96	1.30E-13	47.98	51.16	0.51
5	2.27E-11	8.21E-12	342.50	345.00	2.50	63.79	9.28E-14	42.81	45.99	0.50
6	2.07E-11	8.72E-12	363.75	366.25	2.50	57.94	1.02E-13	45.28	48.46	0.50
Mean	2.14E-11	7.99E-12	354.38	357.50	3.13	62.33	1.10E-13	**Mean**		0.51
Std. Dev	1.99E-12	1.05E-12	15.22	15.08	0.68	6.23	2.12E-14	**Std. Dev**		0.01
95 % CI	2.09E-12	1.11E-12	15.98	15.83	0.72	6.53	2.22E-14	**95 % CI**		0.01

Table A- 20 SGL 10CA (1.0 mgcm^{-2}) Vulcan XC-72R.

SGL 10CA										
1.0 mgcm^{-2} (Vulcan XC-72R)										
Sample Number	**Permeability k (m^2)**		**Thickness (μm)**		**Thickness change (L_{MPL}) (μm)**	**Percentage reduction in permeability (%)**	**MPL permeability (k_{MPL}) (m^2)**	**Mass of samples (mg)**		**Actual carbon loading ($mgcm^{-2}$)**
	Uncoated (k_{GDL})	**Coated (k_{GDM})**	**Uncoated (L_{GDL})**	**Coated (L_{GDM})**				**Uncoated**	**Coated**	
1	2.13E-11	4.87E-12	340.00	356.25	16.25	77.15	2.84E-13	41.93	48.27	1.36
2	2.33E-11	5.30E-12	335.00	350.00	15.00	77.32	2.90E-13	42.06	48.40	1.05
3	2.18E-11	6.22E-12	335.00	351.25	16.25	71.43	3.96E-13	42.28	48.62	0.98
4	2.13E-11	5.54E-12	361.25	373.75	12.50	74.05	2.47E-13	44.51	50.85	1.01
5	2.35E-11	5.14E-12	341.25	353.75	12.50	78.16	2.30E-13	42.20	48.54	1.02
6	2.14E-11	4.85E-12	338.75	353.75	15.00	77.36	2.62E-13	41.80	48.14	1.03
Mean	2.21E-11	5.32E-12	341.88	356.46	14.58	75.91	2.85E-13	**Mean**		1.07
Std. Dev	1.03E-12	5.13E-13	9.83	8.75	1.71	2.61	5.89E-14	**Std. Dev**		0.14
95 % CI	1.08E-12	5.39E-13	10.32	9.18	1.79	2.74	6.18E-14	**95 % CI**		0.15

Table A- 21 SGL 10CA (2.0 $mgcm^{-2}$) Vulcan XC-72R.

SGL 10CA										
2.0 $mgcm^{-2}$ (Vulcan XC-72R)										
Sample Number	**Permeability $k\ (m^2)$**		**Thickness (μm)**		**Thickness change (L_{MPL}) (μm)**	**Percentage reduction in permeability (%)**	**MPL permeability (k_{MPL}) (m^2)**	**Mass of samples (mg)**		**Actual carbon loading $(mgcm^{-2})$**
	Uncoated (k_{GDL})	**Coated (k_{GDM})**	**Uncoated (L_{GDL})**	**Coated (L_{GDM})**				**Uncoated**	**Coated**	
1	2.08E-11	2.65E-12	378.75	401.25	22.50	87.30	1.69E-13	47.44	60.16	2.01
2	2.04E-11	2.76E-12	328.75	362.50	33.75	86.48	2.93E-13	42.70	55.42	2.00
3	2.20E-11	3.76E-12	355.00	381.25	26.25	82.87	3.08E-13	43.30	56.02	1.99
4	2.16E-11	3.61E-12	341.25	372.50	31.25	83.26	3.58E-13	44.30	57.02	2.02
5	2.34E-11	3.77E-12	345.00	377.50	32.50	83.85	3.81E-13	43.81	56.53	2.03
6	2.15E-11	3.80E-12	358.75	391.25	32.50	82.27	3.77E-13	44.72	57.44	2.03
Mean	2.16E-11	3.39E-12	351.25	381.04	29.79	84.34	3.14E-13	**Mean**		2.01
Std. Dev	1.03E-12	5.40E-13	17.16	13.73	4.43	2.06	7.99E-14	**Std. Dev**		0.02
95 % CI	3.60E-12	1.88E-13	3.59	8.94	6.46	2.16	8.38E-14	**95 % CI**		0.02

Table A- 22 SGL 10CA (0.5 mgcm^{-2}) Ketjenblack EC-300J.

SGL 10CA										
0.5 mgcm^{-2} (Ketjenblack EC-300J)										
Sample Number	**Permeability k (m^2)**		**Thickness (μm)**		**Thickness change (L_{MPL}) (μm)**	**Percentage reduction in permeability (%)**	**MPL permeability (k_{MPL}) (m^2)**	**Mass of samples (mg)**		**Actual carbon loading $(mgcm^{-2})$**
	Uncoated (k_{GDL})	**Coated (k_{GDM})**	**Uncoated (L_{GDL})**	**Coated (L_{GDM})**				**Uncoated**	**Coated**	
1	2.23E-11	7.88E-12	375.00	380.00	5.00	64.72	1.59E-13	47.78	50.96	0.50
2	2.15E-11	9.52E-12	358.75	367.50	8.75	55.63	4.00E-13	45.30	48.48	0.53
3	2.14E-11	8.90E-12	338.75	343.75	5.00	58.41	2.19E-13	42.11	45.29	0.51
4	2.15E-11	7.16E-12	342.50	352.50	10.00	66.68	3.00E-13	42.23	45.41	0.50
5	2.37E-11	8.37E-12	343.75	351.25	7.50	64.69	2.73E-13	42.58	45.76	0.51
6	2.08E-11	7.86E-12	377.50	386.25	8.75	62.25	2.82E-13	46.98	50.16	0.50
Mean	2.19E-11	8.28E-12	356.04	363.54	7.50	62.07	2.72E-13	**Mean**		0.51
Std. Dev	1.02E-12	8.38E-13	17.09	17.13	2.09	4.24	8.09E-14	**Std. Dev**		0.01
95 % CI	1.07E-12	8.80E-13	17.94	17.98	2.20	4.45	8.50E-14	**95 % CI**		0.01

Table A- 23 SGL 10CA (1.0 $mgcm^{-2}$) Ketjenblack EC-300J.

SGL 10CA										
1.0 $mgcm^{-2}$ (Ketjenblack EC-300J)										
Sample Number	**Permeability $k\ (m^2)$**		**Thickness (μm)**		**Thickness change (L_{MPL}) (μm)**	**Percentage reduction in permeability (%)**	**MPL permeability (k_{MPL}) (m^2)**	**Mass of samples (mg)**		**Actual carbon loading $(mgcm^{-2})$**
	Uncoated (k_{GDL})	**Coated (k_{GDM})**	**Uncoated (L_{GDL})**	**Coated (L_{GDM})**				**Uncoated**	**Coated**	
1	2.01E-11	7.89E-12	375.00	387.50	12.50	60.72	4.10E-13	45.60	51.94	1.00
2	2.34E-11	6.92E-12	345.00	376.25	31.25	70.40	7.89E-13	42.87	49.21	1.10
3	2.06E-11	6.26E-12	382.50	400.00	17.50	69.66	3.86E-13	47.26	53.60	1.11
4	2.36E-11	7.79E-12	342.50	373.75	31.25	66.98	9.34E-13	42.21	48.55	1.03
5	2.14E-11	7.74E-12	341.25	371.25	30.00	63.84	9.37E-13	42.15	48.49	1.03
6	2.19E-11	6.29E-12	353.75	382.50	28.75	71.25	6.44E-13	44.79	51.13	1.00
Mean	2.18E-11	7.15E-12	356.67	381.88	25.21	67.14	6.83E-13	**Mean**		1.05
Std. Dev	1.43E-12	7.60E-13	17.81	10.69	8.12	4.15	2.46E-13	**Std. Dev**		0.05
95 % CI	2.22E-12	2.58E-12	5.25	5.34	6.29	4.35	2.58E-13	**95 % CI**		0.05

Table A- 24 SGL 10CA (2.0 $mgcm^{-2}$) Ketjenblack EC-300J.

SGL 10CA										
2.0 $mgcm^{-2}$ (Ketjenblack EC-300J)										
Sample Number	**Permeability $k\ (m^2)$**		**Thickness (μm)**		**Thickness change (L_{MPL}) (μm)**	**Percentage reduction in permeability (%)**	**MPL permeability (k_{MPL}) (m^2)**	**Mass of samples (mg)**		**Actual carbon loading $(mgcm^{-2})$**
	Uncoated (k_{GDL})	**Coated (k_{GDM})**	**Uncoated (L_{GDL})**	**Coated (L_{GDM})**				**Uncoated**	**Coated**	
1	2.43E-11	6.55E-12	371.25	486.25	115.00	73.03	1.95E-12	44.73	57.45	2.11
2	2.25E-11	6.99E-12	340.00	460.00	120.00	68.92	2.37E-12	43.23	55.95	2.07
3	2.07E-11	5.70E-12	363.75	468.75	105.00	72.50	1.62E-12	45.44	58.16	2.00
4	2.44E-11	5.61E-12	373.75	486.25	112.50	77.05	1.58E-12	44.91	57.63	2.00
5	2.07E-11	5.88E-12	363.75	473.75	110.00	71.63	1.75E-12	45.55	58.27	1.99
6	2.13E-11	5.77E-12	361.25	468.75	107.50	72.96	1.67E-12	45.30	58.02	2.00
Mean	2.23E-11	6.08E-12	362.29	473.96	111.67	72.68	1.82E-12	**Mean**		2.03
Std. Dev	1.69E-12	5.56E-13	11.95	10.50	5.40	2.63	2.97E-13	**Std. Dev**		0.05
95 % CI	1.78E-12	5.84E-13	12.54	11.02	5.67	2.76	3.12E-13	**95 % CI**		0.05

Table A- 25 SGL 10EA (0.5 $mgcm^{-2}$) Vulcan XC-72R.

SGL 10EA										
0.5 $mgcm^{-2}$ (Vulcan XC-72R)										
Sample Number	**Permeability $k\ (m^2)$**		**Thickness (μm)**		**Thickness change (L_{MPL}) (μm)**	**Percentage reduction in permeability (%)**	**MPL permeability (k_{MPL}) (m^2)**	**Mass of samples (mg)**		**Actual carbon loading $(mgcm^{-2})$**
	Uncoated (k_{GDL})	**Coated (k_{GDM})**	**Uncoated (L_{GDL})**	**Coated (L_{GDM})**				**Uncoated**	**Coated**	
1	2.24E-11	4.05E-12	406.25	408.75	2.50	81.88	3.02E-14	52.95	56.13	0.50
2	2.12E-11	3.85E-12	390.00	396.25	6.25	81.81	7.40E-14	54.54	57.72	0.51
3	1.73E-11	3.23E-12	408.75	411.25	2.50	81.35	2.41E-14	56.03	59.21	0.52
4	1.62E-11	4.58E-12	387.50	392.50	5.00	71.78	8.08E-14	55.20	58.38	0.51
5	1.77E-11	4.67E-12	360.00	365.00	5.00	73.63	8.65E-14	52.50	55.68	0.51
6	1.94E-11	6.22E-12	365.00	368.75	3.75	67.93	9.27E-14	51.30	54.48	0.50
Mean	1.90E-11	4.43E-12	386.25	390.42	4.17	76.40	6.47E-14	**Mean**		0.51
Std. Dev	2.39E-12	1.02E-12	20.31	19.62	1.51	6.07	2.98E-14	**Std. Dev**		0.01
95 % CI	2.51E-12	1.07E-12	21.32	20.59	1.59	6.38	3.13E-14	**95 % CI**		0.01

Table A- 26 SGL 10EA (1.0 mgcm^{-2}) Vulcan XC-72R.

SGL 10EA										
1.0 mgcm^{-2} (Vulcan XC-72R)										
Sample Number	**Permeability k (m^2)**		**Thickness (μm)**		**Thickness change (L_{MPL}) (μm)**	**Percentage reduction in permeability (%)**	**MPL permeability (k_{MPL}) (m^2)**	**Mass of samples (mg)**		**Actual carbon loading $(mgcm^{-2})$**
	Uncoated (k_{GDL})	**Coated (k_{GDM})**	**Uncoated (L_{GDL})**	**Coated (L_{GDM})**				**Uncoated**	**Coated**	
1	1.53E-11	1.99E-12	351.25	366.25	15.00	87.00	9.32E-14	54.25	60.59	1.01
2	1.77E-11	1.20E-12	360.00	376.25	16.25	93.22	5.54E-14	52.12	58.46	1.10
3	1.94E-11	1.86E-12	365.00	381.25	16.25	90.41	8.73E-14	50.30	56.64	1.04
4	1.80E-11	1.19E-12	361.25	378.75	17.50	93.39	5.86E-14	52.88	59.22	1.06
5	1.56E-11	2.02E-12	353.75	370.00	16.25	87.05	1.01E-13	55.10	61.44	0.99
6	1.97E-11	1.74E-12	366.25	381.25	15.00	91.18	7.47E-14	52.30	58.64	1.03
Mean	1.76E-11	1.67E-12	359.58	375.63	16.04	90.38	7.85E-14	**Mean**		1.04
Std. Dev	1.84E-12	3.80E-13	6.00	6.21	0.94	2.84	1.88E-14	**Std. Dev**		0.04
95 % CI	1.93E-12	3.98E-13	6.30	6.52	0.99	2.98	1.97E-14	**95 % CI**		0.04

Table A- 27 SGL 10EA (2.0 mgcm^{-2}) Vulcan XC-72R.

SGL 10EA										
2.0 mgcm^{-2} (Vulcan XC-72R)										
Sample Number	**Permeability k (m^2)**		**Thickness (μm)**		**Thickness change (L_{MPL}) (μm)**	**Percentage reduction in permeability (%)**	**MPL permeability (k_{MPL}) (m^2)**	**Mass of samples (mg)**		**Actual carbon loading ($mgcm^{-2}$)**
	Uncoated (k_{GDL})	**Coated (k_{GDM})**	**Uncoated (L_{GDL})**	**Coated (L_{GDM})**				**Uncoated**	**Coated**	
1	1.74E-11	1.28E-12	373.75	410.00	36.25	92.61	1.22E-13	52.71	65.43	2.05
2	1.76E-11	1.17E-12	377.50	427.50	50.00	93.35	1.45E-13	52.06	64.78	2.01
3	1.62E-11	8.99E-13	386.25	435.00	48.75	94.44	1.06E-13	54.31	67.03	2.03
4	1.55E-11	1.16E-12	377.50	421.25	43.75	92.53	1.29E-13	54.20	66.92	2.01
5	1.77E-11	9.64E-13	380.00	430.00	50.00	94.55	1.18E-13	55.60	68.32	2.04
6	1.62E-11	1.09E-12	387.50	432.50	45.00	93.30	1.20E-13	55.90	68.62	2.04
Mean	1.67E-11	1.09E-12	380.42	426.04	45.63	93.46	1.23E-13	**Mean**		2.03
Std. Dev	9.22E-13	1.42E-13	5.40	9.17	5.29	0.87	1.31E-14	**Std. Dev**		0.01
95 % CI	9.67E-13	1.49E-13	5.67	9.62	5.55	0.91	1.37E-14	**95 % CI**		0.01

Table A- 28 SGL 10EA (0.5 mgcm^{-2}) Ketjenblack EC-300J.

SGL 10EA										
0.5 mgcm^{-2} (Ketjenblack EC-300J)										
Sample Number	**Permeability k (m^2)**		**Thickness (μm)**		**Thickness change (L_{MPL}) (μm)**	**Percentage reduction in permeability (%)**	**MPL permeability (k_{MPL}) (m^2)**	**Mass of samples (mg)**		**Actual carbon loading ($mgcm^{-2}$)**
	Uncoated (k_{GDL})	**Coated (k_{GDM})**	**Uncoated (L_{GDL})**	**Coated (L_{GDM})**				**Uncoated**	**Coated**	
1	2.21E-11	1.15E-11	403.75	431.25	27.50	47.91	1.43E-12	56.05	59.23	0.50
2	1.86E-11	8.84E-12	391.25	407.50	16.25	52.39	6.49E-13	55.16	58.34	0.50
3	2.14E-11	6.07E-12	355.00	367.50	12.50	71.67	2.84E-13	54.21	57.39	0.50
4	2.24E-11	7.27E-12	360.00	385.00	25.00	67.58	6.77E-13	52.50	55.68	0.52
5	2.35E-11	6.09E-12	351.25	372.50	21.25	74.04	4.60E-13	52.89	56.07	0.52
6	2.26E-11	7.11E-12	348.75	366.25	17.50	68.48	4.86E-13	52.30	55.48	0.49
Mean	2.18E-11	7.82E-12	368.33	388.33	20.00	63.68	6.65E-13	**Mean**		0.51
Std. Dev	1.70E-12	2.08E-12	23.25	26.05	5.65	10.82	4.03E-13	**Std. Dev**		0.01
95 % CI	1.79E-12	2.18E-12	24.40	27.34	5.93	11.36	4.23E-13	**95 % CI**		0.01

Table A- 29 SGL 10EA (1.0 mgcm^{-2}) Ketjenblack EC-300J.

SGL 10EA										
1.0 mgcm^{-2} (Ketjenblack EC-300J)										
Sample Number	**Permeability k (m^2)**		**Thickness (μm)**		**Thickness change (L_{MPL}) (μm)**	**Percentage reduction in permeability (%)**	**MPL permeability (k_{MPL}) (m^2)**	**Mass of samples (mg)**		**Actual carbon loading ($mgcm^{-2}$)**
	Uncoated (k_{GDL})	**Coated (k_{GDM})**	**Uncoated (L_{GDL})**	**Coated (L_{GDM})**				**Uncoated**	**Coated**	
1	1.54E-11	5.97E-12	382.50	425.00	42.50	61.25	9.16E-13	63.43	69.77	1.01
2	1.67E-11	6.80E-12	381.25	425.00	43.75	59.32	1.10E-12	56.80	63.14	1.03
3	2.51E-11	6.10E-12	408.75	440.00	31.25	75.66	5.60E-13	54.39	60.73	1.00
4	2.24E-11	5.68E-12	360.00	407.50	47.50	74.68	8.52E-13	49.84	56.18	0.99
5	2.35E-11	6.57E-12	351.25	402.50	51.25	72.00	1.11E-12	48.74	55.08	1.02
6	2.26E-11	6.09E-12	348.75	402.50	53.75	73.03	1.06E-12	47.90	54.24	1.06
Mean	2.09E-11	6.20E-12	372.08	417.08	45.00	69.32	9.33E-13	**Mean**		1.02
Std. Dev	3.92E-12	4.12E-13	23.07	15.28	7.98	7.14	2.10E-13	**Std. Dev**		0.02
95 % CI	4.11E-12	4.33E-13	24.22	16.04	8.38	7.50	2.21E-13	**95 % CI**		0.03

Table A- 30 SGL 10EA (2.0 mgcm^{-2}) Ketjenblack EC-300J.

SGL 10EA										
2.0 mgcm^{-2} (Ketjenblack EC-300J)										
Sample Number	**Permeability k (m^2)**		**Thickness (μm)**		**Thickness change (L_{MPL}) (μm)**	**Percentage reduction in permeability (%)**	**MPL permeability (k_{MPL}) (m^2)**	**Mass of samples (mg)**		**Actual carbon loading ($mgcm^{-2}$)**
	Uncoated (k_{GDL})	**Coated (k_{GDM})**	**Uncoated (L_{GDL})**	**Coated (L_{GDM})**				**Uncoated**	**Coated**	
1	1.64E-11	3.59E-12	412.50	537.50	125.00	78.15	1.00E-12	65.27	77.99	2.03
2	1.75E-11	3.33E-12	395.00	521.25	126.25	80.92	9.43E-13	62.83	75.55	2.00
3	1.66E-11	3.04E-12	388.75	500.00	111.25	81.63	7.90E-13	59.43	72.15	2.02
4	1.54E-11	4.82E-12	382.50	505.00	122.50	68.67	1.53E-12	59.70	72.42	2.04
5	1.69E-11	3.45E-12	381.25	493.75	112.50	79.56	9.34E-13	58.80	71.52	2.07
6	1.64E-11	3.20E-12	388.75	515.00	126.25	80.45	9.22E-13	59.20	71.92	2.04
Mean	1.65E-11	3.57E-12	391.46	512.08	120.63	78.23	1.02E-12	**Mean**		2.03
Std. Dev	6.77E-13	6.41E-13	11.44	15.94	6.93	4.83	2.61E-13	**Std. Dev**		0.02
95 % CI	7.10E-13	6.73E-13	12.01	16.73	7.27	5.07	2.74E-13	**95 % CI**		0.02

Appendix B

Chapter 5 Results

Table B- 1 SGL 10EA (1.0 mgcm^{-2}) Carbon composite mixture (80 % Vulcan XC-72R – 20% Ketjenblack EC-300J).

SGL 10EA								
1.0 mgcm^{-2} (80 % Vulcan XC-72R – 20% Ketjenblack EC-300J)								
Sample Number	**Permeability k (m^2)**		**Thickness (μm)**		**Thickness change (L_{MPL}) (μm)**	**Mass of samples (mg)**		**Actual carbon loading ($mgcm^{-2}$)**
	Uncoated (k_{GDL})	**Coated (k_{GDM})**	**Uncoated (L_{GDL})**	**Coated (L_{GDM})**		**Uncoated**	**Coated**	
1	2.09E-11	3.85E-12	373.75	402.50	28.75	54.77	61.23	1.02
2	2.14E-11	2.98E-12	405.00	422.50	17.50	60.55	66.91	1.00
3	1.76E-11	1.16E-12	398.75	417.50	18.75	62.10	68.48	1.01
4	2.08E-11	3.82E-12	385.00	397.50	12.50	55.56	61.91	1.00
5	1.95E-11	3.69E-12	376.25	392.50	16.25	56.61	62.98	1.01
6	2.11E-11	3.73E-12	375.00	392.50	17.50	54.73	61.11	1.01
Mean	2.02E-11	3.21E-12	385.63	404.17	18.54	**Mean**		1.01
Std. Dev	1.44E-12	1.05E-12	13.34	12.91	5.44	**Std. Dev**		0.01
95 % CI	1.52E-12	1.11E-12	14.00	13.55	5.71	**95 % CI**		0.01

Table B- 2 SGL 10EA (1.0 $mgcm^{-2}$) Carbon composite mixture (50 % Vulcan XC-72R – 50% Ketjenblack EC-300J).

SGL 10EA								
1.0 $mgcm^{-2}$ (50 % Vulcan XC-72R – 50% Ketjenblack EC-300J)								
Sample Number	**Permeability $k\ (m^2)$**		**Thickness (μm)**		**Thickness change (L_{MPL}) (μm)**	**Mass of samples (mg)**		**Actual carbon loading $(mgcm^{-2})$**
	Uncoated (k_{GDL})	**Coated (k_{GDM})**	**Uncoated (L_{GDL})**	**Coated (L_{GDM})**		**Uncoated**	**Coated**	
1	2.18E-11	5.94E-12	362.50	382.50	20.00	58.99	65.40	1.01
2	1.80E-11	4.93E-12	397.50	420.00	22.50	63.75	70.07	1.00
3	2.19E-11	4.96E-12	398.75	425.00	26.25	56.62	62.99	1.01
4	1.96E-11	6.09E-12	380.00	397.50	17.50	48.53	54.92	1.01
5	1.67E-11	4.85E-12	388.75	416.25	27.50	56.07	62.43	1.00
6	1.95E-11	4.23E-12	338.75	363.75	25.00	54.37	61.20	1.08
Mean	1.96E-11	5.17E-12	377.71	400.83	23.13	**Mean**		1.02
Std. Dev	2.06E-12	7.11E-13	23.28	24.13	3.85	**Std. Dev**		0.03
95 % CI	2.17E-12	7.46E-13	24.44	25.33	4.04	**95 % CI**		0.03

Table B- 3 SGL 10EA (1.0 mgcm^{-2}) Carbon composite mixture (20 % Vulcan XC-72R – 80% Ketjenblack EC-300J).

SGL 10EA								
1.0 mgcm^{-2} (20 % Vulcan XC-72R – 80% Ketjenblack EC-300J)								
Sample Number	**Permeability k (m^2)**		**Thickness (μm)**		**Thickness change (L_{MPL}) (μm)**	**Mass of samples (mg)**		**Actual carbon loading ($mgcm^{-2}$)**
	Uncoated (k_{GDL})	**Coated (k_{GDM})**	**Uncoated (L_{GDL})**	**Coated (L_{GDM})**		**Uncoated**	**Coated**	
1	2.00E-11	5.58E-12	357.50	392.50	35.00	52.80	59.16	1.00
2	2.23E-11	6.34E-12	367.50	395.00	27.50	59.93	66.30	1.01
3	1.72E-11	5.72E-12	381.25	413.75	32.50	63.95	70.45	1.03
4	2.38E-11	5.49E-12	350.00	392.50	42.50	62.50	68.91	1.01
5	2.03E-11	5.83E-12	383.75	421.25	37.50	54.46	60.86	1.01
6	2.05E-11	5.46E-12	426.25	457.50	31.25	59.67	66.10	1.01
Mean	2.07E-11	5.73E-12	377.71	412.08	34.38	**Mean**		1.01
Std. Dev	2.25E-12	3.28E-13	27.15	25.33	5.23	**Std. Dev**		0.01
95 % CI	2.36E-12	3.44E-13	28.50	26.59	5.49	**95 % CI**		0.01

Table B- 4 SGL 10EA (2.0 mgcm^{-2}) Carbon composite mixture (80 % Vulcan XC-72R – 20% Ketjenblack EC-300J).

SGL 10EA								
2.0 mgcm^{-2} (80 % Vulcan XC-72R – 20% Ketjenblack EC-300J)								
Sample Number	**Permeability k (m^2)**		**Thickness (μm)**		**Thickness change (L_{MPL}) (μm)**	**Mass of samples (mg)**		**Actual carbon loading ($mgcm^{-2}$)**
	Uncoated (k_{GDL})	**Coated (k_{GDM})**	**Uncoated (L_{GDL})**	**Coated (L_{GDM})**		**Uncoated**	**Coated**	
1	1.71E-11	1.75E-12	410.00	458.75	48.75	68.02	80.91	2.03
2	1.81E-11	1.20E-12	415.00	462.50	47.50	65.79	78.65	2.03
3	2.20E-11	1.11E-12	386.25	433.75	47.50	63.45	76.30	2.03
4	2.08E-11	1.67E-12	385.00	437.50	52.50	64.25	77.20	2.04
5	1.95E-11	1.63E-12	376.25	423.75	47.50	67.12	79.74	1.99
6	2.11E-11	1.62E-12	375.00	421.25	46.25	65.18	78.20	2.05
Mean	1.98E-11	1.50E-12	391.25	439.58	48.33	**Mean**		2.03
Std. Dev	1.89E-12	2.72E-13	17.14	17.42	2.19	**Std. Dev**		0.02
95 % CI	1.98E-12	2.86E-13	17.99	18.29	2.30	**95 % CI**		0.02

Table B- 5 SGL 10EA (2.0 mgcm^{-2}) Carbon composite mixture (50 % Vulcan XC-72R – 50% Ketjenblack EC-300J).

SGL 10EA								
2.0 mgcm^{-2} (50 % Vulcan XC-72R – 50% Ketjenblack EC-300J)								
Sample Number	**Permeability k (m^2)**		**Thickness (μm)**		**Thickness change (L_{MPL}) (μm)**	**Mass of samples (mg)**		**Actual carbon loading ($mgcm^{-2}$)**
	Uncoated (k_{GDL})	**Coated (k_{GDM})**	**Uncoated (L_{GDL})**	**Coated (L_{GDM})**		**Uncoated**	**Coated**	
1	2.00E-11	3.13E-12	388.75	436.25	47.50	65.03	78.10	2.06
2	2.15E-11	2.18E-12	345.00	402.50	57.50	56.83	69.93	2.07
3	1.89E-11	3.21E-12	378.75	423.75	45.00	52.44	65.23	2.02
4	1.68E-11	2.52E-12	408.75	465.00	56.25	57.25	70.12	2.03
5	2.24E-11	2.33E-12	371.25	431.25	60.00	63.43	76.06	1.99
6	2.04E-11	2.53E-12	406.25	468.75	62.50	61.34	74.72	2.11
Mean	2.00E-11	2.65E-12	383.13	437.92	54.79	**Mean**		2.05
Std. Dev	1.98E-12	4.26E-13	23.82	25.24	7.00	**Std. Dev**		0.04
95 % CI	2.08E-12	4.47E-13	25.00	26.50	7.35	**95 % CI**		0.04

Table B- 6 SGL 10EA (2.0 mgcm^{-2}) Carbon composite mixture (20 % Vulcan XC-72R – 80% Ketjenblack EC-300J).

SGL 10EA								
2.0 mgcm^{-2} (20 % Vulcan XC-72R – 80% Ketjenblack EC-300J)								
Sample Number	**Permeability k (m^2)**		**Thickness (μm)**		**Thickness change (L_{MPL}) (μm)**	**Mass of samples (mg)**		**Actual carbon loading ($mgcm^{-2}$)**
	Uncoated (k_{GDL})	**Coated (k_{GDM})**	**Uncoated (L_{GDL})**	**Coated (L_{GDM})**		**Uncoated**	**Coated**	
1	1.73E-11	2.92E-12	373.75	437.50	63.75	65.27	76.15	2.03
2	1.70E-11	2.91E-12	362.50	437.50	75.00	62.90	75.91	2.05
3	1.80E-11	3.03E-12	395.00	457.50	62.50	66.82	79.67	2.03
4	1.68E-11	3.43E-12	408.75	512.50	103.75	65.65	78.29	1.99
5	2.24E-11	3.02E-12	371.25	452.50	81.25	61.42	74.18	2.01
6	2.04E-11	3.23E-12	406.25	486.25	80.00	64.13	76.91	2.02
Mean	1.86E-11	3.09E-12	386.25	463.96	77.71	**Mean**		2.02
Std. Dev	2.26E-12	2.02E-13	19.64	29.75	15.03	**Std. Dev**		0.02
95 % CI	2.37E-12	2.12E-13	20.61	31.23	15.78	**95 % CI**		0.02

Table B- 7 Toray TGP-H-60 (1.0 $mgcm^{-2}$) Vulcan XC-72R.

Toray TGP-H-60								
1.0 $mgcm^{-2}$ (Vulcan XC-72R)								
Sample Number	**Permeability k (m^2)**		**Thickness (μm)**		**Thickness change (L_{MPL}) (μm)**	**Mass of samples (mg)**		**Actual carbon loading ($mgcm^{-2}$)**
	Uncoated (k_{GDL})	**Coated (k_{GDM})**	**Uncoated (L_{GDL})**	**Coated (L_{GDM})**		**Uncoated**	**Coated**	
1	7.43E-12	3.21E-13	197.50	207.50	10.00	43.10	50.10	1.10
2	7.73E-12	3.22E-13	198.75	208.75	10.00	43.10	49.50	1.01
3	7.49E-12	3.19E-13	193.75	206.25	12.50	43.06	49.50	1.02
4	7.88E-12	3.15E-13	193.75	203.75	10.00	42.70	49.10	1.01
Mean	7.33E-12	3.19E-13	195.94	206.56	10.63	**Mean**		1.04
Std. Dev	7.84E-13	3.18E-15	2.58	2.13	1.25	**Std. Dev**		0.05
95 % CI	1.25E-12	5.06E-15	4.10	3.40	1.99	**95 % CI**		0.07

Table B- 8 Toray TGP-H-60 (1.0 $mgcm^{-2}$) Ketjenblack EC-300J.

Toray TGP-H-60								
1.0 $mgcm^{-2}$ (Ketjenblack EC-300J)								
Sample Number	**Permeability k (m^2)**		**Thickness (μm)**		**Thickness change (L_{MPL}) (μm)**	**Mass of samples (mg)**		**Actual carbon loading ($mgcm^{-2}$)**
	Uncoated (k_{GDL})	**Coated (k_{GDM})**	**Uncoated (L_{GDL})**	**Coated (L_{GDM})**		**Uncoated**	**Coated**	
1	7.28E-12	1.96E-12	187.50	231.25	43.75	44.62	51.06	1.02
2	6.32E-12	2.14E-12	188.75	228.75	40.00	44.37	50.74	1.01
3	7.51E-12	1.88E-12	191.25	231.25	40.00	43.19	49.79	1.04
4	8.22E-12	2.06E-12	195.00	233.75	38.75	44.77	51.5	1.06
Mean	7.33E-12	2.01E-12	190.63	231.25	40.63	**Mean**		1.03
Std. Dev	7.84E-13	1.16E-13	3.31	2.04	2.17	**Std. Dev**		0.03
95 % CI	1.25E-12	1.85E-13	5.26	3.25	3.44	**95 % CI**		0.04

Table B- 9 SGL 35BA (1.0 mgcm^{-2}) Vulcan XC-72R.

SGL 35BA								
1.0 mgcm^{-2} (Vulcan XC-72R)								
Sample Number	**Permeability k (m^2)**		**Thickness (μm)**		**Thickness change (L_{MPL}) (μm)**	**Mass of samples (mg)**		**Actual carbon loading ($mgcm^{-2}$)**
	Uncoated (k_{GDL})	**Coated (k_{GDM})**	**Uncoated (L_{GDL})**	**Coated (L_{GDM})**		**Uncoated**	**Coated**	
1	4.02E-11	3.77E-12	295.00	301.25	6.25	28.94	35.28	1.16
2	3.77E-11	3.74E-12	281.25	287.50	6.25	28.21	34.55	1.26
3	3.82E-11	5.28E-12	288.75	296.25	7.50	28.39	34.73	1.09
4	3.79E-11	3.38E-12	295.00	302.50	7.50	28.89	35.23	1.03
Mean	3.85E-11	4.04E-12	290.00	296.88	6.88	**Mean**		1.14
Std. Dev	1.15E-12	8.44E-13	6.54	6.81	0.72	**Std. Dev**		0.10
95 % CI	1.83E-12	1.34E-12	10.40	10.83	1.15	**95 % CI**		0.16

Table B- 10 SGL 35BA (1.0 $mgcm^{-2}$) Ketjenblack EC-300J.

SGL 35BA								
1.0 $mgcm^{-2}$ (Ketjenblack EC-300J)								
Sample Number	**Permeability k (m^2)**		**Thickness (μm)**		**Thickness change (L_{MPL}) (μm)**	**Mass of samples (mg)**		**Actual carbon loading ($mgcm^{-2}$)**
	Uncoated (k_{GDL})	**Coated (k_{GDM})**	**Uncoated (L_{GDL})**	**Coated (L_{GDM})**		**Uncoated**	**Coated**	
1	4.26E-11	1.02E-11	297.50	340.00	42.50	28.75	35.09	1.01
2	3.90E-11	9.92E-12	290.00	350.00	60.00	29.37	35.71	1.05
3	3.73E-11	9.35E-12	292.50	338.75	46.25	29.06	35.40	1.03
4	4.26E-11	1.10E-11	297.50	345.00	47.50	29.15	35.49	1.02
Mean	4.04E-11	1.01E-11	294.38	343.44	49.06	**Mean**		1.03
Std. Dev	2.66E-12	6.86E-13	3.75	5.14	7.59	**Std. Dev**		0.02
95 % CI	4.23E-12	1.09E-12	5.97	8.18	12.08	**95 % CI**		0.03

Table B- 11 Sintering data for Toray TGP-H-60 (1.0 $mgcm^{-2}$) Vulcan XC-72R.

Toray TGP-H-60						
1.0 $mgcm^{-2}$ (Vulcan XC-72R)						
Sample Number	**Permeability k (m^2)**					
	Sintering Time (hours)					
	0	**0.5**	**2**	**4**	**6**	**8**
1	3.21E-13	3.20E-13	3.18E-13	3.21E-13	3.23E-13	3.21E-13
2	3.22E-13	3.21E-13	3.16E-13	3.22E-13	3.28E-13	3.21E-13
3	3.19E-13	3.18E-13	3.10E-13	3.13E-13	3.17E-13	3.13E-13
4	3.15E-13	3.12E-13	3.08E-13	3.10E-13	3.19E-13	3.17E-13
Mean	3.19E-13	3.18E-13	3.13E-13	3.16E-13	3.22E-13	3.18E-13
Std. Dev	3.18E-15	3.87E-15	4.58E-15	5.73E-15	4.82E-15	3.92E-15
95 % CI	5.06E-15	6.15E-15	7.28E-15	9.11E-15	7.67E-15	6.24E-15

Table B- 12 Sintering data for Toray TGP-H-60 (1.0 $mgcm^{-2}$) Ketjenblack EC-300J.

Toray TGP-H-60						
1.0 $mgcm^{-2}$ (Ketjenblack EC-300J)						
Sample Number	**Permeability $k\ (m^2)$**					
	Sintering Time (hours)					
	0	**0.5**	**2**	**4**	**6**	**8**
1	1.96E-12	2.00E-12	1.95E-12	2.54E-12	2.08E-12	3.12E-12
2	2.14E-12	1.98E-12	2.19E-12	2.30E-12	3.98E-12	5.24E-12
3	1.88E-12	1.94E-12	1.92E-12	1.94E-12	1.99E-12	2.04E-12
4	2.06E-12	2.17E-12	2.21E-12	2.19E-12	3.15E-12	3.38E-12
Mean	2.01E-12	2.02E-12	2.07E-12	2.24E-12	2.80E-12	3.45E-12
Std. Dev	1.16E-13	1.01E-13	1.55E-13	2.49E-13	9.45E-13	1.33E-12
95 % CI	1.85E-13	1.60E-13	2.46E-13	3.95E-13	1.50E-12	2.12E-12

Table B- 13 Sintering data for SGL 35BA (1.0 $mgcm^{-2}$) Vulcan XC-72R.

SGL 35BA						
1.0 $mgcm^{-2}$ (Vulcan XC-72R)						
Sample Number	**Permeability k (m^2)**					
	Sintering Time (hours)					
	0	**0.5**	**2**	**4**	**6**	**8**
1	3.77E-12	4.07E-12	3.63E-12	3.81E-12	3.79E-12	3.59E-12
2	3.74E-12	3.75E-12	3.68E-12	3.67E-12	4.01E-12	3.63E-12
3	5.28E-12	4.98E-12	5.39E-12	5.18E-12	5.32E-12	5.20E-12
4	3.38E-12	3.39E-12	3.19E-12	3.33E-12	3.38E-12	3.19E-12
Mean	4.04E-12	4.05E-12	3.97E-12	4.00E-12	4.13E-12	3.90E-12
Std. Dev	8.45E-13	6.81E-13	9.70E-13	8.12E-13	8.39E-13	8.87E-13
95 % CI	1.34E-12	1.08E-12	1.54E-12	1.29E-12	1.34E-12	1.41E-12

Table B- 14 Sintering data for SGL 35BA (1.0 $mgcm^{-2}$) Ketjenblack EC-300J.

SGL 35BA						
1.0 $mgcm^{-2}$ (Ketjenblack EC-300J)						
Sample Number	**Permeability k (m^2)**					
	Sintering Time (hours)					
	0	**0.5**	**2**	**4**	**6**	**8**
1	1.02E-11	9.42E-12	9.07E-12	9.38E-12	9.35E-12	9.40E-12
2	9.92E-12	9.54E-12	9.37E-12	9.48E-12	9.86E-12	9.64E-12
3	9.35E-12	8.98E-12	8.82E-12	8.98E-12	8.98E-12	8.88E-12
4	1.08E-11	8.71E-12	8.76E-12	8.90E-12	8.99E-12	8.72E-12
Mean	1.01E-11	9.16E-12	9.00E-12	9.19E-12	9.29E-12	9.16E-12
Std. Dev	5.94E-13	3.83E-13	2.77E-13	2.90E-13	4.14E-13	4.31E-13
95 % CI	9.46E-13	6.09E-13	4.41E-13	4.62E-13	6.59E-13	6.86E-13

Table B- 15 Sintering data for SGL 10BC.

SGL 10BC							
Sample Number	**Thickness** (μm)	**Permeability** $k\ (m^2)$					
		Sintering Time (hours)					
		0	**0.5**	**2**	**4**	**6**	**8**
1	345.00	5.06E-13	5.22E-13	5.16E-13	5.15E-13	5.05E-13	5.01E-13
2	338.75	5.51E-13	5.51E-13	5.53E-13	5.46E-13	5.46E-13	5.45E-13
3	340.00	5.32E-13	5.58E-13	5.72E-13	5.91E-13	5.44E-13	5.49E-13
4	345.00	5.06E-13	5.22E-13	5.16E-13	5.15E-13	5.05E-13	5.01E-13
Mean	342.19	5.24E-13	5.38E-13	5.39E-13	5.42E-13	5.25E-13	5.24E-13
Std. Dev	3.29	2.22E-14	1.89E-14	2.77E-14	3.62E-14	2.32E-14	2.67E-14
95 % CI	5.23	3.54E-14	3.01E-14	4.41E-14	5.76E-14	3.69E-14	4.24E-14

Table B- 16 Sintering data for SGL 10BE.

SGL 10BE							
Sample Number	**Thickness** (μm)	**Permeability** $k\ (m^2)$					
		Sintering Time (hours)					
		0	**0.5**	**2**	**4**	**6**	**8**
1	397.50	7.59E-13	8.05E-13	8.02E-13	8.04E-13	8.38E-13	8.10E-13
2	378.75	8.22E-13	8.60E-13	8.57E-13	8.36E-13	9.17E-13	9.05E-13
3	380.00	8.25E-13	8.63E-13	8.59E-13	8.38E-13	9.20E-13	9.08E-13
4	395.00	7.54E-13	7.99E-13	7.97E-13	7.99E-13	8.33E-13	8.05E-13
Mean	387.81	7.90E-13	8.32E-13	8.29E-13	8.19E-13	8.77E-13	8.57E-13
Std. Dev	9.81	3.89E-14	3.46E-14	3.37E-14	2.08E-14	4.79E-14	5.72E-14
95 % CI	15.61	6.19E-14	5.50E-14	5.36E-14	3.31E-14	7.62E-14	9.11E-14

Appendix C

Chapter 6 Results

Table C- 1 Toray TGP-H-60 (1.0 $mgcm^{-2}$) Vulcan XC-72R – Ultrasonic Bath Sonication.

Toray TGP-H-60									
1.0 $mgcm^{-2}$ (Vulcan XC-72R)- Ultrasonic bath sonication									
Sample Number	**Permeability $k\ (m^2)$**		**Thickness (μm)**		**Thickness change (L_{MPL}) (μm)**	**Percentage reduction in permeability (%)**	**Mass of samples (mg)**		**Actual carbon loading $(mgcm^{-2})$**
	Uncoated (k_{GDL})	**Coated (k_{GDM})**	**Uncoated (L_{GDL})**	**Coated (L_{GDM})**			**Uncoated**	**Coated**	
1	7.20E-12	4.70E-13	200.00	216.25	16.25	93.48	43.57	50.20	1.05
2	6.80E-12	4.40E-13	197.50	212.50	15.00	93.53	43.29	49.80	1.03
3	6.94E-12	3.31E-13	198.75	213.75	15.00	95.23	43.56	50.10	1.03
4	7.06E-12	4.63E-13	201.25	215.00	13.75	93.44	43.47	49.95	1.02
Mean	7.00E-12	4.26E-13	199.38	214.38	15.00	93.92	**Mean**		1.03
Std. Dev	1.73E-13	6.47E-14	1.61	1.61	1.02	0.88	**Std. Dev**		0.01
95 % CI	2.76E-13	1.03E-13	2.57	2.57	1.62	1.39	**95 % CI**		0.02

Table C- 2 Toray TGP-H-60 (1.0 $mgcm^{-2}$) Vulcan XC-72R – Magnetic Stirring.

Toray TGP-H-60									
1.0 $mgcm^{-2}$ (Vulcan XC-72R)- Magnetic Stirring									
Sample Number	**Permeability $k\ (m^2)$**		**Thickness (μm)**		**Thickness change (L_{MPL}) (μm)**	**Percentage reduction in permeability (%)**	**Mass of samples (mg)**		**Actual carbon loading $(mgcm^{-2})$**
	Uncoated (k_{GDL})	**Coated (k_{GDM})**	**Uncoated (L_{GDL})**	**Coated (L_{GDM})**			**Uncoated**	**Coated**	
1	7.11E-12	9.89E-13	197.50	222.50	25.00	86.09	43.66	50.10	1.02
2	6.43E-12	9.33E-13	191.25	215.00	23.75	85.49	41.33	47.60	0.99
3	6.94E-12	9.64E-13	192.50	216.25	23.75	86.12	43.92	50.50	1.04
4	6.89E-12	7.43E-13	192.50	220.00	27.50	89.22	43.64	50.10	1.02
Mean	6.85E-12	9.07E-13	193.44	218.44	25.00	86.73	**Mean**		1.02
Std. Dev	2.91E-13	1.12E-13	2.77	3.44	1.77	1.68	**Std. Dev**		0.02
95 % CI	4.63E-13	1.78E-13	4.41	5.48	2.81	2.68	**95 % CI**		0.03

Table C- 3 Toray TGP-H-60 (1.0 $mgcm^{-2}$) Ketjenblack EC-300J – Ultrasonic Bath Sonication.

Toray TGP-H-60									
1.0 $mgcm^{-2}$ (Ketjenblack EC-300J)- Ultrasonic bath sonicaation									
Sample Number	**Permeability $k\ (m^2)$**		**Thickness (μm)**		**Thickness change (L_{MPL}) (μm)**	**Percentage reduction in permeability (%)**	**Mass of samples (mg)**		**Actual carbon loading $(mgcm^{-2})$**
	Uncoated (k_{GDL})	**Coated (k_{GDM})**	**Uncoated (L_{GDL})**	**Coated (L_{GDM})**			**Uncoated**	**Coated**	
1	6.88E-12	3.09E-12	198.75	243.75	45.00	55.02	43.28	49.5	0.98
2	7.07E-12	3.77E-12	193.75	236.25	42.50	46.69	44.29	50.71	1.01
3	7.27E-12	4.17E-12	200.00	245.00	45.00	42.63	41.96	48.32	1.00
4	7.26E-12	4.02E-12	198.75	245.00	46.25	44.65	42.75	49.3	1.03
Mean	7.12E-12	3.76E-12	197.81	242.50	44.69	47.25	**Mean**		1.01
Std. Dev	1.88E-13	4.77E-13	2.77	4.21	1.57	5.44	**Std. Dev**		0.02
95 % CI	2.99E-13	7.58E-13	4.41	6.70	2.50	8.66	**95 % CI**		0.03

Table C- 4 Toray TGP-H-60 (1.0 mgcm^{-2}) Ketjenblack EC-300J – Magnetic Stirring.

Toray TGP-H-60									
1.0 mgcm^{-2} (Ketjenblack EC-300J)- Magnetic Stirring									
Sample Number	**Permeability $k\ (m^2)$**		**Thickness (μm)**		**Thickness change (L_{MPL}) (μm)**	**Percentage reduction in permeability (%)**	**Mass of samples (mg)**		**Actual carbon loading $(mgcm^{-2})$**
	Uncoated (k_{GDL})	**Coated (k_{GDM})**	**Uncoated (L_{GDL})**	**Coated (L_{GDM})**			**Uncoated**	**Coated**	
1	6.72E-12	3.99E-12	191.25	242.50	51.25	40.59	42.59	42.59	1.03
2	7.42E-12	4.15E-12	205.00	258.75	53.75	44.06	42.37	42.37	1.03
3	7.08E-12	3.75E-12	195.00	243.75	48.75	46.97	43.16	43.16	1.07
4	7.23E-12	3.93E-12	196.25	247.50	51.25	45.65	43.04	43.04	1.02
Mean	7.11E-12	3.96E-12	196.88	248.13	51.25	44.32	**Mean**		1.04
Std. Dev	2.97E-13	1.64E-13	5.82	7.40	2.04	2.76	**Std. Dev**		0.02
95 % CI	4.72E-13	2.62E-13	9.26	11.77	3.25	4.39	**95 % CI**		0.04

Table C- 5 SGL 10DA (1.0 mgcm^{-2}) Vulcan XC-72R – Ultrasonic Bath Sonication.

SGL 10DA									
1.0 mgcm^{-2} (Vulcan XC-72R)- Ultrasonic bath sonication									
Sample Number	**Permeability $k\ (m^2)$**		**Thickness (μm)**		**Thickness change (L_{MPL}) (μm)**	**Percentage reduction in permeability (%)**	**Mass of samples (mg)**		**Actual carbon loading $(mgcm^{-2})$**
	Uncoated (k_{GDL})	**Coated (k_{GDM})**	**Uncoated (L_{GDL})**	**Coated (L_{GDM})**			**Uncoated**	**Coated**	
1	1.70E-11	2.89E-12	360.00	376.25	16.25	83.05	54.73	61.05	1.00
2	1.82E-11	2.89E-12	350.00	367.50	17.50	84.16	51.35	58.03	1.05
3	1.85E-11	3.04E-12	372.50	390.00	17.50	83.56	55.42	62.01	1.04
4	2.22E-11	2.96E-12	347.50	363.75	16.25	86.67	47.37	54.18	1.07
Mean	1.90E-11	2.95E-12	357.50	374.38	16.88	84.36	**Mean**		1.04
Std. Dev	2.25E-12	7.29E-14	11.37	11.66	0.72	1.61	**Std. Dev**		0.03
95 % CI	3.57E-12	1.16E-13	18.08	18.55	1.15	2.56	**95 % CI**		0.05

Table C- 6 SGL 10DA (1.0 $mgcm^{-2}$) Vulcan XC-72R – Magnetic Stirring.

SGL 10DA									
1.0 $mgcm^{-2}$ (Vulcan XC-72R)- Magnetic Stirring									
Sample Number	**Permeability $k\ (m^2)$**		**Thickness (μm)**		**Thickness change (L_{MPL}) (μm)**	**Percentage reduction in permeability (%)**	**Mass of samples (mg)**		**Actual carbon loading $(mgcm^{-2})$**
	Uncoated (k_{GDL})	**Coated (k_{GDM})**	**Uncoated (L_{GDL})**	**Coated (L_{GDM})**			**Uncoated**	**Coated**	
1	1.93E-11	5.77E-12	358.75	380.00	21.25	70.09	49.88	56.50	1.04
2	1.98E-11	4.29E-12	358.75	383.75	25.00	78.32	52.73	59.30	1.04
3	1.63E-11	3.21E-12	325.00	348.75	23.75	80.36	47.66	54.40	1.06
4	2.07E-11	3.81E-12	340.00	367.50	27.50	81.59	48.39	55.12	1.06
Mean	1.90E-11	4.27E-12	345.63	370.00	24.38	77.59	**Mean**		1.05
Std. Dev	1.89E-12	1.09E-12	16.35	15.78	2.60	5.18	**Std. Dev**		0.01
95 % CI	3.00E-12	1.74E-12	26.01	25.10	4.14	8.24	**95 % CI**		0.02

Table C- 7 SGL 10DA (1.0 mgcm^{-2}) Ketjenblack EC-300J – Ultrasonic Bath Sonication.

SGL 10DA									
1.0 mgcm^{-2} (Ketjenblack EC-300J)- Ultrasonic bath sonicaation									
Sample Number	**Permeability $k\ (m^2)$**		**Thickness (μm)**		**Thickness change (L_{MPL}) (μm)**	**Percentage reduction in permeability (%)**	**Mass of samples (mg)**		**Actual carbon loading $(mgcm^{-2})$**
	Uncoated (k_{GDL})	**Coated (k_{GDM})**	**Uncoated (L_{GDL})**	**Coated (L_{GDM})**			**Uncoated**	**Coated**	
1	1.97E-11	6.65E-12	346.25	388.75	42.50	66.17	47.79	54.09	0.99
2	2.00E-11	7.22E-12	356.25	393.75	37.50	63.89	48.5	54.9	1.01
3	2.03E-11	7.20E-12	351.25	390.00	38.75	64.50	49.15	55.34	0.98
4	2.05E-11	7.00E-12	337.50	373.75	36.25	65.85	46.66	53.01	1.00
Mean	2.01E-11	7.02E-12	347.81	386.56	38.75	65.10	**Mean**		1.00
Std. Dev	3.63E-13	2.64E-13	8.00	8.80	2.70	1.08	**Std. Dev**		0.01
95 % CI	5.78E-13	4.20E-13	12.72	14.00	4.30	1.73	**95 % CI**		0.02

Table C- 8 SGL 10DA (1.0 mgcm^{-2}) Ketjenblack EC-300J – Magnetic Stirring.

SGL 10DA									
1.0 mgcm^{-2} (Ketjenblack EC-300J)- Magnetic Stirring									
Sample Number	**Permeability $k\ (m^2)$**		**Thickness (μm)**		**Thickness change (L_{MPL}) (μm)**	**Percentage reduction in permeability (%)**	**Mass of samples (mg)**		**Actual carbon loading $(mgcm^{-2})$**
	Uncoated (k_{GDL})	**Coated (k_{GDM})**	**Uncoated (L_{GDL})**	**Coated (L_{GDM})**			**Uncoated**	**Coated**	
1	1.85E-11	7.08E-12	365.00	407.50	42.50	61.67	53.9	60.89	1.10
2	2.12E-11	6.89E-12	331.25	375.00	43.75	67.57	49.09	55.96	1.08
3	2.13E-11	8.69E-12	362.50	405.00	42.50	59.18	51.19	57.9	1.06
4	2.07E-11	8.64E-12	352.50	402.50	50.00	58.20	51.24	57.87	1.05
Mean	2.04E-11	7.82E-12	352.81	397.50	44.69	61.65	**Mean**		1.07
Std. Dev	1.33E-12	9.73E-13	15.36	15.14	3.59	4.21	**Std. Dev**		0.03
95 % CI	2.11E-12	1.55E-12	24.43	24.08	5.71	6.69	**95 % CI**		0.04